8.901 Lecture Notes
Astrophysics I, Spring 2019

I.J.M. Crossfield (with S. Hughes and E. Mills)[*]

MIT

6th February, 2019 – 15th May, 2019

Contents

[*]iancross@mit.edu

1 Introduction to Astronomy and Astrophysics

Lecture 1

- **Course overview.** Hand out syllabus, discuss schedule & assignments.

- **Astrophysics**: effort to understand the nature of astronomical objects. Union of quite a few branches of physics --- gravity, E&M, stat mech, quantum, fluid dynamics, relativity, nuclear, plasma --- all matter, and have impact over a wide range of length & time scales

- **Astronomy:** providing the observational data upon which astrophysics is built. Thousands of years of history, with plenty of intriguing baggage. E.g.:

  - Sexagesimal notation: Base-60 number system, originated in Sumer in ~3000 BC. Origin uncertain (how could it not be?), but we still use this today for time and angles: 60'' in 1', 60' in 1°, 360° in one circle.

  - **Magnitudes**: standard way of measuring brightnesses of stars and galaxies.
    - Originally based on the human eye by Hipparchus of Greece (~135 BC), who divided visible stars into six primary brightness bins. This arbitrary system continued for ~2000 years, and it makes it fun to read old astronomy papers ("I observed a star of the first magnitude," etc.).
    - Revised by Pogson (1856), who semi-arbitrarily decreed that a one-magnitude jump meant a star was ~2.512x brighter. This is only an approximation to how the eye works! So given two stars with brightness l_1 and l_2:
    - Apparent/relative magnitude: $m_1 - m_2 = 2.5 \log_{10} (l_1/l_2)$ (2 stars)
      - So 2.5 mag difference = 10x brighter.
      - Also, 2.5x brighter ~ 1 mag difference. Nice coincidence!
      - Also, 1 mmag difference = 10^{-3} mag = 1.001x brighter
    - Absolute magnitude (1 star): $m - M = 2.5 \log_{10} [(d / 10\text{pc})^2] = 5 \log_{10} (d / 10\text{pc})$ (assumes no absorption of light through space)
    - Magnitudes can be :
      - "bolometric," relating the total EM power of the object (of course, we can never actually measure this – need models!) or
      - wavelength-dependent, only relating the power in a specific wavelength range
    - There are two different kinds of magnitude systems – these use different "zero-points" defining the magnitude of a given brightness. These are:
      - Vega – magnitudes at different wavelengths are always relative to a 10,000 K star
      - AB – a given magnitude at any wavelength always means the same flux density

- **Astronomical observing**:
  - Most astro observations are electromagnetic: photons (high energy) or waves (low energy)
  - EM: Gamma rays X-ray UV Optical Infrared sub-mm radio
  - Non-EM: cosmic rays, neutrinos, gravitational waves. Except for a blip in 1987 (SN1987A), we only recently entered the era of "multi-messenger astronomy"

- **Key scales and orders of magnitude.**
  - We'll spend a lot of time on stars, so it's important to understand some key scales to get ourselves correctly oriented.
  - Mass:
    - Electron, $m_e \sim 10^{-27}$ g
      Proton, $m_p \sim 2 \times 10^{-24}$ g
      $m_p/m_e \sim 1800 \sim R_{WD} / R_{NS}$ ← not a coincidence!
    - Meanwhile, $M_{sun} \sim 2 \times 10^{33}$ g
    - So it might seem that this course is astronomically far from considerations of fundamental physics. This couldn't be further from the truth! Many quantities we will calculate are almost 'purely' derived from fundamental constants. E.g.:
      - $M_{WD} = (hbar\ c / G)^{3/2}\ m_H^{-2}$ maximum mass of a white dwarf
      - $R_S = 2\ G / c^2\ M_{BH}$ Schwarzschild radius of a black hole
    - Assume N hydrogen atoms in an object with mass M, packed maximally tightly under classical physics. When are the electrostatic and gravitational binding energies roughly comparable?
      - $E_{ES} = N\ k\ e^2 / a$ a = *Bohr radius*
      - $E_G = G\ M^2 / R$
        - $M = N\ m_p$
        - $R \sim N^{1/3}\ a$
          - $E_G = G\ N^{5/3}\ m_p^2 / a$
      - So the ratio is:
        - $E_G / E_{ES} = \dfrac{G\ N^{2/3} m_p^2}{e^2} \approx (N / 10^{54})^{2/3}$
        - So the biggest hydrogen blob that can be supported only by electrostatic pressure has
          M = $10^{54}\ m_p \sim 0.9\ M_{Jup}$
          R ~ $(10^{54})^{1/3}\ a \sim 0.7\ R_{jup}$ Roughly a Jovian gas giant!
  - **Physical state of the sun:**
    - $T_{center} \sim$ 1.5e7 K
      $\rho_{center} \sim 150$ g/cc
      (we'll see why later; one of our key goals will be to build models that relate interiors to observable, surface conditions)
      Is the center of the Sun still in the classical physics regime?
    - Simple criterion: atomic separation is much greater than their de Broglie wavelength:
      $d >> \lambda_D$ $\lambda_D = h / p$
      So, classical means $n << \lambda_D^{-3} << (p/h)^3$
      where $kT \sim p^2/2m$
    - So for electrons, $\dfrac{p}{h} = \dfrac{\sqrt{2\ m_e\ k\ T}}{h}$
      and so $n \ll \left(\dfrac{2\ m_e k\ T}{h^2} \right)^{3/2}$

- How do we relate n and ρ? Sun is ~totally ionized, so both electrons and protons contribute by number; but only protons contribute substantially to mass.:
  $\rho = m_p\, n / 2$
- Then our requirement for classical physics means:
  $$\rho \ll \frac{m_p}{2}\left(\frac{2 m_e k T}{h^2}\right)^{3/2} \quad or$$
  $$\rho \ll \left(2800\, g\, cm^{-3}\right)\left(\frac{T}{10^7\, K}\right)^{3/2}$$ … classical, but only by a factor of ~10. Not so far off!
- Is the sun an ideal gas? If so, thermal energy dominates:
  kT >> e^2 / a, so
  T >> $e^2\, n^{1/3} / k$
  T >> $e^2\, (2\,\rho / m_p)^{1/3} / k$
  T >> (15000 K) $(\rho$ / 1g/cc$)^{1/3}$
  This is satisfied throughout the entire sun: it's valid to treat the Sun's interior (and most other stars) as an ideal gas.

2 The Two-Body Problem and Kepler's Laws

Lecture 2

- Space is Big.
- Last time we talked about mass scales; today we'll talk about **size scales**:
  - Bohr radius → $p^2/2m \sim \hbar^2 / (2\ m\ a^2) \sim e^2/a \rightarrow$ 5.3e-9 cm
  - Rearth = 6.3e8 cm = (20000 / pi) km
  - Rsun = 7e10 cm
  - 1 AU = 1.5e13 cm ~ 8 light-minutes
  - 1 parsec = 1 pc = 3e18 cm = 3.26 light years (note that l.y. are ~never used in astrophysics)

- **Parsec** is the fundamental unit of distance; it is ~the typical distance between stars (though that's just a coincidence). It is observationally defined:

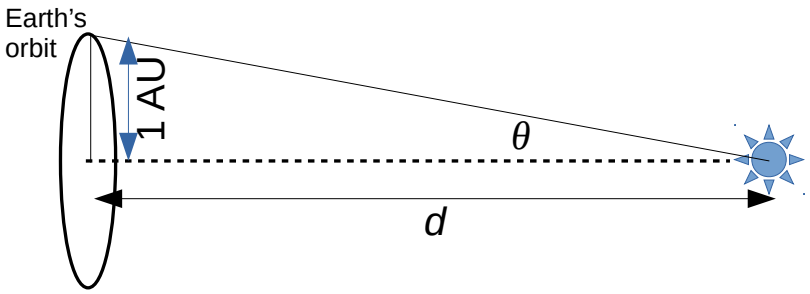

Over one year, the Earth's displacement is 2 AU and an object at distance *d* changes apparent position by 2θ, where
tan θ = 1 AU / d, or
d = 1 AU / θ, or
d / 1 pc = 1 arcsec / θ

  - Nearest star: 1.3 pc
    To our galactic center: 8 kpc (kiloparsecs)
    To the nearest big galaxy: 620 kpc !!

- **Cosmic Distance Ladder:**
  - Distance is a key concept in astrophysics – e.g. the revolution currently underway thanks to ESA's Gaia mission (measuring parallax for billions of objects with sub-milliarcsec precision)
  - "Distance ladder" refers to the bootstrapping of distance measurements, from nearby stars to the furthest edges of the observable universe.
  - Within solar system: light travel time. Radar, spacecraft communication, etc.
  - Parallax: the first rung outside the Solar system. Measured by Gaia (2nd data release) for ~1 billion stars across ~half of the Galaxy. A revolution is underway!

- Standard candles: if Luminosity L is known, then observed flux F gives distance:
  $F = L / 4\pi d^2 \quad \rightarrow \quad d = (L / 4\pi F)^{1/2}$
  Most important types:
  - Cepheid variables - giant pulsating stars, period varies with absolute magnitude
  - Type Ia Supernovae – exploding stars (probably white dwarf)
  - Neither of these are truly standard – only "standardizable" (which is almost as good)
  - Other types (for other galaxies):
    - Tully-Fisher: $L \sim V^2$ (rotational velocity of spiral galaxies)
    - Faber-Jackson: $L \sim \sigma^2$ (velocity dispersion of elliptical galaxies)
- Hubble's Law – for very distant Galaxies.
  - The universe is expanding at a nearly-constant rate (more on that in 8.902). Roughly, it expands evenly everywhere, so a distant galaxy's apparent velocity is $v = H_0 d$. So, $d = v / H_0$.
  - Note that this doesn't work for nearby galaxies like Andromeda (which is moving toward us due to gravity dominating over cosmic expansion).

- **The two-body problem** ← see Ch. 2 of Murray & Dermott
  - The motion of two bodies about one another due to their mutual gravity.
    - Planets orbiting stars
    - Stars orbiting each other
    - Objects orbiting white dwarf; neutron star; black hole
  - Certain quantities can be measured very precisely, enabling precise measurements of masses and sizes of bodies. E.g., binary pulsars (neutron stars): masses measured to within $10^{-3}\ M_{sun}$ (~0.1%)
  - Goal here: Go through the gravitational two-body problem with an eye on features that are observationally testable, and on features specific to the $1/r^2$ nature of gravity. Many "details" of the real world push us away from exact $1/r^2$ – e.g. physical sizes, non-spherical shapes, general relativity
  - Key behavior we will use:
    - (1) Bodies move in elliptical trajectories (**Kepler's 1st Law**)

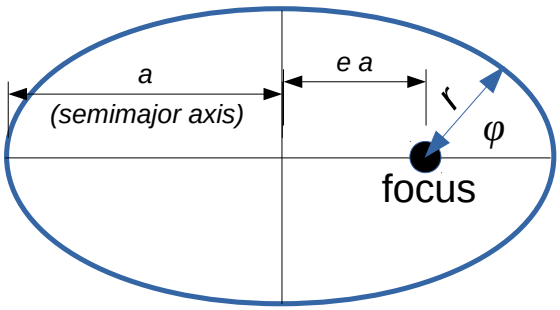

$$r(\varphi) = \frac{a(1-e^2)}{1+e\cos\varphi}$$

    - **2nd Law:** Motion sweeps out equal areas in equal times: $dA/dt = \frac{1}{2} r^2 \, d\varphi/dt$ = constant
    - **3rd Law:** $a^3/P^2 \sim (M_{tot})$ ← our eventual goal. P=orbital period, M_{tot} = total system mass

- To fully describe two pointlike bodies in 3D, we need 6 position components and 6 velocity components. (If they are not pointlike we need even more – in this case we use, e.g., Euler angles to define bodies' orientations.) Regardless, we need to reduce this to make things tractable!

- FIRST, go from 2 bodies to 1 … we can do this for any central force (not just $1/r^2$). This means converting potential: $V(r_1, r_2) = V(|r_2 - r_1|)$ ← since potential depends only on relative position

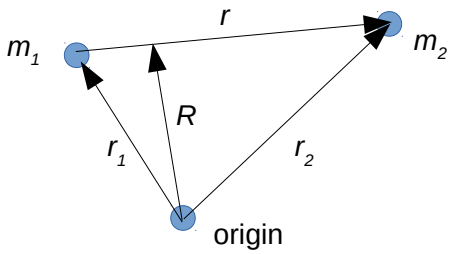

- $\vec{r} = \vec{r}_2 - \vec{r}_1$ (eq 1)
  $\vec{R} = \frac{m_1\vec{r}_1 + m_2\vec{r}_2}{m_1 + m_2}$ (position of center of mass)
  $\ddot{\vec{R}} = 0$ IF no external forces operate on the system.

- We can always set ***Rdot*** = 0 by choosing an intertial reference frame, and we can choose our origin so that ***R*** = 0 too.
  That means that $m_1\vec{r}_1 + m_2\vec{r}_2 = 0$ – combining with (eq 1) above shows that
  $\vec{r}_2 = \frac{\vec{r}}{1 + m_2/m_1}$ and $\vec{r}_1 = -\frac{m_2}{m_1}\vec{r}_2$

- … Which gives us the motions and velocities of both bodies in terms of the single variable *r.* So, we've reduced the 2-body problem to a one-body problem.

3 The Two-Body Problem, Continued

Lecture 3

- So, we've reduced the **2-body problem** to a one-body problem. Next, we reduce the dimensionality:
  - We have a central force, so $\vec{F} \propto \vec{r}$
    Thus we have no torque, since $\vec{\tau} = \vec{r} \times \vec{F} = 0$
    Thus angular momentum is conserved in the 2-body system.

  - That angular momentum is always perpendicular to the orbital plane, since
    $\vec{L} \cdot \hat{r} = (\vec{r} \times \mu \dot{\vec{r}}) \cdot \hat{r}$
    $... = (\hat{r} \times \vec{r}) \cdot \mu \dot{\vec{r}} = 0$

  - Since the orbit is always in a single, constant plane we can just describe it using 2D polar coordinates, r and φ
    Thus we have $\vec{L} = \vec{r} \times \mu \vec{v}$ (by definition of L)
    $... = \mu r v \varphi = \mu r^2 \dot{\varphi}$ = constant
    → **Equal area law (Kepler's 2nd) follows – true for <u>any central force</u> (not just $1/r^2$)**

  - Next, we go from 2D to 1D:
    - $E = \frac{1}{2} \mu \vec{v} \cdot \vec{v} + V(r)$
      $... = \frac{1}{2} \mu \dot{r}^2 + \frac{1}{2} \mu r^2 \dot{\varphi}^2 + V(r)$
      $L = \mu r^2 \dot{\varphi}$ (from above), and so $\dot{\varphi}^2 = \frac{L^2}{\mu^2 r^4}$
      and so $E = \frac{1}{2} \mu \dot{r}^2 + \frac{L^2}{2 \mu r^2} + V(r)$. We call those last two terms V_{eff}.
    - The formal solution to solve for the orbital motion is:
      $dt = \frac{dr}{\sqrt{\frac{2}{\mu}[E - V_{eff}(r)]}}$
    - For any given potential, one can integrate to get *t(r)* and then invert to find *r(t)*. Usually one gets nasty-looking Elliptic integrals for a polynomial potential.

- Get more insight from graphical analysis.

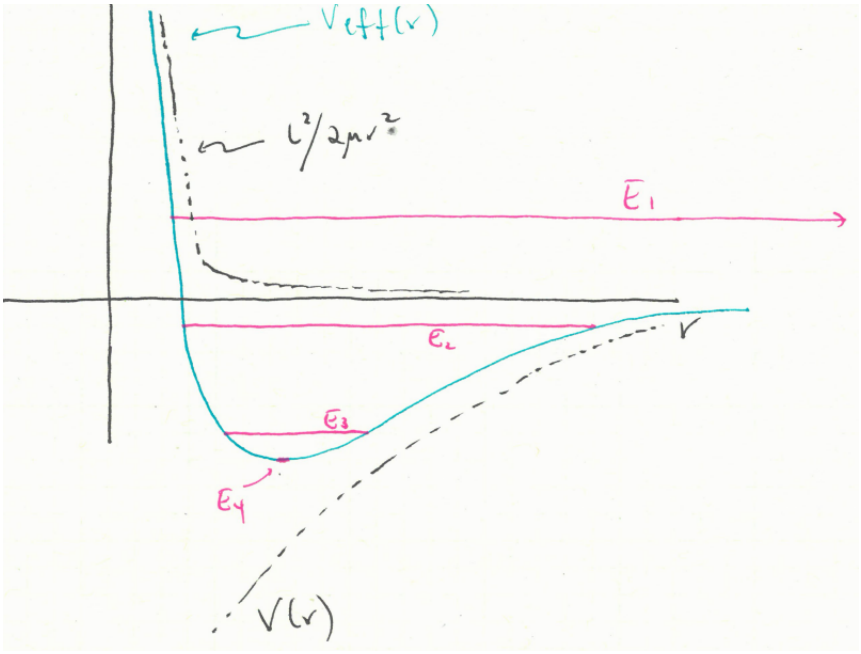

  - Plot V_{eff}, and then the total system E on the same graph. Given L & E:
    - Must have $V_{eff} < E$ (otherwise $v^2 < 0$)
    - Motion shows a turning point whenever $V_{eff} = E$.

  - For different energies plotted:
    - E_1: unbound orbit. Hyperbolic – interstellar comets!
    - E_2, E_3: bound, eccentric orbits (outer (apastron) and inner (periastron) points)
    - E_4: circular orbit (single radius).
    - $E < E_4$: not allowed!

- Let's look at this motion in the plane (for the bound case):

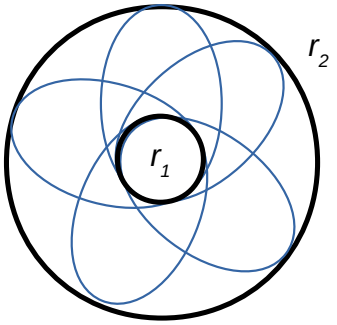

We see that the possible paths will fill in the regions between an inner and an outer radius (r_1 and r_2). But there's no guarantee that the orbits actually repeat periodically.

- We get **periodic orbits, and closed ellipses, for two special cases**:
  - $V(r) \propto \frac{1}{r}$ (Keplerian motion)
  - $V(r) \propto r^2$ (simple harmonic oscillator)
  - "Bertrand's Theorem" says that these are the only two closed-orbit forms.

▪ These closed-form cases are also special because they have **an "extra" conserved quantity.**

- Consider gravity: $V(r) = -\frac{G\mu M}{r}$ where $M = m_1 + m_2$
- Define the "Laplace-Runge-Lenz" (LRL) vector,
  $\vec{A} \equiv \vec{p} \times \vec{L} - GM\mu^2 \hat{r}$ ← this is **conserved**! Describes shape & orientation of orbit
- $\frac{d\vec{A}}{dt} = \frac{d\vec{p}}{dt} \times \vec{L} + \vec{p} \times \frac{d\vec{L}}{dt} - GM\mu^2 \frac{d\hat{r}}{dt}$ (second term goes to zero; L conserved!)

  $\frac{d\vec{p}}{dt} = -G\frac{\mu M}{r^2}\hat{r}$

  $\frac{d\hat{r}}{dt} = \frac{d\varphi}{dt}\hat{\varphi}$

  $\vec{L} = \mu r^2 \dot{\varphi} \hat{z}$

- So, $\frac{d\vec{A}}{dt} = \left(-\frac{G\mu M}{r^2}\hat{r}\right) \times \left(\mu r^2 \dot{\varphi} \hat{z}\right) - GM\mu^2 \dot{\varphi}\hat{\varphi}$, which gives

  $\frac{d\vec{A}}{dt} = +GM\mu^2 \dot{\varphi}\hat{\varphi} - GM\mu^2 \dot{\varphi}\hat{\varphi} = 0$ … A is a conserved quantity!
- But, what does the LRL vector *mean*?
  → It describes the elliptical equations of motion!

- *A* points in the orbital plane. Define it to point along the x-axis of our polar system:
  $\vec{r}\cdot\vec{A}\equiv r\,A\cos\varphi=\vec{r}\cdot(\vec{p}\times\vec{L})-G\,M\,\mu^2\,r$
  $...=\vec{L}\cdot(\vec{r}\times\vec{p})-G\,M\,\mu^2\,r \quad \rightarrow$
  $r\,A\cos\varphi=L^2-G\,M\,\mu^2 r$

- We can solve this for *r*:
  $r(\varphi)=\dfrac{L^2/G\,M\,\mu^2}{1+(A/G\,M\,\mu^2)\cos\varphi}$
  and this is just the **equation of an ellipse** that we saw in Lecture 2, with
  $e=\dfrac{A}{G\,M\,\mu^2}$ and
  $L=\sqrt{G\,M\,\mu^2\,a(1-e^2)}$

- We defined *A* to point along the x-axis (φ = 0). This is the same direction where *r* is minimized – so *A* (the LRL) points toward the closest approach in the orbit ("pericenter").

- One remaining law: K**epler's 3rd Law**
  - Consider the area of a curve in polar coordinates.
    $d\,Area=\dfrac{1}{2}r^2\,d\,\varphi$, so
    $\dfrac{d\,Area}{d\,t}=\dfrac{1}{2}r^2\,\dot{\varphi}=\dfrac{1}{2}\dfrac{L}{\mu}=constant$

  - If we integrate over a full period, we get the area of an ellipse:
    $A_{ellipse}=\int_0^P \dfrac{d\,Area}{dt}=\dfrac{1}{2}\int_0^P \dfrac{L}{\mu}dt=\dfrac{L\,P}{2\,\mu}$.
  - And from geometry, $A_{ellipse}=\pi\,a\,b$ (where $b=a\sqrt{1-e^2}$ is the semi*minor* axis)
  - So set these equal:
    $\dfrac{L\,P}{2\,\mu}=\pi\,a^2\sqrt{1-e^2}$. Plugging the previous expression for *L* in:
    $\dfrac{1}{2}\dfrac{\sqrt{G\,M\,\mu^2\,a(1-e^2)}}{\mu}P=\pi a^2\sqrt{1-e^2}$, which simplifies to
    $\sqrt{\dfrac{G\,M}{a^3}}=\dfrac{2\,\pi}{P}=\Omega_{Kepler}$

  - Rearranging to the more familiar form, we find:
    $P^2=\left(\dfrac{4\,\pi^2}{G\,M}\right)a^3$. Or in Solar units, $\left(\dfrac{P}{1\,yr}\right)^2=\left(\dfrac{M}{M_{sun}}\right)^{-1}\left(\dfrac{a}{1\,AU}\right)^3$

- Other interesting bits and bobs:
  - A useful exercise for the reader is to show that $E = -\frac{G M \mu}{2a}$

    (use *rdot* = 0 at pericenter, $r = a(1 - e)$, $\varphi = 0$)

  - We have r(phi) --- **what about r(t) and phi(t) ?**
    - Unfortunately there's no general, closed-form solution – this is typically calculated iteratively using a numerical framework.
    - One can find parametric solutions (see Psets)

  - The position vector moves on an ellipse, but you can show that the velocity vector actually moves on a circle:

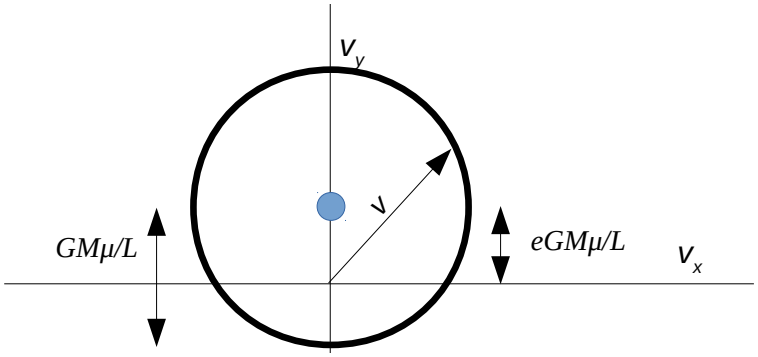

  - Really esoteric: all these conservation laws are tied to particular symmetries:
    - Energy conservation comes from time translation
    - Angular momentum conservation comes from SO(3) rotations
    - The RLR vector *A* is conserved because of rotations in *4D* (!!). *r* & *p* map onto the 3D surface of a 4D Euclidean sphere. Cool – but not too useful.

Other bits and bobs: Kozai-Lidov mechanism. Allows a tight binary with a wide tertiary to trade inner eccentricity with outer inclination. Secular calculations show that in these cases, $(\cos I)(\sqrt{1-e^2})$ is a conserved quantity. Important for multiple systems from asteroids to exoplanets to black holes.

4 Binary Systems

Having dealt with the two-body problem, we'll leave the three-body problem to science fiction authors and begin an in-depth study of stars. Our foray into Kepler's laws was appropriate, because about 50% of all stars are in binary (or higher-multiplicity) systems. With our fundamental dynamical model, plus data, we get a lot of stellar information from binary stars.

Stars in binaries are best characterized by mass M, radius R, and luminosity L. Note that an effective temperature $T_{\rm eff}$ is often used in place of L (see Eq. 66). An alternative set of parameters from the perspective of stellar evolution would be M; heavy-element enhancement "metallicity" [Fe/H], reported logarithmically; and age.

4.1 *Empirical Facts about binaries*

The distribution of stellar systems between singles, binaries, and higher-order multiples is roughly 55%, 35%, and 10% (Raghavan et al. 2010) – so the average number of stars per system is something like 1.6.

Orbital periods range from $<$ 1day to $\sim 10^{10}$ days ($\sim 3 \times 10^6$ yr). Any longer, and Galactic tides will disrupt the stable orbit (the Sun takes ~ 200 Myr to orbit the Milky Way). The periods have a log-normal distribution – for Sun-like stars, this peaks at $\log_{10}(P/d) = 4.8$ with a width of 2.3 dex (Duquennoy & Mayor 1992).

There's also a wide range of eccentricities, from nearly circular to highly elliptical. For short periods, we see $e \approx 0$. This is due to **tidal circularization**. Stars and planets aren't point-masses and aren't perfect spheres; tides represent the differential gradient of gravity across a physical object, and they bleed off orbital energy while conserving angular momentum. It turns out that this means e decreases as a consequence.

4.2 *Parameterization of Binary Orbits*

Two bodies orbiting in 3D requires 12 parameters, three for each body's position and velocity. Three of these map to the 3D position of the center of mass – we get these if we measure the binary's position on the sky and the distance to it. Three more map to the 3D velocity of the center of mass – we get these if we can track the motion of the binary through the Galaxy.

So we can translate any binary's motion into its center-of-mass rest frame, and we're left with **six numbers describing orbits** (see Fig. 2):

- P – the orbital period
- a – semimajor axis
- e – orbital eccentricity
- I – orbital inclination relative to the plane of the sky
- Ω – the longitude of the ascending node
- ω – the argument of pericenter

The first give the relevant timescale; the next two give us the shape of the ellipse; the last three describe the ellipse's orientation (like Euler angles in classical mechanics).

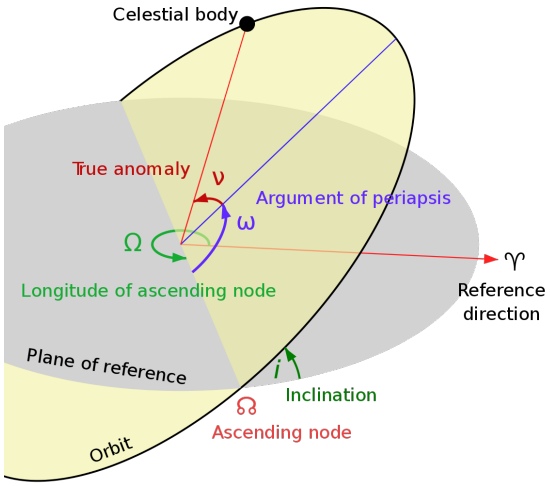

Figure 1: Geometry of an orbit. The observer is looking down along the z axis, so x and y point in the plane of the sky.

4.3 *Binary Observations*

The best way to measure L comes from basic telescopic observations of the apparent bolometric flux F (i.e., integrated over all wavelengths). Then we have

$$F = \frac{L}{4\pi d^2} \tag{1}$$

where ideally d is known from parallax.

But the most precise way to measure M and R almost always involve stellar binaries (though asteroseismology can do very well, too). But if we can observe enough parameters to reveal the Keplerian orbit, we can get masses (and separation); if the stars also undergo eclipses, we also get sizes.

In general, how does this work? We have two stars with masses $m_1 > m_2$ orbiting their common center of mass on elliptical orbits. Kepler's third law says that

$$\frac{GM}{a^3} = \left(\frac{2\pi}{P}\right)^2 \tag{2}$$

so if we can measure P and a we can get M. For any type of binary, we usually want $P \lesssim 10^4$ days if we're going to track the orbit in one astronomer's career.

If the binary is nearby and we can see the elliptical motion of at least one component, then we have an "astrometric binary." If we know the distance

d, we can then directly determine a as well (or both a_1 and a_2 if we see both components). The first known astrometric binary was the bright, northern star Sirius – from its motion on the sky, astronomers first identified its tiny, faint, but massive white dwarf companion, Sirius b.

More often, the data come from spectroscopic observations that measure the stars' Doppler shifts. If we can only measure the periodic velocity shifts of one star (e.g. the other is too faint), then the "spectroscopic binary" is an "SB1". If we can measure the Doppler shifts of both stars, then we have an "SB2": we get the individual semimajor axes a_1 and a_2 of both components, and we can get the individual masses from $m_1 a_1 = m_2 a_2$.

If we have an SB1, we measure the radial velocity of the visible star. Assuming a circular orbit,

$$v_{r1} = \frac{2\pi a_1 \sin I}{P} \cos\left(\frac{2\pi t}{P}\right) \tag{3}$$

where P and v_{r1} are the observed quantities. What good is $a_1 \sin I$? We know that $a_1 = (m_2/M)a$, so from Kepler's Third Law we see that

$$\left(\frac{2\pi}{P}\right)^2 = \frac{G m_2^3}{a_1^3 M^2} \tag{4}$$

Combining Eqs. 3 and 4, and throwing in an extra factor of $\sin^3 I$ to each side, we find

$$\frac{1}{G}\left(\frac{2\pi}{P}\right)^2 a_a^3 \sin^3 I = \frac{1}{G}\frac{v_{r1}^3}{(2\pi/P)} \tag{5}$$

$$= \frac{m_2^3 \sin^3 I}{M^2} \tag{6}$$

where this last term is the spectroscopic "mass function" – a single number built from observables that constrains the masses involved.

$$f_m = \frac{m_2^3 \sin^3 I}{(m_1 + m_2)^2} \tag{7}$$

In the limit that $m_1 << m_2$ (e.g. a low-mass star or planet orbiting a more massive star), then we have

$$f_m \approx m_2 \sin^3 I \leq m_2 \tag{8}$$

Another way of writing this out in terms of the observed radial velocity semi-amplitude K (see Lovis & Fischer 2010) is:

$$K = \frac{28.4 \text{ m s}^{-1}}{(1-e^2)^{1/2}} \frac{m_2 \sin I}{M_{Jup}} \left(\frac{m_1 + m_2}{M_\odot}\right)^{-2/3} \left(\frac{P}{1 \text{ yr}}\right)^{-1/3} \tag{9}$$

Fig. 2 shows the situation if the stars are eclipsing. In this example one star is substantially larger than the other; as the sizes become roughly equal (or as

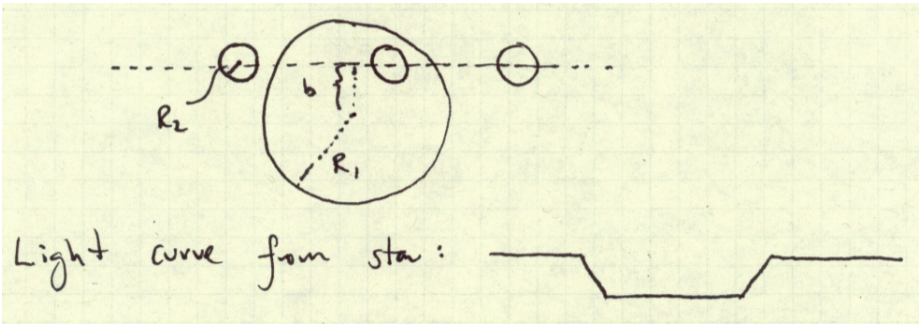

Figure 2: Geometry of an eclipse (top), and the observed light curve (bottom).

the impact parameter b reaches the edge of the eclipsed star), the transit looks less flat-bottomed and more and more V-shaped.

If the orbits are roughly circular then the duration of the eclipse (T_{14}) relates directly to the system geometry:

$$T_{14} \approx \frac{2R_1\sqrt{1-(b/R_1)^2}}{v_2} \tag{10}$$

while the fractional change in flux when one star blocks the other just scales as the fractional area, $(R_2/R_1)^2$.

There are a lot of details to be modeled here: the proper shape of the light curve, a way to fit for the orbit's eccentricity and orientation, also including the flux contribution during eclipse from the secondary star. Many of these details are simplified when considering extrasolar planets that transit their host stars: most of these have roughly circular orbits, and the planets contribute negligible flux relative to the host star.

Eclipses and spectroscopy together are very powerful: visible eclipses typically mean $I \approx 90^o$, so the $\sin I$ degeneracy in the mass function drops out and gives us an absolute mass. Less common is astrometry and spectroscopy – the former also determines I; this is likely to become much more common in the final *Gaia* data release (DR4, est. 2022).

5 Gravitational Waves

A subset of binary objects can be studied in an entirely different way than astrometry, spectroscopy, and eclipses: this is through **gravitational waves,** undulations in the fabric of spacetime itself caused by rapidly-orbiting, massive objects. For our description of that, I follow Choudhuri's textbook, parts of chapters 12 and 13. Note that in much of what follows, we skip details about a number of different factors (e.g. "projection tensors") that introduce angular dependencies, and enforce certain rules that radiation must obey. For a detailed treatment of all this, consult a modern gravitational wave textbook (even Choudhuri doesn't cover everything that follows, below).

Recall that in relativity we describe spacetime through the four-vector

$$x^i = (x^0, x^1, x^2, x^3) \tag{11}$$
$$= (ct, x, y, z) \tag{12}$$

(note that those are indices, not exponents!). The *special* relativistic metric that describes the geometry of spacetime is

$$ds^2 = -(dx^0)^2 + (dx^1)^2 + (dx^2)^2 + (dx^3)^2 \tag{13}$$
$$= \eta_{ik} dx^i dx^k \tag{14}$$

But this is only appropriate for special (not general) relativity – and we definitely need GR to treat accelerating, inspiraling compact objects. For 8.901, we'll assume weak gravity and an only slightly modified form of gravity; "first-order general relativity." Then our new metric is

$$g_{ik} = \eta_{ik} + h_{ik} \tag{15}$$

where it's still true that $ds^2 = g_{ik} dx^i dx^k$, and h_{ik} is the GR perturbation. For ease of computation (see the textbook) we introduce a modified definition,

$$\bar{h_{ik}} = h_{ik} - \frac{1}{2}\eta_{ik} h \tag{16}$$

where here h is the trace (the sum of the elements on the main diagonal) of h_{ik}.

Now recall that Newtonian gravity gives rise to the gravitational Poisson equation

$$\nabla^2 \Phi = 4\pi G \rho \tag{17}$$

– this is the gravitational equivalent of Gauss' Law in electromagnetism. The GR equations above then lead to an equivalent expression in GR – the **inhomogeneous wave equation**,

$$\Box^2 \bar{h_{ik}} = -\frac{16\pi G}{c^4} T_{ik} \tag{18}$$

where $\Box^2 = -1\frac{1}{c^2}\frac{\partial^2}{\partial t^2} + \nabla^2$ is the 4D differential operator and T_{ik} is the energy-momentum tensor, describing the distribution of energy and momentum in spacetime. This tensor is a key part of the **Einstein Equation** that describes how mass-energy leads to the curvature of spacetime, which unfortunately we don't have time to fully cover in 8.901.

One can solve Eq. 18 using the Green's function treatment found in almost all textbooks on electromagnetism. The solution is that

$$\bar{h_{ik}}(t,\vec{r}) = \frac{4G}{c^4}\int_S \frac{T_{ik}(t-|\vec{r}-\vec{r'}|/c,\vec{r'})}{|\vec{r}-\vec{r'}|}d^3r' \tag{19}$$

(where $t_r = t - |\vec{r}-\vec{r'}|/c$ is the 'Retarded Time'; see Fig. 3 for the relevant geometry). This result implies that the effects of gravitation propagate outwards at speed c, just as do the effects of electromagnetism.

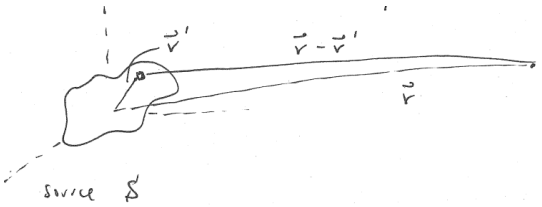

Figure 3: General geometry for Eq. 19.

We can simplify Eq. 19 in several ways. First, assuming than an observer is very far from the source implies $|\vec{r}| >> |\vec{r'}|$ for all points in the source S. Therefore,

$$\frac{1}{|\vec{r}-\vec{r'}|} \approx \frac{1}{r} \tag{20}$$

If the mass distribution (the source S) is also relatively small, then

$$t - |\vec{r}-\vec{r'}|/c \approx t - r/c \tag{21}$$

. Finally, general relativity tells us that the timelike components of h_{ik} do not radiate (see GR texts) – so we can neglect them in the analysis that follows.

Putting all this together, we have a simplified solution of Eq. 19, namely

$$\bar{h_{ik}} = \frac{4G}{c^4 r}\int_S T_{ik}(\vec{r'},t_R)d^3r' \tag{22}$$

We can combine this with one more trick. The properties of the stress-energy tensor (see text, again) turn out to prove that

$$\int_S T_{ik}(\vec{r'})d^3r' = \frac{1}{2}\frac{d^2}{dt^2}\int_S T_{00}(\vec{r'})\cdot x'_i x'_k d^3r' \tag{23}$$

This is possibly the greatest help of all, since in the limit of a weak-gravity source $T_{00} = \rho c^2$, where ρ is the combined density of mass and energy.

If we then define the **quadrupole moment tensor** as

$$I_{ik} = \int_S \rho(\vec{r}') x_i' x_j' d^3 r' \tag{24}$$

then we have as a result

$$h_{ik} = \frac{2G}{c^4 r} \frac{d^2}{dt^2} I_{ik} \tag{25}$$

which is the **quadrupole formula** for the gravitational wave amplitude.

What is this quadrupole moment tensor, I_{ik}? We can use it when we treat a binary's motion as approximately Newtonian, and then use I_{ik} to infer how gravitational wave emission causes the orbit to change. If we have a circular binary orbiting in the xy plane, with separation r and m_1 at $(x > 0, y = 0)$. In the reduced description, we have a separation r, total mass M, reduced mass $\mu = m_1 m_2 / M$, and orbital frequency $\Omega = \sqrt{GM/r^3}$. This means that the binary's position in space is

$$x_i = r(\cos \Omega t, \sin \Omega t, 0) \tag{26}$$

Treating the masses as point particles, we have $\rho = \rho_1 + \rho_2$ where

$$\rho_n = \delta(x - x_n)\delta(y - y_n)\delta(z) \tag{27}$$

so the moment tensor becomes simply $I_{ik} = \mu x_i x_k$, or

$$I_{ik} = \mu r^2 \begin{bmatrix} \cos^2 \Omega t & \sin \Omega t \cos \Omega t & 0 \\ \sin \Omega t \cos \Omega t & \sin^2 \Omega t & 0 \\ 0 & 0 & 0 \end{bmatrix} \tag{28}$$

As we will see below, this result implies that gravitational waves are emitted at twice the orbital frequency.

5.1 *Gravitational Radiation*

Why gravitational *waves*? Eq. 18 above implies that in empty space, we must have simply

$$\Box^2 \bar{h_{lm}} = \Box^2 h_{lm} = 0 \tag{29}$$

This implies the existence of the aforementioned propagating gravitational waves, in an analogous fashion to the implication of Maxwell's Equations for traveling electromagnetic waves. In particular, if we define the wave to be traveling in the x^3 direction then a plane gravitational wave has the form

$$h_{lm} = A_{lm} e^{ik(ct - x^3)} \tag{30}$$

(where i and k now have their usual wave meanings, rather than referring to indices). It turns out that the A_{lm} tensor can be written as simply

$$A_{lm} = \begin{pmatrix} 0 & 0 & 0 & 0 \\ 0 & a & b & 0 \\ 0 & b & -a & 0 \\ 0 & 0 & 0 & 0 \end{pmatrix} \tag{31}$$

The implication of just two variables in A_{lm} is that gravitational waves have just two polarizations, "$+$" and "$\times$". This is why each LIGO and VIRGO detector needs just two arms – one per polarization mode.

Just like EM waves, GW also carry energy. The **Isaacson Tensor** forms part of the expression describing how much energy is being carried, namely:

$$\frac{dE}{dAdt} = \frac{1}{32\pi} c^3/G < \dot{h}_{ij}\dot{h}_{ij} > \tag{32}$$

This is meaningful only on distance scales of at least one wavelength, and when integrated over a large sphere (and accounting for better-unmentioned terms like the projection tensors), we have

$$\frac{dE}{dt} = \frac{1}{5}\frac{G}{c^5} < \dddot{I}_{ij}\dddot{I}_{ij} > \tag{33}$$

which is the **quadrupole formula** for the energy carried by gravitational waves.

5.2 *Practical Effects*

In practice, this means that the energy flux carried by a gravitational wave of frequency f and amplitude h is

$$F_{gw} = 3 \text{ mW m}^{-2} \left(\frac{h}{10^{-22}}\right)^2 \left(\frac{f}{1 \text{ kHz}}\right)^2 \tag{34}$$

In contrast, the Solar Constant is about 1.4×10^6 mW m^{-2}. But the full moon is $\sim 10^6\times$ fainter than the sun, and gravitational waves carry energy comparable to that!

For a single gravitational wave event of duration τ, the observed "strain" (amplitude) h scales approximately as:

$$h = 10^{-21} \left(\frac{E_{GW}}{0.01 M_\odot c^2}\right)^{1/2} \left(\frac{r}{20 \text{ Mpc}}\right)^{-1} \left(\frac{f}{1 \text{ kHz}}\right)^{-1} \left(\frac{\tau}{1 \text{ ms}}\right)^{-1/2} \tag{35}$$

With today's LIGO strain sensitivity of $< 10^{-22}$, this means they should be sensitive to events out to at least the Virgo cluster (or further for stronger signals).

And as a final aside, note that the first detection of the presence of grav-

itational waves came not from LIGO but from observations of binary neutron stars. As the two massive objects rapidly orbit each other, gravitational waves steadily sap energy from the system, causing the orbits to steadily decay. When at least one of the neutron stars is a pulsar, this orbital decay can be measured to high precision.

6 Radiation

The number of objects directly detected via gravitational waves can be counted on two hands and a toe (11 as of early 2019). In contrast, billions and billions of astronomical objects have been detected via *electromagnetic* radiation. Throughout history and up to today, astronomy is almost completely dependent on EM radiation, as photons and/or waves, to carry the information we need to observatories on or near Earth.

To motivate us, let's compare two spectra of similarly hot sources, shown in Fig. 4.

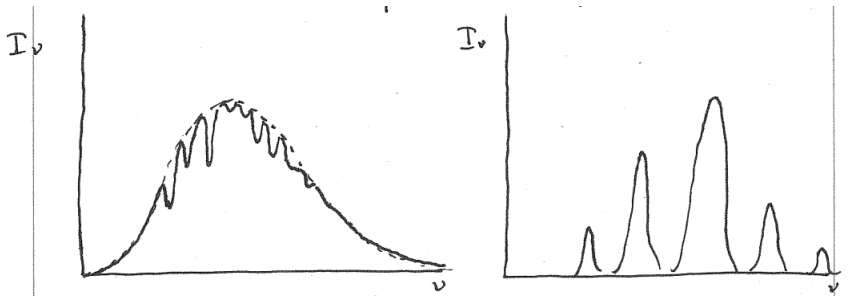

Figure 4: Toy spectra of two hot sources, $\sim 10^4$ K. Left: a nearly-blackbody Ao star with a few absorption lines. Right: central regions of Orion Nebula, showing only emission lines and no continuum.

In a sense we're moving backward: we'll deal later with how these photons are actually created. For now, our focus is on the **radiative transfer** from source to observer. We want to develop the language to explain and describe the difference between these spectra of two hot gas masses.

6.1 *Radiation from Space*

The light emitted from or passing through objects in space is almost the only way that we have to probe the vast majority of the universe we live in. The most distant object to which we have traveled and brought back samples, besides the moon, is a single asteroid. Collecting solar wind gives us some insight into the most tenuous outer layers of our nearby star, and meteorites on earth provide insight into planets as far away as Mars, but these are the only things from space that we can study in laboratories on earth. Beyond this, we have sent unmanned missions to land on Venus, Mars, and asteroids and comets. To study anything else in space we have to interpret the radiation we get from that source. As a result, understanding the properties of radiation, including the variables and quantities it depends on and how it behaves as it moves through space, is then key to interpreting almost all of the fundamental observations we make as astronomers.

Energy

To begin to define the properties of radiation from astronomical objects, we will start with the energy that we receive from an emitting source somewhere in space. Consider a source of radiation in the vacuum of space (for familiarity, you can think of the sun). At some point in space away from our source of radiation we want to understand the amount of energy dE that is received from this source. What is this energy proportional to?

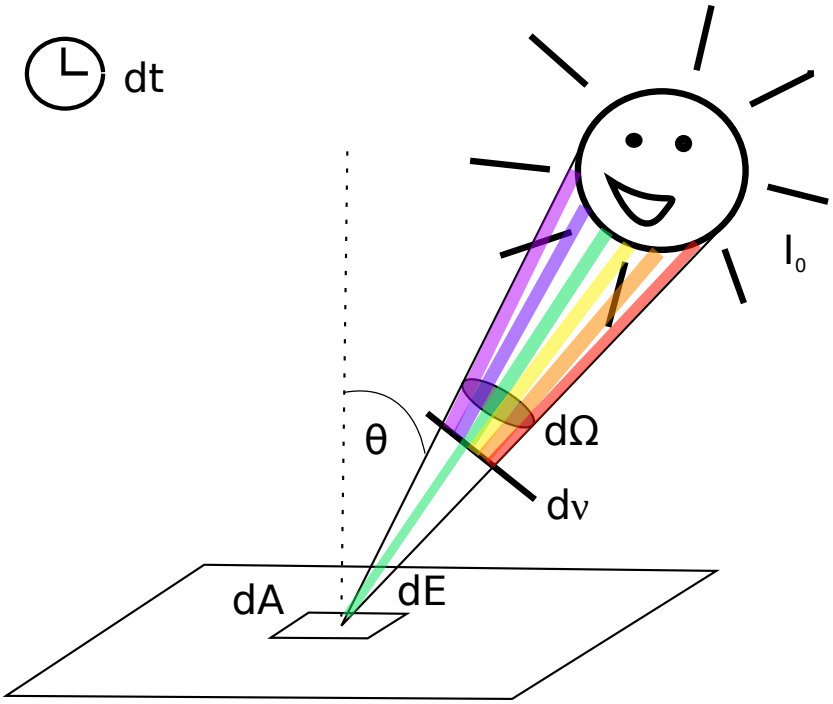

Figure 5: Description of the energy detected at a location in space for a period of time dt over an area dA arriving at an angle θ from an object with intensity I_0, an angular size $d\Omega$, through a frequency range $d\nu$ (in this case, only the green light).

As shown in Figure 5, our source of radiation has an intensity I_0 (we will get come back to this in a moment) over an apparent angular size (solid angle) of $d\Omega$. Though it may give off radiation over a wide range of frequencies, as is often the case in astronomy we only concern ourselves with the energy emitted in a specific frequency range $\nu+d\nu$ (think of using a filter to restrict the colors of light you see, or even just looking at something with your eyeball, which only detects radiation in the visible range). At the location of detection, the radiation passes through some area dA in space (an area perhaps like a spot on the surface of Earth) at an angle θ away from the normal to that surface. The last property of the radiation that we might want to consider is that we are detecting it over a given window of time (and many astronomical sources are time-variable). You might be wondering why the distance between

our detector and the source is not being mentioned yet: we will get to this.

Considering these variables, the amount of energy that we detect will be proportional to the apparent angular size of our object, the range of frequencies over which we are sensitive, the time over which we collect the radiation, and the area over which we do this collection. The constant of proportionality is the **specific intensity** of our source: I_0. Technically, as this is the intensity just over a limited frequency range, we will write this as $I_{0,\nu}$.

In equation form, we can write all of this as:

$$dE_\nu = I_{0,\nu}\, cos\theta\, dA\, d\Omega\, d\nu\, dt \quad (36)$$

Here, the cos θ dA term accounts for the fact that the area that matters is actually the area "seen" from the emitting source. If the radiation is coming straight down toward our unit of area dA, it "sees" an area equal to that of the full dA (cos $\theta = 1$). However, if the radiation comes in at a different angle θ, then it "sees" our area dA as being tilted: as a result, the apparent area is smaller (cos $\theta < 1$). You can test this for yourself by thinking of the area dA as a sheet of paper, and observing how its apparent size changes as you tilt it toward or away from you.

Intensity

Looking at Equation 36, we can figure out the units that the specific intensity must have: energy per time per frequency per area per solid angle. In SI units, this would be W Hz^{-1} m^{-2} sr^{-1}. Specific intensity is also sometimes referred to as **surface brightness**, as this quantity refers to the brightness over a fixed angular size on the source (in O/IR astronomy, surface brightness is measured in magnitudes per square arcsec). Technically, the specific intensity is a 7-dimensional quantity: it depends on position (3 space coordinates), direction (two more coordinates), frequency (or wavelength), and time. As we'll see below, we can equivalently parameterize the radiation with three coordinates of position, three of momentum (for direction, and energy/frequency), and time.

Flux

The **flux density** from a source is defined as the total energy of radiation received from all directions at a point in space, per unit area, per unit time, per frequency. Given this definition, we can modify equation 36 to give the flux density at a frequency ν:

$$F_\nu = \int_\Omega \frac{dE_\nu}{dA\, dt\, d\nu} = \int_\Omega I_\nu cos\theta d\Omega \quad (37)$$

The total flux at all frequencies (the **bolometric flux**) is then:

$$F = \int_\nu F_\nu\, d\nu \quad (38)$$

As expected the SI units of flux are W m^{-2}; e.g., the aforementioned Solar Constant (the flux incident on the Earth from the Sun) is roughly 1400 W m^{-2}.

The last, related property that one should consider (particularly for spatially well-defined objects like stars) is the **Luminosity**. The luminosity of a source is the total energy emitted per unit time. The SI unit of luminosity is just Watts. Luminosity can be determined from the flux of an object by integrating over its entire surface:

$$L = \int F \, dA \tag{39}$$

As with flux, there is also an equivalent luminosity density, L_ν, defined analogously to Eq. 38.

Having defined these quantities, we now ask how the flux you detect from a source varies as you increase the distance to the source. Looking at Figure 6, we take the example of our happy sun and imagine two spherical shells or bubbles around the sun: one at a distance R_1, and one at a distance R_2. The amount of energy passing through each of these shells per unit time is the same: in each case, it is equal to the luminosity of the sun, $L_\odot$. However, as $R_2 > R_1$, the surface area of the second shell is greater than the first shell. Thus, the energy is spread thinner over this larger area, and the flux (which by definition is the energy per unit area) must be smaller for the second shell. Comparing the equations for surface area, we see that flux decreases proportionally to $1/d^2$.

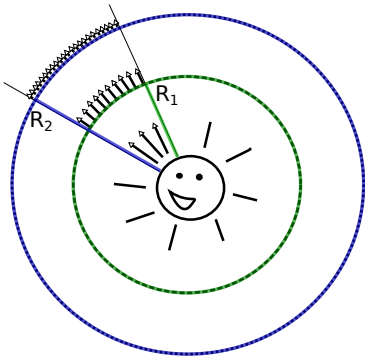

Figure 6: A depiction of the flux detected from our sun as a function of distance from the sun. Imagining shells that fully enclose the sun, we know that the energy passing through each shell per unit time must be the same (equal to the total luminosity of the sun). As a result, the flux must be less in the larger outer shell: reduced proportionally to $1/d^2$

6.2 *Conservation of Specific Intensity*

We have shown that the flux obeys an inverse square law with distance from a source. How does the specific intensity change with distance? The specific

intensity can be described as the flux divided by the angular size of the source, or $I_\nu \propto F_\nu/\Delta\Omega$. We have just shown that the flux decreases with distance, proportional to $1/d^2$. What about the angular source size? It happens that the source size also decreases with distance, proportional to $1/d^2$. As a result, the specific intensity (just another name for surface brightness) is independent of distance.

Let's now consider in a bit more detail this idea that I_ν is conserved in empty space – this is a key property of radiative transfer. This means that in the absence of any material (the least interesting case!) we have $dI_\nu/ds = 0$, where s measures the path length along the traveling ray. And we also know from electrodynamics that a monochromatic plane wave in free space has a single, constant frequency ν. Ultimately our goal will be to connect I_ν to the flow of energy dE – this will eventually come by linking the energy flow to the number flow dN and the energy per photon,

$$dE = dN(h\nu) \tag{40}$$

We mentioned above that I_ν can be parameterized with three coordinates of position, three of momentum (for direction, and energy/frequency), and time. So $I_\nu = I_\nu(\vec{r}, \vec{p}, t)$. For now we'll neglect the dependence on t, assuming a constant radiation field – so our radiation field fills a particular six-dimensional phase space of $\vec{r}$ and $\vec{p}$.

This means that the particle distribution N is proportional to the phase space density f:

$$dN = f(\vec{r}, \vec{p}) d^3r d^3p \tag{41}$$

By **Liouville's Theorem**, given a system of particles interacting with conservative forces, the phase space density $f(\vec{r}, \vec{p})$ is conserved along the flow of particles; Fig. 7 shows a toy example in 2D (since 6D monitors and printers aren't yet mainstream).

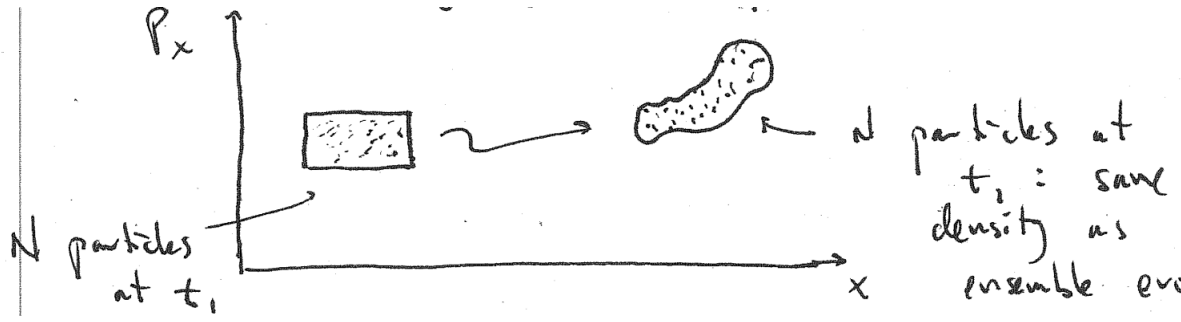

Figure 7: Toy example of Liouville's Theorem as applied to a 2D phase space of (x, p_x). As the system evolves from t_1 at left to t_2 at right, the density in phase space remains constant.

In our case, the particles relevant to Liouville are the photons in our ra-

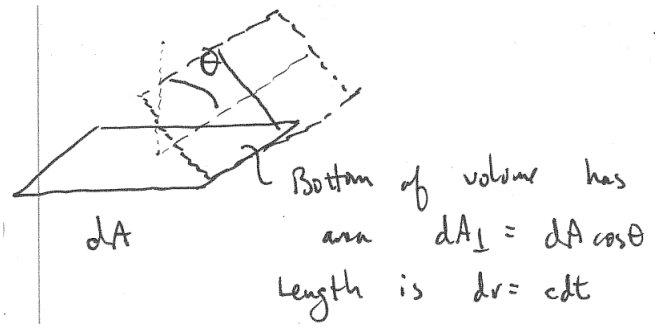

Figure 8: Geometry of the incident radiation field on a small patch of area dA.

diation field. Fig. 8 shows the relevant geometry. This converts Eq. 41 into

$$dN = f(\vec{r}, \vec{p}) c dt dA \cos\theta d^3 p \tag{42}$$

As noted previously, $\vec{p}$ encodes the radiation field's direction and energy (equivalent to frequency, and to linear momentum p) of the radiation field. So we can expand d^3p around the propagation axis, such that

$$d^3 p = p^2 dp d\Omega \tag{43}$$

This means we then have

$$dN = f(\vec{r}, \vec{p}) c dt dA \cos\theta p^2 dp d\Omega \tag{44}$$

Finally recalling that $p = h\nu/c$, and throwing everything into the mix along with Eq. 40, we have

$$dE = (h\nu) f(\vec{r}, \vec{p}) c dt dA \cos\theta \left(\frac{h\nu}{c}\right)^2 \left(\frac{h d\nu}{c}\right) d\Omega \tag{45}$$

We can combine this with Eq. 36 above, to show that specific intensity is directly proportional to the phase space density:

$$I_\nu = \frac{h^4 \nu^3}{c^2} f(\vec{r}, \vec{p}) \tag{46}$$

Therefore whenever phase space density is conserved, I_ν/ν^3 is conserved. And since ν is constant in free space, I_ν is conserved as well.

6.3 *Blackbody Radiation*

For radiation in thermal equilibrium, the usual statistical mechanics references show that the Bose-Einstein distribution function, applicable for photons, is:

$$n = \frac{1}{e^{h\nu/k_BT} - 1} \tag{47}$$

The phase space density is then

$$f(\vec{r}, \vec{p}) = \frac{2}{h^3} n \tag{48}$$

where the factor of two comes from two photon polarizations and h^3 is the elementary phase space volume. Combining Eqs. 46, 47, and 48 we find that in empty space

$$I_\nu = \frac{2h\nu^3}{c^2} \frac{1}{e^{h\nu/k_BT} - 1} \equiv B_\nu(T) \tag{49}$$

Where we have now defined $B_\nu(T)$, the **Planck blackbody function**. The Planck function says that the specific intensity (i.e., the surface brightness) of an object with perfect emissivity depends only on its temperature, T.

Finally, let's define a few related quantities for good measure:

$$J_\nu = \text{specific mean intensity} \tag{50}$$
$$= \frac{1}{4\pi} \int I_\nu d\Omega \tag{51}$$
$$= B_\nu(T) \tag{52}$$

$$u_\nu = \text{specific energy intensity} \tag{53}$$
$$= \int \frac{I_\nu}{c} d\Omega \tag{54}$$
$$= \frac{4\pi}{c} B_\nu(T) \tag{55}$$

$$P_\nu = \text{specific radiation pressure} \tag{56}$$
$$= \int \frac{I_\nu}{c} \cos^2\theta d\Omega \tag{57}$$
$$= \frac{4\pi}{3c} B_\nu(T) \tag{58}$$

The last quantity in each of the above is of course only valid in empty space, when $I_\nu = B_\nu$. Note also that the correlation $P_\nu = u_\nu/3$ is valid whenever I_ν is isotropic, regardless of whether we have a blackbody radiation.

6.4 *Radiation, Luminosity, and Temperature*

The Planck function is of tremendous relevance in radiative calculations. It's worth plotting $B_\nu(T)$ for a range of temperatures to see how the curve behaves. One interesting result is that the location of maximal specific intensity turns out to scale linearly with T. When we write the Planck function in terms of wavelength λ, where $\lambda B_\lambda = \nu B_\nu$, we find that the **Wien Peak** is approximately

$$\lambda_{\max} T \approx 3000 \mu m \; K \tag{59}$$

So radiation from a human body peaks at roughly 10μm, while that from a 6000 K, roughly Sun-like star peaks at 0.5μm = 500 nm — right in the response range of the human eye.

Another important correlation is the link between an object's luminosity L and its temperature T. For any specific intensity I_ν, the bolometric flux F is given by Eqs. 37 and 38. When $I_\nu = B_\nu(T)$, the **Stefan-Boltzmann Law** directly follows:

$$F = \sigma_{SB} T^4 \tag{60}$$

where σ_{SB}, the Stefan-Boltzmann constant, is

$$\sigma_{SB} = \frac{2\pi^5 k_B^4}{15 c^2 h^3} \tag{61}$$

(or $\sim 6 \times 10^{-8}$ W m^{-2} K^{-4}).

Assuming isotropic emission, the luminosity of a sphere with radius R and temperature T is

$$L = 4\pi R^2 F = 4\pi \sigma_{SB} R^2 T^4 \tag{62}$$

.

If we assume that the Sun is a blackbody with $R_\odot = 7 \times 10^8$ m and $T = 6000$ K, then we would calculate

$$L_{\odot,approx} = 4 \times 3 \times (6 \times 10^{-8}) \times (7 \times 10^8)^2 \times (6 \times 10^3)^4 \tag{63}$$

$$= 72 \times 10^{-8} \times (50 \times 10^{16}) \times (1000 \times 10^{12}) \tag{64}$$

$$= 3600 \times 10^{23} \tag{65}$$

which is surprisingly close to the IAU definition of $L_\odot = 3.828 \times 10^{26}$ W m^{-2}.

Soon we will discuss the detailed structure of stars. Spectra show that they are not perfect blackbodies, but they are often pretty close. This leads to the common definition of an **effective temperature** linked to a star's size and luminosity by the Stefan-Boltzmann law. Rearranging Eq. 62, we find that

$$T_{\text{eff}} = \left(\frac{L}{4\pi \sigma_{SB} R^2} \right)^{1/4} \tag{66}$$

7 Radiative Transfer

Radiation through empty space is what makes astronomy possible, but it isn't so interesting to study on its own. **Radiative transfer**, the effect on radiation of its passage through matter, is where things really get going.

7.1 *The Equation of Radiative Transfer*

We can use the fact that the specific intensity does not change with distance to begin deriving the radiative transfer equation. For light traveling in a vacuum along a path length s, we say that the intensity is a constant. As a result,

$$\frac{dI_\nu}{ds} = 0 \ (for\ radiation\ traveling\ through\ a\ vacuum) \tag{67}$$

This case is illustrated in the first panel of Figure 9. However, space (particularly objects in space, like the atmospheres of stars) is not a vacuum everywhere. What about the case when there is some junk between our detector and the source of radiation? This possibility is shown in the second panel of Figure 9. One quickly sees that the intensity you detect will be less than it was at the source. You can define an **extinction coefficient** α_ν for the space junk, with units of extinction (or fractional depletion of intensity) per distance (path length) traveled, or m^{-1} in SI units. For our purposes right now, we will assume that this extinction is uniform and frequency-independent (but in real life of course, it never is).

We also define

$$\alpha_\nu = n\sigma_\nu \tag{68}$$

$$= \rho\kappa_\nu \tag{69}$$

Where n is the number density of absorbing particles and σ_ν is their frequency-dependent cross-section, while ρ is the standard mass density and κ_ν is the frequency-dependent **opacity**. Now, our equation of radiative transfer has

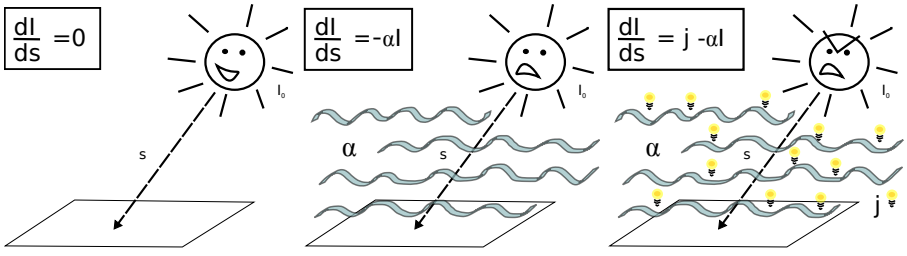

Figure 9: The radiative transfer equation, for the progressively more complicated situations of: (left) radiation traveling through a vacuum; (center) radiation traveling through a purely absorbing medium; (right) radiation traveling through an absorbing and emitting medium.

been modified to be:

$$\frac{dI_\nu}{ds} = -\alpha_\nu I_\nu \ (\textit{when there is absorbing material between us and our source}) \tag{70}$$

As is often the case when simplifying differential equations, we then find it convenient to try to get rid of some of these pesky units by defining a new unitless constant: τ_ν, or **optical depth**. If α_ν is the fractional depletion of intensity per path length, τ_ν is just the fractional depletion. We then can define

$$d\tau_\nu = \alpha_\nu ds \tag{71}$$

and re-write our equation of radiative transfer as:

$$\frac{dI_\nu}{d\tau} = -I_\nu \tag{72}$$

Remembering our basic calculus, we see that this has a solution of the type

$$I_\nu(s) = I_\nu(0) \exp\left(-\int_0^s d\tau_\nu\right) \tag{73}$$

$$= I_\nu(0) e^{-\tau_\nu} \ (\textit{for an optically thin source}) \tag{74}$$

So, at an optical depth of unity (the point at which something begins to be considered optically thick), your initial source intensity I_0 has decreased by a factor of e.

However, radiation traveling through a medium does not always result in a net decrease. It is also possible for the radiation from our original source to pass through a medium or substance that is not just absorbing the incident radiation but is also emitting radiation of its own, adding to the initial radiation field. To account for this, we define another coefficient: j_ν. This **emissivity coefficient** has units of energy per time per volume per frequency per solid angle. Note that these units (in SI: W m^{-3} Hz^{-1} sr^{-1}) are slightly different than the units of specific intensity. Including this coefficient in our radiative transfer equation we have:

$$\frac{dI_\nu}{ds} = j_\nu - \alpha_\nu I_\nu \tag{75}$$

or, putting it in terms of the dimensionless optical depth τ, we have:

$$\frac{dI_\nu}{d\tau_\nu} = \frac{j_\nu}{\alpha_\nu} - I_\nu \tag{76}$$

After defining the so-called **source function**

$$S_\nu = \frac{j_\nu}{\alpha_\nu} \tag{77}$$

we arrive at the final form of the **radiative transfer equation**:

$$\frac{dI_\nu}{d\tau_\nu} = S_\nu - I_\nu \tag{78}$$

7.2 *Solutions to the Radiative Transfer Equation*

What is the solution of this equation? For now, we will again take the simplest case and assume that the medium through which the radiation is passing is uniform (i.e., S_ν is constant). Given an initial specific intensity of $I_\nu(s = 0) = I_{\nu,0}$, we obtain

$$I_\nu = I_{\nu,0}e^{-\tau_\nu} + S_\nu\left(1 - e^{-\tau_\nu}\right) \ (for\ constant\ source\ function) \tag{79}$$

What happens to this equation when τ is small? In this case, we haven't traveled very far through the medium and so should expect that absorption or emission hasn't had a strong effect. And indeed, in the limit that $\tau_\nu = 0$ we see that $I_\nu = I_{\nu,0}$.

What happens to this equation when τ becomes large? In this case, we've traveled through a medium so optically thick that the radiation has "lost all memory" of its initial conditions. Thus $e^{-\tau_\nu}$ becomes negligible, and we arrive at the result

$$I_\nu = S_\nu \ (for\ an\ optically\ thick\ source) \tag{80}$$

So the only radiation that makes it out is from the emission of the medium itself. What is this source function anyway? For a source in thermodynamic equilibrium, any opaque (i.e., optically thick) medium is a "black body" and so it turns out that $S_\nu = B_\nu(T)$, the Planck blackbody function. For an optically-thick source (say, a star like our sun) we can use Eq. 80 to then say that $I_\nu = B_\nu$.

The equivalence that $I_\nu = S_\nu = B_\nu$ gives us the ability to define key properties of stars – like their flux and luminosity – as a function of their temperature. As described in the preceding chapter, using Eq. 37 and 38 we can integrate the blackbody function to determine the flux of a star (or other blackbody) as a function of temperature, the Stefan-Boltzmann law:

$$F = \sigma T^4 \tag{81}$$

Another classic result, the peak frequency (or wavelength) at which a star (or other blackbody) radiates, based on its temperature, can be found by differentiating the blackbody equation with respect to frequency (or wavelength). The result must be found numerically, and the peak wavelength can be ex-

pressed in **Wien's Law** as

$$\lambda_{peak} = \frac{2.898 \times 10^{-3} \text{ m K}}{T} \tag{82}$$

We can improve on Eq. 79 and build a formal, general solution to the radiative transfer equation as follows. Starting with Eq. 78, we have

$$\frac{dI_\nu}{d\tau_\nu} = S_\nu - I_\nu \tag{83}$$

$$\frac{dI_\nu}{d\tau_\nu} e^{\tau_\nu} = S_\nu e^{\tau_\nu} - I_\nu e^{\tau_\nu} \tag{84}$$

$$\frac{d}{d\tau_\nu} \left(I_\nu e^{\tau_\nu} \right) = S_\nu e^{\tau_\nu} \tag{85}$$

We can integrate this last line to obtain the formal solution:

$$I_\nu(\tau_\nu) = I_\nu(0) e^{-\tau_\nu} + \int_0^{\tau_\nu} S_\nu(\tau'_\nu) e^{(\tau'_\nu - \tau_\nu)} d\tau'_\nu \tag{86}$$

As in our simpler approximations above, we see that the initial intensity $I_\nu(0)$ decays as the pathlength increases; at the same time we pick up an increasing contribution from the source function S_ν, integrated along the path. In practice S_ν can be fairly messy (i.e., when it isn't the Planck function), and it can even depend on I_ν. Nonetheless Eq. 86 lends itself well to a numerical solution.

7.3 *Kirchhoff's Laws*

We need to discuss one additional detail before getting started on stars and nebulae: **Kirchhoff's Law for Thermal Emission.** This states that a thermally emitting object in equilibrium with its surrounding radiation field has $S_\nu = B_\nu(T)$.

Note that the above statement does *not* require that our object's thermal radiation is necessarily blackbody radiation. Whether or not that is true depends on the interactions between photons and matter – which means it depends on the optical depth τ_ν.

Consider two lumps of matter, both at T. Object one is optically thick, i.e. $\tau_\nu >> 1$. In this case, Eq. 86 does indeed require that the emitted radiation has the form $I_\nu(\tau_\nu) = S_\nu = B_\nu(T)$ — i.e., blackbody radiation emerges from an optically thick object. This is mostly the case for a stellar spectrum, but not quite (as we'll see below).

First, let's consider the other scenario in which our second object is optically thin, i.e. $0 < \tau_\nu << 1$. If our initial specific intensity $I_\nu(0) = 0$, then we have

$$I_\nu(\tau_\nu) = 0 + S_\nu \left(1 - (1 - \tau_\nu)\right) \tag{87}$$

$$= \tau_\nu B_\nu(T) \tag{88}$$

Thus for an optically thin object, the emergent radiation will be blackbody radiation, scaled down by our low (but nonzero) τ_ν.

It's important to remember that τ_ν is frequency-dependent (hence the ν subscript!) due to its dependence on the extinction coefficient α_ν. So most astronomical objects represent a combination of the two cases discussed immediately above. At frequencies where atoms, molecules, etc. absorb light most strongly, α_ν will be higher than at other frequencies.

So in a simplistic model, assume we have a hot hydrogen gas cloud where α_ν is zero everywhere except at the locations of H lines. The location of these lines is given by the Rydberg formula,

$$\frac{1}{\lambda_{\text{vac},1,2}} = R\left(\frac{1}{n_1^2} - \frac{1}{n_2^2}\right) \tag{89}$$

(where $R = 1/(91.2\text{ nm})$ is the Rydberg constant and $n_1 = 1, 2, 3, 4, 5$, etc. for the Lyman, Balmer, Paschen, and Brackett series, respectively).

In a thin gas cloud of temperature T, thickness s, and which is "backlit" by a background of empty space (so $I_{\nu,0} \approx 0$), from Eq. 88 all we will see is $\tau_\nu B_\nu(T) = \alpha_\nu s B_\nu(T)$ — so an **emission-line spectrum** which is zero away from the lines and has strong emission at the locations of each line.

What about in a stellar atmosphere? A single stellar T (an **isothermal atmosphere**) will yield just a blackbody spectrum, regardless of the form of α_ν. The simplest atmosphere yielding an interesting spectrum is sketched in Fig. 10: an optically thick interior at temperature T_H and a cooler, optically thin outer layer at $T_C < T_H$.

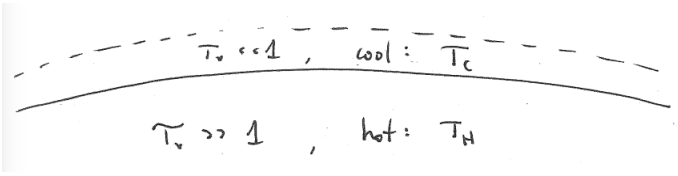

Figure 10: The simplest two-layer stellar atmosphere: an optically thick interior at temperature T_H and a cooler, optically thin outer layer at $T_C < T_H$.

The hot region is optically thick, so we have $I_\nu = S_\nu = B_\nu(T_H)$ emitted from the lower layer – again, regardless of the form of α_ν. The effect of the upper, cooler layer which has small but nonzero τ_ν is to slightly diminish the contribution of the lower layer while adding a contribution from the cooler layer:

$$I_\nu = I_\nu(0)e^{-\tau_\nu} + S_\nu\left(1 - e^{-\tau_\nu}\right) \tag{90}$$
$$= B_\nu(T_H)e^{-\tau_\nu} + B_\nu(T_C)\left(1 - e^{-\tau_\nu}\right) \tag{91}$$
$$\approx B_\nu(T_H)(1 - \tau_\nu) + B_\nu(T_C)\tau_\nu \tag{92}$$
$$\approx B_\nu(T_H) - \tau_\nu\left(B_\nu(T_H) - B_\nu(T_C)\right) \tag{93}$$
$$\approx B_\nu(T_H) - \alpha_\nu s\left(B_\nu(T_H) - B_\nu(T_C)\right) \tag{94}$$

So a stellar spectrum consists of two parts, roughly speaking. The first is $B_\nu(T_H)$, the contribution from the blackbody at the base of the atmosphere (the **spectral continuum**). Subtracted from this is a contribution wherever α_ν is strong – i.e., at the locations of strongly-absorbing lines. As we will see later, we can typically observe in a stellar atmosphere only down to $\tau_\nu \sim 1$. So at the line locations where (absorption is nonzero), we observe approximately $B_\nu(T_C)$. Thus in this toy model, the lines probe higher in the atmosphere (we can't observe as deeply into the star, because absorption is stronger at these frequencies – so we effectively observe the cooler, fainter upper layers). Meanwhile there is effectively no absorption in the atmosphere, so we see down to the hotter layer where emission is brighter. Fig. 11 shows a typical example.

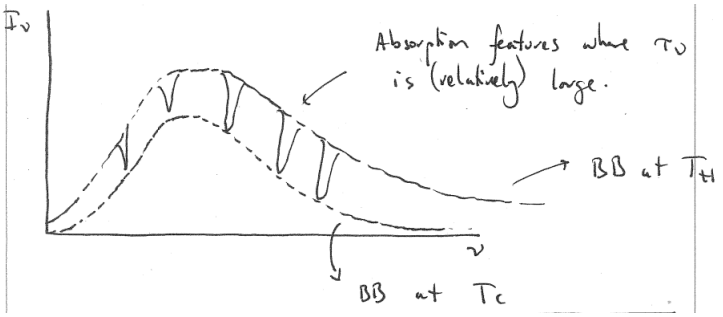

Figure 11: Toy stellar spectrum (solid line) for the toy stellar model graphed in Fig. 10.

Note that our assumption has been that temperature in the star decreases with increasing altitude. More commonly, stellar models will parameterize an atmosphere in terms of its **pressure-temperature profile**, with pressure P decreasing monotonically with increasing altitude. An interesting phenomenon occurs when T increases with decreasing P (increasing altitude): in this case we have a **thermal inversion**, all the arguments above are turned on their heads, and the lines previously seen in absorption now appear in emission over the same continuum. Thermal inversions are usually a second-order correction to atmospheric models, but they are ubiquitous in the atmospheres of the Sun, Solar System planets, and exoplanets.

8 Stellar Classification, Spectra, and Some Thermodynamics

Questions you should be able to answer after this lecture:

- How are stars classified?
- What is the difference between Thermal equilibrium and Thermodynamic equilibrium?
- What are the different temperatures that must be equal in Thermodynamic equilibrium?
- When is Local Thermodynamic Equilibrium valid for a region?

Classification is a key step toward understanding any new class of objects. When modern astronomy began, classification of the stars was a key goal — also an elusive one, until the physical processes became better understood. We're now going to begin to peel back the onion that is a Star. And the first step in peeling an onion is to look at it from the outside.

8.1 *Classification*

One of the first successful frameworks used **photometry** (broadband, $\Delta\nu/\nu \approx 20\%$, measurements of stellar flux density) at different colors. Assuming again that stellar spectra are approximately blackbodies, the Planck function shows that we should see the hotter stars have bluer colors and be intrinsically brighter. This led to the **Hertzsprung-Russell diagram** (HR diagram), which plots absolute magnitude against color – we'll see the HR diagram again when we discuss stellar evolution.

It's fair to say that spectroscopy is one of our key tools for learning about astronomical objects, including stars. Fig. 12 shows a sequence of stars arranged from hot to cool: one can easily see the Wien peak shift with temperature, although none of the stars are perfect blackbodies. Other features come and go, determined (as we will see) mainly by stellar temperature but also surface gravity (or equivalently, surface pressure).

Table 1: Stellar spectral types.

SpT	$T_{\rm eff}$	Spectral features
O	$> 3 \times 10^4$	Ionized He or Si; no H (or only very weak)
B	$10^4 - 3 \times 10^4$	H Balmer lines, neutral He lines
A	$7500 - 10^4$	Strong H lines
F	$6000 - 7500$	H Balmer, first metal lines appear (Ca)
G	$5200 - 6000$	Fading H lines, increasing metal lines
K	$3700 - 5200$	Strong Ca and other metals, hydride molecules appear
M	$2400 - 3700$	Molecular bands rapidly strengthen: hydrides, TiO, H_2O
L	$1400 - 2400$	A melange of atomic and molecular bands; dust appears
T	$\sim 400 - 1400$	CH_4 strengthens, dust clears
Y	$\lesssim 400$	NH_3 strengthens

Through decades of refinement, spectra are now classified using **Morgan-Keenan spectral types**. These include a letter to indicate the approximate temperature, an Arabic numeral to refine the temperature, and a roman numeral to indicate the star's luminosity. The order of letters seems disjointed because stars were classified before the underlying physical causes were well-understood. The temperature sequence is OBAFGKMLTY, where the last three typically apply to brown dwarfs (intermediate in mass between planets and stars) and the rest apply to stars. Table 8.1 briefly describes each of the alpha-

Table 2: Stellar luminosity classes.

Lum	name	examples
VI	subdwarf	Kapteyn's Star (M1VI)
V	dwarf	Sun (G2V), Vega (A0V)
IV	subgiant	Procyon (F5IV)
III	giant	Arcturus (K1III)
II	bright giant	
I	supergiant	Rigel (B8Ia), Betelgeuse (M1Ia)
0	hypergiant	η Carinae, Pistol Star

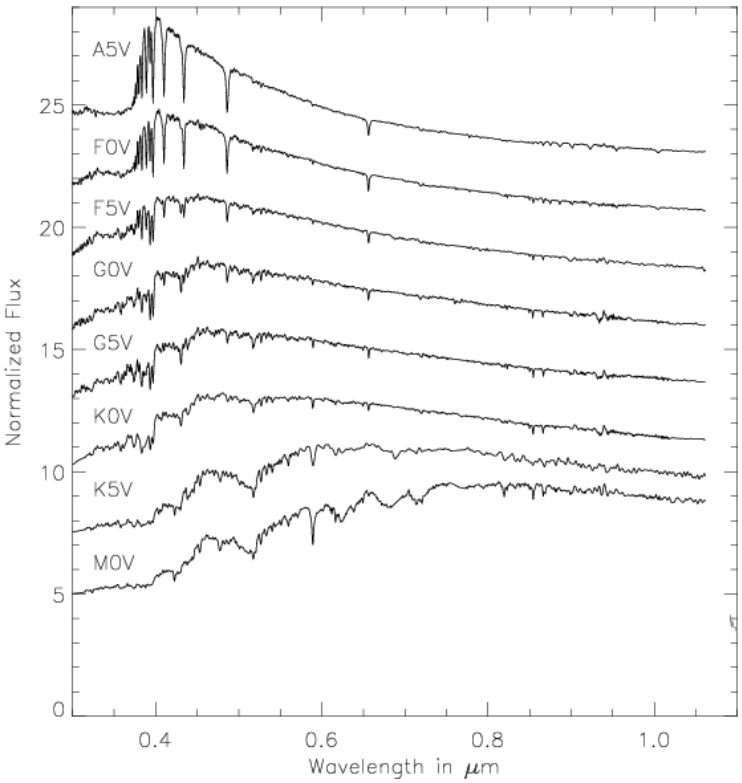

Figure 12: Optical-wavelength spectra of main-sequence stars across a range of spectral types.

betic spectral types. Additional resolution is added to the system through the use of numbers 0–9, so that F9–G0–G1 is a sequence of steadily decreasing $T_{\rm eff}$. Finally, the Roman numerals described in Table 2 indicate the luminosity class, which typically correlates with the stellar radius (and inversely with the surface gravity).

8.2 *Thermodynamic Equilibrium*

Our goal is to quantitatively explain the trends observed in Fig. 12. To do that, we need the tools provided to us by thermodynamics and statistical mechanics. We claimed earlier that $S_\nu = B_\nu(T)$, the source function is equal to the blackbody function, for a source in thermodynamic equilibrium. So, what are the conditions of thermodynamic equilibrium, and in what typical astronomical sources are these conditions satisfied?

There are two main conditions for thermodynamic equilibrium.

1. **Thermal equilibrium**: There is no heat transfer in a source: classically, it is at a constant, uniform temperature. However, as we will describe further in Section 11.2, for a star we generally take this just to mean that the temperature can vary spatially (but not in time), and that local energy losses (say, due to energy transport) are exactly balanced by gains (say, due to nuclear fusion).

2. Every temperature in the source is the same: the source is also in a radiation, ionization, and excitation equilibrium.

So, how do we define all of these different temperatures a source or system can have?

First, there is the **kinetic temperature** T_{kin}. This temperature describes the random motion of particles in a system. For a system in thermodynamic equilibrium, the distribution of speeds of particles (atoms or molecules) in this system is given by the **Maxwell-Boltzmann distribution**:

$$dN_v = 4\pi\, n \left(\frac{m}{2\pi\, k_B T_{kin}}\right)^{3/2} v^2 \exp\left(-\frac{m v^2}{2\, k_B T_{kin}}\right) dv \tag{95}$$

Here, dN_v is the number of particles with mass m and number density n between speeds v and $v + dv$.

Second, there is the **excitation temperature** T_{ex}. This temperature describes the distribution of internal energies in the particles in a system. This internal energy can be the energy of different electronic states of an atom, or the energy of rotation or vibration in a molecule. For a system in thermodynamic equilibrium, the fraction of atoms (or molecules) occupying a particular energy state is given by the **Boltzmann distribution** (not to be confused with Eq. 95!):

$$\frac{N_1}{N_2} = \frac{g_1}{g_2} \exp\left(-\frac{E_1 - E_2}{k_B\, T_{ex}}\right) \tag{96}$$

Here, N_1 is the number of atoms or molecules in a state with an energy E_1 above the ground state, and N_2 is the number of atoms or molecules in a state with an energy E_2 above the ground state. The statistical weight of each state is given by g, which accounts for multiple configurations that might all have the same energy (i.e., the statistical degeneracy).

Next is T_{rad}, the **radiation temperature** in the system. This temperature is defined by an equation we have seen before: the Planck distribution, or the Blackbody law of Equation 49.

Finally, there is the **ionization temperature** T_i. This temperature describes the degree to which electrons are bound to the particles in a system. The fraction of the atoms in a gas which are ionized is given by the **Saha equation**, derived below and given as Eq. 124.

8.3 *Local Thermodynamic Equilibrium*

How typical is it for astronomical sources (like stars or planets or gas clouds) to be in thermodynamic equilibrium? In general, it is rare! Most sources are going to have significant temperature variations (for example, from the interior to the exterior of a star or planet). However, the situation is not hopeless, as in most sources, these changes are slow and smooth enough that over a small region, the two conditions we described are sufficiently satisfied. Such a situation is referred to as Local Thermodynamic Equilibrium or LTE.

When does LTE hold? First, for particles to have a Maxwell-Boltzmann distribution of velocities, and so to have a single kinetic temperature, the particles must have a sufficient opportunity to 'talk' to each other through collisions. Frequent collisions are also required for particles to have a uniform distribution of their internal energy states. The frequency of collisions is inversely proportional to the mean free path of the gas: the typical distance a particle travels before undergoing a collision. In general, for a region to be in LTE, the mean free path should be small compared to the distance over which the temperature varies appreciably. As LTE further requires that the radiation temperature is equal to the kinetic and excitation temperature, the matter and radiation must also be in equilibrium. For this to happen, not only must the mean free path for particles to undergo collisions with each other be small, but the mean free path for photons to undergo collisions with matter must be small as well. We have actually already introduced the mean free path for photons: it is equal to α^{-1}, where α was given in Equation 70 as the extinction coefficient, with units of fractional depletion of intensity per distance traveled. As intensity is depleted by being absorbed by matter, the inverse of the extinction coefficient describes the typical distance a photon will travel before interacting with matter.

Very qualitatively then, our two conditions for LTE are that the mean free path for particle-particle and particle-photon interactions must be less than the distance over which there is a significant temperature variation.

8.4 *Stellar Lines and Atomic Populations*

When we study stellar spectra, we examine how the strengths of various features change. Fig. 12 suggests that this is a continuous process as a function of $T_{\rm eff}$. For example, we never see lines of both He I (i.e., neutral He) and Ca II (i.e., singly-ionized Ca, i.e. Ca^+) at the same time – these lines appear at completely different temperatures. What we want is a quantitative understanding of spectra.

When do we expect substantial excitation of these various atoms? Let's consider the electronic lines of atomic hydrogen. The H atom's energy levels are given by:

$$E_n = -\frac{13.6 \text{ eV}}{n^2} \tag{97}$$

which gives rise to the Rydberg formula (Eq. 89) for the locations of individual lines.

To see conditions we need to excite these H atoms, we might make use of the relative probability of 2 atomic states with different energies (given by the Boltzmann distribution, Eq. 96). Statistical mechanics tells us that the statistical weight of each level in a hydrogen atom is

$$g_n = 2n^2 \tag{98}$$

So for transitions between the ground state (-13.6 eV, $n = 1$) and the first excited state (-3.4 eV, $n = 2$) the relative fraction is given by

$$\frac{n_1}{n_2} = \frac{g_1}{g_2} \exp\left[-\left(E_1 - E_2\right)/k_B T\right] \tag{99}$$

When the levels are approximately equal, we then have

$$1 = \frac{2}{8} \exp\left[10.2 \text{ eV}/k_B T\right] \tag{100}$$

The calculation above would thus imply that to get appreciable levels of excited hydrogen, we would need $T \approx 90,000$ K — much hotter than the observed temperatures of stars. In fact, H is totally ionized (not just mildly excited) even at much lower temperatures. Meanwhile, even A and F stars (with $T_{\rm eff} \leq 10,000$ K) show prominent $n = 2$ hydrogen lines. We got the energetics right, but missed some other important thermodynamic quantities.

8.5 *The Saha Equation*

Let's investigate our hydrogen atom in further detail. From statistical mechanics, the distribution function of particles leads to the phase space density (see Eqns. 47 and 48):

$$f(\vec{r}, \vec{p}) = \frac{g}{h^3} \frac{1}{e^{[E-\mu]/k_B T \pm 1}} \tag{101}$$

where μ is the chemical potential and g is still the degeneracy factor:

(102)
$$g = 2s + 1 (\text{for fermions})$$

(103)
$$g = 2 (\text{for photons})$$

and where the $\pm$ operator is positive for Fermi-Dirac statistics and negative for Bose-Einstein statistics.

Again, we'll transform this six-dimensional density into a number density by integrating over momentum (see Eq. 43):

(104) $$n = 4\pi \int_0^\infty f(p) p^2 dp$$

But integrating Eq. 101 is going to be a bear of a job, so we'll make two additional approximations. First, we'll assume for now that all particles are non-relativistic – so their energy is given classically by

(105) $$E = \frac{p^2}{2m} + mc^2$$

And we'll also assume that we're dealing with large energies, such that $E - \mu >> k_B T$. In practice, this second point means we can neglect the ± 1 in the denominator of Eq. 101. Both these assumptions are reasonable for the gas in most stars. We'll come back later to some especially interesting astrophysical cases, when these assumptions no longer hold.

We can now make the attempt to calculate n from Eq. 104.

(106)
$$n = 4\pi \int_0^\infty f(p) p^2 dp$$

(107)
$$= \frac{4\pi g}{h^3} \int_0^\infty p^2 dp \exp\left(\frac{\mu}{k_B T}\right) \exp\left(-\frac{mc^2}{k_B T}\right) \exp\left(-\frac{p^2}{2mk_B T}\right)$$

(108)
$$= \frac{4\pi g}{h^3} \exp\left[\left(\mu - mc^2\right)/k_B T\right] \int_0^\infty p^2 \exp\left(-\frac{p^2}{2mk_B T}\right)$$

(109)
$$= \frac{g}{h^3} \left(2\pi m k_B T\right)^{3/2} \exp\left[\left(\mu - mc^2\right)/k_B T\right]$$

So now we have a relation between the number density and other relevant

quantities. We can rearrange this expression to get

$$\exp\left(\frac{\mu - mc^2}{k_B T}\right) = \frac{1}{g}\frac{n}{n_Q} \tag{110}$$

where n_Q is the "quantum density"

$$n_Q \equiv (2\pi m k_B T/h^2)^{3/2} \tag{111}$$

When $n = n_Q$, then the spacing between particles $n^{-1/3}$ is roughly equal to the thermal de Broglie wavelength — the particles' wave functions start to overlap, quantum effects ramp up, and degeneracy effects become increasingly important.

Ideally we want to get rid of the pesky μ and set things in terms of other quantities. Recall from thermodynamics that the **chemical potential** μ is just the energy absorbed or released during reactions. At constant volume V and entropy S, μ is determined by the change in internal energy U:

$$\mu \equiv \left(\frac{\partial U}{\partial n}\right)\Bigg|_{V,S} \tag{112}$$

The implication is that in equilibrium, all chemical potentials in a reaction sum to zero. So given a notional reaction

$$\mathrm{A} + \mathrm{B} \longleftrightarrow \mathrm{C} + \mathrm{D}$$

we must have both

$$A + B = C + D \tag{113}$$

and also

$$\mu_A + \mu_B = \mu_C + \mu_D \tag{114}$$

Just as energies flow to equalize temperature and reach thermal equilibrium, numbers of different particle species flow to reach chemical equilibrium. For the H system under consideration, the reaction to ionize our hydrogen is

$$e^- + \mathrm{p} \longleftrightarrow \mathrm{H} + \gamma$$

In chemical equilibrium, we will then have

$$\mu_e + \mu_p = \mu_H \tag{115}$$

since the chemical potential of a photon is zero. Why is this useful? Because we can rearrange Eq. 110 to find an expression for μ, and then use this in what follows (we're getting close). We find

$$\mu_i = m_i c^2 + k_B T \ln\left(\frac{n_i}{g_i n_{Q_i}}\right) \tag{116}$$

and of course mass-energy must also be conserved in the reaction:

$$m_H c^2 = m_p c^2 + m_e c^2 + \epsilon_n \tag{117}$$

where $\epsilon_1 = -13.6$ eV for full ionization. The statistical weights are a tad trickier, but for our fermions we have $g_p = g_e = 2$ while for ionizing atomic H we have $g_H = n^2 g_p g_e = 4$.

Requiring that the chemical potentials must balance, following Eq. 115 we then have:

$$m_p c^2 + m_e c^2 + k_B T \left[\ln\left(\frac{n_p}{2n_{Q_p}}\right) + \ln\left(\frac{n_e}{2n_{Q_e}}\right) \right] = m_H c^2 + k_B T \ln\left(\frac{n_H}{4n_{Q_H}}\right) \tag{118}$$

Bringing in the results of Eq. 117, we then have

$$\ln\left(\frac{n_p n_e}{4n_{Q_p} n_{Q_e}}\right) = \frac{-13.6 \text{ eV}}{k_B T} + \ln\left(\frac{n_H}{4n_{Q_H}}\right) \tag{119}$$

Rearranging terms, we then have

$$\frac{n_p n_e}{n_H} \frac{n_{Q_H}}{n_{Q_p} n_{Q_e}} = e^{-(13.6 \text{ eV}/k_B T)} \tag{120}$$

We can simplify this one more step by recalling from Eq. 111 that $n_{Q_P} \approx n_{Q_H}$. This means that we have finally reached our goal:

$$\frac{n_p n_e}{n_H} = n_{Q_e} e^{-(13.6 \text{ eV}/k_B T)} \tag{121}$$

which is famous as the **Saha equation** for hydrogen ionization. This tells us how the relative number densities of p, e^-, and H atoms will depend on the temperature of the system of particles.

It's traditional to refactor Eq. 121 by defining yet two more terms, the baryon number

$$n_B = n_H + n_p \tag{122}$$

(which is conserved) and the ionization fraction

$$y = \frac{n_e}{n_B} \tag{123}$$

which goes from zero (all neutral H) to unity (full ionization). When we divide both sides of Eq. 121 by n_B, we find the classical form of the **Saha equation**,

$$\frac{y^2}{1-y} = \frac{n_{Q_e}}{n_B} e^{-(13.6 \text{ eV}/k_B T)} \tag{124}$$

In a stellar photosphere, decent estimates are that $n_B \sim 10^{16}$ cm^{-3} and

$n_{Q_e} \approx 10^{21}\ \mathrm{cm}^{-3} \left(T/10^4\ \mathrm{K}\right)^{3/2}$. Eq. 124 is easily solved or plotted with numerical tools — the result, shown in Fig. 13, is a steep function of temperature that indicates ionization setting in at much lower temperatures than inferred in Eq. 100 alone. Instead, we see essentially no ionization in the 5800 K Solar photosphere, but we expect an ionization fraction of 5% at 9,000 K, rising to 50% at 12,000 K and 95% at 16,000 K. Although the Saha equation is a toy model with only two level populations, it still does an excellent job in predicting that H lines should be absent (as they are) from the hottest O and B stars.

In general, we also want to be able to properly treat the fact that there are an infinite number of energy levels (not just two) between the ground state and full ionization. This means that we need to account for the **partition function** $Z(\bar{T})$,

$$Z(\bar{T}) \equiv \Sigma g_s e^{-E_s/k_B T} \tag{125}$$

In principle one can calculate one's own partition functions, but in practice one often leaves that to the experts and borrows appropriately from the literature. So then the number density becomes

$$n = \left(\frac{2\pi m_e k_B T}{h^2}\right)^{3/2} e^{\mu/k_B T} Z(\bar{T}) \tag{126}$$

Using this new form to repeat the analysis above, equality of chemical potentials for the generic species A, B, and C will then yield

$$\frac{n_B n_C}{n_A} = \left(\frac{2\pi k_B T}{h^2}\right)^{3/2} \left(\frac{m_B m_C}{m_A}^{3/2}\right)^{3/2} \left(\frac{\bar{Z}_B \bar{Z}_C}{\bar{Z}_A}\right) \tag{127}$$

If the partition function is dominated by a single state (as in our simple two-

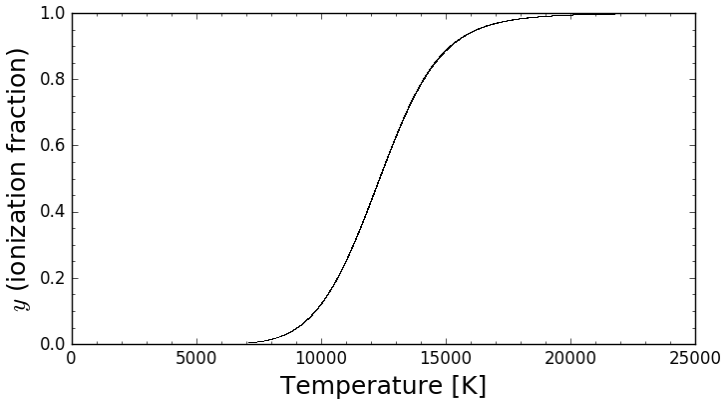

Figure 13: Ionization fraction y as a function of temperature T as inferred from the two-level Saha equation (Eq. 124).

level example), we recover the earlier form:

$$\frac{n_B n_C}{n_A} = \left(\frac{2\pi k_B T}{h^2}\right)^{3/2} \left(\frac{m_B m_C}{m_A}^{3/2}\right)^{3/2} \frac{g_B g_C}{g_A} e^{(E_A - E_B - E_C)/k_B T} \tag{128}$$

Note that for simple level-change reactions within atomic H, most factors cancel and we recover the usual Boltzmann distribution:

$$\frac{n_B}{n_A} = \frac{g_B}{g_A} e^{(E_A - E_B)/k_B T} \tag{129}$$

As a few final remarks, note that the above analysis only applies for excitation caused by the thermal distribution of particles in our system. So this won't properly treat **photoionization** (i.e. ejection of an electron due to an incoming, highly-energetic photon). Also, everything here also requires mostly-classical conditions, i.e. $n << n_Q$ for all species involved. In very dense plasmas, pressure begins to affect electron orbital shapes and subsequently affects both intermediate energy levels as well as ionization.

9 Stellar Atmospheres

Having developed the machinery to understand the spectral lines we see in stellar spectra, we're now going to continue peeling our onion by examining its thin, outermost layer – the stellar atmosphere. Our goal is to understand how specific intensity I_ν varies as a function of increasing depth in a stellar atmosphere, and also how it changes depending on the angle relative to the radial direction.

9.1 *The Plane-parallel Approximation*

Fig. 14 gives a general overview of the geometry in what follows. The star is spherical (or close enough as makes no odds), but when we zoom in on a small enough patch the geometry becomes essentially plane-parallel. In that geometry, S_ν and I_ν depend on both altitude z as well as the angle θ from the normal direction. We assume that the radiation has no intrinsic dependence on either t or ϕ – i.e., the radiation is in steady state and is isotropic.

We need to develop a few new conventions before we can proceed. This is because in our definition of optical depth, $d\tau_\nu = \alpha_\nu ds$, the path length ds travels along the path. This Lagrangian description can be a bit annoying, so it's common to formulate our radiative transfer in a path-independent, Eulerian, prescription.

Let's call our previously-defined optical depth (Eq. 71) τ'_ν. We'll then create a slightly altered definition of optical depth – a vertical, ingoing optical depth (this is the convention). The new definition is almost identical to the old one:

$$d\tau_\nu = -\alpha_\nu dz \tag{130}$$

But now our optical depth, is vertical and oriented to measure inward, toward the star's interior. In particular since $dz = ds\cos\theta$, relative to our old optical depth we now have

$$d\tau_\nu = -d\tau'_\nu \cos\theta \tag{131}$$

Our radiative transfer equation, Eq. 78, now becomes

$$-\cos\theta \frac{dI_\nu}{d\tau_\nu} = S_\nu(\tau_\nu, \theta) - I_\nu(\tau_\nu, \theta) \tag{132}$$

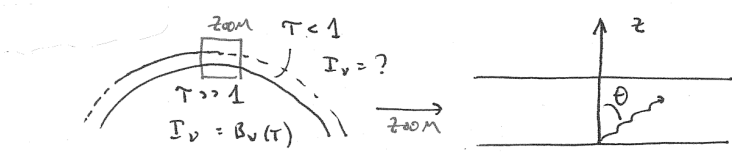

Figure 14: Schematic view of a stellar atmosphere, and at right a zoomed-in view showing the nearly plane-parallel nature on small scales.

It's conventional to also define $\mu = \cos\theta$, so our **radiative transfer equation** for stellar atmospheres now becomes

$$\mu \frac{dI_\nu}{d\tau_\nu} = I_\nu(\tau_\nu, \mu) - S_\nu(\tau_\nu, \mu). \tag{133}$$

We can solve this in an analogous manner to how we treated Eq. 85, multiplying all terms by $e^{-\tau_\nu/\mu}$, then rearranging to see that

$$\frac{d}{d\tau_\nu}\left(I_\nu e^{-\tau_\nu/\mu}\right) = -\frac{S_\nu}{\mu} e^{-\tau_\nu/\mu}. \tag{134}$$

Our solution looks remarkably similar to Eq. 86, except that we now explicitly account for the viewing angle μ:

$$I_\nu(\tau_\nu, \mu) = \int_{\tau_\nu}^{\infty} \frac{S_\nu(\tau'_\nu, \mu)}{\mu} e^{(\tau'_\nu - \tau_\nu)/\mu} d\tau'_\nu \tag{135}$$

So we now have at least a formal solution that could explain how I_ν varies as a function of the vertical optical depth τ_ν as well as the normal angle θ. It's already apparent that I_ν at a given depth is determined by the contributions from S_ν at all deeper levels, but these S_ν themselves depend on I_ν there. So we'd like to develop a more intuitive understanding than Eq. 135 provides.

Our goal will be to make a self-consistent model for S_ν and I_ν (or, as we'll see, I_ν and T). We'll again assume local thermodynamic equilibrium (LTE), so that

$$S_\nu = B_\nu(T) = B_\nu\left[T(\tau_\nu)\right] \tag{136}$$

(since T increases with depth into the star).

First, let's assume a simple form for S_ν so we can solve Eq. 135. We already tried a zeroth-order model for S_ν (i.e. a constant; see Eq. 79), so let's add a first-order perturbation, assuming that

$$S_\nu = a_\nu + b_\nu \tau_\nu \tag{137}$$

Where a_ν and b_ν are independent of τ_ν – for example, two blackbodies of different temperatures. When we plug this form into the formal solution of Eq. 135 and turn the crank, we find that the **emergent intensity** from the top of the star's atmosphere ($\tau_\nu = 0$) is

$$I_\nu(\tau_\nu = 0, \mu) = a_\nu + b_\nu \mu \tag{138}$$

Fig. 15 explains graphically what this solution means: namely, that the *angular* dependence of a star's emergent radiation encodes the *depth* dependence of its atmosphere's source function. If the depth dependence is small, so will the angular dependence be – and the reverse will also hold. So if $b_\nu \approx 0$, I_ν will be nearly isotropic with θ.

This describes the phenomenon of **limb darkening**, wherein the center

of a stellar disk appears brighter than the edge. This is commonly seen in photographs of the Sun – it often looks to the eye like merely shadow effects of a 3D sphere, but in fact this represents temperature stratification.

Another interesting consequence involves the fact that an observer can only typically observe down to $\tau_\nu \approx 1$. Because of the depth and angular dependencies we have just identified, this means that the surface where $\tau_\nu = 1$ (or any other constant value) occurs higher in the stellar atmosphere at the limb than at the disk center. Fig. 16 shows this effect. Since (as previously mentioned) temperature drops with decreasing pressure for most of a star's observable atmosphere, this means that we observe a cooler blackbody at the limb than at the center – and so the center appears brighter. (This is just a different way of thinking about the same limb-darkening effect mentioned above.) For the same reason, spectral lines look dark because at these lines α_ν is largest and so τ_ν occurs higher in the atmosphere, where temperatures are lower.

9.2 *Gray Atmosphere*

Now let's try to build a more self-consistent atmospheric model. To keep things tractable, we'll compensate for adding extra complications by simplifying another aspect: we'll assume a **gray atmosphere** in which the absorption coefficient (and derived quantities are independent of frequency). So we will use α instead of α_ν, and τ in place of τ_ν.

In this case, the equation of radiative transfer still has the same form as in

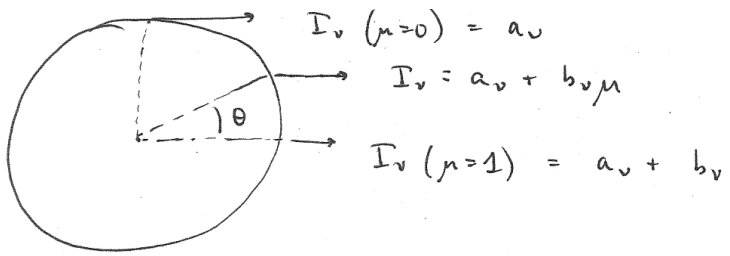

Figure 15: Emergent intensity as a function of θ assuming the linear model for S_ν given by Eq. 137.

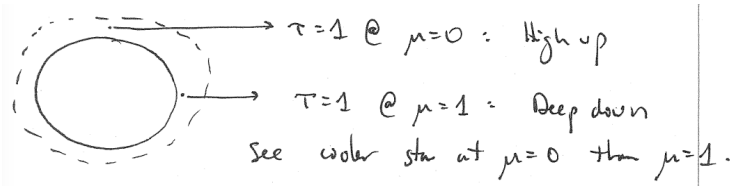

Figure 16: Depth dependence on the depth to which an observer can see into a stellar atmosphere: we see deeper at the center than at the limb.

Eq. 133 above:

$$\mu \frac{dI}{d\tau} = I(\tau, \mu) - S(\tau, \mu) \tag{139}$$

With the difference that by ignoring frequency effects, we are now equivalently solving for the **bolometric quantities**

$$I = \int_\nu I_\nu \, d\nu \tag{140}$$

and

$$S = \int_\nu S_\nu \, d\nu \tag{141}$$

Up until now, we've always assumed LTE with a Planck blackbody source function whose temperature varies with depth. But we've only used ad hoc models for this source — now, let's introduce some physically meaningful constraints. Specifically, let's require that flux is conserved as it propagates through the atmosphere. This is equivalent to saying there is no energy generation in the atmosphere: we just input a bunch of energy at the base and let it transport through and escape from the top.

This requirement of **flux conservation** means that $\frac{dF}{dt} = 0$, where

$$F = \int I \cos\theta d\Omega = \int \mu I d\Omega \tag{142}$$

(by definition; see Eq. 37).

To apply this reasonable physical constraint, let's integrate Eq. 139 over all solid angles:

$$\int \mu \frac{\partial I}{\partial \tau} d\Omega = \int (I - S) d\Omega \tag{143}$$

which implies that

$$\frac{dF}{d\tau} = 4\pi \langle I \rangle - 4\pi S \tag{144}$$

which equals zero due to flux conservation. Note that S is isotropic, while in general I may not be (i.e. more radiation comes out of a star than goes into it from space). The perhaps-surprising implication is that in our gray atmosphere,

$$S = \langle I \rangle \tag{145}$$

at all altitudes.

We can then substitute $\langle I \rangle$ for S in Eq. 139, to find

(146)
$$S = I - \mu \frac{dI}{d\tau}$$

(147)
$$\langle I \rangle = I - \mu \frac{dI}{d\tau}$$

(148)
$$\frac{1}{2} \int_{-1}^{1} I d\mu = I - \mu \frac{dI}{d\tau}$$

This is an integro-differential equation for gray atmospheres in radiative equilibrium. Though it looks odd, it is useful because an exact solution exists. After finding $\langle I \rangle = S$, we can use our formal solution to the radiative transfer equation to show that

(149) $$S = \frac{3F_0}{4\pi} [\tau + q(\tau)]$$

where F_0 is the input flux at the base of the atmosphere and $q(\tau)$ is the Hopf function, shown in Fig. 17. Let's examine an approximation to this function that provides a lot of insight into what's going on.

We'll start by examining the moments of the radiative transfer equation, where moment n is defined as

(150) $$\mu^{n+1} \int \frac{\partial I}{\partial \tau} d\Omega = \int \mu^n (I - S) d\Omega$$

We already did $n = 0$ back in Eq. 143, so let's consider $n = 1$. We'll need each

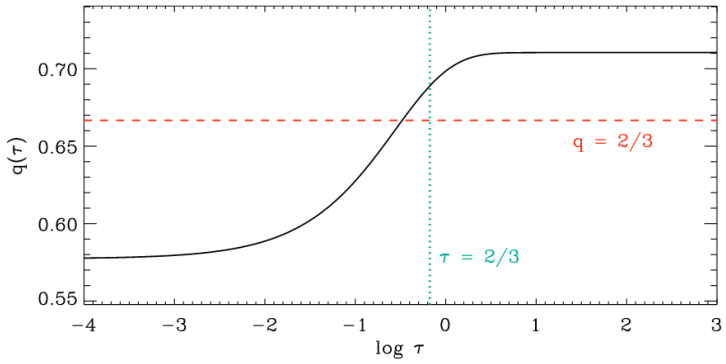

Figure 17: Hopf function $q(\tau)$, which has as its limits $q(0) = 1/\sqrt{3}$ and $q(\infty) = 0.7101....$

of the following terms, given in Eqs. 151–153:

$$\int \mu S d\Omega = 2\pi S \int_{-1}^{1} \mu d\mu \tag{151}$$

which equals zero, since S is isotropic.

$$\int \mu I d\Omega \equiv F \tag{152}$$

(the definition of flux), and finally

$$\int \mu^2 I d\Omega = \int I \cos^2\theta d\Omega \equiv c P_{\rm rad} \tag{153}$$

from Eq. 58.

The first moment then becomes

$$c\frac{dP}{d\tau} = F \tag{154}$$

which we have required to be constant. Thus, we find that

$$P_{\rm rad} = \frac{F}{c}(\tau + Q) \tag{155}$$

where here Q is a constant of integration; when certain assumptions are lifted, this becomes the Hopf function $q(\tau)$ of Fig. 17.

9.3 *The Eddington Approximation*

Eq. 155 is a potentially powerful result, because it tells us that in our gray, flux-conserving atmosphere the radiation pressure is just a linear function of the bolometric flux. This will become even more useful, since we are about to connect this back to S, and thence to I (a more useful observational diagnostic than P).

From the expression for the radiation pressure of a blackbody field (Eq. 58) we have that

$$P = \frac{4\pi}{3c}\int B_\nu d\nu \tag{156}$$

$$= \frac{4\pi}{3c} S \tag{157}$$

since we assume LTE, and thus our source function is the Planck function. *However*, remember that our atmosphere exhibits a temperature gradient, so our radiation field isn't actually a pure blackbody. We therefore make the key assumption — the **Eddington approximation** — that the temperature gradient is weak enough that the above expression for P is valid (correcting this

assumption turns Q into $q(\tau)$).

Under these assumptions, we then combine Eq. 157 and 155 to find

(158)
$$S = \frac{3F}{4\pi}(\tau + Q)$$

(159)
$$= \frac{3F}{4\pi}\left(\tau + \frac{2}{3}\right)$$

Thus the stellar atmosphere's source function is just a linear function of optical depth – just as we had blithely assumed in Eq. 137 when introducing limb darkening. The value of $2/3$ comes from a straightforward but tedious derivation described in Sec. 2.4.2 of the Choudhuri textbook.

We can also use Eq. 159 to clarify our previous discussion of limb darkening. Since we now know the particular linear dependence of S on τ, we can dispense with the arbitrary constants in Eq. 138 to show that the emergent intensity is

(160) $$I(\tau = 0, \mu) = \frac{3F}{4\pi}\left(\mu + \frac{2}{3}\right)$$

which shows decent agreement with observational data. This type of expression is called a **linear limb-darkening "law"**. Because of our assumptions this doesn't perfectly fit observed stellar limb-darkening profiles, so there is a whole family of various relations that people use (some physically justified, some empirical).

Finally, given the exact functional form of S in Eq. 159, we can now compute the stellar atmosphere's **thermal structure** – how its temperature changes with optical depth, pressure, or altitude. This relation is derived by relating S to the Stefan-Boltzmann flux F from Eq. 60:

(161)
$$S = \int S_\nu d\nu$$

(162)
$$= \int B_\nu d\nu$$

(163)
$$= \frac{\sigma_{SB} T^4}{\pi}$$

(as for that factor of π, see Sec. 1.3 of the Rybicki & Lightman). We now have $S(T)$ as well as $S(\tau)$, so combining Eqs. 159, Eq. 163, and the Stefan-Boltzmann flux (Eq. 60) we obtain a relation that

(164) $$T^4(\tau) = \frac{3}{4} T_{\text{eff}}^4 \left(\tau + \frac{2}{3}\right)$$

This gives us the thermal profile through the star's atmosphere. As we move deeper into the star the vertical optical depth τ increases (Eq. 130) and the temperature rises as well (Eq. 164). Note too that the atmospheric temperature $T = T_{\text{eff}}$ when $\tau = 2/3$. Earlier we have claimed that we see down to a depth of $\tau \approx 1$, so we have no refined that statement to say that we see into a stellar atmosphere down to the $\tau = 2/3$ surface.

9.4 *Frequency-Dependent Quantities*

We've achieved quite a bit, working only with frequency-integrated quantities: in particular, the temperature structure in Eq. 164 and the formal solution Eq. 135. However, although our earlier treatment of excitation and ionization of atomic lines (Sec. 8.5) qualitatively explains some of the trends in absorption lines seen in stellar spectra, we have so far only discussed line formation in the most qualitative terms.

We expect intensity to vary only slowly with frequency when temperatures are low. This because we expect the ratio $R(\nu)$ between intensities at two temperatures to scale as:

(165)
$$R(\nu) = \frac{I_\nu(T_B)}{I_\nu(T_A)}$$

(166)
$$\approx \frac{B_\nu(T_B)}{B_\nu(T_A)}$$

(167)
$$= \frac{e^{h\nu/kT_A} - 1}{e^{h\nu/kT_B} - 1}$$

This is consistent with the observed frequency dependence of limb darkening, which is seen to be much weaker at longer (infrared) wavelengths and stronger at shorter (e.g., blue-optical) wavelengths.

Let's now consider a more empirical way to make progress, based on the fact that we can observe the intensity emerging from the top of the atmosphere, $I_\nu(\tau_\nu = 0, \mu)$, across a wide range of frequencies. Expanding on our earlier, linear model of S_ν (Eq. 137), a fully valid expression for the source function is always

(168) $$S_\nu = \sum_{n=0}^{\infty} a_{\nu,n} \tau_\nu^n$$

Putting this into our formal solution, Eq. 135, and invoking the definition of the gamma function gives

(169) $$I_\nu(0, \mu) = \sum_{n=0}^{\infty} a_{\nu,n}(n!)\mu^n$$

So long as we are in LTE, then we also have $S_\nu(\tau_\nu) = B_\nu[T(\tau_\nu)]$. This lets us

map out $T(\tau_\nu)$, which we can do for multiple frequencies – as shown in Fig. 18. Each T corresponds to a particular physical depth in the stellar atmosphere, so we have successfully identified a mapping between optical depth, frequency, and temperature.

Since for any ν we typically observe only down to a constant $\tau_\nu \approx 2/3$, we can rank the absorption coefficients α_{ν_i} for each of the ν_i sketched in Fig. 18. For any given τ_ν, $T(\tau_\nu)$ is greatest for ν_1 and least for ν_3. Thus we are seeing deepest into the star at ν_1 and α_{ν_1} must be relatively small, while on the other hand we see only to a shallow depth (where T is lower) at ν_3 and so α_{ν_3} must be relatively large.

9.5 *Opacities*

What affects a photon as it propagates out of a stellar atmosphere? So far we haven't talked much about the explicit frequency dependence of α_ν, but this is essential in order to interpret observations.

From the definition of α_ν in Eq. 69, one sees that

(170) $n\sigma_\nu = \rho\kappa_\nu$

A lot of work in radiative transfer is about calculating the opacity κ_ν given ρ, T, and composition. In practice most desired opacities are tabulated and one uses a simple look-up table for ease of calculation. Nonetheless we can still consider some of the basic cases. These include:

1. Thomson (electron) scattering
2. Bound-bound reactions
3. Bound-free: photoionization & recombination
4. Free-free: Bremsstrahlung

Thomson scattering

The simplest effect is **Thomson scattering**, also known as electron scattering. In this interaction a photon hits a charged particle, shakes it up a bit (thus

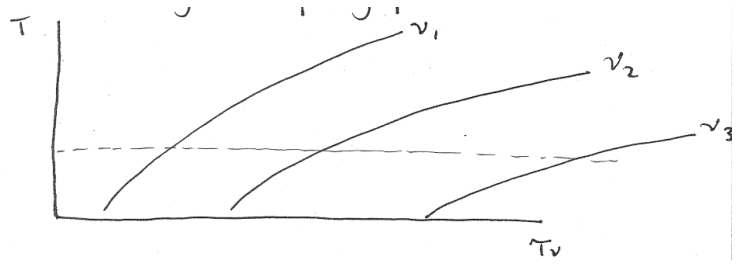

Figure 18: Notional atmospheric structure, $T(\tau_\nu)$, with different frequencies ν_i.

taking energy out of the radiation field), and is then re-radiated away. The basic (frequency-independent) cross-section is derived in many textbooks (e.g. Rybicki & Lightman, Sec. 3.4), which shows that in cgs units,

$$\sigma_T = \frac{8\pi}{3}\left(\frac{e^2}{m_e c^2}\right)^2 \tag{171}$$

or approximately $2/3 \times 10^{-24}$ cm^2 (or 2/3 of a "barn").

Notice that $\sigma_T \propto m^{-2}$, so the lightest charge-carriers are the most important – this means electrons. Eq. 171 suggests that in a notional medium composed solely of electrons, we would have

$$\kappa_\nu = \frac{n_e \sigma_T}{\rho_e} = \frac{\sigma_T}{m_e} \tag{172}$$

In any real astrophysical situation our medium will contain a wide range of particles, not just electrons. So in actuality we have

$$\kappa_\nu = \frac{n_e \sigma_T}{\rho_{\rm tot}} \equiv \frac{1}{\mu_e}\frac{\sigma_T}{m_p} \tag{173}$$

where we have now defined the **mean molecular weight of the electron** to be

$$\mu_e = \frac{\rho_{tot}}{n_e m_p} \tag{174}$$

The quantity μ_e represents the mean mass of the plasma per electron, in units of m_p (note that this is a bit different from the mean molecular weight for ions, which is important in stellar interior calculations). But in a fully ionized H-only environment, $n_e = N$ cm^{-3} while $\rho = Nm_p$ cm^{-3} — so $\mu_e = 1$. Meanwhile in a fully ionized, 100% He plasma, $n_e = 2N$ cm^{-3} while $\rho = 4N$ cm^{-3} — so in this case, $\mu_e = 2$.

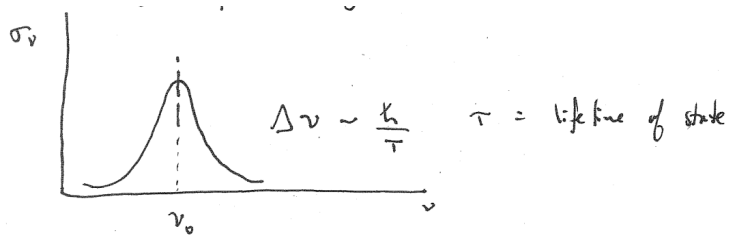

Figure 19: Schematic of σ_ν for bound-bound reactions, showing a line centered at ν_0 and with intrinsic width $\Delta\nu \sim \hbar/\tau$.

Bound-bound transitions

As the name implies, these involve changes between energy levels that still leave all particles bound. Most stellar opacity sources are of this type, which give rise to lines such as those depicted schematically in Fig. 19. In all cases the *intrinsic* line width $\Delta\nu \sim \hbar/\tau$ is given by the Heisenberg uncertainty principle and by τ, the typical lifetime of the state. Depending on the system being studied. But τ can change considerably depending on the system under analysis.

The general expression for the line's cross-section will be that

$$\sigma_\nu = \frac{\pi e^2}{m_e c} f \Phi(\nu - \nu_0) \tag{175}$$

where f is the transition's dimensionless oscillator strength (determined by the atomic physics) and $\Phi(\nu - \nu_0)$ is the line profile shape as sketched in Fig. 19. Note that Eq. 175 will also sometimes be written not in terms of f but rather as

$$\sigma_\nu = \frac{B_{LU} h\nu}{4\pi} \Phi(\nu - \nu_0) \tag{176}$$

where B_{LU} is the "Einstein B" coefficient for the transition from the lower to the upper state.

Regardless, the lifetime of the state may be intrinsic (and long-lived) if the particles involved are isolated and non-interacting, and undergo only **spontaneous emission**. This gives rise to the narrowest lines, which are said to be **naturally broadened.**

When conditions are denser and the particle interaction timescale $\lesssim \tau$, then collisions perturb the energy levels and so slightly higher- or lower-energy photons can couple to the particles involved. This leads to **pressure broadening** (or collisional broadening), which leads (as the name implies) to broader lines in higher-pressure environments.

Finally, particle velocities will impart a range of Doppler shifts to the observed line profile, causing various types of extrinsic broadening. In general these can all be lumped under the heading of **Doppler broadening**, in which the line width is set by the material's velocity,

$$\frac{\Delta\nu}{\nu_0} = \frac{v_r}{c} \tag{177}$$

This is an important effect for the accretion (or other) disks around black holes and around young stars, and also for the nearly-solid-body rotation of individual stars.

There's a lot more to say about bound-bound transitions than we have time for here. But whatever the specific situation, our approach will always be the following: use the Saha and Boltzmann equations to establish the populations in the available energy levels; then use atomic physics to determine the oscillator strength f and line profile $\Phi(\nu - \nu_0)$.

Figure 20: Bremsstrahlung (braking radiation) — an electron decelerates near an ion and emits a photon.

Bremsstrahlung

If you speak German, you might recognize that this translates as "braking radiation" — and Bremsstrahlung (or "free-free") is radiation caused by the deceleration of charged particles (typically electrons), as shown schematically in Fig. 20. Under time reversal, this phenomenon also represents absorption of a photon and acceleration of the electron. Typically this is modeled as occurring as the e^- is near (but not bound to) a charged but much more massive ion, which is assumed to be stationary during the interaction. Rybicki & Lightman devote a whole chapter to Bremsstrahlung, but we'll just settle for two useful rules of thumb:

$$\alpha_\nu^{ff} \approx 0.018 T^{-3/2} Z^2 n_e n_i \nu^{-2} \bar{g_{ff}} \tag{178}$$

and

$$\epsilon_\nu^{ff} \approx (6.8 \times 10^{-38}) Z^2 n_e n_i T^{-1/2} e^{-h\nu/kT} \bar{g_{ff}}$$

where Z is the ionic charge and $\bar{g_{ff}}$ is the **Gaunt factor**, typically of order unity.

Free-free absorption is dependent on both temperature and density, and is often commonly described by Kramer's opacity law:

$$\kappa_{ff} = \frac{1}{2} \kappa_{ff,0} (1 + X) \langle \frac{\mathcal{Z}^2}{\mathcal{A}} \rangle \rho T^{-7/2} \tag{179}$$

Bound-free

In this case, electrons transition between a bound (possibly excited) state and the free (i.e., ionized) state. If the initial state is bound, then an incoming photon comes in and (possibly) ejects an electron. Thus the e^- begins within a series of discretized, quantum, atomic energy levels and ends unbound, with a continuum of energy levels available to it. A full derivation shows that for a given bound transition we find $\sigma_\nu \propto \nu^{-3}$. But as ν decreases toward the

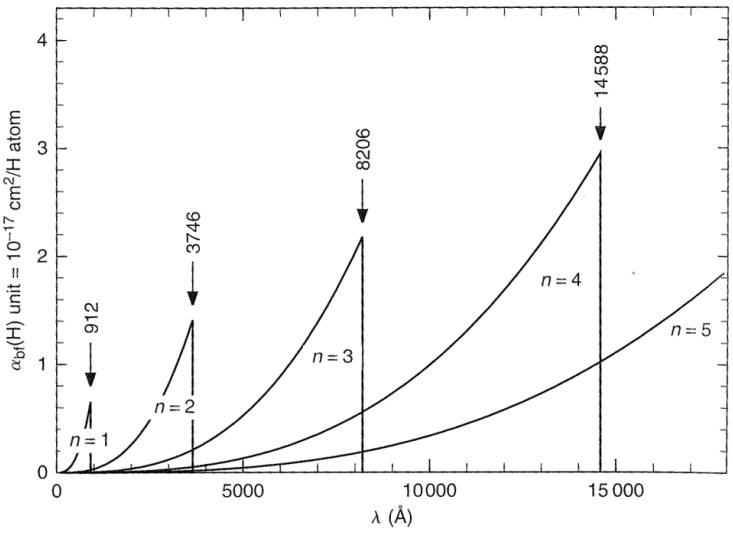

Figure 21: Extinction coefficient α_ν for bound-free transitions of the H atom (from Gray's *Stellar Photospheres*, Fig. 8.2). The characteristic scaling with $\nu^{-3} \propto \lambda^3$ is clearly apparent.

ionization threshold ν_i (e.g., 13.6 ev$/h$ for H in the ground state), then σ_ν will sharply drop when the photon is no longer able to ionize. But assuming there is some excited hydrogen (e.g., ν_2=13.6$/4h$ for H in the $n = 2$ state), then there will be a second one-sided peak located at ν_2, and so on as shown in Fig. 21.

H-minus opacity

For years after astronomers first turned their spectrographs toward the Sun, it was unclear which processes explained the observed Solar opacity. It was apparent that the opacity was fairly large, despite the fact that H and He are almost entirely neutral in the Solar photosphere and bound-bound transitions also weren't able to explain the data.

The solution turned out to be the **negative hydrogen ion**, H^-, which is stable because the normal H atom is highly polarized and can hold another e^-. The electron is bound only weakly, with a dissociation energy of just 0.75 eV (no stable, excited states exist). Thus all photons with $\lambda \lesssim 1.7\mu$m can potentially break this ion and, being absorbed, contribute to an overall continuum opacity that is strongest from 0.4–1.4μm. The magnitude of the total H^- opacity depends sensitively on the ion's abundance: it drops off steeply in stars much hotter than the Sun (when most H^- is ionized) and in the very coolest stars (when no free e^- are available to form the ion). In addition to being a key opacity source in many stars, H^- has only recently been recognized as a key opacity source in the atmospheres of the hottest extrasolar planets (see e.g. Lothringer et al., 2018).

10 Timescales in Stellar Interiors

Having dealt with the stellar photosphere and the radiation transport so relevant to our observations of this region, we're now ready to journey deeper into the inner layers of our stellar onion. Fundamentally, the aim we will develop in the coming chapters is to develop a connection between M, R, L, and T in stars (see Table 10 for some relevant scales).

More specifically, our goal will be to develop equilibrium models that describe stellar structure: $P(r)$, $\rho(r)$, and $T(r)$. We will have to model gravity, pressure balance, energy transport, and energy generation to get everything right. We will follow a fairly simple path, assuming spherical symmetric throughout and ignoring effects due to rotation, magnetic fields, etc.

Before laying out the equations, let's first think about some key timescales. By quantifying these timescales and assuming stars are in at least short-term equilibrium, we will be better-equipped to understand the relevant processes and to identify just what stellar equilibrium means.

10.1 *Photon collisions with matter*

This sets the timescale for radiation and matter to reach equilibrium. It depends on the **mean free path** of photons through the gas,

$$\ell = \frac{1}{n\sigma} \tag{180}$$

So by dimensional analysis,

$$\tau_\gamma \approx \frac{\ell}{c} \tag{181}$$

If we use numbers roughly appropriate for the average Sun (assuming full

Table 3: Relevant stellar quantities.

Quantity	Value in Sun	Range in other stars
M	2×10^{33} g	$0.08 \lesssim (M/M_\odot) \lesssim 100$
R	7×10^{10} cm	$0.08 \lesssim (R/R_\odot) \lesssim 1000$
L	4×10^{33} erg s^{-1}	$10^{-3} \lesssim (L/L_\odot) \lesssim 10^6$
$T_{\rm eff}$	5777 K	3000 K $\lesssim (T_{\rm eff}/mathrmK) \lesssim$ 50,000 K
ρ_c	150 g cm^{-3}	$10 \lesssim (\rho_c/\text{g cm}^{-3}) \lesssim 1000$
T_c	1.5×10^7 K	$10^6 \lesssim (T_c/\text{K}) \lesssim 10^8$

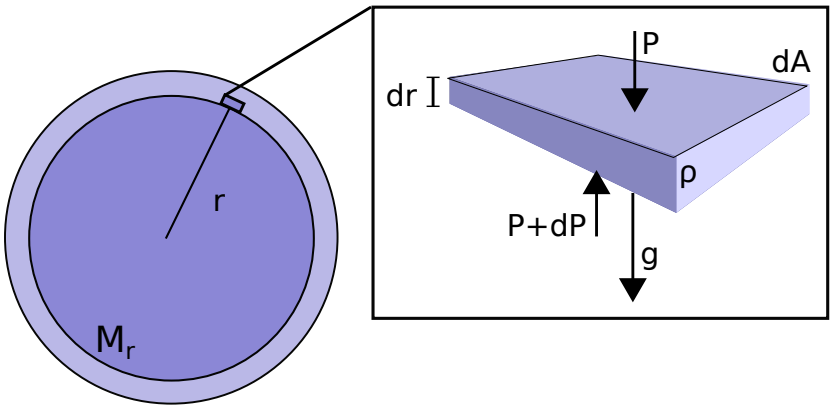

Figure 22: The state of hydrostatic equilibrium in an object like a star occurs when the inward force of gravity is balanced by an outward pressure gradient. This figure illustrates that balance for a packet of gas inside of a star

ionization, and thus Thomson scattering), we have

(182)
$$\ell = \frac{1}{n\sigma}$$

(183)
$$= \frac{m_p}{\rho\sigma_T}$$

(184)
$$= \frac{1.7 \times 10^{-24}\ \mathrm{g}}{(1.4\ \mathrm{g\ cm^{-3}})(2/3 \times 10^{-24}\ \mathrm{cm^{-2}})}$$

(185)
$$\approx 2\ \mathrm{cm}$$

So the matter-radiation equilibration timescale is roughly $\tau_\gamma \approx 10^{-10}$ s. Pretty fast!

10.2 *Gravity and the free-fall timescale*

For stars like the sun not to be either collapsing inward due to gravity or expanding outward due to their gas pressure, these two forces must be in balance. This condition is known as hydrostatic equilibrium. This balance is illustrated in Figure 22

As we will see, gravity sets the timescale for fluid to come into mechanical equilibrium. When we consider the balance between pressure and gravity on a small bit of the stellar atmosphere with volume $V = Adr$ (sketched in Fig. 22), we see that in equilibrium the vertical forces must cancel.

The small volume element has mass dm and so will feel a gravitational

force equal to

$$F_g = \frac{GM_r\, dm}{r^2} \tag{186}$$

where M_r is the mass of the star enclosed within a radius r,

$$M(r) \equiv 4\pi \int_{r'=0}^{r'=r} \rho(r') r'^2 dr' \tag{187}$$

Assuming the volume element has a thickness dr and area dA, and the star has a uniform density ρ, then we can replace dm with $\rho dr dA$. This volume element will also feel a mean pressure which we can define as dP, where the pressure on the outward facing surface of this element is P and the pressure on the inward facing surface of this element is $P + dP$. The net pressure force is then $dPdA$, so

$$F_P(r) = F_g(r) \tag{188}$$

$$A\left(P(r) - P(r+dr)\right) = -\rho V g \tag{189}$$

$$= \rho A dr g \tag{190}$$

(191)

which yields the classic expression for **hydrostatic equilibrium**,

$$\frac{dP}{dr} = \rho(r) g(r) \tag{192}$$

where

$$g \equiv -\frac{GM(r)}{r^2} \tag{193}$$

and $M(r)$ is defined as above.

When applying Eq. 192 to stellar interiors, it's common to recast it as

$$\frac{dP}{dr} = -\frac{GM(r)\rho(r)}{r^2} \tag{194}$$

In Eqs. 192 and 194 the left hand side is the pressure gradient across our volume element, and the right hand side is the gravitational force averaged over that same volume element. So it's not that pressure balances gravity in a star, but rather gravity is balanced by the gradient of increasing pressure from the center to the surface.

The gradient dP/dr describes the pressure profile of the stellar interior in equilibrium. What if the pressure changes suddenly – how long does it take

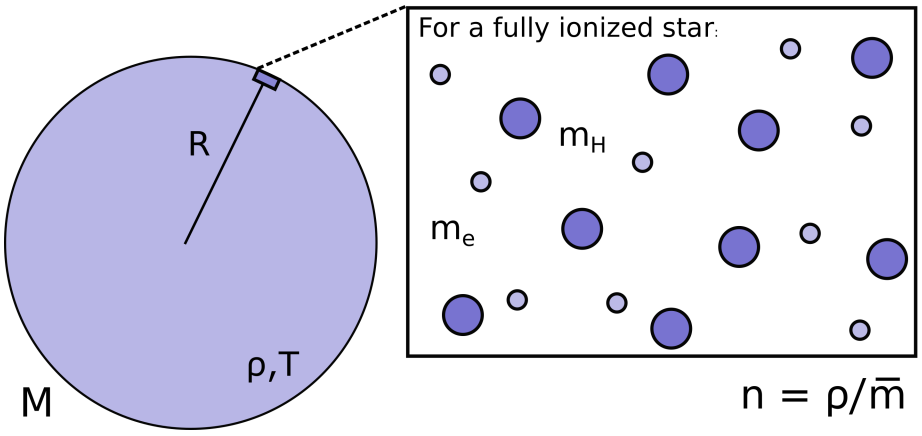

Figure 23: A simple model of a star having a radius R, mass M, constant density ρ, a constant temperature T, and a fully ionized interior. This simple model can be used to derive a typical free-fall time and a typical sound-crossing time for the sun.

us to re-establish equilibrium? Or equivalently: if nothing were holding up a star, how long would it take to collapse under its own gravity? Looking at Figure 23, we can model this as the time it would take for a parcel of gas on the surface of a star, at radius R, to travel to its center, due to the gravitational acceleration from a mass M.

Looking at Figure 23, we can model this as the time it would take for a parcel of gas on the surface of a star, at radius R, to travel to its center, due to the gravitational acceleration from a mass M. To order of magnitude, we can combine the following two equations

$$a = -\frac{GM}{r^2} \tag{195}$$

and

$$d = -\frac{1}{2}at^2. \tag{196}$$

Setting both r and d equal to the radius of our object R, and assuming a constant density $\rho = \frac{3M}{4\pi R^3}$, we find

$$\tau_{ff} \sim \frac{1}{\sqrt{G\rho}} \tag{197}$$

which is within a factor of two of the exact solution,

$$\tau_{ff} = \sqrt{\frac{3\pi}{32G\rho}} \tag{198}$$

Note that the free-fall timescale does not directly depend on the mass of an object or its radius (or in fact, the distance from the center of that object). It only depends on the density. Since $G \approx 2/3 \times 10^{-7}$ (cgs units), with $\langle \rho_\odot \rangle \approx 1$ g cm^{-3}, the average value is $\tau_{dyn} \sim 30$ min.

In real life, main-sequence stars like the sun are stable and long-lived structures that are not collapsing. Even if you have a cloud of gas that is collapsing under its own gravity to form a star, it does not collapse all the way to $R = 0$ thanks to its internal hydrostatic pressure gradient.

10.3 *The sound-crossing time*

We have an expression for the time scale upon which gravity will attempt to force changes on a system (such changes can either be collapse, if a system is far out of hydrostatic equilibrium and gravity is not significantly opposed by pressure, or contraction, if a system is more evenly balanced). What is the corresponding time scale upon which pressure will attempt to cause a system to expand?

The pressure time scale in a system can be characterized using the sound speed (as sound is equivalent to pressure waves in a medium). This isothermal sound speed is given by the relation

$$c_s = \sqrt{\frac{P}{\rho}} \tag{199}$$

Although gas clouds in the interstellar medium may be reasonably approximated as isothermal, the same is not true for stars. We will ignore that fact for now, but will return to this point later.

Referring back to Figure 23, we can define the sound-crossing time for an object as the time it takes for a sound wave to cross the object. Using a simple equation of motion $d = vt$ and approximating $2R$ just as R we can then define a sound-crossing time as

$$\tau_s \sim R\sqrt{\frac{\rho}{P}} \tag{200}$$

Using the ideal gas equation, we can substitute $\frac{\rho}{\bar{m}}kT$ for P and get an expression for the sound crossing time in terms of more fundamental parameters for an object:

$$\tau_s \sim R\sqrt{\frac{\bar{m}}{kT}} \tag{201}$$

Unlike the free-fall time we derived earlier, the sound-crossing time depends directly upon the size of the object, and its temperature. At the center of the Sun, $T_c \approx 1.5 \times 10^7$ K and $\bar{m} \sim m_p$ and so the sound-crossing timescale is roughly 30 min.

Note that by Eq. 198 we see that τ_s is also approximately equal to the free-fall timescale τ_{ff}. For an object not just to be in hydrostatic equilibrium but to remain this way, the pressure must be able to respond to changes in gravity, and vice versa. This response requires that a change in one force is met with a change in another force on a timescale that is sufficiently fast to restore the force balance. In practice, this means that for objects in hydrostatic equilibrium, the free-fall time is more or less equivalent to the sound-crossing time. In that way, a perturbation in pressure or density can be met with a corresponding response before the object moves significantly out of equilibrium.

10.4 *Radiation transport*

If photons streamed freely through a star, they'd zip without interruption from the core to the stellar surface in $R_\odot/c \approx 2$ s. But as we saw above in Eq. 185, the photons actually scatter every $\sim$1 cm. With each collision they "forget" their history, so the motion is a random walk with N steps. So for a single photon[1] to reach the surface from the core requires

$$\ell\sqrt{N} \sim R_\odot \tag{202}$$

which implies that the **photon diffusion timescale** is

$$\tau_{\gamma,\mathrm{diff}} \sim \frac{N\ell}{c} \sim \frac{R_\odot^2}{\ell}\frac{1}{c} \tag{203}$$

or roughly 10^4 yr.

10.5 *Thermal (Kelvin-Helmholtz) timescale*

The thermal timescale answers the question, How long will it take to radiate away an object's gravitational binding energy? This timescale also governs the contraction of stars and brown dwarfs (and gas giant planets) by specifying the time it takes for the object to radiate away a significant amount of its gravitational potential energy. This is determined by the **Kelvin-Helmholtz timescale**. This thermal time scale can generally be given as:

$$\tau_{KH} = \frac{E}{L}, \tag{204}$$

where E is the gravitational potential energy released in the contraction to its final radius and L is the luminosity of the source. Approximating the Sun as a uniform sphere, we have

$$\tau_{KH} \sim \frac{GM_\odot^2}{R_\odot}\frac{1}{L_\odot} \tag{205}$$

[1] This is rather poetic – of course a given photon doesn't survive to reach the surface, but is absorbed and re-radiated as a new photon $\sim (R_\odot/\ell)^2$ times. Because of this, it may be better to think of the timescale of Eq. 203 as the **radiative energy transport timescale**.

which is roughly 3×10^7 yr.

Before nuclear processes were known, the Kelvin-Helmholtz timescale was invoked to argue that the Sun could be only a few 10^7 yr old – and therefore much of geology and evolutionary biology (read: Darwin) must be wrong. There turned out to be missing physics, but τ_{KH} turns out to still be important when describing the contraction of large gas clouds as they form new, young stars.

The time that a protostar spends contracting depends upon its mass, as its radius slowly contracts. A 0.1 $M_\odot$ star can take 100 million years on the Hayashi track to finish contracting and reach the main sequence. On the other hand, a 1 $M_\odot$ star can take only a few million years contracting on the Hayashi track before it develops a radiative core, and then spends up to a few tens of millions of years on the Henyey track before reaching the main sequence and nuclear burning equilibrium. The most massive stars, 10 $M_\odot$ and above, take less than 100,000 years to evolve to the main sequence.

10.6 *Nuclear timescale*

The time that a star spends on the main sequence – essentially the duration of the star's nuclear fuel under a constant burn rate – is termed the **the nuclear timescale**. It is a function of stellar mass and luminosity, essentially analogous to the thermal time scale of Equation 204. Here, the mass available (technically, the mass difference between the reactants and product of the nuclear reaction) serves as the energy available, according to $E = mc^2$.

If we fuse 4 protons to form one He^4 nucleus (an **alpha particle**), then the fractional energy change is

$$\frac{\Delta E}{E} = \frac{4m_p c^2 - m_{He} c^2}{4m_p c^2} \approx 0.007 \tag{206}$$

This is a handy rule of thumb: fusing H to He liberates roughly 0.7% of the available mass energy. As we will see, in more massive stars heavier elements can also fuse; further rules of thumb are that fusing He to C and then C to Fe (through multiple intermediate steps) each liberates another 0.1% of mass energy. But for a solar-mass star, the main-sequence nuclear timescale is

$$\tau_{nuc} = \frac{\Delta E}{E_{\rm tot}} \approx \frac{0.007 M_\odot c^2}{L_\odot} \approx 10^{11} \text{ yr} \tag{207}$$

which implies a main-sequence lifetime of roughly 100 billion years. The actual main-sequence lifetime for a $1 M_\odot$ star is closer to 10 billion years; it turns out that significant stellar evolution typically occurs by the time $\sim$10% of a star's mass has been processed by fusion.

10.7 *A Hierarchy of Timescales*

So if we arrange our timescales, we find a strong separation of scales:

$$\begin{array}{ccccccccc} \tau_{nuc} & \gg & \tau_{KH} & \gg & \tau_{\gamma,diff} & \gg & \tau_{dyn} & \gg & \tau_\gamma \\ 10^{11} \text{ yr} & \gg & 3 \times 10^7 \text{ yr} & \gg & 10^4 \text{ yr} & \gg & 30 \text{ min} & \gg & 10^{-10} \text{ s} \end{array}$$

This separation is pleasant because it means whenever we consider one timescale, we can assume that the faster processes are in equilibrium while the slower processes are static.

Much excitement ensues when this hierarchy breaks down. For example, we see convection occur on τ_{dyn} which then fundamentally changes the thermal transport. Or in the cores of stars near the end of their life, τ_{nuc} becomes much shorter. If it gets shorter than τ_{dyn}, then the star has no time to settle into equilibrium – it may collapse.

10.8 *The Virial Theorem*

In considering complex systems as a whole, it becomes easier to describe important properties of a system in equilibrium in terms of its energy balance rather than its force balance. For systems in equilibrium– not just a star now, or even particles in a gas, but systems as complicated as planets in orbit, or clusters of stars and galaxies– there is a fundamental relationship between the internal, kinetic energy of the system and its gravitational binding energy.

This relationship can be derived in a fairly complicated way by taking several time derivatives of the moment of inertia of a system, and applying the equations of motion and Newton's laws. We will skip this derivation, the result of which can be expressed as:

$$\frac{d^2I}{dt^2} = 2\langle K\rangle + \langle U\rangle, \tag{208}$$

where $\langle K\rangle$ is the time-averaged kinetic energy, and $\langle U\rangle$ is the time-averaged gravitational potential energy. For a system in equilibrium, $\frac{d^2I}{dt^2}$ is zero, yielding the form more traditionally used in astronomy:

$$\langle K\rangle = -\frac{1}{2}\langle U\rangle \tag{209}$$

The relationship Eq. 209 is known as the Virial Theorem. It is a consequence of the more general fact that whenever $U \propto r^n$, we will have

$$\langle K\rangle = \frac{1}{n}\langle U\rangle \tag{210}$$

And so for gravity with $U \propto r^{-1}$, we have the Virial Theorem, Eq. 209.

When can the Virial Theorem be applied to a system? In general, the system must be in equilibrium (as stated before, this is satisfied by the second time derivative of the moment of inertia being equal to zero). Note that this is not necessarily equivalent to the system being stationary, as we are considering the time-averaged quantities $\langle K\rangle$ and $\langle U\rangle$. This allows us to apply the Virial Theorem to a broad diversity of systems in motion, from atoms swirling within a star to stars orbiting in a globular cluster, for example. The system also generally must be isolated. In the simplified form we are using, we don't consider so-called 'surface terms' due to an additional external pressure from a medium in which our system is embedded. We also assume that there are

not any other sources of internal support against gravity in the system apart from the its internal, kinetic energy (there is no magnetic field in the source, or rotation). Below, we introduce some of the many ways we can apply this tool.

Virial Theorem applied to a Star

For stars, the Virial Theorem relates the internal (i.e. thermal) energy to the gravitational potential energy. We can begin with the equation of hydrostatic equilibrium, Eq. 192. We multiply both sides by $4\pi r^3$ and integrate as follows

$$\int_0^R \frac{dP}{dr} 4\pi r^3 dr = -\int_0^R \left(\frac{GM(r)}{r}\right)\left(4\pi r^2 \rho(r)\right) dr \tag{211}$$

The left-hand side can be integrated by parts,

$$\int_0^R \frac{dP}{dr} 4\pi r^3 dr = 4\pi r^3 P|_0^R - 3\int_0^R P 4\pi r^2 dr \tag{212}$$

and since $r(0) =$ and $P(R) = 0$, the first term equals zero. We can deal with the second term by assuming that the star is an ideal gas, replacing $P = nkT$, and using the thermal energy density

$$u = \frac{3}{2} nkT = \frac{3}{2} P \tag{213}$$

This means that the left-hand side of Eq. 211 becomes

$$-2\int_0^R u(4\pi r^2 dr) = -2E_{th} \tag{214}$$

Where E_{th} is the total thermal energy of the star.

As for the right-hand side of Eq. 211, we can simplify it considerably by recalling that

$$\Phi_g = -\frac{GM(r)}{r} \tag{215}$$

and

$$dM = 4\pi r^2 \rho(r) dr. \tag{216}$$

Thus the right-hand side of Eq. 211 becomes simply

$$\int_0^R \Phi_g(M') dM' = E_{\text{grav}} \tag{217}$$

And so merely from the assumptions of hydrostatic equilibrium and an ideal gas, it turns out that

(218) $E_{\text{grav}} = -2E_{th}$

or alternatively,

(219) $E_{tot} = -E_{th} = E_{\text{grav}}/2$

The consequence is that the total energy of the bound system is negative, and that it has negative heat capacity – a star heats up as it loses energy! Eq. 219 shows that if the star radiates a bit of energy so that E_{tot} decreases, E_{th} increases while E_{grav} decreases by even more. So energy was lost from the star, causing its thermal energy to increase while it also becomes more strongly gravitationally bound. This behavior shows up in all gravitational systems with a thermal description — from stars to globular clusters to Hawking radiation near a black hole to the gravitational collapse of a gas cloud into a star.

Virial Theorem applied to Gravitational Collapse

We can begin by restating the Virial Theorem in terms of the average total energy of a system $\langle E \rangle$:

(220) $\langle E \rangle = \langle K \rangle + \langle U \rangle = \frac{1}{2}\langle U \rangle$

A classic application of this relationship is then to ask, if the sun were powered only by energy from its gravitational contraction, how long could it live? To answer this, we need to build an expression for the gravitational potential energy of a uniform sphere: our model for the gravitational potential felt at each point inside of the sun. We can begin to put this into equation form by considering what the gravitational potential is for an infinitesimally thin shell of mass at the surface of a uniformly-dense sphere.

Using dM as defined previously, the differential change in gravitational potential energy that this shell adds to the sun is

(221) $dU = -\frac{GM(r)dM}{r}.$

The simplest form for $M(r)$ is to assume a constant density. In this case, we can define

(222) $M(r) = \frac{4}{3}\pi r^3 \rho$

To determine the total gravitational potential from shells at all radii, we must integrate Equation 221 over the entire size of the sphere from 0 to R, substi-

tuting our expressions for dM and $M(r)$ from Equations 216 and 222:

$$U = -\frac{G(4\pi\rho)^2}{3}\int_0^R r^4 dr. \quad (223)$$

Note that if this were not a uniform sphere, we would have to also consider ρ as a function of radius: $\rho(r)$ and include it in our integral as well. That would be a more realistic situation for a star like our sun, but we will keep it simple for now.

Performing this integral, and replacing the average density ρ with the quantity $\frac{3M}{4\pi R^3}$, we then find

$$U = -\frac{G(3M)^2}{R^6}\frac{R^5}{5} = -\frac{3}{5}\frac{GM^2}{R} \quad (224)$$

which is the gravitational potential (or binding energy) of a uniform sphere. All together, this is equivalent to the energy it would take to disassemble this sphere, piece by piece, and move each piece out to a distance of infinity (at which point it would have zero potential energy and zero kinetic energy).

To understand how this relates to the energy available for an object like the sun to radiate as a function of its gravitational collapse, we have to perform one more trick, and that is to realize that Equation 220 doesn't just tell us about the average energy of a system, but how that energy has evolved. That is to say,

$$\Delta E = \frac{1}{2}\Delta U \quad (225)$$

So, the change in energy of our sun as it collapsed from an initial cloud to its current size is half of the binding energy that we just calculated. How does our star just lose half of its energy as it collapses, and where does it go? The Virial Theorem says that as a cloud collapses it turns half of its potential energy into kinetic energy (Equation 209). The other half then goes into terms that are not accounted for in the Virial Theorem: radiation, internal excitation of atoms and molecules and ionization (see the Saha Equation, Equation 124).

Making the simplistic assumption that all of the energy released by the collapse goes into radiation, then we can calculate the energy available purely from gravitational collapse and contraction to power the luminosity of the sun. Assuming that the initial radius of the cloud from which our sun formed is not infinity, but is still large enough that the initial gravitational potential energy is effectively zero, the energy which is radiated from the collapse is half the current gravitational potential energy of the sun, or

$$E_{radiated} = -\frac{3}{10}\frac{GM_\odot^2}{R_\odot} \quad (226)$$

Eq. 226 therefore links the Virial Theorem back to the Kelvin-Helmholtz

timescale of Sec. 10.5. For the sun, this is a total radiated energy of $\sim 10^{41}$ J. If we assume that the sun radiates this energy at a rate equal to its current luminosity ($\sim 10^{26}$ W) then we can calculate that the sun could be powered at its current luminosity just by this collapse energy for 10^{15} s, or 3×10^7 years. While this is a long time, it does not compare to our current best estimates for the age of the earth and sun: $\sim$4.5 billion years. As an interesting historical footnote, it was Lord Kelvin who first did this calculation to estimate the age of the sun (back before we knew that the sun must be powered by nuclear fusion). He used this calculation to argue that the Earth must only be a few million years old, he attacked Charles Darwin's estimate of hundreds of millions of years for the age of the earth, and he argued that the theory of evolution and natural selection must be bunk. In the end of course, history has shown who was actually correct on this point.

11 Stellar Structure

Questions you should be able to answer after these lectures:

- What equations, variables, and physics describe the structure of a star?
- What are the two main types of pressure in a star, and when is each expected to dominate?
- What is an equation of state, and what is the equation of state that is valid for the sun?

11.1 *Formalism*

One of our goals in this class is to be able to describe not just the observable, exterior properties of a star, but to understand all the layers of these cosmic onions — from the observable properties of their outermost layers to the physics that occurs in their cores. This next part will then be a switch from some of what we have done before, where we have focused on the "surface" properties of a star (like size, total mass, and luminosity), and considered many of these to be fixed and unchanging. Our objective is to be able to describe the entire internal structure of a star in terms of its fundamental physical properties, and to model how this structure will change over time as it evolves.

Before we define the equations that do this, there are two points that may be useful to understand all of the notation being used here, and the way in which these equations are expressed.

First, when describing the evolution of a star with a set of equations, we will use mass as the fundamental variable rather than radius (as we have mostly been doing up until this point.) It is possible to change variables in this way because mass, like radius, increases monotonically as you go outward in a star from its center. We thus will set up our equations so that they follow individual, moving shells of mass in the star. There are several benefits to this. For one, it makes the problem of following the evolution of our star a more well-bounded problem. Over a star's lifetime, its radius can change by orders of magnitude from its starting value, and so a radial coordinate must always be defined with respect to the hugely time-varying outer extent of the star. In contrast, as our star ages, assuming its mass loss is insignificant, its mass coordinate will always lie between zero and its starting value M — a value which can generally be assumed to stay constant for most stars over most of stellar evolution. Further, by following shells of mass that do not cross over each other, we implicitly assume conservation of mass at a given time, and the mass enclosed by any of these moving shells will stay constant as the star evolves, even as the radius changes. This property also makes it easier to follow compositional changes in our star.

In general, the choice to follow individual fluid parcels rather than reference a fixed positional grid is known as adopting Lagrangian coordinates instead of Eulerian coordinates. For a **Lagrangian** formulation of a problem:

- This is a particle-based description, following individual particles in a fluid over time
- Conservation of mass and Newton's laws apply directly to each particle being followed
- However, following each individual particle can be computationally expensive
- This expense can be somewhat avoided for spherically-symmetric (and thus essentially '1D') problems

In contrast, for a **Eulerian** formulation of a problem:

- This is a field-based description, recording changes in properties at each point on a fixed positional grid in space over time
- The grid of coordinates is not distorted by the fluid motion
- Problems approached in this way are generally less computationally expensive, and are generally easier for 2D and 3D problems

There are thus trade-offs for choosing each formulation. For stellar structure, Lagrangian coordinates are generally preferred, and we will rely heavily on equations expressed in terms of a stellar mass variable going forward.

Second, it might be useful to just recall the difference between the two types of derivatives that you may encounter in these equations. The first is a partial derivative, written as ∂f. The second is a total derivative, written as df. To illustrate the difference, let's assume that f is a function of a number of variables: $f(x,t)$. The partial derivative of f with respect to x is just $\frac{\partial f}{\partial x}$. Here, we have assumed in taking this derivative that x is held fixed with time and does not vary. However, most of the quantities that we will deal with in the equations of stellar structure *do* vary with time. The use of a partial derivative with respect to radius or mass indicates that we are considering the change in this space(like) coordinate for an instantaneous, fixed time value. In contrast, the total derivative does not hold any variables to be fixed, and considers how all of the dependent variables changes as a function of the variable considered. Note that when you see a quantity like $\dot{r}$ in an equation, this is actually the partial rather than total derivative with respect to time.

11.2 *Equations of Stellar Structure*

In this class, we will define four fundamental equations of stellar structure, and several additional relationships that, taken all together, will define the structure of a star and how it evolves with time. Depending on the textbook that you consult, you will find different versions of these equations using slightly different variables, or in a slightly different format.

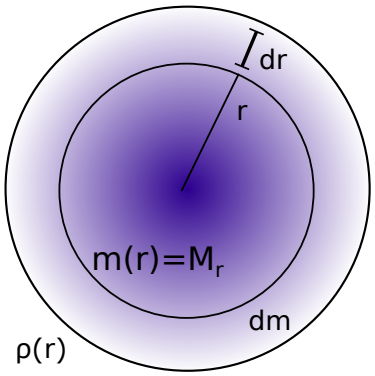

Figure 24: An illustration of a shell with mass dm and thickness dr. The mass enclosed inside of the shell is $m(r)$ (or M_r, depending on how you choose to write it). Assume that this object has a density structure $\rho(r)$

Mass continuity

The first two equations of stellar structure we have already seen before, as the conversion between the mass and radius coordinates

$$\frac{dr}{dm} = \frac{1}{4\pi r^2 \rho} \tag{227}$$

and as the equation of hydrostatic equilibrium (Eq. 192), now recast in terms of mass:

$$\frac{dP}{dm} = -\frac{Gm}{4\pi r^4} \tag{228}$$

Eq. 227 and its variant forms are known variously as the **Mass Continuity Equation** or the **Equation of Conservation of Mass**. Either way, this is the first of our four fundamental equations of stellar structure, and relates our mass coordinate m to the radius coordinate r, as shown in Fig. 24.

Note that up until now we have been generally either been assuming a uniform constant density in all of the objects we have considered, or have been making approximations based on the average density $\langle\rho\rangle$. However, to better and more realistically describe stars we will want to use density distributions that are more realistic (e.g., reaching their highest value in the center of the star, and decreasing outward to zero at the edge of the star). This means we should start trying to think about ρ as a function rather than a constant (even when it is not explicitly written as $\rho(r)$ or $\rho(m)$ in the following equations).

Hydrostatic equilibrium

The second equation of stellar structure (Eq. 228, the equation of hydrostatic equilibrium) concerns the motion of a star, and we derived it in Sec. 10.2. As we noted earlier, stars can change their radii by orders of magnitude over

the course of their evolution. As a result, we must consider how the interiors of stars move due the forces of pressure and gravity. We have already seen a specific case for this equation: the case in which gravity and pressure are balanced such that there is no net acceleration, and the star is in hydrostatic equilibrium (Equation 192).

We want to first consider a more general form of Eq. 228 that allows for the forces to be out of balance and thus there to be a net acceleration, and second to change variables from a dependence on radius to a dependence on mass. We can begin by rewriting our condition of force balance in Equation 192 as

$$0 = -\frac{Gm(r)}{r^2} - \frac{1}{\rho}\frac{\partial P}{\partial r}. \tag{229}$$

Each term in this equation has units of acceleration. Thus, this equation can be more generally written as

$$\ddot{r} = -\frac{Gm(r)}{r^2} - \frac{1}{\rho}\frac{\partial P}{\partial r}. \tag{230}$$

Using Equation 216 we can recast this expression in terms of a derivative with respect to m rather than r. This gives us the final form that we will use:

$$\ddot{r} = -\frac{Gm(r)}{r^2} - 4\pi r^2 \frac{\partial P}{\partial m}. \tag{231}$$

This is the most general form of our second equation of stellar structure. When $\ddot{r}$ is zero we are in equilibrium and so we obtain Eq. 228, the equation of **hydrostatic equilibrium**. This more general form, Eq. 231, is sometimes referred to as the **Equation of Motion** or the **Equation of Momentum Conservation**.

The Thermal Transport Equation

We also need to know how the temperature profile of a star changes with depth. If we do that, we can directly connect the inferred profile of temperature vs. optical depth (Eq. 164) to a physical coordinate within the star.

Assume there is a luminosity profile (determined by the energy equation, to be discussed next), such that the flux at radius r is

$$F(r) = \frac{L(r)}{4\pi r^2} \tag{232}$$

In a plane-parallel atmosphere, we learned (Eq. 155) that the flux is related to the gradient of the radiation pressure. The assumptions we made then don't restrict the applicability of that relation only to the outer atmosphere, so we can apply it anywhere throughout the interior of our star. The only (minor) adjustment is that we replace dz with dr since we are now explicitly considering a spherical geometry, so we now have

$$F = -\frac{c}{\alpha}\frac{dP_{rad}}{dr} \tag{233}$$

Since we know that $P_{rad} = 4/3c\ \sigma_{SB} T^4$ (Eq. 258), we see that

$$\frac{dP_{rad}}{dr} = \frac{16\sigma_{SB}}{3c} T^3 \frac{dT}{dr}. \tag{234}$$

When combined with Eq. 232, we find the thermal profile equation,

$$\frac{dT}{dr} = -\frac{3\rho\kappa L(r)}{64\pi\sigma_{SB} T^3 r^2} \tag{235}$$

The Energy Equation

Eq. 235 shows that we need to know the luminosity profile in order to determine the thermal profile. In the outer photosphere we earlier required that flux is conserved (Sec. 9.2), but go far enough in and all stars (until the ends of their lives) are liberating extra energy via fusion.

Thus the next equation of stellar structure concerns the generation of energy within a star. As with the equation of motion, we will first begin with a simple case of equilibrium. In this case, we are concerned with the thermodynamics of the star: this is the equation for Thermal Equilibrium, or a constant flow of heat with time for a static star (a situation in which there is no work being done on any of our mass shells).

Consider the shell dm shown in Fig. 24. Inside of this shell we define a quantity ϵ_m that represents the net local gain of energy per time per unit mass (SI units of J s^{-1} kg^{-1}) due to local nuclear processes. Note that sometimes the volumetric power ϵ_r will also sometimes be used, but the power per unit mass ϵ_m is generally the more useful form. Regardless, we expect either ϵ to be very large deep in the stellar core and quickly go to zero in the outer layers where fusion is negligible – in those other regions, $\epsilon = 0$, L is constant, and we are back in the flux-conserving atmosphere of Sec. 9.2.

We then consider that the energy per time entering the shell is L_r (note that like M_r, this is now a local and internal rather than global or external property: it can be thought of as the luminosity of the star as measured at a radius r inside the star) and the energy per time that exits the shell is now $L_r + dL_r$ due to this local gain from nuclear burning in the shell. To conserve energy, we must then have (note that these are total rather than partial derivatives as there is no variation with time):

$$\frac{dL_r}{dm} = \epsilon_m. \tag{236}$$

This is the equation for **Thermal Equilibrium** in a star. While Thermal Equilibrium and Hydrostatic Equilibrium are separate conditions, it is generally unlikely that a star will be in Thermal Equilibrium without already being in Hydrostatic equilibrium, thus guaranteeing that there is no change in the energy flow in the star with time or with work being done. In general, Thermal Equilibrium and Eq. 236 require that any local energy losses in the shell (typically from energy propagating outward in the star) are exactly balanced by the rate of energy production in that shell due to nuclear burning. On a

macroscopic scale, it means that the rate at which energy is produced in the center of the star is exactly equal to the star's luminosity: the rate at which that energy exits the surface.

How likely is it that a star satisfies this requirement? While a star may spend most of its life near Thermal Equilibrium while it is on the main sequence, most of the evolutionary stages it goes through do not satisfy Eq. 236: for example, pre-main sequence evolution (protostars) and post-main sequence evolution (red giants). How can we describe conservation of energy for an object that is not in Thermal equilibrium?

Following standard texts (e.g., Prialnik), we can make use of u, the internal energy density in a shell in our star. We can change u either by doing work on the shell, or by having it absorb or emit heat. We have already described how the heat in the shell can change with L_r and ϵ_m. Similarly, the incremental work done on the shell can be defined as a function of pressure and the incremental change in volume:

(237)
$$dW = -PdV$$

(238)
$$= -P\left(\frac{dV}{dm}dm\right)$$

(239)
$$= -P\ d\left(\frac{1}{\rho}\right)dm$$

The change in internal energy per unit mass (du) is equal to the work done per unit mass ($\frac{dW}{dm}$), so finally we can rewrite Eq. 239 as:

(240) $$du = -Pd\left(\frac{1}{\rho}\right)$$

Taking the time derivative of each side,

(241) $$\frac{du}{dt} = -P\frac{d}{dt}\left(\frac{1}{\rho}\right)$$

Compression of the shell will decrease dV, and thus require energy to be added to the shell, while expansion increases dV and is a way to release energy in the shell.

Changes in the internal energy of the shell u with time can then be described in terms of the both the work done on the shell and the changes in heat:

(242) $$\frac{du}{dt} = \epsilon_m - \frac{\partial L_r}{\partial m} - P\frac{d}{dt}\left(\frac{1}{\rho}\right)$$

The general form of Eq. 242 is the next equation of stellar structure, known either as the **Energy Equation** or the **Equation of Conservation of Energy**.

You may also sometimes see this equation written in various other forms, such as in terms of the temperature T and entropy S of the star. In this form, you then have

$$\frac{\partial L_r}{\partial m} = \epsilon_m - T\frac{dS}{dt} \tag{243}$$

Chemical Composition

An additional relationship that is useful for determining stellar evolution is the change in a star's composition.This relation will be less of an 'equation' for the purposes of this class, and more a rough depiction of how the composition of a star can vary with time.

We can define the composition of a star using a quantity called the mass fraction of a species:

$$X_i = \frac{\rho_i}{\rho}. \tag{244}$$

Here, ρ_i is the partial density of the i^{th} species.

Particles in a star are defined by two properties: their baryon number $\mathcal{A}$ (or the number of total protons and neutrons they contain) and their charge $\mathcal{Z}$. Using the new notation of baryon number, we can rewrite

$$n = \frac{\rho}{\bar{m}}, \tag{245}$$

as the corresponding partial number density of the i^{th} species:

$$n_i = \frac{\rho_i}{\mathcal{A}_i\, m_H}. \tag{246}$$

We can then slightly rewrite our expression for the composition as

$$X_i = n_i \frac{\mathcal{A}_i}{\rho} m_H. \tag{247}$$

Changes in composition must obey (at least) two conservation laws. Conservation of charge:

$$\mathcal{Z}_i + \mathcal{Z}_j = \mathcal{Z}_k + \mathcal{Z}_l. \tag{248}$$

and conservation of baryon number:

$$\mathcal{A}_i + \mathcal{A}_j = \mathcal{A}_k + \mathcal{A}_l. \tag{249}$$

If you also consider electrons, there must also be a conservation of lepton number.

Without attempting to go into a detailed formulation of an equation for the rate of change of X we can see that it must depend on the starting composition and the density, and (though it does not explicitly appear in these equations) the temperature, as this will also govern the rate of the nuclear reactions responsible for the composition changes (analogous to the collision timescale $t_{col} = \frac{v}{nA}$ as shown in Figure 31, in which the velocity of particles is set by the gas temperature). This leads us to our last 'equation' of stellar structure, which for us will just be a placeholder function **f** representing that the change in composition is a function of these variables:

$$\dot{\mathbf{X}} = \mathbf{f}(\rho, T, \mathbf{X}). \tag{250}$$

Technically, this **X** is a vector representing a series of equations for the change of each X_i.

The final fundamental relation we need in order to derive the structure of a star is an expression for the temperature gradient, which will be derived a bit later on.

11.3 *Pressure*

We have already seen a relationship for the gas pressure for an ideal gas, $P = nkT$. However, now that we have begun talking more about the microscopic composition of the gas we can actually be more specific in our description of the pressure. Assuming the interior of a star to be largely ionized, the gas will be composed of ions (e.g., H^+) and electrons. Their main interactions ('collisions') that are responsible for pressure in the star will be just between like particles, which repel each other due to their electromagnetic interaction. As a result, we can actually separate the gas pressure into the contribution from the ion pressure and the electron pressure:

$$P_{gas} = P_e + P_{ion} \tag{251}$$

For a pure hydrogen star, these pressures will be equivalent, however as the metallicity of a star increases, the electron pressure will be greater than the ion pressure, as the number of free electrons per nucleon will go up (for example, for helium, the number of ions is half the number of electrons).

Assuming that both the ions and electrons constitute an ideal gas, we can rewrite the ideal gas equation for each species:

$$P_e = n_e kT \tag{252}$$

and

$$P_{ion} = n_{ion} kT \tag{253}$$

However, this is not the full story: there is still another source of pressure in addition to the gas pressure that we have not been considering: the pressure from radiation.

Considering this pressure then at last gives us the total pressure in a star:

$$P = P_{ion} + P_e + P_{rad} \tag{254}$$

We can determine the radiation pressure using an expression for pressure that involves the momentum of particles:

$$P = \frac{1}{3} \int_0^\infty v\ p\ n(p)\ dp \tag{255}$$

Here v is the velocity of the particles responsible for the pressure, p is their typical momentum, and $n(p)$ is the number density of particles in the momentum range $(p, p + dp)$. We first substitute in values appropriate for photons ($v = c$, $p = \frac{h\nu}{c}$). What is $n(p)$? Well, we know that the Blackbody (Planck) function (Equation 49) has units of energy per volume per interval of frequency per steradian. So, we can turn this into number of particles per volume per interval of momentum by (1) dividing by the typical energy of a particle (for a photon, this is $h\nu$), then (3) multiplying by the solid angle 4π, and finally (4) using $p = \frac{E}{c}$ to convert from energy density to momentum density.

$$P_{rad} = \frac{1}{3}\ 4\pi \int_0^\infty c \left(\frac{h\nu}{c}\right) \left(\frac{1}{h\nu}\right) \left(\frac{1}{c}\right) \frac{2h\nu^3}{c^2} \left[e^{\frac{h\nu}{kT}} - 1\right]^{-1} d\nu \tag{256}$$

Putting this all together,

$$P_{rad} = \frac{1}{3}\ \left(\frac{4}{c}\right) \left[\pi \int_0^\infty \left(\frac{1}{c}\right) \frac{2h\nu^3}{c^2} \left[e^{\frac{h\nu}{kT}} - 1\right]^{-1} d\nu\right] \tag{257}$$

Here, the quantity in brackets is the same integral that is performed in order to yield the Stefan-Boltzmann law (Equation 79). The result is then

$$P_{rad} = \frac{1}{3}\ \left(\frac{4}{c}\right) \sigma T^4 \tag{258}$$

The quantity $\frac{4\sigma}{c}$ is generally defined as a new constant, a.

We can also define the specific energy (the energy per unit mass) for radi-

ation, using the relation

$$u_{rad} = 3\frac{P_{rad}}{\rho} \tag{259}$$

When solving problems using the Virial theorem, we have encountered a similar expression for the internal energy of an ideal gas:

$$KE_{gas} = \frac{3}{2}NkT \tag{260}$$

From the ideal gas law for the gas pressure ($P = nkT$), we can see that the specific internal energy $\frac{KE}{\bar{m}}$ then can be rewritten in a similar form:

$$u_{gas} = \frac{P_{gas}}{\rho} \tag{261}$$

11.4 *The Equation of State*

In a star, an equation of state relates the pressure, density, and temperature of the gas. These quantities are generally dependent on the composition of the gas as well. An **equation of state** then has the general dependence $P = P(\rho, T, X)$. The simplest example of this is the ideal gas equation. Inside some stars radiation pressure will actually dominate over the gas pressure, so perhaps our simplest plausible (yet still general) equation of state would be

$$P = P_{gas} + P_{rad} \tag{262}$$

$$= nkT + \frac{4F}{3c} \tag{263}$$

$$= \frac{\rho kT}{\mu m_p} + \frac{4\sigma_{SB}}{3c}T^4 \tag{264}$$

where μ is now the **mean molecular weight per particle** – e.g., $\mu = 1/2$ for fully ionized H.

But a more general and generally applicable equation of state is often that of an adiabatic equation of state. As you might have encountered before in a physics class, an adiabatic process is one that occurs in a system without any exchange of heat with its environment. In such a thermally-isolated system, the change in internal energy is due only to the work done on or by a system. Unlike an isothermal process, an adiabatic process will by definition change the temperature of the system. As an aside, we have encountered both adiabatic and isothermal processes before, in our description of the early stages of star formation. The initial collapse of a star (on a free-fall time scale) is a

roughly isothermal process: the optically thin cloud is able to essentially radiate all of the collapse energy into space unchecked, and the temperature does not substantially increase. However, once the initial collapse is halted when the star becomes optically thick, the star can only now radiate a small fraction of its collapse energy into space at a time. It then proceeds to contract nearly adiabatically.

Adiabatic processes follow an equation of state that is derived from the first law of thermodynamics: for a closed system, the internal energy is equal to the amount of heat supplied, minus the amount of work done.

As no heat is supplied, the change in the specific internal energy (energy per unit mass) u comes from the work done by the system. We basically already derived this in Equation 240:

$$du = -Pd\left(\frac{1}{\rho}\right) \tag{265}$$

As we have seen both for an ideal gas and from our expression for the radiation pressure, the specific internal energy is proportional to $\frac{P}{\rho}$:

$$u = \phi\frac{P}{\rho} \tag{266}$$

Where ϕ is an arbitrary constant of proportionality. If we take a function of that form and put it into Equation 265 we recover an expression for P in terms of ρ for an adiabatic process:

$$P \propto \rho^{\frac{\phi+1}{\phi}} \tag{267}$$

We can rewrite this in terms of an adiabatic constant K_a and an adiabatic exponent γ_a:

$$P = K_a\rho^{\gamma_a} \tag{268}$$

For an ideal gas, $\gamma_a = \frac{5}{3}$.

This adiabatic relation can also be written in terms of volume:

$$PV^{\gamma_a} = K_a \tag{269}$$

This can be compared to the corresponding relationship for an ideal gas, in which PV = constant.

11.5 *Summary*

In summary, we have a set of coupled stellar structure equations (Eq. 227, Eq. 231, Eq. 235, Eq. 242, and Eq. 268):

$$\frac{dr}{dm} = \frac{1}{4\pi r^2 \rho} \tag{270}$$

$$\ddot{r} = -\frac{Gm(r)}{r^2} - 4\pi r^2 \frac{\partial P}{\partial m}. \tag{271}$$

$$\frac{dT}{dr} = -\frac{3\rho\kappa L(r)}{64\pi\sigma_{SB} T^3 r^2} \tag{272}$$

$$\frac{du}{dt} = \epsilon_m - \frac{\partial L_r}{\partial m} - P\frac{d}{dt}\left(\frac{1}{\rho}\right) \tag{273}$$

$$P = K_a \rho^{\gamma_a} \tag{274}$$

If we can solve these together in a self-consistent way, we have good hope of revealing the unplumbed depths of many stars. To do this we will also need appropriate boundary conditions. Most of these are relatively self-explanatory:

$$M(0) = 0 \tag{275}$$

$$M(R) = M_{tot} \tag{276}$$

$$L(0) = 0 \tag{277}$$

$$L(R) = 4\pi R^2 \sigma_{SB} T_{\text{eff}}^4 \tag{278}$$

$$\rho(R) = 0 \tag{279}$$

$$P(R) \approx 0 \tag{280}$$

$$T(R) \approx T_{\text{eff}} \tag{281}$$

(282)

To explicitly solve the equations of stellar structure even with all these constraints in hand is still a beast of a task. In practice one integrates numerically, given some basic models (or tabulations) of opacity and energy generation.

12 Stability, Instability, and Convection

Now that we have the fundamental equations of stellar structure, we would like to examine some interesting situations in which they apply. One such interesting regime is the transition from stable stars to instability, either in a part of the star or throughout its interior. We will examine this by answering the following question: if we perturb the system (or a part of it), does it settle back into equilibrium?

12.1 *Thermal stability*

Suppose we briefly exceed thermal equilibrium; what happens? In equilibrium, the input luminosity from nuclear burning balances the energy radiated away:

$$\frac{dE_{\rm tot}}{dt} = L_{\rm nuc} - L_{\rm rad} = 0 \tag{283}$$

If the star briefly overproduces energy, then (at least briefly) $L_{\rm nuc} > L_{\rm rad}$ and we overproduce a clump ΔE of energy. Over a star's main-sequence lifetime its core temperature steadily rises, so this slight imbalance is happening all the time. Whenever it does, the star must be responding on the photon diffusion timescale, $\tau_{\gamma,\rm diff} \approx 10^4$ yr... but how?

From the virial theorem, we know that

$$\Delta E = -\Delta E_{\rm th} = \frac{1}{2}\Delta E_{\rm grav} \tag{284}$$

So if nuclear processes inject an extra ΔE into the star, we know we will *lose* an equivalent amount ΔE of thermal energy and simultaneously *gain* $2\Delta E$ of gravitational energy. Thus the star must have cooled, and – since its mass has not appreciably changed –its radius must have expanded.

Of the two, the temperature change is the more relevant for thermal stability because nuclear reaction rates depend very sensitively on temperature. For Sun-like stars, $\epsilon \propto T^{16}$ – so even a slight cooling will strongly diminish the nuclear energy production rate and will tend to bring the star back into thermal equilibrium. This makes sense, because stars are stable during their slow, steady evolution on the main sequence.

12.2 *Mechanical and Dynamical Stability*

Suppose that a fluid element of the star is briefly pushed away from hydrostatic equilibrium; what happens? We expect the star to respond on the dynamical timescale, $\tau_{\rm dyn} \approx 30$ min... but how?

Let's consider a toy model of this scenario, in which we squeeze the star slightly and see what happens. (A full analysis would require us to compute a full eigenspectrum of near-equilibrium Navier-Stokes equations, and is definitely beyond the scope of our discussion here.) If we start with Eq. 228, we

can integrate to find $P(M)$:

(285)
$$P(M) = \int_0^P dP$$

(286)
$$= \int_{M_{\rm tot}}^{M} \frac{dP}{dM} dM$$

(287)
$$= -\int_{M_{\rm tot}}^{M} \frac{GM}{4\pi r^4} dM$$

Initially, in equilibrium the gas pressure must be equal to the pressure required to maintain hydrostatic support – i.e., we must have $P_{hydro} = P_{gas}$.

If we squeeze the star over a sufficiently short period of time (shorter than the thermal diffusion timescale), heat transfer won't occur during the squeezing and so the contraction is adiabatic. If the contraction is also homologous, then we will have

$r \longleftrightarrow r' = r(1-\epsilon)$

$\rho \longleftrightarrow \rho' = \rho(1+3\epsilon)$

How will the star's pressure respond? Since the contraction was sufficiently rapid, we have an adiabatic equation of state

(288) $P \propto \rho^{\gamma_{ad}}$,

where

(289) $\gamma_{ad} \equiv \frac{c_P}{c_V}$

where c_P and c_V are the heat capacities at constant pressure and volume, respectively. Statistical mechanics shows that we have $\gamma_{ad} = 5/3$ for an ideal monoatomic gas, and $4/3$ for photon radiation (or a fully relativistic, degenerate gas).

Thus our perturbed star will have a new internal gas pressure profile,

(290)
$$P'_{gas} = P_{gas}(1+3\epsilon)^{\gamma_{ad}}$$

(291)
$$\approx P_{gas}(1+3\gamma_{ad}\epsilon)$$

Will this new gas pressure be enough to maintain hydrostatic support of the star? To avoid collapse, we need $P_{gas} > P_{hydro}$ always. We know from Eq. 287 that the new *hydrostatic* pressure required to maintain equilibrium

will be

(292)
$$P'_{hydro} = -\int_{M_{\rm tot}}^{M} \frac{GM}{4\pi(r')^4} dM$$

(293)
$$= -(1+4\epsilon)\int_{M_{\rm tot}}^{M} \frac{GM}{4\pi r^4} dM$$

(294)
$$= (1+4\epsilon)P_{hydro}$$

Thus our small perturbation may push us out of equilibrium! The new pressures are in the ratio

(295) $$\frac{P'_{gas}}{P'_{hydro}} \approx \frac{1+3\gamma_{ad}\epsilon}{1+4\epsilon}$$

and so the star will only remain in equilibrium so long as

(296) $$\gamma_{ad} > \frac{4}{3}$$

This is pretty close; a more rigorous treatment of the same question yields

(297) $$\int_0^M \left(\gamma_{ad} - \frac{4}{3}\right)\frac{P}{\rho} dM > 0.$$

Regardless of the exact details, Eqs. 296 and 297 indicate that a star comes ever closer to collapse as it becomes more fully supported by relativistic particles (whether photon radiation, or a relativistic, degenerate gas).

The course reading from Sec. 3.6 of Prialnik shows another possible source of instability, namely via partial ionization of the star. γ_{ad} can also drop below $4/3$, thus also leading to collapse, via the reaction $\mathrm{H} \longleftrightarrow \mathrm{H}^+ + \mathrm{e}^-$.

In this reaction, both c_v and c_P change because added heat can go into ionization rather then into increasing the temperature. c_v changes more rapidly than c_P, so γ_{ad} gets smaller (as low as 1.2 or so). Qualitatively speaking, a stellar contraction reverses some of the ionization, reducing the number of particles and also reducing the pressure opposing the initial squeeze. As in the relativistic support case, when $\gamma_{ad} \leq 4/3$, the result is instability.

12.3 *Convection*

Not all structural instabilities lead to stellar collapse. One of the most common instabilities is almost ubiquitous in the vast majority of stars: convection. **Convection** is easily visualized by bringing a pot of water to a boil, and dropping in dark beans, rice grains, or other trace particles. We will now show how the

same situation occurs inside of stars.

Convection is one of several dominant modes of energy transport inside of stars. Up until now, we have considered energy transport only by radiation, as described by Eq. 235,

$$\frac{dT}{dr} = -\frac{3\rho\kappa L(r)}{64\pi\sigma_{SB}T^3r^2}. \tag{298}$$

In a few cases energy can also be transported directly by conduction, which is important in the dense, degenerate white dwarfs and neutron stars. Whereas radiation transports heat via photon motions and conduction transports heat through microscopic particle motion, convection transports heat via bulk motions of large parcels of gas or fluid.

When a blob of stellar material is pushed upwards by some internal perturbation, how does it respond: will it sink back down, or continue to rise? Again, a consideration of different timescales is highly relevant here. An outward motion typically corresponds to a drop in both pressure and temperature. The pressure will equilibrate on $\tau_{dyn} \approx 30$ min, while heat will flow on the much slower $\tau_{\gamma,diff} \approx 10^4$ yr. So the motion is approximately adiabatic, and a rising blob will transport heat from the lower layers of the star into the outer layers.

The fluid parcel begins at r with some initial conditions $P(r)$, $\rho(r)$, and $T(r)$. After moving outward to $(r + dr)$ the parcel's temperature will remain unchanged even as the pressure rapidly equilibrates, so that the new pressure $P'(r + dr) = P(r + dr)$. Meanwhile (as in the previous sections) we will have an adiabatic equation of state (Eq. 288), which determines the parcel's new density ρ'.

The gas parcel will be stable to this radial perturbation so long as $\rho' > \rho(r + dr)$. Otherwise, if the parcel is less dense than its surroundings, it will be like a child's helium balloon and continue to rise: instability! A full analysis shows that this stability requirement can be restated in terms of P and ρ as

$$\left(\frac{dP/dr}{d\rho/dr}\right) < \frac{dP}{d\rho}|_{\text{adiabatic}} \tag{299}$$

$$< \gamma_{ad}\frac{P}{\rho}. \tag{300}$$

Since dP/dr and $d\rho/dr$ are both negative quantities, this can be rearranged as

$$\frac{\rho}{\gamma_{ad}P}\frac{dP}{dr} > \frac{d\rho}{dr}. \tag{301}$$

If we also assume that the stellar material is approximately an ideal gas, then

$P = \rho kT/\mu m_p$ and so

$$\left|\frac{dT}{dr}\right| < \frac{T}{P}\left|\frac{dP}{dr}\right|\left(1 - \frac{1}{\gamma_{ad}}\right) \tag{302}$$

Eq. 302 is the **Schwarzschild stability criterion** against convection. The absolute magnitudes are not strictly necessary, but can help to mentally parse the criterion: as long as the thermal profile is shallower than the modified pressure profile, the star will remain stable to radial perturbations of material.

Modeling convection

Fully self-consistent models of stellar convection are an active area of research and require considerable computational resources to accurately capture the three-dimensional fluid dynamics. The simplest model of convection is to assume that the process is highly efficient – so much so that it drives the system to saturate the Schwarzschild criterion, and so

$$\frac{dT}{dr} = \frac{T}{P}\frac{dP}{dr}\left(1 - \frac{1}{\gamma_{ad}}\right) \tag{303}$$

The somewhat *ad hoc,* but long-tested, framework of **mixing length theory** (MLT) allows us to refine our understanding of convection. In MLT one assumes that gas parcels rise some standard length ℓ, deliver their heat there, and sink again. Accurately estimating ℓ can be as much art as science; at least for nearly Solar stars, ℓ can be calibrated against a host of other observations.

Another way to understand convection comes from examining the relevant equations of stellar structure. Since the star is unstable to convection when the thermal profile becomes too steep, let's consider the thermal transport equation:

$$\frac{dT}{dr} = -\frac{3}{64\pi}\frac{\rho\kappa}{\sigma_{SB}T^3}\frac{L}{r^2} \tag{304}$$

Convection may occur either when $|dT/dr|$ is especially large, or when the Schwarzschild criterion's factor of $(1 - 1/\gamma_{ad})$ is especially small:

1. **Large** κ **and/or low** T: sometimes met in the outer layers (of Sun-like stars);
2. **Large** $F \equiv L/r^2$: potentially satisfied near cores
3. **Small** γ_{ad}: near ionization layers and molecular dissociation layers.

Overall, we usually see convection across a range of stellar types. Descending along the main sequence, energy transport in the hottest (and most massive) stars is dominated by radiation. Stars of somewhat lower mass (but still with $M_* > M_\odot$) will retain radiative outer atmospheres but acquire interior convective regions. By the time one considers stars of roughly Solar mass, we see a convective exterior that surrounds an internal radiative core. Many years of Solar observations shows the outer surface of the Sun bubbling away,

just like a boiling pot. Large, more evolved stars (e.g., red giants) also have convective outer layers; in these cases, the size of the convective cells $\ell \gtrsim R_\odot$!

As one considers still lower masses along the main sequence, the convection region deepens; below spectral types of M2V-M3V, the stars become **fully convective** — i.e., $\ell = R_*$. The Gaia DR2 color-magnitude diagram shows a narrow break in the main sequence which is interpreted as a direct observational signature of the onset of full convection for these smallest, coolest stars. These stars therefore have a fully adiabatic equation of state throughout their interior.

12.4 *Another look at convection vs. radiative transport*

Again, we already know that radiative transport is the default mechanism for getting energy from a star's center to its surface. However, it turns out that within a star, a second mechanism can take over from radiative transport and become dominant. To understand when this happens, we need to bring back two concepts we have previously discussed.

First, we have the temperature gradient. We will use the version that defines the temperature change as a function of radius:

$$\frac{dT}{dr} = -\frac{3}{4ac}\frac{\kappa\rho}{T^3}\frac{L_r}{4\pi r^2} \tag{305}$$

Second, we have the definition of an adiabatic process: a process in which no heat is exchanged between a system and its environment.

Again, we begin by considering a blob of gas somewhere within a star. It has a temperature T_{blob} and is surrounded by gas at an ambient, local temperature T_*. At this point, they are in thermal equilibrium so that $T_{blob} = T_*$. What happens if this blob is given a quick nudge upward so that now it is warmer than the gas around it: $T_{blob} > T_*$? Just as warm air does, we expect that it will rise. In order for the blob to stop rising, it must become cooler than its environment.

There are two ways for our blob to cool. One way is for it to radiate (that is, exchange heat with its environment). The other way is for it to do work on its environment (essentially, to expand in order to reach pressure equilibrium with its surroundings). Which one is going to be more effective in a star? To answer this, we can just look at time scales. Heat exchange will occur on a roughly thermal (or Kelvin-Helmholtz) time scale. For the sun, this time scale is on the order of ten million years. In contrast, work can be done on the blob's environment on a dynamical time scale (technically, the sound-crossing time scale, as this work is done by the expansion of the blob due to pressure). For the sun, this time scale is only about 30 minutes. The enormous difference in magnitude of these scales suggests that there will be almost no chance for the blob to exchange heat with its environment over the time scale in which it expands to reach pressure equilibrium with its environment: our blob will expand and cool nearly entirely adiabatically.

Once the blob has expanded enough to cool down to the ambient temperature, it will cease its upward motion and become stable again. The question

is: how quickly will this happen? If an overly warm blob can quickly become cooler than the surrounding gas, then it will not travel far, and upward gas motions will be swiftly damped out. As the gas does not then move in bulk, energy in the star is transported just through the radiation field. However, if the blob cannot quickly become cooler than the ambient gas, it will rise and rise until it encounters a region where it finally satisfies this criterion. This sets up a convective zone in the star: an unstable situation that results in significant movement of gas in the star (think of a pot of water boiling). Warm gas travels upward through this region and eventually reaches the top of the convective zone (which could be the surface of the star, or a region inside the star where the physical conditions have changed significantly) where it is able to cool and return downward. Through the work that it does on its environment over this journey, it carries significant energy from the inner to the outer regions of the star. For this 'convective' zone of the star (which could be a small region or the entire star) convective transport is then the primary means by which energy is transported.

To determine whether convection will dominate, we compare the temperature gradient of the star (the ambient change in temperature as a function of radius) and the rate at which a parcel of gas will cool adiabatically (the so-called adiabatic temperature gradient). These are shown visually in Figure 25 for both convective stability and instability.

If the adiabatic temperature gradient is steeper than the temperature gradient in a star (as set by purely radiative energy transport) then the rate at which a blob of gas will rise and expand and cool will be more rapid than the rate at which the ambient gas in the star cools over the same distance. As a result, if a blob experiences a small displacement upward, it will very quickly become cooler than its surroundings, and sink back to its original position. No significant motion or convection will occur (this region is convectively stable) and the star will continue to transport energy radiatively.

However, if the adiabatic temperature gradient is shallower than the (radiative) temperature gradient in a star, then the rate at which a parcel of gas expands and cools as it rises will be slower than the rate at which the surrounding gas of the star cools over the same distance. Because of this, if a blob is displaced upward, it will remain hotter than its surroundings after it adiabatically expands to reach pressure equilibrium with its surroundings, and it will continue to rise. This sets up convection in the star: as long as the adiabatic temperature gradient is shallower than the radiative temperature gradient, the blob will rise. Only when the blob reaches an area of the star with different physics (such that the temperature gradient becomes shallower than the adiabatic gradient) will it stop rising. The region in which

$$\left(\frac{dT}{dr}\right)_{ad} < \left(\frac{dT}{dr}\right)_{*} \tag{306}$$

defines the convective zone and the region in which convection dominates the energy transport.

Convection can then be favored in several ways. One way is through mak-

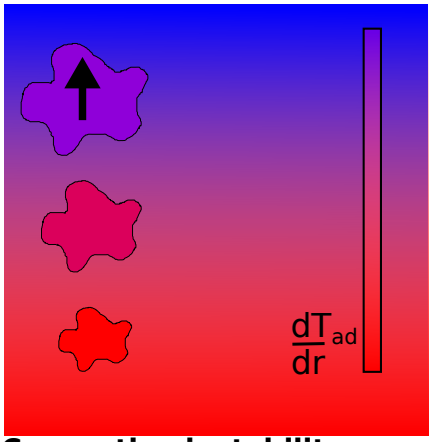

Convective instability
The adiabatic temperature gradient is shallower than the ambient temperature gradient

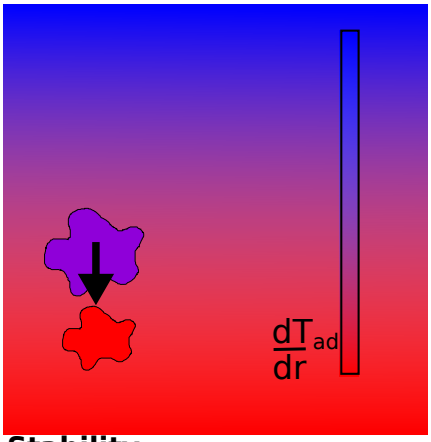

Stability
The adiabatic temperature gradient is steeper than the ambient temperature gradient

Figure 25: **Left**: An illustration of convective instability in a star. The ambient (background) temperature gradient, set by radiative transport of energy in the star, is steeper than the rate at which a parcel of gas can cool adiabatically. Because of this, a parcel of gas that becomes slightly warmer than the gas around it will rise uncontrollably, resulting in convection, which then is responsible for transporting energy in that region of the star. **Right**: An illustration of a stable situation. The ambient (background) temperature gradient, is shallower than the rate at which a parcel of gas can cool adiabatically. Because of this, a parcel of gas that becomes slightly warmer than the gas around it will very quickly become cooler than the gas around it, and will not rise significantly. In this situation, radiative energy transport dominates.

ing the adiabatic temperature gradient more shallow (this is set by the equation of state for the gas, and requires a deviation from the ideal gas law that lowers the adiabatic exponent). While this can and does occur, it is beyond the scope of this class, so we will not consider this in more detail. Alternatively then, we can ask what causes the temperature gradient of a star to steepen? Looking at Equation 305, we can see that the temperature gradient in a star is proportional to a number of variables, including the opacity κ and the energy flux L_r. Regions of high opacity are in fact a significant cause of convective zones in stars. As we saw in Section 7.1, many of the processes that cause opacity in stars favor conditions in which there are bound electrons. This will occur in cooler regions of a star, particularly in regions where the gas (Hydrogen or Helium) is only partially ionized. In fact, partially ionized gas also has a slightly lower adiabatic exponent than fully ionized gas, which further contributes to the development of convective instability. The sun's outer layers are convective for these reasons (its core is radiative, as this region is fully ionized). Cooler stars like red dwarfs are actually fully convective from their

core to surface. As we will discuss further when we reach the topic of nuclear burning in stars, nuclear processes that release substantial amounts of energy can significantly increase L_r and thus also drive convection. This is the reason that stars more massive than the sun (which have a slightly different fusion reaction occurring) have convective cores.

Note that in defining convective instability we can also swap variables, and instead of temperature, consider the density and pressure of the blob (as both of these are connected to the temperature through our equation of state (the ideal gas equation, which is a good description of the conditions in the interior of stars). This approach is taken by Prialnik, and is the basis of the historical argument first made by Karl Schwarzschild in evaluating the convective stability of stars. Here, we assume that we have a blob that has pressure and density equal to the ambient values in the surrounding gas. When it is displaced upward, its pressure now exceeds the ambient pressure, and it expands adiabatically to reach pressure equilibrium with its surroundings. In expanding, not only has its pressure decreased, but its density as well. If the blob is now less dense than its surroundings, it will experiences a force that will displace it upward. However, if the blob remains more dense than its surroundings, it will instead experience a downward displacement force. This argument is in a sense more physical, as we are not appealing to 'warm air rising' but rather the underlying physical mechanism: the Archimedes buoyancy law. Using these variables, our condition for convective instability is now

$$\left(\frac{dP}{dr}\right)_{ad} < \left(\frac{dP}{dr}\right)_{*}. \tag{307}$$

All of this actually has an interesting application not just to stars, but to earth's atmosphere as well: the formation of thunderstorms! The formation of extremely tall (up to 12 miles!) clouds that lead to severe thunderstorms and tornadoes are driven by a convective instability in earth's lower atmosphere. The conditions that lead to this convective instability can be measured, and factor into forecasts of severe weather outbreaks. The criterion for convective instability is exactly the same as we just discussed for stars: the adiabatic temperature gradient, or the rate at which a parcel of gas displaced from ground level will cool as it rises, must be less than the temperature gradient (or profile) of the atmosphere:

$$\left(\frac{dT}{dr}\right)_{ad} < \left(\frac{dT}{dr}\right)_{atm} \tag{308}$$

The conditions that lead to thunderstorms have two things going on that make this more likely. First, weather systems that lead to thunderstorms are typically driven by the approach of a cold air mass (a cold front) that is pushing like a wedge into the upper atmosphere. This steepens the temperature gradient of the atmosphere: problem #1. The second thing that happens in advance of these weather systems is the buildup of a moist air mass in advance

of the cold front, which drives high humidity. As you may have experienced firsthand (think of how quickly it gets cold at night in the desert, or alternatively, how warm a humid summer night can be, and how hard it is to stay cool on a humid day) air with a high moisture content is better at retaining heat, and thus cools more slowly. In essence, it has a shallower adiabatic temperature gradient: problem #2. Together, these two conditions are a recipe for strong convection. Humid air that is heated near the sunbaked ground will dramatically rise, unchecked, into the upper atmosphere, depositing energy and water vapor to make enormous, powerful cumulonimbus (thunderhead) clouds. The strength of the convection is measured by meteorologists with the CAPE (Convective Available Potential Energy) index. It measures this temperature differential, and uses it to determine how strong the upward buoyancy force will be. An extremely large CAPE for a given region could be a reason to issue a tornado watch.

12.5 *XXXX – extra material on convection in handwritten notes*

13 Polytropes

Much of the challenge in making self-consistent stellar models comes from the connection between T and L. The set of so-called **polytrope models** derives from assuming that we can just ignore the thermal and luminosity equations of stellar structure. This assumption is usually wrong, but it is accurate in some cases, useful in others, and historically was essential for making early progress toward understanding stellar interiors. A polytrope model assumes that for some proportionality constant K and index γ (or equivalently, n),

(309)
$$P = K\rho^{\gamma}$$

(310)
$$= K\rho^{1+1/n}$$

We have already discussed at least two types of stars for which a polytrope is an accurate model. For fully convective stars, energy transport is dominated by bulk motions which are essentially adiabatic (since $\tau_{dyn} \langle \tau_{\gamma,\mathrm{diff}}$); thus $\gamma = \gamma_{ad} = 5/3$. It turns out that the same index also holds for degenerate objects (white dwarfs and neutron stars); in the non-relativistic limit these also have $\gamma = 5/3$, even though heat transport is dominated by conduction not convection. When degenerate interiors become fully relativistic, γ approaches $4/3$ and (as we saw previously) the stars can come perilously close to global instability.

The key equation in polytrope models is that of hydrostatic equilibrium (Eq. 192),

$$\frac{dP}{dr} = -\frac{GM}{r^2}\rho$$

which when rearranged yields

(311) $$\frac{r^2}{\rho}\frac{dP}{dr} = -GM.$$

Taking the derivative of each side, we have

(312) $$\frac{d}{dr}\left(\frac{r^2}{\rho}\frac{dP}{dr}\right) = -GdM,$$

and substituting in the mass-radius equation (Eq. 227) for dM gives

(313) $$\frac{1}{r^2}\frac{d}{dr}\left(\frac{r^2}{\rho}\frac{dP}{dr}\right) = -4\pi G\rho.$$

It is then customary to define the density in terms of a dimensionless density function $\phi(r)$, such that

(314) $$\rho(r) = \rho_c \phi(r)^n$$

and n is the polytrope index of Eq. 310. Note that $\phi(r=0)=1$, so ρ_c is the density at the center of the star, while $\phi(r=R)=0$ defines the stellar surface. Combining Eq. 314 with Eq. 310 above gives

$$P(r) = K\rho_c^{1+1/n}\phi(r)^{n+1}. \tag{315}$$

Plugging this back into Eq. 313 and rearranging yields the formidable-looking

$$\lambda^2 \frac{1}{r^2}\frac{d}{dr}\left(r^2\frac{d\phi}{dr}\right) = -\phi^n \tag{316}$$

where we have defined

$$\lambda = \left(\frac{K(n+1)\rho_c^{1/n-1}}{4\pi G}\right)^{1/2}. \tag{317}$$

When one also then defines

$$r = \lambda\xi, \tag{318}$$

then we finally obtain the famous **Lane-Emden Equation**

$$\frac{1}{\xi^2}\frac{d}{d\xi}\left(\xi^2\frac{d\phi}{d\xi}\right) = -\phi^n. \tag{319}$$

The solutions to the Lane-Emden equation are the set of functions $\phi(\xi)$, each of which corresponds to a different index n and each of which completely specifies a star's density profile in the polytrope model via Eq. 314. The solution for a given n is conventionally denoted $\phi_n(\xi)$. Each solution also determines the temperature profile $T(r)$ (as you will see in Problem Set 5).

What are the relevant boundary conditions for $\phi(\xi)$, and what are the possible values of this dimensionless ξ anyway? Well, just as with $\phi(r)$ we must also have that $\phi(\xi=0)=1$, and analogously we will have $\phi(\xi=\xi_{\rm surf})=0$. As for $\xi_{\rm surf}$ (the value of ξ at the stellar surface), its value will depend on the particular form of the solution, $\phi(\xi)$. A final, useful boundary condition is that we have no cusp in the central density profile – i.e., the density will be a smooth function from $r=+\epsilon$ to $-\epsilon$. So our boundary conditions are thus

$$\phi(\xi=0)=1 \tag{320}$$

$$\phi(\xi=\xi_{\rm surf})=0 \tag{321}$$

$$\frac{d\phi}{d\xi}|_{\xi=0}=0 \tag{322}$$

Just three analytic forms of $\phi(\xi)$ exist, corresponding to $n=0,\ 1,\ 5$. So-

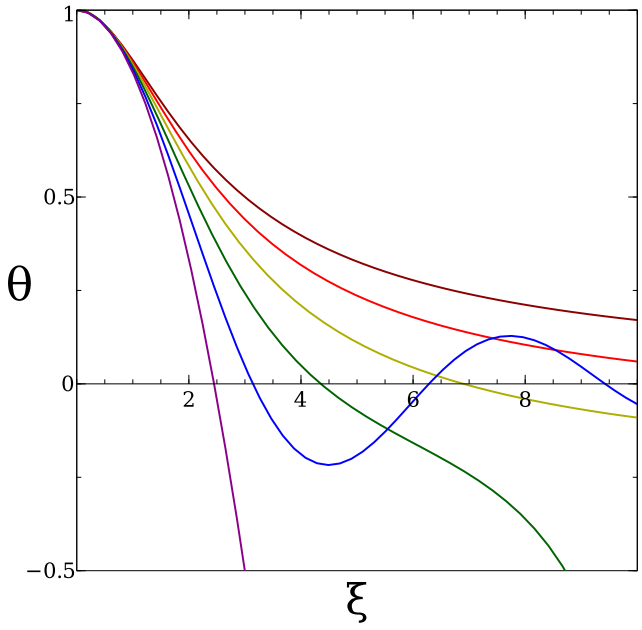

Figure 26: Solutions to the Lane-Emden Equation, here denoted by θ instead of ϕ, for $n = 0$ (most concentrated) to 5 (least concentrated). The applicability of each curve to stellar interiors ends at the curve's first zero-crossing. Figure from Wikipedia, used under a Creative Commons CCO 1.0 license.

lutions give finite stellar mass only for $n \leq 5$. Textbooks on stellar interiors give examples of these various solutions. One example is $n = 1$, for which the solution is

$$\phi_1(\xi) = a_0 \frac{\sin \xi}{\xi} + a_1 \frac{\cos \xi}{\xi} \tag{323}$$

where a_0 and a_1 are determined by the boundary conditions. A quick comparison to those conditions, above, shows that the solution is

$$\phi_1(\xi) = \frac{\sin \xi}{\xi} \tag{324}$$

which is the well-known sinc function. For a reasonable stellar model in which ρ only decreases with increasing r, this also tells us that for $n = 1$, $\xi_{\rm surf} = \pi$.

The point of this dense thicket of ϕ's and ξ's is that once n is specified, you only have to solve the Lane-Emden equation once. (And this has already been done – Fig. 26 shows the solutions for $n = 0$ to 5.) Merely by scaling K and ρ_c one then obtains an entire family of stellar structure models for each ϕ_n – each model in the family has its own central density and total mass, even though the structure of all models in the family (i.e., for each n) are homologously related.

13.1 *XXXX – extra material in handwritten notes*

14 An Introduction to Nuclear Fusion

14.1 *Useful References*

- Choudhuri, Secs. 4.1–4.2
- Kippenhahn, Weiger, and Weiss, 2nd ed., Chap. 18
- Hansen, Kawaler, and Trimble, Sec. 6.2

14.2 *Introduction*

Commercial nuclear fusion may be perpetually 50 years away, but stellar fusion has powered the universe for billions of years and (for the lowest-mass stars) will continue to do so for trillions of years to come.

Our two goals here are (1) to understand ϵ, the volumetric energy production rate (see Eq. 242), and how it depends on ρ and T; and (2) to identify and describe the key nuclear reaction pathways that are important in stars.

14.3 *Nuclear Binding Energies*

Stars derive their energy from the fusion of individual atomic nuclei, as we described briefly in Sec. 10.6. Fusion involves true elemental transmutation of the sort that the ancients could only dream of. For better or for worse, our own discussions of this natural alchemy will involve relatively more considerations of the detailed physics involved and relatively less boiling of one's own urine.

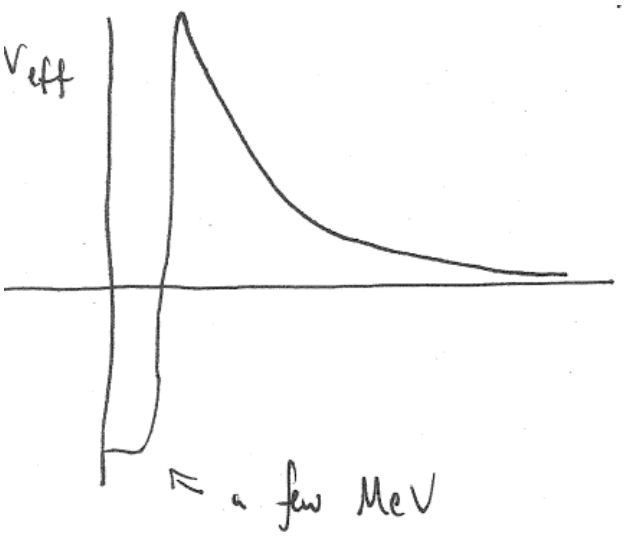

Figure 27: Rough sketch of the nuclear potential. Coulomb repulsion dominates at large separations, and is overwhelmed by Strong nuclear attraction at the smallest separations.

For one nucleus to reach another and fuse, it must overcome the strong Coulomb repulsion generated by the two positively-charged nuclei. Fig. 27 gives a rough sketch of the situation: Coulomb repulsion dominates at large separations, but it is overwhelmed by Strong nuclear attraction at the smallest separations. The fundamental nuclear size is set by the typical radius of protons and neutrons, $r_p \approx r_n \approx 0.8$ fm, as

$$r_{\rm nuc} \approx 2 r_p A^{1/3} \tag{325}$$

where A is the number of nucleons (neutrons plus protons, also approximately the atomic weight). We will also deal shortly with Z, the nuclear charge (i.e., number of protons).

The key thing that matters is the nuclear binding energy. Strong force has typical binding energies of a few MeV per nucleon. For astrophysical purposes we don't need to descend all the way into the realm of detailed nuclear physics. For our purposes an empirically-calibrated, semiclassical model (the "Bethe-Weizsäcker formula) is sufficiently accurate. This posits that a nucleus' binding energy E_B is

$$E_B \approx a_V A - a_S A^{2/3} - \frac{a_C Z^2}{A^{1/3}} - a_A \frac{(A-2Z)^2}{A} \tag{326}$$

Each of the terms in Eq. 326 has a particular significance. These are:

a_V	≈ 14 MeV	Volumetric term, describes bulk assembly of the nucleus.
a_S	≈ 13.1 MeV	Surface term, since surface nucleons have few neighbors.
a_C	≈ 0.58 MeV	Coulomb term, describes mutual repulsion of protons.
a_A	≈ 19.4 MeV	Asymmetry term, preferring $N_n = N_p$ (Fermi exclusion).

This model does a decent job: Eq. 326 correctly demonstrates that the nuclei with the greatest binding energy *per nucleon* have $Z \sim 25$. In fact the most tightly-bound, and thus most stable, nucleus is that of iron (Fe) with $Z = 26$, $A = 56$. Thus elements near Fe represent an equilibrium state toward which all nuclear processes will try to direct heavier or lighter atoms. For example, we will see that lighter atoms (from H on up) typically fuse into elements as high as Fe but no higher (except in unusual circumstances).

14.4 *Let's Get Fusing*

The Big Bang produced a universe whose baryonic matter was made of roughly 75% H and 25% He, with only trace amounts of heavier elements. Stellar fusion created most of the heavier elements, with supernovae doing the rest. For fusion to proceed, something must occur to either fuse H or He. Since He will have a $4\times$ greater Coulomb barrier, we'll focus on H; nonetheless we immediately encounter two huge problems.

Problem one is the huge Coulomb barrier shown in Fig. 27. At the separation of individual nucleons, the electronic (or protonic) repulsion is $e^2/\text{fm} \sim 1$ MeV, of roughly comparable scale to the strong nuclear attraction at shorter scales. But how to breach this Coulomb wall? Even at the center of the Sun where

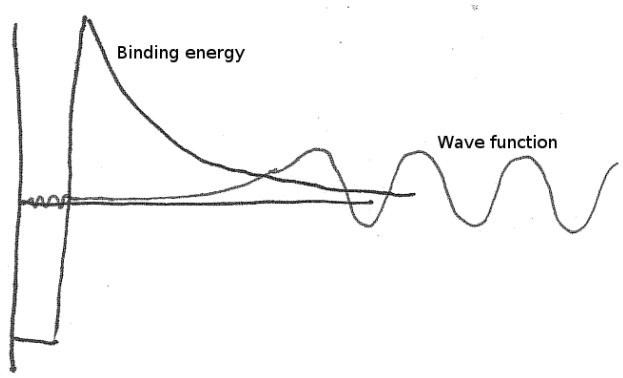

Figure 28: Rough sketch of quantum tunneling, with the wave function (just barely) penetrating the forbidding Coulomb barrier.

$T_c = 1.5 \times 10^7$ K (Sec. 10) the typical thermal energies per particle are of order $k_B T_C \sim 1$ keV — a thousand times too low. (Problem Set 5 will show that even all the way out on the tail of the Maxwell-Boltzmann distribution, there are zero nuclei in a star with thermal energy sufficient to cross the barrier.) The second problem is that the fusion product of two protons would be ^{2}He, an isotope so unstable it is not entirely clear whether it has ever been observed.

Problem one: quantum tunneling

The first problem was solved by recognizing that at the nuclear scale one doesn't climb a mountain — rather, one tunnels through it. Quantum mechanics states that each particle has a wave function $\Psi(x)$ given by the Schrödinger Equation, and the probability of finding the particle at x is $\propto |\Psi(x)|^2$. When the particle's energy is less than required to classically overcome an energy barrier, the wavefunction decays exponentially but remains nonzero. To order of magnitude, the protons only need to get close enough to each other that their thermal de Broglie wavelengths overlap; when this happens, tunneling becomes plausible (as sketched in Fig. 28).

The Coulomb barrier for two protons separated by a de Broglie wavelength λ_D (which may be substantially larger than the nucleon size of $\sim$1 fm) is

$$E_C = \frac{e^2}{\lambda_D} = \frac{e^2 p}{h}. \tag{327}$$

If the protons only need enough thermal energy to reach a separation of λ_D, then proton's required thermal momentum will be

$$p \approx \sqrt{2 m_p E_C}. \tag{328}$$

Solving for E_C, we see that

$$E_C^2 = \frac{e^4 p^2}{h^2} \approx \frac{2e^4 m_p E_C}{h^2} \tag{329}$$

and so

$$E_C \approx \frac{2e^4 m_p}{h^2}. \tag{330}$$

If the nuclei have thermal energies of order that given by Eq. 330, then quantum tunneling may happen. It turns out that E_C is of order a few keV, comparable to the thermal energy in the Sun's core.

The discussion above was merely phenomenological, but a more rigorous approach is the so-called "WKB approximation." WKB is described in more detail in advanced reference texts. Under certain fairly reasonable assumptions, the quantum wavefunction Ψ can be expressed as

$$\Psi(x) \propto \exp\left[\frac{i}{\hbar}\int \sqrt{2m\,(E - V(x)]}dx\right] \tag{331}$$

with probability $\propto |\Psi|^2$, as noted above. When one calculates the full probability by integrating from the classical turning point to the bound state, one finds that

$$P \approx e^{-bE^{-1/2}} \tag{332}$$

where

$$b = \frac{1}{\hbar} Z_1 Z_2 e^2 \sqrt{2\mu} \tag{333}$$

where μ is the reduced mass of the system. So as the typical particle energy E increases the probability of tunneling becomes exponentially more likely. On the other hand, more strongly charged particles have larger Coulomb barriers and more massive particles have smaller de Broglie wavelengths; both of these effects will tend to make tunneling more difficult to achieve.

The probability of tunneling given by Eq. 332 directly relates to the cross section for nuclear interactions $\sigma(E)$. This is given approximately by

$$\sigma(E) \approx \lambda_D^2 e^{-bE^{-1/2}} \tag{334}$$

where

$$\lambda_D = \frac{h}{p} \propto \frac{1}{\sqrt{E}}. \tag{335}$$

This is pretty close. More accurate is a very similar form:

$$\sigma(E) = \frac{S(E)}{E} e^{-bE^{-1/2}} \tag{336}$$

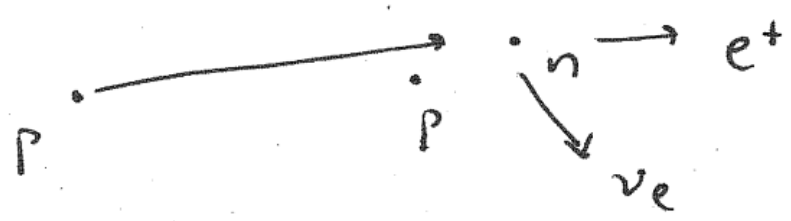

Figure 29: Rough sketch of inverse beta decay: $p + p$ yields $p + n + e^+ + \nu_e$.

where $S(E)$ is essentially a fudge factor (albeit one that varies only slowly with E).

Problem two: avoiding the ^{2}He trap

The key to our second problem (that the product of H + H, ^{2}He, is incredibly unstable) lies in the humble neutron. Given sufficient neutrons we could form the stable isotope ^{2}H (deuterium) instead of ^{2}He and open up new reaction pathways.

The challenge is that the neutron half-life is only $\sim$15 min, after which they undergo beta decay and produce $p + e^- + \bar{\nu}_e$. The opportunity lies in a related reaction, inverse beta decay. In this process (sketched in Fig. 29) two of the many, common protons interact via the weak process. The full reaction is

$$p + p \rightarrow p + n + e^+ + \nu_e \rightarrow {}^2\mathrm{H} + e^+ + \nu_e$$

and perhaps surprisingly, this can provide all the neutrons we need to produce sufficient ^{2}H to make the universe an interesting place to be. The cross-section is tiny (it's a weak process):

$$\sigma_{\mathrm{p-p}} \approx 10^{-22} \text{ barnes} = 10^{-46} \text{ cm}^2 \tag{337}$$

(recall that the electron scattering, or Thomson, cross section of Sec. 9.5 was $\sigma_T = 0.67$ barns!). Put another way, the reaction rate in the Sun will be just once per $\sim$few Gyr, per proton. But it's enough, and once we have ^{2}H we can start producing heavier (and more stable) He isotopes: fusion becomes energetically feasible. Thus the solution to the ^{2}He fusion barrier is similar in a way to the H^- story of Sec. 9.5: to get everything right required both hydrogen and some imagination.

14.5 *Reaction pathways*

With these most basic rudiments of nuclear considerations laid out, we can now start to consider some of the reaction pathways that might produce the energy we need to support the stars we see. This means that we're going to return to our volumetric energy production rate, ϵ, of Eq. 242 and determine what the quantity really means.

Imagine we have a reaction

$$\mathrm{A} + \mathrm{B} \rightarrow \mathrm{C}$$

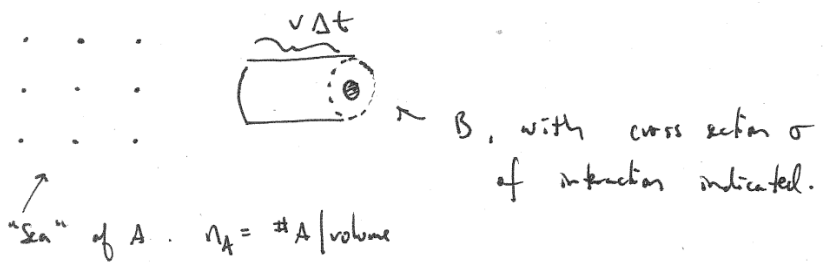

Figure 30: Particle B, moving at velocity v and impinging on a sea of particles A.

which releases Q units of energy and has some cross-section σ. What is ϵ? Fig. 30 shows the situation shortly before the reaction has occurred, with a particle B moving at speed v relative to a sea of particles A with number density n_A. In a short period of time Δt, the total volume contributing to the reaction is

(338) $V_{\text{eff}} = \sigma v \Delta t$

and so the total reaction rate (per time, per particle B) will be

(339) $\frac{n_A v \Delta t \sigma}{\Delta t} = n_A v \sigma.$

Since we have n_B B particles per volume, the volumetric reaction rate (reactions per time, per volume) will then be

(340) $r_{AB} = n_A n_B v \sigma.$

Since each interaction liberates an amount of energy Q, the volumetric power density (energy per time per volume) will then be

(341) $\epsilon = Q n_A n_B v \sigma.$

To be more accurate, we need to account for the fact that there is not a single relative velocity v but rather two separate velocity distributions (for particles A and B). Each distribution is given by Eq. 95,

$$\Phi_v = 4\pi n \left(\frac{m}{2\pi k_B T_{kin}} \right)^{3/2} v^2 \exp\left(-\frac{m v^2}{2 k_B T_{kin}} \right) dv$$

It is an intriguing (and not too onerous) exercise to show that for two species in thermal equilibrium (and at the same T) that both obey Eq. 95, then their relative velocities also follow the same distribution but with m now replaced by μ, the reduced mass.

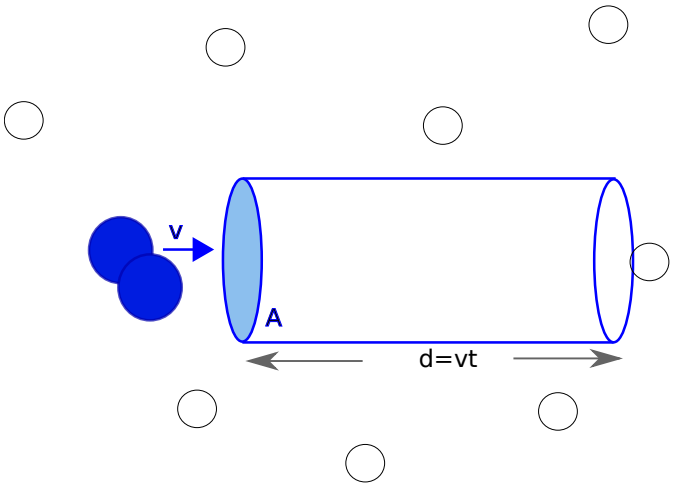

Figure 31: A diagram illustrating the probability of collision for a molecule moving at a speed v through a medium of other particles (assumed to have a number density n). The collisional cross section of the molecule is A. In this diagram, the molecule is presumed to undergo a single collision in a time t after traveling a distance d.

Alternatively, Eq. 95 can also be written in terms of energy instead of v:

$$\Phi_E = \sqrt{\frac{2}{\pi}}(k_B T)^{-3/2} E^{1/2} e^{-E/k_B T} \tag{342}$$

and it must be true that

$$\Phi_v dv = \Phi_E dE. \tag{343}$$

Then, instead of the simple Eq. 341 we have instead

$$\epsilon = Q n_A n_B \int_0^\infty \sigma(E) v(E) \Phi_E dE \tag{344}$$

where $\sigma(E)$ comes from Eq. 336 and

$$v(E) = \sqrt{2E/\mu}. \tag{345}$$

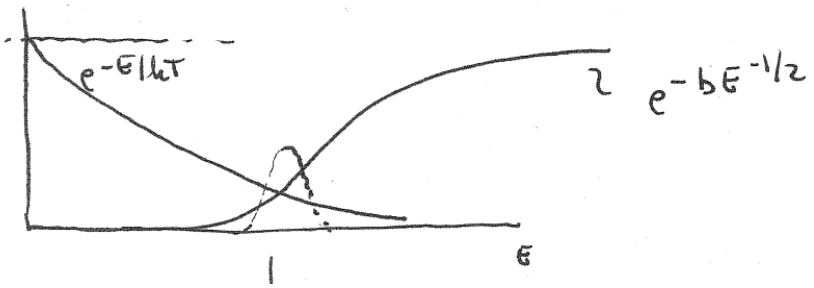

Figure 32: The two exponential terms in Eq. 347 cancel out everywhere but in a narrow region of overlap: the Gamow-Teller peak of nuclear energy production.

Neglecting everything but the T and E dependencies, we then have

(346)
$$\epsilon \propto Q n_A n_B T^{-3/2} \int_0^\infty \frac{S(E)}{E} e^{-bE^{-1/2}} E^{1/2} E^{1/2} e^{-E/k_B T} dE$$

(347)
$$\propto Q n_A n_B T^{-3/2} \int_0^\infty S(E) e^{-bE^{-1/2}} e^{-E/k_B T} dE$$

The two exponentials inside the integral combine in an interesting way. As shown in Fig. 32, they cancel each other out everywhere but in a fairly narrow energy regime. This region of overlap, where ϵ reaches its greatest value, is known as the **Gamow-Teller peak**. This feature is all that's left after we've combined the Maxwell-Boltzmann distribution with the energy needed for tunneling to proceed.

To actually solve the integral in Eq. 347 and calculate ϵ directly is more tricky. A straightforward and reasonable simplification is to approximate the Gamow-Teller peak as a normal (Gaussian) profile centered on the energy E_0 where ϵ reaches its maximum. The result is then

(348) $$\epsilon \propto Q n_A n_B T^{-2/3} S(E_0) e^{-BT_6^{-1/3}}$$

where

(349) $$B = 42.6 (Z_1 Z_2)^{2/3} \left(\frac{A_1 A_2}{A_1 + A_2} \right)^{1/3}$$

and $T_6 = T/(10^6 \mathrm{K})$.

Eq. 348 will go to zero in the limit of both large and small T, indicating that there is some optimal temperature range for any particular nuclear reaction. (Technically, this is an optimal range in T-n space.) The formula above can

also be recast in logarithmic form, by noting that

(350)
$$\ln \epsilon = -\frac{2}{3} \ln T_6 - B T_6^{-1/3} + C$$

(351)
$$= -\frac{2}{3} \ln T_6 - B \exp\left(-\frac{1}{3} \ln T_6\right) + C$$

It is common to then speak of a power index ν that describes the steepness of the dependence of ϵ on T, such that

(352) $\epsilon \propto T^{\nu}$.

The index ν can be calculated

(353) $\nu \equiv \frac{d(\ln \epsilon)}{d \ln T_6} = -\frac{2}{3} + \frac{B}{3} T_6^{-1/3}$.

For one of the main reaction chains in the Sun, $\nu \approx 3.8$ — so nuclear power generation depends fairly strongly on the central T. $\nu \approx 5$ for the lightest nuclei, and for other, much larger values of B involving more massive nuclei ν can take on much larger values, up to $n \approx 20$. This occurs in the most massive stars, which therefore show an extraordinary dependence of ϵ on T.

Traditionally the reactions described above are termed **thermonuclear** because the reaction rates and power generation depend most strongly on T. In dense environments with large compositions of heavy nuclei, electron shielding leads to an additional dependence on density as well, such that

(354) $\epsilon \propto \left(\frac{\rho}{\rho_0}\right)^{\lambda} \left(\frac{T}{T_0}\right)^{\nu}$.

One then obtains

(355) $\nu = \frac{B}{2} T_6^{-1/3} - \frac{2}{3} - \frac{E_D}{k_B T}; \;\; \lambda = 1 + \frac{1}{3} \frac{E_D}{k_B T}$

and E_D is the electrostatic energy when two nuclei are separated by the radii of their electron clouds, r_D,

(356) $E_D = \frac{Z_1 Z_2 e^2}{r_D}$.

At high densities and moderate temperatures, ν decreases and λ steepens considerably. This is the regime of **pyconuclear** reactions whose rates depend primarily on density not temperature. These conditions are typically seen in the latest stages of stellar evolution.

15 Nuclear Reaction Pathways

15.1 *Useful references*

- Choudhuri, Sec. 4.3
- Kippenhahn, Weiger, and Weiss, 2nd ed., Secs. 18.5–18.6
- Hansen, Kawaler, and Trimble, Secs. 6.3–6.8

15.2 *First fusion: the p-p chain*

For stars with $M \lesssim 1 M_\odot$, the dominant fusion pathway builds ${}^4_2\mathrm{He}$ nuclei (i.e., α particles) from individual protons, and is termed the **p-p chain**. The overall reaction can be described as

$$4p \rightarrow {}^4_2\mathrm{He} + 26.4\ \mathrm{MeV} \tag{357}$$

which liberates roughly 0.7% of the mass energy of the individual protons.

We've already encountered the first, weakest, and rate-limiting step in this process, namely

$$p + p \rightarrow {}^2_1\mathrm{H} + e^+ + \nu. \tag{358}$$

As we saw in the preceding chapter, the cross-section for this inverse beta-decay reaction is so low that a given proton will only undergo it in a $\sim$few Gyr. The next step,

$$p + {}^2_1\mathrm{H} \rightarrow {}^3_2\mathrm{He} + \gamma \tag{359}$$

happens very quickly – it takes only about 1.4 s in the Sun.

After ^{3}He is produced, there are three different pathways to ^{4}He. These are termed pp1, pp2, and pp3. You might think that in a H-dominated universe we could proceed via

$$p + {}^3_2\mathrm{He} \rightarrow {}^4_3\mathrm{Li} \tag{360}$$

and another inverse beta decay, but ^{4}Li is highly unstable and its dominant decay mode is the emission of a proton, so that gets us nowhere.

Instead, we have to use larger building blocks and build up via collisions of ${}^3_2$He. If we have a paucity of ${}^4_2$He (as was the case shortly after the Big Bang), then we must use the **pp1 pathway**:

$${}^3_2\mathrm{He} + {}^3_2\mathrm{He} \rightarrow {}^4_2\mathrm{He} + 2p \tag{361}$$

which produces roughly 70% of the total Solar luminosity.

If ${}^4_2$He is available (and especially at higher temperatures) the pp2 and pp3 pathways will dominate. These both begin via

$${}^3_2\mathrm{He} + {}^4_2\mathrm{He} \rightarrow {}^7_4\mathrm{Be} + \gamma \tag{362}$$

and then branch off. In the Sun, almost all the rest of the luminosity comes from the pp2 pathway,

(363)
$$^{7}_{4}\mathrm{Be} + e^{-} \rightarrow ^{7}_{3}\mathrm{Li} + \nu_e$$

(364)
$$^{7}_{3}\mathrm{Li} + p \rightarrow ^{4}_{2}\mathrm{He} + ^{4}_{2}\mathrm{He}.$$

Whereas $< 1\%$ of the Sun's power comes from the pp3 pathway:

(365)
$$^{7}_{4}\mathrm{Be} + p \rightarrow ^{8}_{5}\mathrm{B} + \gamma$$

(366)
$$^{8}_{5}\mathrm{B} \rightarrow ^{8}_{4}\mathrm{Be} + e^{+} + \nu_e$$

(367)
$$^{8}_{4}\mathrm{Be} \rightarrow ^{4}_{2}\mathrm{He} + ^{4}_{2}\mathrm{He}.$$

As noted above, all three pp chains convert protons into $^{4}_{2}$He and so all release the same amount of energy, 26.4 MeV per α particle. But not all of that energy goes into heating the star (and ultimately to observable electromagnetic radiation): an appreciable fraction can be carried away by the neutrinos. The neutrino produced by the pp3 decay of $^{8}_{5}$B can carry away up to 15 MeV (with an average of more like 7 MeV).

As a final aside, these pp3 neutrinos are energetic enough that they can be detected via

(368) $^{37}_{17}\mathrm{Cl} + \nu_e \rightarrow ^{37}_{18}\mathrm{Ar} + e^{-}$.

The argon produced is radioactive, and its decay can be easily detected. Neutrinos have tiny interaction cross-sections, but the chlorine needed to capture the neutrino is cheap in bulk – it's historically used in dry-cleaning.

15.3 *The triple-α process*

Via the several p-p chains, stars build up helium nuclei (α particles) from elementary hydrogen nuclei (protons). Many heavier elements now populate the universe that weren't present immediately after the Big Bang. How were they created? The trouble is that both of the next two most likely reactions are endothermic, removing energy from the star instead of contributing to it:

(369) $^{4}_{2}\mathrm{He} + ^{4}_{2}\mathrm{He} \rightarrow ^{8}_{4}\mathrm{Be} - - \mathbf{94keV}$

and

(370) $^{4}_{2}\mathrm{He} + p \rightarrow ^{5}_{3}\mathrm{Li} - - \mathbf{2MeV}$.

As with the first step in the pp chain, the solution turns out to be a relatively rare reaction; nonetheless, it is the most effective pathway available.

That is the **triple-alpha process**, in which three $^4_2$He nuclei interact almost simultaneously, forming a $^{12}_6$C nucleus. This reaction was predicted long before the reaction was known to be feasible, just because there was no other good explanation for the formation of heavier elements; it involves a resonance in the triple-α cross-section that allows this to proceed. The reaction therefore proceeds as

$$3\,{}^4_2\mathrm{He} \rightarrow {}^{12}_6\mathrm{C} + 7.5\mathrm{MeV}. \tag{371}$$

Note that whereas the pp chain has a mass-to-energy conversion efficiency of 0.7%, the triple-α process is an order of magnitude less efficient ($\sim 0.07\%$). So to support a star of given mass and temperature, the triple-α process would have to burn $\sim 10\times$ faster. This new reaction pathway also turns out be highly temperature-sensitive, with

$$\epsilon_{3\alpha} \propto T^{40} \tag{372}$$

when temperatures approach $\sim 10^8$ K.

15.4 *On Beyond ^{12}C*

Once we have ^{12}C, multiple additional pathways open up for the stellar nucleosynthesis.

The CNO cycle

The first of these, the **CNO cycle**, is an alternative to the pp chains for producing $^4_2$He from protons. However, the process here is rather less straightforward and requires the $^{12}_6$C as a kind of catalyst. Multiple variants exist, but all rely on C to produce intermediate isotopes of N and O that are then broken back down to C in the production of an α particle. One common CNO cycle proceeds as follows:

$$ {}^{12}_6\mathrm{C} + {}^1_1\mathrm{H} \rightarrow {}^{12}_7\mathrm{N} + \gamma \tag{373}$$

$$ {}^{13}_7\mathrm{N} \rightarrow {}^{13}_6\mathrm{C} + e^+ + \nu_e \tag{374}$$

$$ {}^{13}_6\mathrm{C} + {}^1_1\mathrm{H} \rightarrow {}^{14}_7\mathrm{N} + \gamma \tag{375}$$

$$ {}^{14}_7\mathrm{N} + {}^1_1\mathrm{H} \rightarrow {}^{15}_8\mathrm{O} + \gamma \tag{376}$$

$$ {}^{15}_8\mathrm{O} \rightarrow {}^{15}_7\mathrm{N} + e^+ + \nu_e \tag{377}$$

$$ {}^{15}_7\mathrm{N} + {}^1_1\mathrm{H} \rightarrow {}^{12}_6\mathrm{C} + {}^4_2\mathrm{He} \tag{378}$$

The CNO cycle does not become highly effective until temperatures are

somewhat higher than in the Sun's core. Thus at present only 1–2% of the Sun's He comes from the CNO cycle. But this ratio will increase as the Sun evolves and its central temperature steadily increases. Interestingly, the conversion of ${}^{14}_{7}\mathrm{N}$ is the slowest step and so nitrogen will tend to build up during this process; the CNO cycle is thus the source of most N.

Alpha-process and higher-order nucleosynthesis

With a sufficient abundance of ${}^{12}_{6}\mathrm{C}$ and ${}^{4}_{2}\mathrm{He}$, **alpha-process nucleosynthesis** can begin and heavier elements can be rapidly produced. This requires higher temperatures and densities (and also higher ${}^{12}_{6}\mathrm{C}$ abundances) than are found in the Sun's core, but the process becomes the dominant central energy source in the most massive stars. These reactions proceed in a much more straightforward manner than does the CNO cycle or p-p chains:

$$(379)\quad {}^{4m}_{2m}\mathrm{X} + {}^{4}_{2}\mathrm{He} \rightarrow {}^{4n}_{2n}\mathrm{Y}$$

for $n = m + 1$, n and m both integers ≥ 3.

${}^{16}\mathrm{O}$ can also be built up in this way (though some species such as ${}^{20}\mathrm{Ne}$ are unstable, and so won't be). Other, related fusion processes also occur in stars that are more massive than the Sun. These are termed "------ burning," where you can fill in the blank with your favorite choice of ${}^{12}\mathrm{C}$, ${}^{16}\mathrm{O}$, ${}^{32}\mathrm{Si}$. Regardless of the specific pathway, Eq. 326 suggests that we will rapidly run out of road as we approach ${}^{56}\mathrm{Fe}$ because it has the highest binding energy per nucleon.

As noted above for the triple-alpha process, each step in the nuclear burning chain becomes progressively less energy efficient. Fusing H→He converts 0.7% of mass into energy, He→C converts just 0.1%, and fusing C→Fe — the end of the line — converts only another 0.1%.

16 End Stages of Nuclear Burning

16.1 *Useful references*

- Prialnik, 2nd ed., Appendix B
- Choudhuri, Secs. 5.1–5.2
- Kippenhahn, Weiger, and Weiss, 2nd ed., Ch. 15
- Hansen, Kawaler, and Trimble, Sec. 3.5

16.2 *Introduction*

Nuclear burning continues until fuel is exhausted. For the Sun, the p-p chain can continue for about 10^{10} yr. Once H is exhausted at the core, thermal pressure is lost: the upper layers of the star are no longer supported, and the core compresses. By the virial theorem, half of that gravitational binding energy goes into heating the gas.

When we hit $T_C \sim 10^8$ K at the core, the triple-α process kicks in and begins converting ^{4}He into ^{12}C. After that, ever-larger nuclei continue to fuse until either (1) we get up to ^{56}Fe or (2) something besides nuclear burning can provide a (non-thermal) pressure source to maintain hydrostatic equilibrium. For Sun-like stars, **degeneracy pressure** provides that support.

16.3 *Degeneracy Pressure*

Degeneracy pressure results from the Pauli exclusion principle, which states that only one fermion is allowed to occupy any particular quantum state. In effect, fermions begin to repel each other in order to keep their quantum wavefunctions from overlapping.

Recall that in the very first lecture (Sec. 1, also in Sec. 16.2) we discussed an order-of-magnitude criterion for a classical ideal gas, namely

$$n \ll \lambda_D^{-3}. \tag{380}$$

For ionized H gas, we found that this was equivalent to requiring

$$\rho \ll 10^3 \text{ g cm}^{-3} \left(\frac{T}{10^7 \text{K}} \right)^{3/2}. \tag{381}$$

We will now improve on this using kinetic theory.

We previously defined the density of states in phase space (Eq. 41) to be

$$\frac{dN}{d^3r d^3p} = f(\vec{r}, \vec{p}). \tag{382}$$

We'll make the simplifying assumption that f is both homogeneous (i.e., there is no $\vec{r}$ dependence) and isotropic (thus replacing $\vec{p}$ with p). For fermions, we

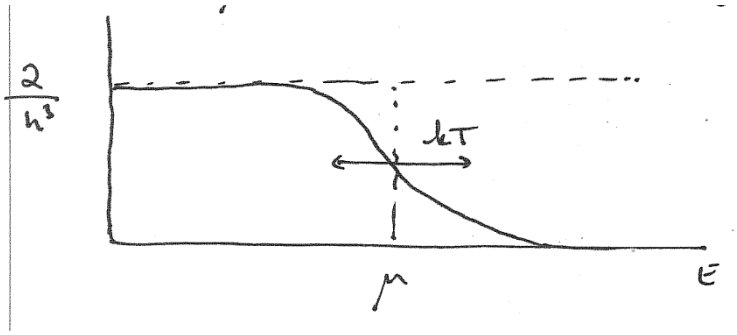

Figure 33: Phase space density of fermions as a function of energy E. The indicated value μ is the Fermi Energy. In the fully degenerate limit, the phase-space density approaches a step function.

have seen that this takes the form (Eq. 101)

$$f(p) = \frac{2}{h^3}\frac{1}{e^{[E-\mu]/k_BT+1}} = \frac{2}{h^3}n_{occ}. \quad (383)$$

Here, μ is not the mean molecular weight but rather E_f, the **Fermi energy** of the distribution. This quantity is derived by maximizing the number of microstates given E, N, and no more than two particles per state (see Fig. 33). So, much above E_f almost no states are occupied; much below it almost all states are full.

The quantities derived from $f(p)$ above are key for us. In particular, we have the number density

$$n = \int f(p)d^3p \quad (384)$$

and also the gas pressure

$$P = \frac{1}{3}\int vpf(p)d^3p. \quad (385)$$

Note that we can relate n, T, and μ – so typically we will solve for μ in terms of these other variables.

Non-degenerate (classical) case:

In the classical limit, particles are widely spaced, $n << \lambda_D^3$, and $n_{occ} << 1$. This means that $\exp[(E-\mu)/kT] >> 1$. Furthermore, if we are fully classical then

$$E = \frac{p^2}{2m}. \quad (386)$$

This means that we have

(387)
$$f \approx \frac{2}{h^3} e^{-E/kT} e^{\mu/kT}$$

(388)
$$\approx \frac{2}{h^3} e^{-p^2/2mkT} e^{\mu/kT}.$$

If we integrate Eq. 388 over momentum to find n, we can solve for μ and find that

(389) $$f(p) \frac{n}{(2\pi mkT)^{3/2})} e^{-p^2/2mkT}$$

which we should recognize as being directly related to the Maxwell-Boltzmann distribution for an ideal gas (Eq. 95).

Degenerate cases:

In the fully degenerate limit, particles are packed as tightly together as their fermionic wavefunctions will allow. This means that

(390)
$$f(p) = 2/h^3 \qquad (E \leq \mu)$$

(391)
$$= 0 \qquad (E > \mu)$$

To calculate the number density from $f(p)$, we again calculate

(392)
$$n = \int f(p) d^3p$$

(393)
$$= 4\pi \int_0^{p_F} \frac{2p^2}{h^3} dp$$

(394)
$$= \frac{8\pi}{h^3} \frac{p_F^3}{3}$$

where p_F is the Fermi momentum, at which $E = \mu$. Given the number density n, this means we can also recast things as

(395) $$p_F = \left(\frac{3nh^3}{8\pi} \right)^{1/3}$$

which will hold regardless of the particular relation between energy and momentum (i.e., whether we are fully relativistic or totally non-relativistic).

Let's then use Eq. 395 to calculate the pressure from a fully degenerate gas. Again, from Eq. 385 we have

$$P = \frac{1}{3}\int_0^{p_F} vp\frac{2}{h^3}4\pi p^2 dp. \tag{396}$$

We'll consider two limits:

1. $v = p/m$ (fully non-relativistic), and
2. $v \approx c$ (ultra-relativistic)

In the **non-relativistic degenerate** case, we calculate Eq. 385 as

$$P = \frac{8\pi}{3}\frac{1}{m}\frac{1}{h^3}\int_0^{p_F} p^4 dp \tag{397}$$

$$= \frac{8\pi}{15}\frac{p_F^5}{mh^3}. \tag{398}$$

If we then plug in Eq. 395, we see that in this limit the gas pressure is

$$P = \frac{8\pi}{15}\frac{1}{mh^3}\left(\frac{3h^3}{8\pi}\right)^{5/3} n^{5/3}. \tag{399}$$

Note this expression for pressure contains the term $1/m$, so the smallest-mass particles dominate the pressure. Thus the electrons are what really matter. If we want to cast P in terms of the mass density, we use Eq. 174 and the mean molecular weight of electrons,

$$n_e = \frac{\rho_{tot}}{\mu_e m_p}, \tag{400}$$

to write

$$P = \left(\frac{3}{\pi}\right)^{2/3}\frac{h^2}{20 m_e m_p^{5/3}}\left(\frac{\rho}{\mu_e}\right)^{5/3} \tag{401}$$

$$= K_{\rm NR}\left(\frac{\rho}{\mu_e}\right)^{5/3}. \tag{402}$$

By comparison back to Eq. 310, we see that a non-relativistic gas is a polytrope (Sec. 13) with index $\gamma = 5/3$.

In the **relativistic degenerate** case, the particle velocities are independent

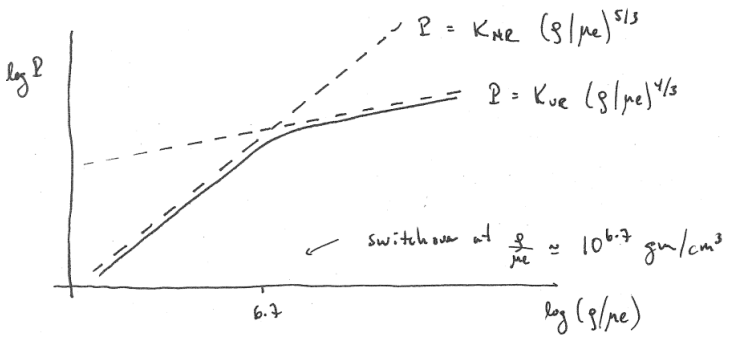

Figure 34: Pressure P vs. density ρ in the non-relativistic (NR) and ultra-relativistic (UR) limits. A switchover occurs at high densities above $\rho/\mu_e \approx 10^{6.7}$ g cm^{-3}.

of p, so we have one less p in our integral for pressure:

(403)
$$P = \frac{1}{3}\int_0^{P_f} cp\frac{2}{h^3}4\pi p^2 dp$$

(404)
$$= \left(\frac{3}{\pi}\right)^{1/3}\frac{hc}{8m_p^{4/3}}\left(\frac{\rho}{\mu_e}\right)^{4/3}$$

(405)
$$= K_{\rm UR}\left(\frac{\rho}{\mu_e}\right)^{4/3}.$$

So the ultra-relativistic degenerate gas is also a polytrope, but now with a slightly shallower index $\gamma = 4/3$.

16.4 *Implications of Degeneracy Pressure*

So our discussion of polytropes in Sec. 13 was fruitful; it now turns out that they give an exact description of the behavior of a degenerate gas. The polytrope indices in the two cases, above, 5/3 vs. 4/3, seem close enough together that there might not be much difference. But comparison to Eqs. 296 and 297 show that the slightly lower index of 4/3 makes all the difference: a fully relativistic and degenerate gas will tend toward instability and collapse.

In the equations of state Eqs. 402 and 405 above, the degeneracy pressure

will dominate over the gas pressure so long as

(406)

$$P_{deg} \gg P_{gas}$$

(407)

$$K_{NR}\left(\frac{\rho}{\mu_e}\right)^{5/3} \gg \frac{\rho k T}{\mu_e m_p}.$$

And assuming a fully ionized medium (so $\mu_e = 1/2$), we then require

(408) $$\frac{\rho}{\mu_e} \gg 750 \text{ g cm}^{-3}\left(\frac{T}{10^7\ K}\right)^{3/2}$$

which is quite similar to our earlier estimate of $n \ll \lambda_D^{-3}$ (Eq. 381, and Sec. 16.2). As the density of a degenerate gas is increased, Fig. 34 demonstrates that the equation of state will switch over from non-relativistic (Eq. 402) to ultra-relativistic (Eq. 405) above densities $\rho/\mu_e \approx 10^{6.7}$ g cm^{-3} or (equivalently) when

(409) $$p_F \approx m_e c = \left(\frac{3nh^3}{8\pi}\right)^{1/3}.$$

16.5 *Comparing Equations of State*

As we start moving into stellar evolution, we will encounter wildly different regimes of pressure, density, and temperature. Which equation of state dominates in each regime? We've seen several examples so far:

Type	EOS		Ideal gas	Temp. dependence
NR degeneracy pressure	$K_{NR}\left(\frac{\rho}{\mu_e}\right)^{5/3}$	=	$\frac{\rho}{\mu_e}\frac{kT}{m_p}$	$T \propto \rho^{2/3}$
Rel degeneracy pressure	$K_{UR}\left(\frac{\rho}{\mu_e}\right)^{4/3}$	=	$\frac{\rho}{\mu_e}\frac{kT}{m_p}$	$T \propto \rho^{1/3}$
Radiation pressure	$\frac{4\sigma}{3c}T^4$	=	$\frac{\rho}{\mu_e}\frac{kT}{m_p}$	$T \propto \rho^{1/3}$

Note that the temperature for radiation pressure and ultra-relativistic degeneracy pressure have the same dependence on temperature; however, the coefficient is larger for the radiation pressure case.

One additional case we haven't yet discussed is: when does treatment as a gas break down? This turns out to happen when Coulomb interactions become increasingly important. Or equivalently, when

(410)

$$E_C \approx E_{Th}$$

(411)

$$\frac{e^2}{a} \approx n^{1/3}e^2 = kT$$

which implies that again, $T \propto \rho^{1/3}$ — but with a smaller coefficient than

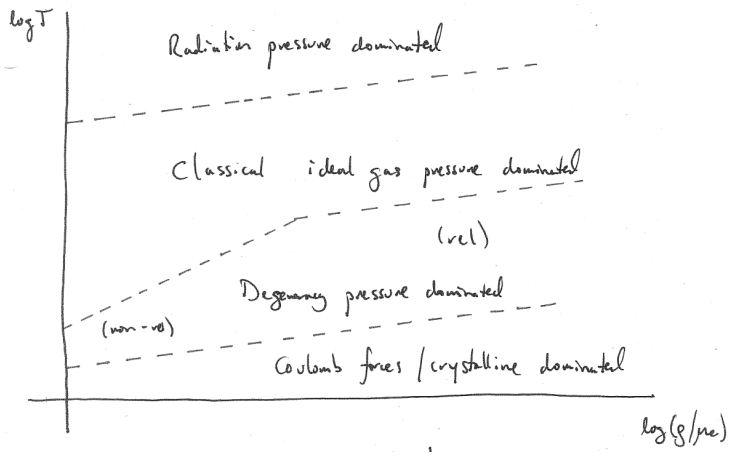

Figure 35: Different regimes in stellar interiors.

for the ultra-relativistic degenerate gas. Fig. 35 summarizes all these different regimes.

Note that degeneracy pressure (like any good polytropic equation of state) is independent of temperature. So it halts stellar contraction even with no power generation. If nuclear power is somehow generated in a degenerate medium, there are interesting consequences:

- **Non-degenerate:** When extra energy is produced, the star expands and cools thanks to the virial theorem. Thus energy production will decreases: negative feedback.
- **Degenerate star:** Extra energy production leads to no expansion of the star. The only place the energy can go is into heating the gas, so its temperature goes up – and thus energy production will increase as well. Positive feedback!

The positive feedback in the degenerate case can accelerate so rapidly that an entire star can become unbound. In other cases, the star will merely be heated up so much that the degenerate state is destroyed; then negative feedback via the virial theorem can once again come into play.

17 Stellar Evolution: The Core

17.1 *Useful References*

- Prialnik, 2nd ed., Ch. 7

17.2 *Introduction*

It's finally time to combine much of what we've introduced in the past weeks to address the full narrative of stellar evolution. This sub-field of astrophysics traces the changes to stellar composition and structure on nuclear burning timescales (which can range from Gyr to seconds). We'll start with a fairly schematic overview – first of the core, where the action is, then zoom out to the view from the surface, where the physics in the core manifest themselves as observables via the equations of stellar structure (Sec. 11.5). Then in Sec. 18 we'll see how stellar evolution behaves in the rest of the star, and its observational consequences.

Critical in our discussion will be the density-temperature plane. For a given composition (which anyway doesn't vary too widely for many stars), a star's evolutionary state can be entirely determined solely by the conditions in the core, T_c and ρ_c. Fig. 36 introduces this plane, in which (as we will see) each particular stellar mass traces out a characteristic, parametric curve.[2]

17.3 *The Core*

There are several key ingredients for our "core view." These include:

[2] We will see that it costs us very little to populate Fig. 36; that is, there's no need to stress over the T-ρ price.

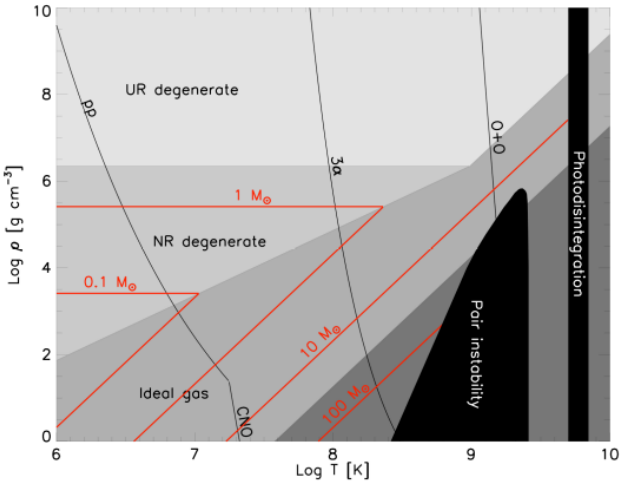

Figure 36: The plane of stellar density and temperature. See text for details.

- **Equation of State.** This could be an ideal gas ($P \propto \rho T$), a non-relativistic degenerate gas (Eq. 402, $P \propto \rho^{5/3}$), an ultra-relativistic degenerate gas (Eq. 405, $P \propto \rho^{4/3}$), or radiation pressure (Eq. 258; $P \propto T^4$). Which equation of state dominates depends on where we are in the (ρ_c, T_c) plane – see Fig. 36.

- **Nuclear Reactions.** The active nuclear reaction pathways, and related reaction rates, depend steeply on T and sometimes on ρ as well(as discussed in Sec. 14.5), with a general form of $\epsilon = \epsilon_0 \rho^\lambda T^\nu$. A given reaction pathway will "ignite" and rapidly start fusing when a given set of T and ρ are reached.

- **Energy Efficiency.** As we saw in Sec. 14.3 (see also Eq. 326), successively later stages of nuclear burning are incrementally less efficient. Each time the nuclear burning ratchets up to the next pathway, less and less binding energy can be liberated per nucleon. Thus τ_{nuc} of Eq. 207 gets shorter and shorter as the end draws near.

- **Stability.** In Sec. 12 we encountered several examples of stellar instabilities. For example, hydrostatic equilibrium breaks down for $\gamma_{ad} < 4/3$ (Eqs. 296 and 297). More generally, we will have to be on the lookout for cases when radiation pressure, degeneracy pressure, and/or ionization become particularly important; these will often correspond to significant dynamical upheavals in the star.

- **Nuclear Runaway.** Another kind of instability occurs if fusion occurs in a degenerate medium (we saw it at the end of Sec. 16). In this case we get a **fusion flash**: all available nuclear fuel is consumed on a thermal conduction timescale (just a few seconds) once burning begins.

17.4 *Equations of State*

Our discussion of stellar polytrope models (Sec. 13) is useful here for giving us a sense of what parts of Fig. 36 certain stars will occupy. What kind of polytrope? Because of the aforementioned stability constraints, for a star to be decently approximated by a polytrope requires

$$\frac{4}{3} < \gamma < \frac{5}{3}. \tag{412}$$

A useful relation comes from assuming a polytrope that is approximately in hydrostatic equilibrium. In this case, we obtain:

$$P_c = G M^{2/3} \rho^{4/3} (4\pi)^{1/3} F(n) \tag{413}$$

where $F(n)$ varies only slowly: from 0.233 to 0.145 for n in the range (1, 3.5).

Core is ideal gas

If we assume the core is an ideal gas, then this means

$$\frac{\rho_c k T_c}{\mu_e m_p} \approx \frac{1}{2} G M^{2/3} \rho_c^{4/3}. \tag{414}$$

Thus regardless of the evolutionary state, for a given star we have the relation

$$T_c \propto M^{2/3} \rho_c^{1/3} \tag{415}$$

or equivalently,

$$\log \rho_c = 3 \log T_c - 2 \log M + C. \tag{416}$$

Thus a star of given mass will lie along a diagonal line in the (logarithmic) plane of Fig. 36, with higher-mass stars lying increasingly toward the right (higher T). It seems that while lower-mass stars will approach and perhaps enter the degenerate regime, more massive stars never do.

Core is degenerate

For those stars whose cores do reach the (non-relativistic) degenerate zone, then degeneracy pressure must be responsible for Eq. 413's pressure calculated from stellar structure considerations. Thus

$$K_{NR} \rho_c^{5/3} \approx \frac{1}{2} G M^{2/3} \rho_c^{4/3}. \tag{417}$$

This result implies instead that

$$\rho_c \propto M^2. \tag{418}$$

or equivalently,

$$\log \rho_c = 2 \log M + C. \tag{419}$$

(Note that we would need to assume a somewhat different polytropic index to gain insight into the ultra-relativistic degenerate zone; but the non-relativistic assumption still gets the point across).

As we saw before, the structure of a degenerate object is independent of its temperature – so a degenerate core of a given mass has a fixed, maximum central density. Note that Eq. 418 also implies that a degenerate object's density increases as the square of its mass, which means that if we add mass to a degenerate white dwarf or neutron star its radius actually decreases. Furthermore, degenerate stars apparently lie along purely horizontal tracks in Fig. 36, with more massive stars at higher densities.

17.5 *Nuclear Reactions*

We've now seen how Fig. 36 can be populated with tracks representing the central conditions for a range of stars. We can now also populate the T-ρ diagram with a set of orthogonal curves describing nuclear energy production in the cores of our stars.

What is a useful characteristic energy production rate ϵ to use for these tracks? We know that in the absence of fusion, stars can be (briefly) heated via gravitational (Kelvin-Helmholtz) contraction. We'll therefore require that nuclear burning produces enough energy to overcome that contraction. In other words,

$$\tau_{KH} \sim \frac{GM^2/R}{L} \sim \frac{u}{\epsilon_V} \tag{420}$$

where

$$u = \frac{3}{2} nkT \tag{421}$$

and the volumetric and mass-based energy rates are related as

$$\epsilon_V = \epsilon_m \rho. \tag{422}$$

This implies that the relevant energy production rate of for any given fusion chain, and over a wide range of stars, is approximately

$$\epsilon_{m,0} \sim 10 \text{ erg g}^{-1} \text{ s}^{-1}. \tag{423}$$

We saw in Sec. 14.5 that the an approximate, general form of ϵ (Eq. 354) is

$$\epsilon = \epsilon_0 \rho^\lambda T^\nu.$$

Thus at the threshold $\epsilon_{m,0}$, we have

$$\log \rho = -\frac{\nu}{\lambda} \log T + \frac{1}{\lambda} \log \left(\frac{\epsilon_{m,0}}{\epsilon_0} \right). \tag{424}$$

Each reaction has its own corresponding coefficient. Successive stages of thermonuclear fusion turn on at higher temperatures and have steeper dependencies on T in particular (with $\lambda \gg 1$ only in the rarely-approached pyconuclear regime).

The features of these curves in Fig. 36 can then be described as follows:

- **p-p chain**: At high ρ, ignites at fairly low T. $\nu \approx 4$.
- **CNO cycle**: Dominates at sufficiently high T and low ρ. Thus given the right raw materials, CNO can actually ignite first as a cloud condenses to form a star. Still just converting protons into He, so continuous with the pp track, but now $\nu \approx 16$.
- **3α**: Ignites at $\sim 10^8$ K, with a very steep T dependence: $\nu \approx 40$.

- **C+C**: Ignites at $\sim 6 \times 10^8$ K, with an even steeper (practically vertical) slope.
- **O+O**: Ignites at $\sim 10^9$ K, with an even steeper (practically vertical) slope.
- **Si**: Ignites at $\sim 2 \times 10^9$ K, with an even steeper (practically vertical) slope.

17.6 *Stability*

For any reasonable duration, dynamical stability will confine our stars to certain regions of the T-ρ diagram. In particular, our stars will become unstable whenever γ approaches $4/3$. Thus the "ideal gas" and "non-relativistic degenerate" zones are fair game, but in both the radiation-dominated regime and in the ultra-relativistic degenerate regime the conditions may verge perilously close to instability.

Other interesting instabilities can also develop. At the highest temperatures $T \gtrsim 10^9$ K, radiation pressure is often the dominant support. But the **pair instability** can remove or decrease that radiation support, leading to collapse. Instead of providing support,

(425) $\gamma \rightarrow e^+ + e^-$

which means

(426) $kT \approx 2m_e c^2$.

Since 1 eV$\sim$12,000 K and m_e=0.5 MeV, this should set in at around

(427) $T_{pp} \approx 10^{10}$ K.

In practice, pair instability sets in considerably earlier because the high-energy tail of the photon distribution can begin pair production long before the kT bulk of the photons reach that level, so it can be relevant for $T \gtrsim 5 \times 10^8$ K.

One final realm of instability is caused by **photodissociation of nuclei**. When $T \gtrsim 3 \times 10^9$ K, individual photons have enough energy to return all the lost binding energy back into heavy nuclei. The most important example is

(428) $\gamma + {}^{56}\mathrm{Fe} \rightarrow 14\,{}^4\mathrm{He}$,

which plays an important role in supernovae of the most massive stars.

17.7 *A schematic overview of stellar evolution*

We're finally in a position to piece together a basic-level astrophysical understanding of the evolution of a star. How do the central conditions of different objects evolve on the T-ρ diagram (Fig. 36).

- **One mass, one fate.** Each particular mass of star follows a distinct track, as described in Sec. 16.5.

- **Start low, end high.** We haven't talked much about the earliest stages of star formation, but we know space is big, empty, and cold. So any star presumably begins the earliest stages of its life at the relatively low temperatures and densities of the interstellar medium.
- **Move along home.** As a gas cloud approaches becoming a *bona fide* star, it contracts and radiates on the Kelvin-Helmholtz timescale (Sec. 10.5). As it contracts, no mass is lost so ρ must increase. And by the Virial Theorem (Eq. 219), T must increase as well.
- **Stop! in the name of fusion.** Eventually the core conditions will hit one of our fusion tracks. We defined our energy production tracks in Sec. 17.5 such that nuclear luminosity balanced the luminosity of gravitational collapse. So the star will remain $\sim$stable at this point for τ_{nuc}.
- **Get up again.** Once nuclear fuel is exhausted in the core, to maintain stability contraction must resume. ρ_c and T_c begin to increase again.
- **Rinse and repeat.** Pause at each nuclear burning threshold, for ever-briefer periods of time, until either a degenerate zone or unstable zone is reached.
- **Just fade away.** Once a star enters the non-relativistic degenerate zone, it's game over. Once any residual fusion is completed, the star can no longer contract to heat and support itself. It will just sit at constant ρ_c, gradually cooling and fading away: it is now a white dwarf. This is the fate of all stars with $M_* \lesssim 1.4 M_\odot$, the **Chandrasekhar Mass**.
- **Do not burn.** Even lowest-mass "stars" will contract and evolve up and to the right in T-ρ space, but for $M \lesssim 0.08 M_\odot$ the track will never intersect the pp-chain burning track. Thus they will become degenerate before ever undergoing fusion; these are **brown dwarfs**.
- **Your star is so massive...** The most massive stars will follow tracks along the upper border of the radiation-dominated regime. This border has the same slope as our equation-of-state tracks, implying that there is some maximum mass that stars can have – any more massive and they would reach $\gamma = 4/3$ and become entirely unstable.
- **Do not pass Go.** Fig. 36 also reveals the final, often-fatal fates of various stars. This includes:
  - Lowest-mass stars: these burn H$\rightarrow$He for many Gyr, then become degenerate **Helium white dwarfs.**
  - Stars $< 1.4 M_\odot \approx M_{Ch}$ produce He and then later also undergo the 3α process. They spend the rest of their days as **carbon/oxygen white dwarfs.**
  - These white dwarfs will occasionally evolve across an ignition line while inside the degenerate region. In this case, we have a **nuclear runaway** and the star will fuse all available fuel almost instantly

(on a thermal conduction timescale, just a few seconds). The best example is the **helium flash**, which occurs for stars at or just below $1M_\odot$. The 3α line is reached right near the non-relativistic degenerate zone, and the core luminosity will spike as high as $10^{11}L_\odot$ for a few seconds. This intense burst only slowly "leaks out" into observable regions, but it quickly melts away the core degeneracy.

– Stars $> M_{Ch}$ will succumb to the instabilities lurking at high T. Most will pass through multiple levels of fusion burning, all the way up to ^{56}Fe, before finally reaching the photodissociation threshold. They will die as **core-collapse supernovae.** The most massive stars are very rare, but some may end their lives via the pair-production instability instead.

17.8 *Timescales: Part Deux*

Note that our discussion so far has left out an explicit treatment of timescales: how long does a star sit at any given nuclear burning threshold, how long does it take to pass from one threshold to the next, and how long does it take a white dwarf to cool? For now, let's merely realize that any given stage of fusion will continue for roughly τ_{nuc} (Eq. 207) while contraction occurs over roughly τ_{KH} (Eq. 205). So the Sun took only a few 10s of Myr to collapse from a gas cloud into a young zero-age main-sequence star, but it will sit on the H→He burning threshold for roughly 10^4 Myr. Since nuclear timescales scale roughly as M^{-3}, more massive stars will fuse up all available hydrogen in just a few 10s of Myr — the lowest-mass stars will take trillions ($> 10^6$ Myr!).

18 Stellar Evolution: The Rest of the Picture

We'll now consider stellar evolution from the external perspective. All the interior physics is now translated through millions of km of starstuff; Plato's cave doesn't have anything on this. As in Fig. 36 we will still observe stars move through a 2D space as their evolution goes on. But now, instead of T_c and ρ_c (which we can only infer and never directly measure) our new coordinates will be the external observables luminosity and effective temperature, L and $T_{\rm eff}$. In truth even these quantities rely on inference at some level; so while the astrophysicist thinks of (L, $T_{\rm eff}$) the observing astronomer will often think in terms of absolute magnitude (a proxy for L) and photometric colors (a proxy for $T_{\rm eff}$). Yes, we've returned once again to the Hertzsprung-Russell diagram first introduced in Sec. 8.

18.1 *Stages of Protostellar Evolution: The Narrative*

The process of star formation is typically divided into a number of separate stages (which may or may not have distinct boundaries). Here, we will consider eight stages, beginning with the initial collapse (which we have already touched on) and ending when a star reaches what is known as the 'main se-

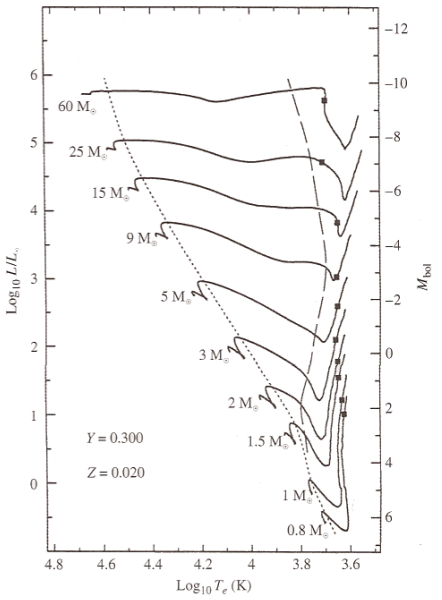

FIGURE 12.11 Classical pre-main-sequence evolutionary tracks computed for stars of various masses with the composition $X = 0.68$, $Y = 0.30$, and $Z = 0.02$. The direction of evolution on each track is generally from low effective temperature to high effective temperature (right to left). The mass of each model is indicated beside its evolutionary track. The square on each track indicates the onset of deuterium burning in these calculations. The long-dash line represents the point on each track where convection in the envelope stops and the envelope becomes purely radiative. The short-dash line marks the onset of convection in the core of the star. Contraction times for each track are given in Table 12.1. (Figure adapted from Bernasconi and Maeder, *Astron. Astrophys.*, *307*, 829, 1996.)

Figure 37:

quence', or a stable state of central nuclear burning of Hydrogen, in which a star will remain for the majority of its life. Note that understanding all of the physics that go into these stages of evolution requires some knowledge of topics we have previously discussed: adiabatic processes (Sec. 11.4), convection (Sec. 12), and opacity (Section7.1) to name a few.

1. **Gravitational Collapse** Initially, the collapse of our Jeans-mass fragment is isothermal: the temperature of the collapsing cloud does not change. The cloud starts at a low density and temperature, and so is optically thin in the infrared, allowing it to efficiently radiate away its collapse energy. However, as the density goes up, the dust grains get closer together until eventually the core becomes optically thick in the infrared, and collapse is halted by the increase in temperature (and thus gas pressure) as the energy from the gravitational collapse is trapped. (Note that theory says that this collapse is an inside-out process: the inner regions collapse faster than the outer regions, and so infall from the collapsing envelope continues during the next few stages). After this point, the core begins to contract nearly adiabatically (as it can no longer exchange heat efficiently with its environment) and continues to heat up as it slowly loses the energy it radiates away. The core will continue to heat up and contract roughly adiabatically, until it reaches a temperature of $\sim$ 2000 K, and some of the energy briefly goes into dissociating all of the H_2 molecules into H, rather than heating the core, causing a second collapse. Once this is finished, the inner region again reaches hydrostatic equilibrium and resumes its slow, adiabatic contraction. This inner object is now referred to as a protostar.

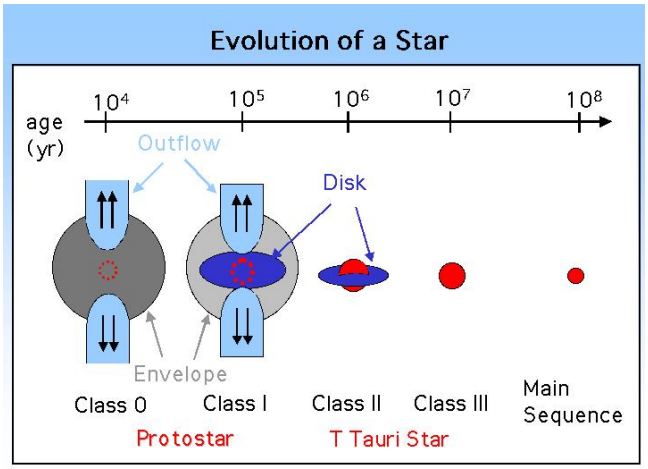

Figure 38: Schematic overview of the early stages of star formation and stellar evolution. (From `http://www-cr.scphys.kyoto-u.ac.jp/research/xray/press200011/figures/`, Apr 2019).

2. **Class 0 protostar** By this stage the envelope may still be collapsing, but a central core has formed which can be seen in cool dust emission at millimeter wavelengths. 'Class 0' is an observational classification indicating that warm dust emission from the core cannot yet be detected at infrared wavelengths. Essentially, the heat generated by the gravitational collapse and accretion has not yet significantly heated a large enough volume of the envelope to destroy the dust, lower the opacity, and make the warm inner regions visible in the infrared. However, there are other observable signatures that show a star is in the process of forming. One key structure that has begun to form at this stage is a flattened, rotating disk. This is a result of the conservation of angular momentum: the smaller the core gets, the faster it spins, causing the initially spherical core to flatten. This actually poses a problem for our forming protostar: if it cannot get rid of this angular momentum, it will never contract to the size of a star, because it would be spinning so fast that it would break up. The solution nature has come up with appears to be bipolar outflows, which begin to be seen at this stage. These rotating flows, launched from the disk (likely with help from the magnetic field, which has also gotten stronger due to conservation of magnetic flux as the cloud collapsed), are believed to carry excess angular momentum away from the system.

3. **Class 1 protostar** In contrast to a Class 0 source, infrared emission from the warm central disk can now be seen. However, material from the envelope is still sufficient to block the protostar from view at optical wavelengths. The outer envelope continues to collapse, infalling onto the central regions. The luminosity that is seen from the central source is largely powered by accretion of this material onto the disk and protostar (this energy comes from a shock, where gas that was in free-fall, traveling at large velocities, suddenly comes to a stop and deposits all of this kinetic energy). The disk continues to drive outflows to remove angular momentum, and by these later stages, now that the disk is larger and better organized, these outflows are better collimated and may even take the form of fast jets.

4. **Classical T-Tauri star (Class 2 protostar)**. The envelope is now sufficiently heated, depleted in mass from infall onto the disk, and/or blown away by the outflows that the central protostar can be seen at optical wavelengths. From this point on the disk will only get smaller as it accretes onto the star and is swept up into planets that are beginning to form. Accretion from the disk remains the primary source of luminosity for the protostar. This accretion is not a continuous process but is extremely stochastic, occurring in large bursts, and so the luminosity of the central object can vary substantially. The 'star' at this point is still much larger than its final radius, and continues to contract. It is also rotating quite quickly at this stage, with rotation periods often around a dozen days (despite its large size), compared to a month for the sun. Its central temperature continues to increase, and though it is still too low for hydrogen fusion, there may be deuterium fusion occurring

(though this does not generate a significant amount of luminosity compared to accretion). T-Tauri stars generally refer exclusively to low mass stars ($\lesssim$ few$M_\odot$). Higher-mass analogues of these systems are known as Herbig Ae/Be stars.

5. **Weak-line T-Tauri star (Class 3 protostar)**. By now, accretion onto the star is almost over (hence, only weak emission lines indicative of hot, accreting gas can be seen in the star's spectrum.) The disk is also only a residual remnant of its former self: exoplanets (especially large gas giant planets) should be well on their way to forming at this point. As the system changes from actively accreting to quiescently contracting, a 'transition disk' may be seen: these objects are expected to have large inner gaps due to planet formation that has cut off the supply of gas to the star, halting its further growth. Remnant disks, which may be mostly rock and dust, having very little gas, can be seen in excess infrared emission from the starlight captured by the dust and re-radiated as heat at longer wavelengths. Such debris disks can be understood as massive analogs of the Kuiper belt and zodiacal dust in our own solar system. These disks are observed to persist up to a few million years, telling us how long planets have to form before the raw materials for doing so are used up.

6. **Pre-main sequence star (Hayashi Track).** At some point during the T-Tauri phase, infall stops, and as we can clearly see the central object at optical wavelengths and place it on a Hertzsprung-Russell (HR) diagram (see Fig. 37), we now begin to refer to it as a 'pre-main sequence' star which has reached its final mass (though not yet its final radius). Once the star is no longer getting energy from accretion, its source of energy is just the potential energy released from its gravitational contraction. No matter the energy source, the large size of the star means that it is extremely bright at this point. Although the central star has for some time been too hot for dust to survive, it is still extremely optically thick. The primary source of its opacity is the H^- ion (see Sec. 7.1), which is an extremely temperature-dependent process: it is much more significant at lower temperatures than higher temperatures. The strong temperature dependency of this process causes the star to become convectively unstable throughout. This time, during which the pre-main sequence star is fully convective, in a state of convective equilibrium, and contracting toward its final size, is known as the **Hayashi track**. The star travels a nearly vertical path (nearly constant temperature) on the HR diagram (Fig. 37) until its central temperature becomes high enough for the core to become radiative rather than convective. As previously mentioned for the T-Tauri phase (which may overlap substantially with this phase) the star may already be fusing deuterium.

7. **Henyey Track** (only for stars greater than 0.8 $M_\odot$). Once a star's core becomes radiative, the star executes a sharp leftward turn on the HR diagram (Fig. 37). This occurs because the core is sufficiently hot for the

opacity to drop, which makes convection less efficient, and the core becomes fully radiative. The star reaches a new equilibrium, and depending on its mass, luminosity remains constant or increases slightly (for intermediate-mass stars), and the surface temperature increases slightly or substantially (for massive stars) as it continues to slowly contract. Stars less than 0.8 $M_\odot$ never develop a radiative core, and so reach the main sequence immediately after the Hayashi track. Higher mass stars may spend very little time at all on the Hayashi track before they develop a radiative core and begin moving nearly horizontally across the HR diagram on the Henyey track. At the end of its time of the Henyey track, the star begins nuclear burning. However, as this process is not yet in equilibrium, the star continues to contract, moving down in luminosity toward its final location on the main sequence.

8. **Zero-age Main Sequence.** Once a star reaches the main sequence, it has now begun stable nuclear burning and reached an equilibrium between pressure from this source of energy generation, and gravity. The star will stay here for the majority of its lifetime (millions to billions of years) however, it will continue to slowly change: getting very slightly larger (and so brighter) as it ages. This leads to a famous problem known as the faint young sun paradox: when life on earth was developing, the sun was only $\sim$70% as bright as its current luminosity, however we believe (since life developed) that there was still able to be liquid water on the earth's surface. Although this change in brightness might seem like a good way to determine the age of a star, it turns out that we need to precisely know the mass to do this, and we cannot directly the mass of a star unless it is in a binary system. Outside of stars in clusters (for which we can measure patterns in the positions of more massive stars on the HR diagram that are evolving into red giants), it is difficult to say more than that a star is on the main sequence (which could mean an age of anywhere from a few million to a few billion years!). Some clues can be seen in its spin rate and magnetic activity (both of which decrease), but we are currently limited, at best, to 10-15% accuracy (a fact which, for example, makes it difficult to construct understandings of the time evolution of exoplanetary systems).

18.2 *Some Physical Rules of Thumb*

Let's now dive into a deeper, more physical discussion of the processes involved. Here are a number of key bits we need to worry about:

- **Opacity vs. Temperature**. Fig. 39 gives a schematic view of what we expect here. Roughly speaking, we will have two extremes:

$$\kappa_R \propto \rho^{1/2} T^9 \ (\textit{below ionization}) \tag{429}$$

and

(430) $\kappa_R \propto \rho T^{-7/2}$ (*above ionization; Kramer's Rule*).

- **Opacity vs. Thermal Gradient**. If κ is very low, radiation streams freely; otherwise, radiative transport of energy is very inefficient. So in the limit of very high opacity, energy will instead by transported by convection; based on the Schwarzschild stability criterion (Eq. 302) we expect

$$\frac{dT}{dr} = -\frac{T}{P}\left|\frac{dP}{dr}\right|\left(1 - \frac{1}{\gamma_{ad}}\right).$$

  Otherwise, we are in the low-opacity limit and have a radiative profile. By the thermal profile equation (Eq. 235) we then expect

$$\frac{dT}{dr} = -\frac{3\rho\kappa L(r)}{64\pi\sigma_{SB}T^3r^2}.$$

- **Virial Theorem.** We saw that stars contract at various stages of their evolution. By Eq. 219, we should also expect that the rate of contraction is limited by a star's ability to radiate energy from its surface.

  1. High opacity → convective → slow contraction
  2. Low opacity → radiative → rapid contraction

18.3 *The Jeans mass and length*

A particularly important application of the Virial Theorem, relevant to the earliest stages of star formation, is to determine the conditions required for a system to be slightly out of equilibrium such that it would tend toward

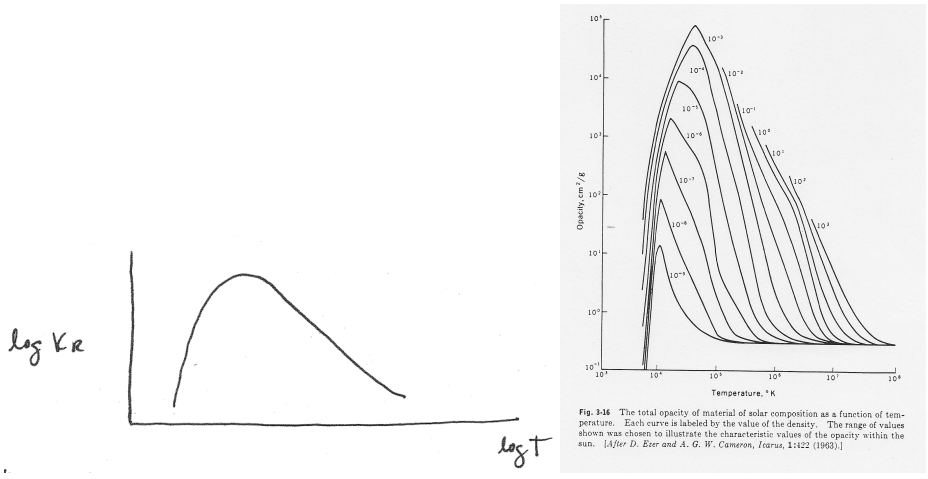

Figure 39: Opacity vs. temperature: *left*, schematic of the Rosseland mean opacity; *right*, an actual calculation (from Ezer and Cameron, 1963).

gravitational collapse or contraction. In this case, we would require that the magnitude of the potential energy term in Equation 209 be larger than the kinetic energy term.

Assuming that we are dealing with an ideal gas, and that we have a spherical, uniform density cloud we can write the total kinetic energy of all the particles in the cloud as

$$K = \frac{3}{2} N k T, \tag{431}$$

where N is the total number of particles in the system. The gravitational potential energy will be the same as Eq. 224,

$$U = -\frac{3}{5}\frac{GM^2}{R}$$

and so we can rewrite the Virial Theorem (Equation 209) as

$$\frac{3}{10}\frac{GM^2}{R} = \frac{3}{2} N k T. \tag{432}$$

the substitutions of $N = M/\bar{m}$ and $R = \left(\frac{3M}{4\pi\rho}\right)^{1/3}$, we can write

$$\frac{1}{5} G M^{2/3} \left(\frac{4\pi\rho}{3}\right)^{1/3} = \frac{kT}{\bar{m}}. \tag{433}$$

Solving Eq. 433 for M gives the mass at which a system will become gravitationally unstable: this is known as the Jeans Mass.

$$M_{\rm Jeans} = \left(\frac{5kT}{G\bar{m}}\right)^{3/2} \left(\frac{3}{4\pi\rho}\right)^{1/2} \tag{434}$$

We can simplify this equation by scaling it to some typical conditions in the star-forming interstellar medium, and conveniently expressing it in Solar mass units.

$$M_{\rm Jeans} = 2.3\, M_\odot \left(\frac{T}{10\ {\rm K}}\right)^{3/2} \left(\frac{n}{10^5\ {\rm cm}^{-3}}\right)^{-1/2} \tag{435}$$

18.4 *Time Scales Redux*

The processes governing each of these stages of stellar evolution are subject to many of the same characteristic time scales that were introduced in Sec. 10.

Collapse and infall

Collapse and infall generally occur on a free-fall time scale (Eq. 198),

$$\tau_{ff} = \sqrt{\frac{3\pi}{32 G \rho}}$$

which, as we discussed, is only ∼30 min for the Sun. But before the Sun became a star its density was much lower. If we cast Eq. 198 in more familiar units, we have instead

(436)
$$\tau_{ff} = 2100\text{s} \left(\frac{R}{R_\odot}\right)^{3/2} \left(\frac{M}{M_\odot}\right)^{-1/2}$$

(437)
$$= 0.2\text{yr} \left(\frac{R}{1\text{AU}}\right)^{3/2} \left(\frac{M}{M_\odot}\right)^{-1/2}$$

(438)
$$= 0.6\text{Myr} \left(\frac{R}{0.1\text{pc}}\right)^{3/2} \left(\frac{M}{M_\odot}\right)^{-1/2}$$

So freefall times can be of order 0.1–1 Myr for solar-type stars.

Contraction

Contraction, in contrast, is governed by the time it takes for the star to radiate a significant amount of its gravitational potential energy. This is determined by the Kelvin-Helmholtz time scale (Eq. 205),

$$\tau_{KH} \sim \frac{GM_\odot^2}{R_\odot} \frac{1}{L_\odot}$$

which is roughly 3×10^7 yr for the Sun; longer for lower-mass bodies, and much shorter for more massive stars (see Sec. 10.5).

18.5 *Protostellar Evolution: Some Physics*

First, recall that it is much easier to measure luminosity L (from broadband photometry) and T_{eff} (from spectra) than it is to measure radii. But we can estimate R via Eq. 66,

(439) $L = 4\pi\sigma_{SB} R^2 T_{\text{eff}}^2.$

As we did with the tracks on the T-ρ diagram (Fig. 36), we will also lay out tracks on the H-R Diagram, Fig. 37. For example:

(440) $\log L = 2 \log R + 4 \log T_{\text{eff}} + C$

Hayashi Track Revisited

The key ingredients are are the following. First, once we reach the Hayashi track opacity is high, and the young objects are fully convective. Thus our equation of state is

(441) $P = \frac{\rho k T}{\mu m_p} = K_{con} \rho^{5/3}$

Though contracting, we are still approximately in hydrostatic equilibrium – this is because contraction occurs on $\tau_{KH} > \tau_{ff}$. So we still have

$$\frac{dP}{dr} = -\frac{GM(r)}{r^2}\rho(r) \tag{442}$$

and optical depth is still given by

$$\frac{d\tau}{dr} = -\rho\kappa_R. \tag{443}$$

Combining the above two equations gives

$$\frac{dP}{d\tau} = \frac{GM(r)}{r^2}\frac{1}{\kappa_R} \tag{444}$$

and since temperatures are low at this point the star is mostly neutral and Eq. 429 gives the opacity:

$$\kappa_R \propto \rho^{1/2}T^9.$$

We then solve the above equations for $\tau = 2/3$ and $T = T_{\text{eff}}$ (see Sec. 9.3). The final solution is that along the Hayashi track (where stars are fully convective because opacity is high), we have

$$\log T_{\text{eff}} \approx 0.2 \log M + 0.05 \log L + C \tag{445}$$

or alternatively,

$$\log L \approx 20 \log T_{\text{eff}} - 4 \log M + C, \tag{446}$$

which matches up fairly well with the nearly-vertical Hayashi track seen on the right-hand side of Fig. 37.

Henyey Track Revisited

As noted above, as the star contracts down the Hayashi track T_c and ρ_c will steadily increase. Eventually, the core will ionize and the opacity will drop (as shown in Fig. 39); as discussed previously in Sec. 12.4 the core will enter the radiative-support regime. At this point L may increase slightly but overall remains fairly constant – all the thermal energy eventually gets out.

With L roughly constant and R decreasing, this means

$$\log T_{\text{eff}} = 0.25 \log L - 0.5 \log R + C \tag{447}$$

must increase. So the star slides to the left along the Henyey Track, leaving the Hayashi Track and heading toward the Main Sequence.

18.6 *Stellar Evolution: End of the Line*

So as we saw when discussing Fig. 36, stellar evolution as seen from the core is a tale of monotonic increases in central ρ and T. From the exterior, it is a story in two parts: each part governed by opacity, ionization, and the transition between convective and radiative interiors.

Once those central ρ and T increases sufficiently, nuclear fusion will begin either via the CNO cycle (for more massive stars) or the p-p chain (for stars of roughly Solar mass and below). In Sec. 15 we already detailed the various nuclear pathways that lead from those earliest stages of fusion to the final endpoints of stellar evolution.

When the central H fuel is finally exhausted, we've seen that the core will contract either until He fusion can be initiated, or until the core becomes degenerate (a He white dwarf). At this point, **shell burning** (Fig. 40) sets in and the star will actually go into reverse, re-ascending along first the Henyey and then the Hayashi track.

Recall that core burning is self-regulating and stable. As a non-degenerate core contracts slightly, its fusion energy production rate will increase dramatically – $\epsilon \propto T^4$ in the pp chain and $\propto T^{16}$ in the CNO cycle. This extra energy will heat the core, causing it to re-expand slightly, cool off, and so decrease the fusion rate.

In contrast, shell burning over a degenerate core is unstable. As fusion proceeds in the shell, the inert core mass grows. Since it is degenerate, by Eq. 418 as its mass increases its radius will decrease slightly. This contraction will compress and heat the fusing shell, leading to an accelerated fusion rate. Thus in shell burning, energy will be produced at a sufficiently rapid rate to essentially run Kelvin-Helmholtz contraction in reverse: the star's outer layers expand and cool off, entering a giant phase. This will initially be the **subgiant**

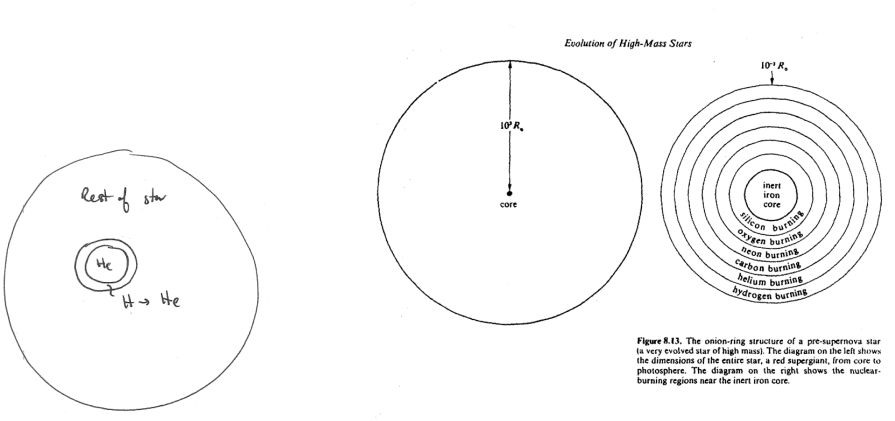

Figure 40: Schematic pictures of shell burning: a degenerate He core surrounded by a thin burning shell surrounded by a mostly-H stellar envelope. Center and left panels are fore an extremely massive star just before the end of its life; Note the linear scales of the two panels.

phase, essentially the reverse Henyey track, followed by the **red giant** phase, essentially a reverse Hayashi track.

18.7 *Red Giants and Cores*

Red Clump

When the core becomes sufficiently hot and dense (i.e. massive), the He in the core will begin to fuse. Most stars avoid the aforementioned helium flash, and undergo steady He fusion. Assuming that happens, the star's contraction along the red giant branch will pause so long as fuel remains for fusion to support the core against further contraction. Thus the star is once again in steady state, but due to He rather than H fusion. The star now sits on what is essentially a second main sequence, but powered by He burning. This phase lasts roughly 5% as long as the original main sequence lifetime. That seems short, but for the sun with a MS lifetime of 10 Gyr this means it will be a red giant for $\sim$500 Myr – short, but $\sim 10\times$ longer than the Kelvin-Helmholtz timescale of expansion.

Because stars spend much more time in this region, they bunch up on the H-R diagram; this region is called the **red clump** and its (infrared) luminosity is roughly independent of composition, ages, etc. Because these giants are much brighter than the main sequence, their luminosities can more easily be measured and so this is often used as a "standard candle" to estimate the distance to a stellar population.

Asymptotic Giant Branch

After sitting on the red clump for a time, the (now carbon-rich) core will again become degenerate. It won't be quite hot and dense enough to initiate higher-order nuclear burning, but He$\rightarrow$C fusion will continue in a shall around the degenerate C core. So it's the same story all over again: the core will grow in mass and (being degenerate) it will shrink, accelerating the burning process – the star is now undergoing a second phase of reverse-Kelvin-Helmholtz contraction (i.e., it is expanding) along the **asymptotic giant branch.** The star is not perturbed by quite as much as before, because there is still an intermediate layer of H$\rightarrow$He fusion (via the CNO cycle) that is providing some energy.

As we briefly alluded to in Sec. 12.3, main-sequence stars hotter and more massive than the Sun have convective interiors beneath radiative envelopes. On the AGB, each fusing shell produces enough energy to exceed Eq. 302 and create its own local convection cell. This mixes the star's internal composition somewhat (it never becomes anywhere close to homogeneous); the star is said to be undergoing **dredge-up** of potentially interesting elements up to the observable surface layers.

Multiple fusion shells also tends to make a star unstable and leads to **stellar pulsations,** periodic expansions and contractions of the outer envelope of the star. These pulsations, combined with high luminosities and very low surface gravity, leads to considerable **mass loss** from the star in its later stages.

Escape velocity is given by

(448)
$$v_{\rm esc} = \left(\frac{2GM}{R}\right)^{1/2}$$

(449)
$$v_{\rm esc} = 620{\rm km\ s}^{-1} \left(\frac{M}{M_\odot}\right)^{1/2} \left(\frac{R}{R_\odot}\right)^{-1/2}$$

(450)

which is then a factor of $\sim \sqrt{200}$ (or more) lower for the largest giants. Winds are indeed observed with Doppler shifts corresponding to about these velocities from evolved red giants and AGB stars.

Mass loss will eventually become sufficiently rapid that the entire envelope is lost to interstellar space; the exceedingly diffuse material around the star will eventually be observed as a **planetary nebula** (whose name is another historical anachronism). Only the degenerate core will remain; the star has finally become a **white dwarf**. This is the fate of all stars with initial masses $\lesssim 6M_\odot$.

19 On the Deaths of Massive Stars

19.1 *Useful References*

- Prialnik, 2nd ed., Ch. 10
- Kippenhahn, Weiger, and Weiss, 2nd ed., Chap. 36
- Hansen, Kawaler, and Trimble, Secs. 2.6–2.8

19.2 *Introduction*

Stars with initial masses $\lesssim 6M_\odot$ will end their days as the degenerate white dwarfs we came to know and love in Sec. 16. But more massive stars will suffer new and different evolution and final fates: in **core-collapse supernovae**.

The most famous such event in living memory was the infamous SN1987A, which occurred "right next door" in the Large Magellanic Cloud (just 50 kpc away) in Feb. 1987. It was the first core-collapse supernova whose progenitor star could be uniquely identified and characterized (from archival data) – it was Sanduleak, a 14,000 K supergiant with mass of $\approx 18M_\odot$ (probably rather more at formation) and pre-collapse luminosity of $\approx 10^5 L_\odot$. Its light curve is shown in Fig. 41.

19.3 *Eddington Luminosity*

One interesting point is that stars with initial masses $\gtrsim 5M_\odot$ never ascend a giant branch. Instead they start much hotter and evolve to the right on the H-R diagram at roughly constant luminosity. This constant L is because the stars are emitting at roughly the maximum permissible luminosity, the so-called **Eddington Luminosity**.

To derive this maximum luminosity, $L_{\rm Edd}$, we need three ingredients: hydrostatic equilibrium, radiation energy transport, and radiation pressure. Recall that for a stable star in hydrostatic equilibrium, Eq. 192 says that its pressure gradient must be

$$\frac{dP}{dr} = \rho(r)g(r).$$

For intense radiation fields (i.e., energy transported by radiation not convection) the thermal profile (Eq. 235) is

$$\frac{dT}{dr} = -\frac{3\rho\kappa L(r)}{64\pi\sigma_{SB}T^3r^2}.$$

And finally, radiation pressure is given by (Eq. 258)

$$P_{rad} = \frac{1}{3}\left(\frac{4}{c}\right)\sigma T^4.$$

An object (whether star or accreting supermassive black hole) has its maximum luminosity, $L_{\rm Edd}$, when the radiation pressure gradient just balances the

hydrostatic gradient. Taking the derivative of P_{rad}, we have

$$\frac{dP_{rad}}{dr} = \frac{16\sigma}{3c}T^3\frac{dT}{dr} \tag{451}$$

$$= \frac{16\sigma}{3c}T^3\left(-\frac{3\rho\kappa L(r)}{64\pi\sigma_{SB}T^3r^2}.\right) \tag{452}$$

$$= -\frac{\rho\kappa L}{4c\pi r^2} \tag{453}$$

(454)

This last expression must just equal $-\rho g$; setting $g = GM/R^2$ we then have

$$L_{\text{Edd}} = \frac{4\pi cGM}{\kappa} \tag{455}$$

$$\approx (3.5\times10^4 L_\odot)\left(\frac{M}{M_\odot}\right) \tag{456}$$

(457)

for an approximate value of $\kappa \approx 0.34$ cm^2 g^{-1}.

19.4 *Core Collapse and Neutron Degeneracy Pressure*

As we saw in Fig. 40, the most massive stars will undergo successive layers of shell burning, each shorter-lived than the last. Eventually the core is composed of ^{56}Fe (up to around $1.5M_\odot$ for $M_* \gtrsim 20M_\odot$), which is inert from a fusion standpoint (just like every other inert core which preceded it during the evolution process).

Two factors cause the core to collapse. First, as we saw in Sec. 17.6, photodisintegration of the Fe nuclei will set in once $T_c \gtrsim 3\times10^9$ K; this absorbs the photons that were previously providing radiation pressure support. Second, electron degeneracy pressure will also eventually drop: the degenerate electrons are forced into ever-higher energy states until they can initiate inverse beta decay:

$$e^- + p \to n + \bar{\nu}_e. \tag{458}$$

The star is undergoing **neutronization** and emitting copious neutrinos. The number of free electrons declines and so electron degeneracy pressure will decrease.

Core collapse

The core is collapsing. What, if anything, can halt the collapse?

The answer is **neutron degeneracy pressure**. This is the same phenomenon we first encountered in Sec. 16.3, but provided by the neutrons instead. The physics is true but the names have been changed to protect the innocent; all relevant scales are all now $m_n/m_e \approx 1800\times$ smaller. We can estimate the size of a neutron star using the same arguments in Eq. 381:

$$N_n \lambda_D^3 \approx R^3 \tag{459}$$

where the de Broglie wavelength of the relativistic neutrons is

$$\lambda_D \approx \frac{h}{m_n c} \approx 1.3 \times 10^{-15} \text{ m} \tag{460}$$

and so

$$N_n \approx 1.5 M_\odot / m_n \approx 1.8 \times 10^{57}. \tag{461}$$

That's a lot of neutrons! At that scale, the expected size is roughly

$$R_{NS} \approx \frac{h}{m_n c} N^{1/3} \approx 12 \text{ km}. \tag{462}$$

Contrast this with the size of a white dwarf (or of the initial degenerate core), which is *roughly* $1800\times$ larger (but actually a bit less, because the composition is more complicated) – $R_{WD} \approx R_\oplus = 6400$ km.

Thus once hydrostatic support is lost, the core collapses from a size of $\approx R_\oplus$ to ≈ 12 km in a free-fall timescale:

$$\tau_{ff} \sim (G\rho)^{-1/2} \tag{463}$$

which is $\lesssim 3$ s for the initial core, and a much shorter timescale by the end of the collapse.

Energy Release

The total gravitational energy liberated by this collapse is considerable:

$$\Delta E \approx \frac{3}{5}\frac{GM^2}{R_f} - \frac{3}{5}\frac{GM^2}{R_i} \tag{464}$$

$$\approx \frac{3}{5}\frac{GM^2}{R_f} \tag{465}$$

$$\approx 3 \times 10^{53} \text{ erg} = 3 \times 10^{46} \text{ J} \tag{466}$$

which is all released in of order a second.

Contrast this with the Solar luminosity, $L_\odot \approx 4 \times 10^{33}$ erg s^{-1}. This collapse (which has now become a **core-collapse supernova**) is over $10^{20}\times$ more luminous than the present-day Sun. Even over the Sun's entire lifetime of 10^{10} yr, it will emit $\sim 10^{51}$ erg. So in a few seconds, a core-collapse supernova releases 100$\times$ more energy than the Sun will in its entire life.

Where does all that energy go?

Photodisintegration captures a bit of it. The destruction of ^{56}Fe releases about 125 MeV per nucleus, or about $\sim$2 MeV per nucleon. There are roughly $N_{Fe} \approx 1.4 M_\odot / 56 m_p \approx 3 \times 10^{55}$ Fe nuclei in the core at collapse, so this absorbs roughly 6×10^{51} erg, or roughly 6% of the total.

Observed outflows from supernovae have velocities of $v_{ej} \sim 10^4$ km s^{-1}, far above the necessary escape speed. With an envelope mass of order $10 M_\odot$, these will carry away an energy roughly equal to

(467)
$$K = \frac{1}{2} M_{env} v_{ej}^2$$

(468)
$$\approx \frac{1}{2} (10 \times 2 \times 10^{33}) (10^9)^2$$

(469)
$$\approx 10^{51} \text{ erg}$$

or roughly 1% of the total.

Ejection of the envelope only uses a smidgen, despite the considerable envelope mass. Even if all that mass were at the core radius, we would still have

(470)
$$\Delta U \approx \frac{G M_{env} M_c}{R_c}$$

(471)
$$\approx \frac{(2/3 \times 10^{-7})(10 \times 2 \times 10^{33})(2 \times 10^{33})}{7 \times 10^{10}}$$

(472)
$$\approx 4 \times 10^{51} \text{ erg}$$

so as much as 4% (and probably a bit less, since some mass started at larger radii).

Supernovae are almost always discovered via their optical/infrared emission, which rises rapidly (see Fig. 41 but persists for weeks to months. Very roughly, assuming one year of emission at a typical supernova luminosity of

$3 \times 10^{10} L_\odot$ gives

(473)
$$L_{SN} \approx (3 \times 10^{10})(4 \times 10^{33})(3 \times 10^{7})$$

(474)
$$\approx 4 \times 10^{51} \text{ erg}$$

which is again just a few percent of the total energy release.

Neutrino Luminosity

Most of the energy actually goes into neutrinos. Despite their *weak* interactions with baryonic matter, these fleeting leptons are created in sufficient numbers (and the collapsing star achieves such high densities) that enough neutrino opacity results to help eject the envelope. In 1987, ∼20 electron neutrinos were observed from SN1987A.

During neutronization, the entire Fe core is converted into a neutron core — the precursor to a **neutron star** — via inverse beta decay. The total number

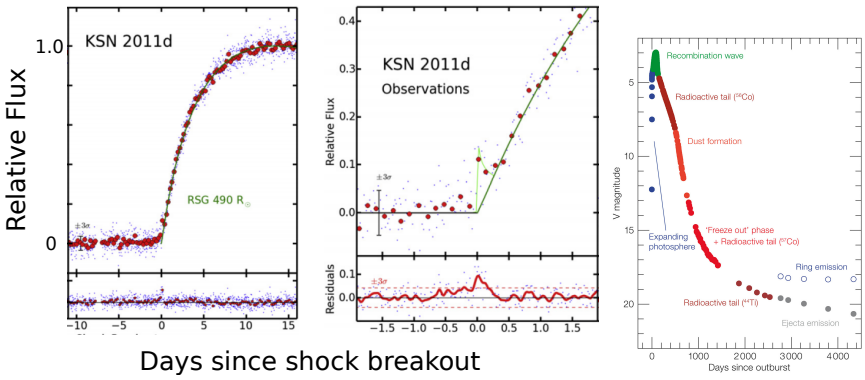

Figure 41: Supernova light curves at visible wavelengths. *Left*: Early phase of a supernova outburst captured by the *Kepler* space telescope (Garnavich et al. 2016). *Right:* Multi-year light curve of SN1987A (`https://www.eso.org/public/images/eso0708c/`).

of neutrinos produced will be roughly

(475)
$$N_\nu = N_p$$

(476)
$$\approx \frac{1.5 M_\odot}{2 m_p}$$

(477)
$$\approx (2 \times 10^{33})(6 \times 10^{23})$$

(478)
$$\approx 10^{57}$$

The neutrinos produced are highly relativistic, and despite their minuscule masses ($\lesssim$ 0.1 eV) they have typical energies of $\sim$30 MeV. Thus they carry away $\gtrsim 5 \times 10^{52}$ erg, and so transport the bulk of the energy liberated by the core's collapse. A wee bit of the copious neutrino flux couples to the dense stellar material; this is still an active area of SN research.

19.5 *Supernova Nucleosynthesis*

Although core fusion has ceased in our dying massive star, nucleosynthesis has not. Given the colossal neutron fluxes present in these final moments, new nuclear pathways open up that were unavailable before; recall that the neutron has no charge, and so can proceed without needing to overcome the strong Coulomb repulsion that hindered us in Sec. 14.3.

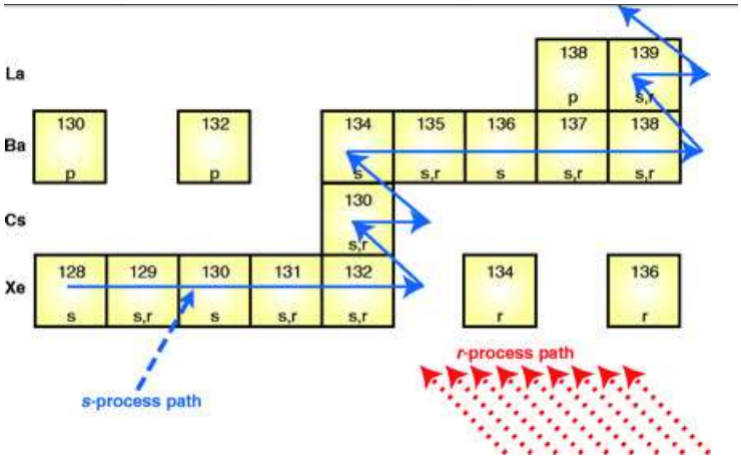

Figure 42: Nucleosynthesis via the s-process and r-process. Only a subset of the possible nuclei (and only the stable isotopes) are shown. Letters indicate which process can form which isotopes. From `http://www.astro.sunysb.edu/lattimer/PHY521/nucleo.pdf`.

As long as stable isotopes are formed, neutron capture can lead to a continuous path of isotopes:

(479)
$$ {}^{A}_{Z}\mathrm{X} + n \rightarrow {}^{A+1}_{Z}\mathrm{X} $$

(480)
$$ {}^{A+1}_{Z}\mathrm{X} + n \rightarrow {}^{A+2}_{Z}\mathrm{X} $$

and so forth. But sooner or later an unstable isotope will be formed. What happens next depends on the relative timescales of neutron capture and beta decay. Fig. 42 depicts the two possible paths; so long as neutron captures occur, the nucleosynthesis track moves steadily to the right.

If neutron captures are relatively infrequent, then the isotope will beta-decay before another neutron can be jammed into the nucleus. This is the **s-process** ("s" for the **s**low neutron capture rate). This occurs, for example, in the cores of asymptotic giant branch (AGB) stars, where the H-shell burning provides the neutrons and large-scale instabilities lead to dredge-up. The beta decay follows its usual course:

(481) $ {}^{A+N}_{Z}\mathrm{X} \rightarrow {}^{A+N}_{Z+1}\mathrm{Y} + e^{-} + \bar{\nu} $

and it could either be followed by more beta decays if the daughter nucleus ${}^{A+N}_{Z+1}\mathrm{Y}$ is unstable

(482) $ {}^{A+N}_{Z+1}\mathrm{Y} \rightarrow {}^{A+N}_{Z+2}\Omega + e^{-} + \bar{\nu} $

(thus moving one step up and one to the left in Fig. 42) or by resuming the train of neutron captures if ${}^{A+N}_{Z+1}\mathrm{Y}$ is stable

(483) $ {}^{A+N}_{Z+1}\mathrm{Y} + n \rightarrow {}^{A+N+1}_{Z+1}\mathrm{Y} $

(and thus moving steadily to the right again in Fig. 42). One of the more unusual s-process products is Technetium, which has no stable isotopes but is still seen in stellar spectra of evolved, late-type stars.

Alternatively, in a high-neutron-flux environment (such as our collapsing, massive star) neutron captures happen more rapidly than beta decays. This is the **r-process** (for **r**apid) and it occurs to some extent in core-collapse supernovae and perhaps reaches its greatest heights in neutron star-neutron star mergers (as were touched upon in Sec. 5). In this case, the chain of neutron captures may continue to quite high atomic mass even given a dearth of protons – i.e., into highly unstable nuclei. But when the neutron flux drops off, it's closing time: the isotopes can't go home and they "can't stay here" – they will undergo a series of beta decays, moving steadily up and to the left in Fig. 42 until a stable isotope is reached.

19.6 *Supernovae Observations and Classification*

The observation and classification of supernovae go back over 1000 years, making this one of the oldest branches of observational astronomy. The name "nova" had been given to "new stars" (actually outbursts from accreting white dwarfs), and "super"-novae were that much brighter. The names are similar in other cultures; e.g., Chinese records refer to them as *kexing*, or "guest stars."

Before the modern era began, there were $\sim$8 supernovae visible without telescopes. The brightest of these, SN 1006, is estimated to have had $m_V \approx -7.5$ mag, roughly 3 mag brighter than Venus and visible even in the daytime. Another famous example is SN 1054, whose ejecta now span a radius of $\approx$1.7 pc – this is the famous Crab Nebula[3] The two most famous, local (i.e., in the Milky Way) supernovae in "recent" times are Tycho's and Kepler's supernovae; these occurred "only" 30 years apart, in 1572 and 1604, and in Europe helped break down beliefs in a static, unchanging heavens and to unleash the modern astronomical revolution. No SN have been seen in the Milky Way since, although we think there should be 1–3 per year.

Like the classification of stars (discussed in Sec. 8), supernovae were classified into groups first and only later associated with underlying physical mechanisms. The observationally-motivated nomenclature comes from optical spectra of the supernova near peak luminosity (when it's easiest to observe), and it is:

- **Type I:** No H-α line seen.
- **Type II:** H-α line seen.

As simple as that! But this was subsequently clarified:

- **Type Ia:** No H-α, but Si lines seen.
- **Type Ib:** No H-α, but He lines seen.
- **Type Ic:** No H-α, and not much else.
- **Type II:** H-α line seen.

There are also multiple types of Type II supernovae, classified on the basis of their light curve morphology. E.g. SN1987A (lightcurve shown in in the rightmost panel of Fig. 41) was classified as Type IIpec, for "peculiar."

A **Type Ia supernova** is caused by fusion detonation on a degenerate white dwarf. Once the main source was thought to be mass transfer from a nearby binary companion onto the white dwarf, until the WD's degeneracy pressure can no longer support itself. But we now know that there are many pathways leading to SNe Ia; different pathways lead to different chemical abundances in the SN ejecta, and these studies now indicate that most SNe Ia (at least in dwarf galaxies) occur from white dwarfs of roughly $\sim 1 M_\odot$, well below the Chandrasekhar Mass of $1.4 M_\odot$. These SNe Ia are typically brighter — less

[3]Note that its ejecta have moved $\sim$5 light years over the past millennium, implying an *average* speed of 0.5% c – and presumably higher (and more relativistic) at earlier times.

total energy is released, but more of the energy here goes into photons rather than into neutrino luminosity.

Types II, Ib, and Ic are all different flavors of core-collapse supernovae probably resulting from progenitor stars with different initial masses and evolutionary histories.

In many supernovae, many of the photons we see actually come from the radioactive decay of unstable isotopes produced in the explosion. The most important pathway comes from the decay of ^{56}Ni, which was itself produced from fusion of Si with a succession of α particles:

(484) $^{28}_{14}\mathrm{Si} + 7^{4}_{2}\mathrm{He} \rightarrow^{56}_{28}$ Ni

or by direct, Si-Si fusion:

(485) $2^{28}_{14}\mathrm{Si} \rightarrow^{56}_{28}$ Ni.

The decay pathway after the supernova is over and nucleosynthesis has ceased is

(486)
$$^{56}\mathrm{Ni} \rightarrow^{56} \mathrm{Co} + e^{+} + \nu_e + \gamma \quad (6.1 \text{ day half} - \text{life})$$

(487)
$$^{56}\mathrm{Co} \rightarrow^{56} \mathrm{Fe} + e^{+} + \nu_e + \gamma \quad (78 \text{ day half} - \text{life})$$

(488)

Note that the ^{56}Co phase of SN1987A is indicated in Fig. 41. That SN was estimated to produce just $0.075 M_{\odot}$ of ^{56}Ni, but others produce as much as $\sim 1 M_{\odot}$ — these are extremely luminous.

20 Compact Objects

20.1 *Useful references*

- Prialnik, 2nd ed., Ch. 10
- Choudhuri, Secs. 5.3–5.6
- Hansen, Kawaler, and Trimble, Ch. 10

20.2 *Introduction*

As we have discussed up to this point, mass is destiny when describing the evolution and final fates of single stars. Fig. 43 breaks down the ultimate states of stars of a range of initial masses. Furthermore, the mass of an object's final remnant (after AGB mass loss, supernova, etc.) is similarly deterministic.

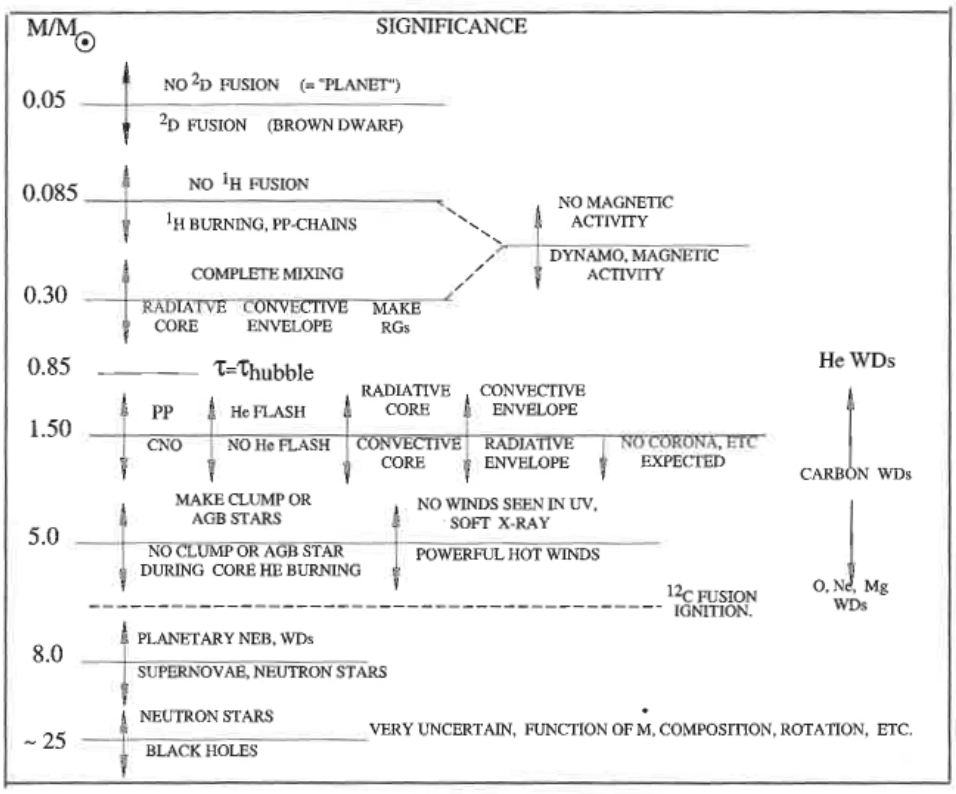

Figure 43: Mass is destiny: final fates of single stars. (Fig. 2.4 of Hansen, Kawaler, and Trimble, 2nd Ed.).

- $\mathbf{M_{fin} < 1.4 M_\odot}$: White dwarf, supported by electron degeneracy pressure.

- $\mathbf{1.4 M_\odot < M_{fin} \lesssim 3 M_\odot}$: Neutron star, supported by neutron degeneracy pressure. The upper limit here is not known with great precision.

- $\mathbf{M_{fin} \gtrsim 3 M_\odot}$: No known support can hold up the remnant; it collapses into a gravitational singularity, a **black hole.**

Fig. 44 shows the masses of known stellar remnants, emphasizing that we know almost nothing about compact objects with masses between 2–5 $M_\odot$. But before we examine these most massive of remnants, let's first reconsider white dwarfs in a bit more detail.

20.3 *White Dwarfs Redux*

Let's construct a more detailed model of a white dwarf than what we've managed before. For example, we've talked before about the WD equation of state and qualitatively estimated their radii, but we can do better.

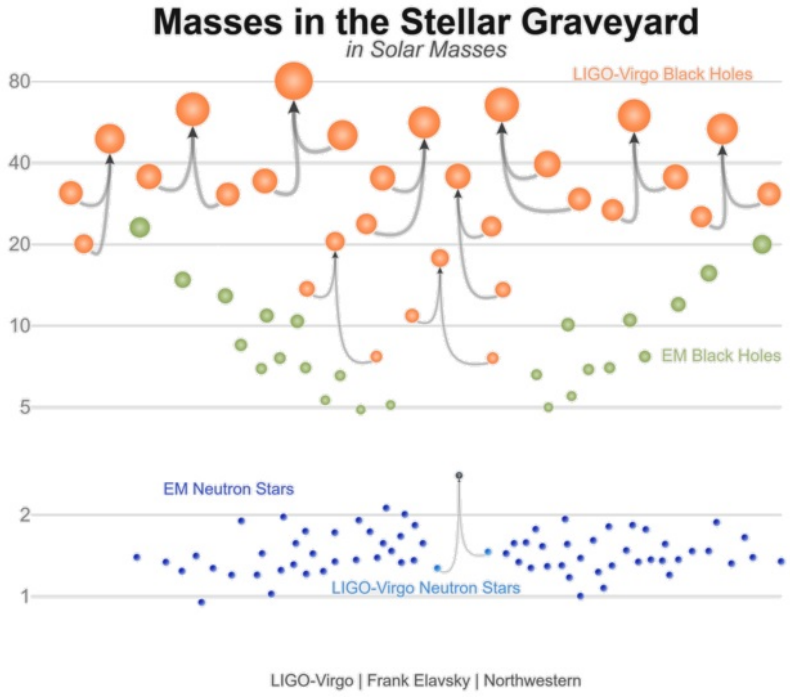

Figure 44: Masses of known extremely compact objects: black holes (above) and neutron stars (below), as of early 2019. Objects joined by arrows indicate mergers observed via gravitational waves.

White dwarf mass-radius relations

Assume we have N electrons that supply the supporting degeneracy pressure, and N protons supplying the mass. Gravity packs the particles closely together (though not as tightly as in a neutron star!). By the Heisenberg uncertainty principle,

$$\Delta x \Delta p \gtrsim \hbar \tag{489}$$

the tight constraints on position imply a correspondingly large momentum dispersion, and so the total kinetic energy will increase.

So the Fermi momentum of the electrons will be approximately

$$p_F \approx \frac{\hbar}{\Delta x} \approx \hbar n^{1/3}. \tag{490}$$

And thus the total Fermi energy will be

$$E_F = \sqrt{p_F^2 c^2 + m_e^2 c^4}. \tag{491}$$

Depending on whether or not the electrons are strongly relativistic, we will have either

$$E_{F,NR} \approx m_e c^2 + \frac{p_F^2}{2m_e} \tag{492}$$

$$\approx C + \frac{\hbar^2}{2m_e}\left(\frac{N}{R^3}\right)^{2/3} \tag{493}$$

or

$$E_{F,UR} \approx p_F c \tag{494}$$

$$\approx \frac{\hbar N^{1/3} c}{R}\left(\frac{N}{R^3}\right)^{2/3} \tag{495}$$

The total gravitational energy will be dominated by the more massive proton, and will be roughly

$$E_G \approx -\frac{GM^2}{R} = -N\frac{GMm_p}{R}. \tag{496}$$

Thus in the non-relativistic limit, the total energy of the system will be

$$E_{NR} \approx C + \frac{\hbar^2}{2m_e}\left(\frac{N^{5/3}}{R^2}\right) - \frac{GM^2}{R}. \tag{497}$$

This expression shows a clear minimum when plotted vs R (see Fig. 45) – this minimum is the equilibrium point, and corresponds to the radius at which a white dwarf is stable. This minimum radius occurs when

(498)
$$\frac{dE}{dR} = 0$$

(499)
$$-\frac{\hbar^2 N^{5/3}}{m_e R^3} + \frac{GM^2}{R^2} = 0$$

or equivalently, when

(500) $$R = \frac{\hbar^2}{G m_e m_p^{5/3} M^{1/3}}.$$

Thus a typical white dwarf with mass $1M_\odot$ will have a radius of just about $1R_\oplus$. Furthermore, note that $R \propto M^{-1/3}$ – so white dwarfs get smaller as we add more mass, as we saw in Sec. 17.4. (We already encountered this while discussing shell burning: as fusion 'ash' is steadily added to a core, it contracts despite its mass having increased.)

Alternatively, in the ultra-relativistic case the total energy of the white

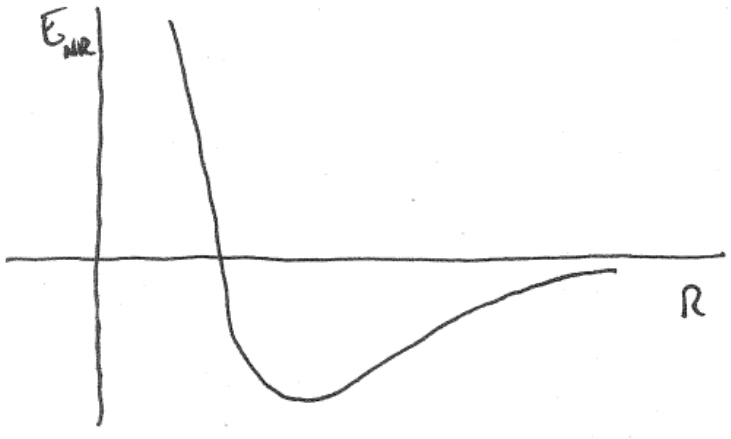

Figure 45: Total energy of a white dwarf in the non-relativistic limit (see Eq. 497). The energy minimum implies an equilibrium point: this will be the radius of the white dwarf.

dwarf will be

(501)
$$E_{UR} \approx \frac{\hbar c N^{4/3}}{R} - \frac{GM^2}{R}$$

(502)
$$= \frac{N^2}{R}\left(\hbar c N^{-2/3} - G m_p^2\right)$$

XXXXXXXXXXXXXX clarify where the above relation comes from

This expression, in contrast to Eq. 497, has no extremum with radius. So rather than a relation between mass and radius, a white dwarf in the ultra-relativistic has a single, limiting mass, given when $E = 0$:

(503) $\hbar c N^{-2/3} = G m_p^2$.

This limiting mass is the aforementioned **Chandrasekhar Mass**, which is approximately

(504)
$$M_{Ch} \approx N_{max} m_p$$

(505)
$$\approx m_p \left(\frac{\hbar c}{G m_p^2}\right)^{3/2}$$

(506)
$$\approx 1.7 M_\odot$$

This is actually not too far off from what a further refinement would predict; we will consider this next.

Polytropic White Dwarf

The next level of refinement is to return to our polytropic model of a white dwarf, which we have discussed previously. As we've seen many times, for white dwarfs we have either

- **Non-relativistic degenerate gas**: $\gamma = 5/3, n = 3/2$.
- **Ultra-relativistic degenerate gas**: $\gamma = 4/3, n = 3$.

And as you just saw in Problem Set 7, the mass of a polytropic white dwarf is

(507) $M = 4\pi\rho_c \lambda_n^3 \xi_{surf}^2 \left.\frac{d\phi_n}{d\xi}\right|_{\xi_{surf}}$

where

$$(508)\quad \lambda_n \left[\frac{(n+1)K\rho_c^{1-n/n}}{4\pi G}\right]^{1/2}$$

and where ξ_{surf} is the Lane-Emden surface coordinate, introduced in Sec. 13.

This means that we have either

$M \propto \rho_c^{1/2}$ (for n=3/2), or

$M \propto \rho_c^0$ =const (for n=3)

and so the mass will steadily increase up to some maximum value, as shown in Fig. 46. To find the transition point and calculate the maximum mass, we need more details. Of particular import is the polytropic constant K_{UR}. The full equation of state turns out to be

$$(509)\quad P = \left(\frac{3}{\pi}\right)^{1/3} \frac{hc}{8m_p^{4/3}} \left(\frac{\rho}{\mu_e}\right)^{4/3}$$

which leads to a more accurate version of the Chandrasekhar Mass,

$$(510)\quad M_{Ch} = 1.4M_\odot \left(\frac{\mu_e}{2}\right)^{-2}.$$

Observations of White Dwarfs

The observational history of white dwarfs is much messier – possibly even more complicated than solving polytropic equations of state. Observations established the existence of unusual celestial objects, but their natures weren't known for some time.

We now know that the first white dwarf was identified in 1783 by William Herschel. He noticed a dim companion to the $V = 4.4$ mag star 40 Eri. The colors of the faint companion indicated that it must be hot (we know now it's $\sim 10^4$ K, hotter than 40 Eri), but it is 5 mag fainter. Thus it must be tiny.

Another, similar object was identified four-score years later; this was Sirius B, discovered using a telescope in Cambridgeport, Massachusetts. Its gravitational connection to Sirius was quickly recognized, and using the tools dis-

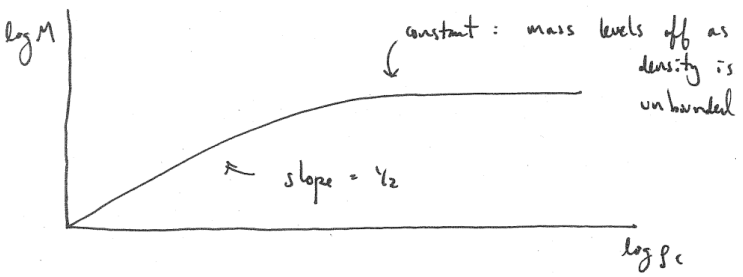

Figure 46: Mass of a white dwarf as its central density increases.

cussed in Sec. 4.3 its mass, luminosity, and (after a "high-contrast" spectrum was obtained in 1915) its temperature were all measured. These indicated $M \approx M_\odot$, $T_{\rm eff} \approx 25,000$ K, and $R \approx 0.01 R_\odot$ — implying $\rho \approx 10^6$ g cm^{-3}.

These numbers were nonsense according to 19^{th} century astrophysics. Quantum mechanics was needed to understand such a bizarre object. It wasn't until 1926 that electron degeneracy pressure was described, and only in 1931 did Chandrasekhar identify his eponymous mass limit. Even so, conservative astronomers resisted for many years.

Other bibs and bobs about white dwarfs:

- As discussed in Sec. 17.7, the final composition of a white dwarf depends on its formation history. If it reached the 3α process, it should be carbon-oxygen. Otherwise, it's probably just a helium white dwarf. (There may be a chance to have O-Ne-Mg WDs, but there's no strong empirical evidence.)
- Some white dwarfs pulsate, permitting asteroseismology to more precisely determine their interior structure from the Fourier spectrum of oscillation modes.
- Gravitational redshifts have been measured from some stars. Since a photon's energy as it leaves a gravitational well changes by

  $$\Delta E = h\nu \Delta\Phi_g / c^2 = h\nu \frac{GM}{c^2} \left(\frac{1}{\infty} - \frac{1}{R_{WD}} \right) \tag{511}$$

  one can measure the wavelength/frequency/energy of a known line relative to its expected location

  $$\frac{\Delta E}{E} = -\frac{GM_{WD}}{R_{WD} c^2} \tag{512}$$

  and so directly measure the WD's mass-to-radius ratio.
- As has been alluded to before, white dwarfs gradually cool down on cosmic timescales. By modeling this, we can estimate the ages of individual (isolated) WDs and also of star clusters. WDs in globular clusters provided one of the first signs that the universe was >10 Gyr old!
- Analysis of white dwarf spectra reveals rotational broadening due to short rotation periods of just $\sim$1000 s, as well as strong magnetic fields of $\sim 10^6$ G (from Zeeman splitting).

20.4 *White Dwarf Cooling Models*

White dwarfs start out extremely hot as the cores of giant stars, but once the stellar envelope is ejected they cool down: first rapidly, then slowly.

White Dwarfs: The Simple Model

In the simplest model of white dwarf cooling, the WD is an isothermal object radiating at temperature T, and its total internal energy is the kinetic energy

of its constituent particles. Thus the total energy available to the WD is

$$E_{tot} \approx NkT = \frac{M}{m_p}kT \tag{513}$$

and its luminosity is

$$L = -\frac{dE_{tot}}{dt} = 4\pi R^2 \sigma T^4. \tag{514}$$

Since the white dwarf is degenerate we will assume that its radius is constant throughout its evolution. Then we have

$$-\frac{M}{m_p}k\frac{dT}{dt} = 4\pi R^2 \sigma T^4 \tag{515}$$

which, after some algebraic manipulation, yields

$$-T^{-4}dT = \frac{4\pi R^2 \sigma m_p}{Mk}dt \tag{516}$$

Thus

$$-\int_{T_{hot}}^{T} T'^{-4}dT' = \int_0^t \frac{4\pi R^2 \sigma m_p}{Mk}dt' \tag{517}$$

where the temperature starts at T_{hot} at $t = 0$ and evolves from there.

The solution is

$$\frac{3}{T^3} - \frac{3}{T_{hot}^3} = \frac{4\pi R^2 \sigma m_p}{Mk}t \tag{518}$$

but because of the rapid cooling, the second term is negligible after a very short time. So after further rearranging, we have

$$T(t) = \left(\frac{3Mk}{4\pi R^2 \sigma m_p}t\right)^{1/3} \tag{519}$$

$$= 5600\ \mathrm{K}\left(\frac{R}{R_\oplus}\right)^{-2/3}\left(\frac{M}{M_\odot}\right)^{1/3}\left(\frac{t}{1\ \mathrm{Gyr}}\right)^{-1/3} \tag{520}$$

This isn't crazy, but it isn't terribly accurate either (and its predicted $L(t)$ will be even further off). We can do better by considering a two-component WD model: the degenerate object remains the same, but its outermost veneer must have sufficiently low density that it is non-degenerate; this outer layer acts like an insulating blanket and slows heat loss from the nearly isothermal interior. Finally, we'll assume that the transition from degenerate to non-degenerate occurs at a transition radius r_{tr}.

The pressure must be continuous at $r_{\rm tr}$; recall from Eq. 408 that the condition for this transition is

$$\rho_{\rm tr} \approx 750 \text{ g cm}^{-3} \mu_e \left(\frac{T}{10^7 \text{ K}} \right)^{3/2}.$$

So the polytropic and ideal-gas equations of state must be equal:

(521)
$$K' T_{\rm tr}^{1+n} = \rho_{\rm tr} \frac{k}{\mu} T_{\rm tr}$$

(522)
$$\approx 2 \times 10^{-8} \mu_e \frac{k}{\mu} T_{\rm tr}^{1+3/2}$$

If we assume that the envelope opacity follows Kramer's Law (Eq. 179),

$$\kappa \approx 4 \times 10^{25} \rho T^{-7/2} \text{ cm}^2 \text{ g}^{-1}$$

then the polytropic coefficient becomes

$$K' \approx 8 \times 10^{-15} \mu^{-1/2} \left[\frac{M/M_\odot}{L/L_\odot} \right]^{1/2} \quad (523)$$

for $n = 3.25$. The result is

$$\frac{L}{L_\odot} \approx 7 \times 10^{-29} \mu \frac{M}{M_\odot} T_{\rm tr}^{7/2}. \quad (524)$$

How does this two-layer white dwarf evolve with time? The specific heat of a mixed (degenerate+ideal gas) is

$$c_V = \frac{3 N_A k}{2 \mu_I} \quad (525)$$

where μ_I is the mean molecular weight of the ions. So the energy output will then be

$$L = -\frac{dE_{\rm ions}}{dt} = -c_V M \frac{dT_{\rm tr}}{dt}. \quad (526)$$

The final solution to all this (see Iben & Tutukov 1984) is

$$\frac{L}{L_\odot} = \left(\frac{A}{12} \right)^{-7/5} \left(\frac{\mu}{2} \right)^{-2/5} \left(\frac{M}{M_\odot} \right) \left(\frac{t}{9 \text{ Myr}} \right)^{-7/5}. \quad (527)$$

This is the **Mestel cooling model** for white dwarfs – not the latest state-of-the-art, but not too bad either. Note that since we have $L \propto t^{-7/5}$ and we know $L \propto T^4$, this implies $T \propto t^{-7/20}$ — remarkably close to the power of $1/3$ we found in our simple model in Eq. 520.

In practice, a number of other factors beyond radiative considerations will

affect white dwarf cooling. E.g., see the Physics Today article on the course website about crystallization effects.

21 Neutron Stars

If a stellar remnant exceeds the Chandrasekhar mass, then even fully relativistic electron degeneracy pressure will be insufficient to support it. As we discussed in Sec. 19.4, only neutron degeneracy pressure can possible halt its final and inevitable collapse. Let's now consider the astrophysics of neutron stars in more detail.

21.1 *Neutronic Chemistry*

For starters: why don't all the neutrons just decay away? An isolated neutron undergoes the decay

(528) $n \to p + e^- + \bar{\nu}_e$

because

(529) $(m_n - m_p)c^2 = 1.3 \text{ MeV}.$

The excess energy will be carried away by the electron and antineutrino.

But in a degenerate medium, the Fermi energy may exceed this 1.3 MeV limit. When this happens, there are no accessible low-energy states for the electron to occupy after decay – so the neutron decay is suppressed (alternatively, imagine the neutron decays but it is energetically favorable for the new electron to immediately recombine with an available proton). We expect this beta-decay suppression to set in when

(530)
$$E_F \gtrsim (m_n - m_p)c^2 = 1.3 \text{ MeV}$$

(531)
$$\sqrt{p_F^2 c^2 + m_e^2 c^4} \gtrsim (m_n - m_p)c^2$$

(532)
$$m_e c^2 \left(\frac{p_F^2}{m_e^2 c^2} + 1 \right)^{1/2} \gtrsim (m_n - m_p)c^2.$$

So to keep the neutrons around, the Fermi momentum must satisfy

(533) $$p_F \gtrsim m_e c \left[\left(\frac{m_n - m_p}{m_e} \right)^2 - 1 \right]^{1/2}$$

or roughly $p_F c \gtrsim 1.2$ MeV. In terms of density, we refer to Eq. 395,

$$p_F = \left(\frac{3n^3\rho}{8\pi m_p} \right)^{1/3}.$$

So combining this with Eq. 533 we see that neutron decay is suppressed for

$$\rho \gtrsim 10^7 \text{ g cm}^{-3}. \tag{534}$$

As ρ_c reaches and exceeds this critical density, the neutron star establishes an equilibrium between neutrons, protons, and electrons. One can develop a Saha-like equation (recall Sec. 8.5) relating the populations of each type of particle; see Sec. 2.6 of Shapiro & Teukolsky for further details. Above the critical density, the so-called **neutron drip** sets in and neutrons slowly leave the individual nuclei. In the extreme end case, the star is indeed entirely neutrons.

21.2 *Tolman-Oppenheimer-Volkoff*

Note also that for neutron stars,

$$\frac{GM}{rc^2} \approx 0.1 - 0.3 \tag{535}$$

and so we are definitely in a range where Newtonian gravity alone will not suffice. General relativity must be used instead.

Recall from Sec. 5 that gravity determines the geometry of spacetime, so that the interval (or distance) ds between two events is

$$ds^2 = g_{\mu\nu} dx^\mu dx^\nu \tag{536}$$

where $g_{\mu\nu}$ is the metric and dx^μ is the coordinate displacement between two events (see Eqs. 12 and 14).

For a spherical, static body, general relativity shows that the appropriate metric is

$$ds^2 = -e^{2\Phi(r)/c^2}(cdt)^2 + \frac{dr^2}{1 = 2GM/rc^2} + r^2(d\theta^2 + \sin^2\theta d\phi^2) \tag{537}$$

where as usual

$$M(r) = \int_0^r = 4\pi(r')^2 \rho(r') dr' \tag{538}$$

and

$$\frac{d\Phi}{dr} = -\frac{G[M(r) + r\pi r^2 P(r)/c^2]}{r(r - 2GM(r)/c^2)}. \tag{539}$$

The boundary conditions are that

$$e^{2\Phi/c^2} = 1 - \frac{2GM}{rc^2} \quad (r > R_*) \tag{540}$$

$$\rho(r) = 0 \quad (r \geq R_*) \tag{541}$$

These equations build in the relativity of distance and time, plus the fact that all forms of energy (including pressure) contribute to gravity. Ultimately the new, relativistic equation of hydrostatic equilibrium is

$$\frac{dP}{dr} = -\left(\frac{G}{r^2}\right)\left[\frac{M + 4\pi r^3 P/c^2}{1 - 2GM(r)/rc^2}\right]\left[\rho + P/c^2\right]. \quad (542)$$

This is the **Tolman-Oppenheimer-Volkoff equation** (or TOV). Note that in the limit of low densities and pressures, all terms with $1/c^2$ drop out and we recover Eq. 192,

$$\frac{dP}{dr} = -\left(\frac{G}{r^2}\right) M\rho = -\rho g.$$

21.3 *Neutron star interior models*

To make a neutron star model, we need to solve the TOV equation – but we also need to have an equation of state to work with. The trouble is that neutron stars push us into a regime where the physics is not accurately known! But we can still consider a few limiting cases.

The first of these is to assume that the neutron star equation of state is so stiff that it is incompressible, i.e., $\rho(r) = \rho_0 =$ constant. Then (as Problem Set 8 demonstrates),

$$P(r) = \rho_0 c^2 \left[\frac{(1 - R_S r^2/R_*^3)^{1/2} - (1 - R_S/R_*)^{1/2}}{3(1 - R_S/R_*)^{1/2} - (1 - R_S r^2/R_*^3)^{1/2}}\right] \quad (543)$$

where R_* is the radius of the neutron star and

$$R_S = \frac{2GM}{c^2} \quad (544)$$

is the **Schwarzschild radius**. This incompressible model shows that $P(r = 0) \to \infty$ if R_* is too small (i.e., if the NS is too compact). The denominator of Eq. 543 must be > 0, so we obtain the constraint that

$$R_* > \frac{9}{8} R_S = 2.25 \frac{GM}{c^2}. \quad (545)$$

The implication is that a star more compact than this cannot be supported even by infinite pressure; it will collapse instead.

In reality, no fluid can be truly incompressible, since this would require an infinite (and super-luminal) sound speed. Rhoades & Ruffini (1974) developed as stiff a NS model as possible that was still consistent with relativity. Their result was that neutron stars must have $M < 3.2 M_\odot$.

21.4 *A bit more neutron star structure*

More typically in modern studies, one chooses an equation of state – or at least, builds up $P(\rho)$ based on your favorite knowledge/assumptions about

dense matter. One picks a central density (informed by your previous model, perhaps) and integrates Eq. 542 until $P = 0$ is reached; this is the surface. One tabulates M_* and R_* for different equations of state; Fig. 47 shows the range of possible models.

Inspection of Fig. 47 shows that predicted radii and maximum masses vary by ∼50% for neutron stars. Typical models (plotted in black) assume "normal" nuclear matter – just standard neutrons at low densities, but at higher densities condensations of hyperons, kaons, pions, etc. may all become important. Different models make different choices for when various mesons (and other particles) play a role. Until the critical density is reached, these models scale roughly as $R_* \propto M_*^{-1/3}$ (as we saw for white dwarfs in Sec. 20.3) since the stars are still explained decently well by straightforward degeneracy calculations.

Another family of models assumes that (under other assumptions) neutron stars may be composed of so-called strange quark matter. These objects would instead be hypothetical condensates of up, down, and strange quarks that would be more stable than normal matter at the high densities involved. In grossly simplified terms, these models amount to a uniform density fluid – so $R_* \propto M_*^{1/3}$.

There are also several forbidden regions:

- **General Relativity:** If a neutron star is to avoid becoming a black hole, it must always satisfy $R > 2GM/c^2$.
- **Causality:** This is the requirement that the soundspeed c_s must satisfy $dP/d\rho = c_s < c^2$.
- **Rotation:** Neutron stars rotate (like stars and other stellar remnants). To

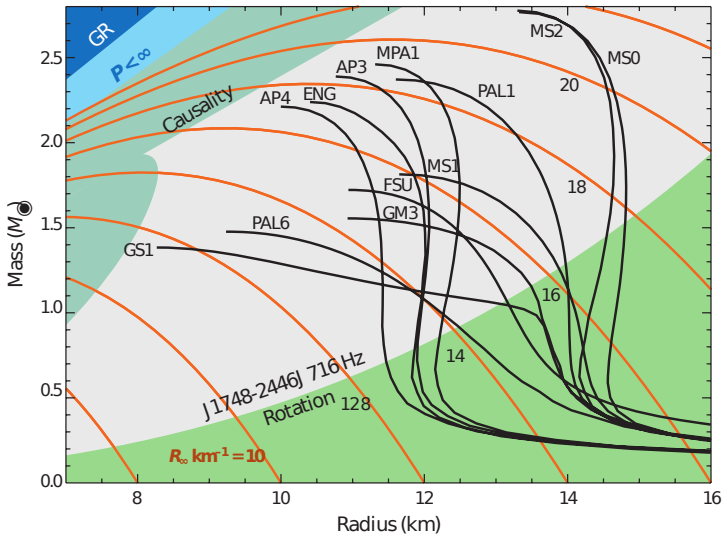

Figure 47: Predicted masses and radii (black curves) for various suggested neutron star equations of state. Orange curves show contours of $R_\infty = R(1 - 2GM/Rc^2)^{-1/2}$. Adapted from Lattimer (2012), *Ann. Rev. Nuc. Part. Sci.*.

hold together, they must satisfy

$$\omega^2 R < \frac{GM}{R^2} \tag{546}$$

or equivalently

$$\omega^2 < \frac{GM}{R^3} \tag{547}$$

and so a spinning neutron star must always satisfy

$$G\rho_{\rm avg} \geq \frac{3\omega^2}{4\pi}. \tag{548}$$

Thus the "rotation" line corresponds to constant average density. In Fig. 47, the particular line plotted corresponds to the fastest-known rotation rate for any neutron star, $f = \omega/2\pi = 716$ Hz.

The orange curves in Fig. 47 indicate lines of constant **radiation radius** R_∞. In principle one could observe the thermal (typically X-ray) spectrum of a young neutron star of known distance, assume a blackbody, and estimate the radius directly. But for such massive, compact objects general relativistic effects will come into play: the temperature, size, and so luminosity observed at large distances are not the "true" values that would be observed in the neutron star's rest frame. In particular, the radiation radius is

$$R_\infty = R_*(1 + z_g) \tag{549}$$

where z_g is the **gravitational redshift** (see Eq. 511). Similarly, the temperature that will be inferred is

$$T_{\rm eff}^\infty = \frac{T_{\rm eff}}{1 + z_g}. \tag{550}$$

21.5 *Neutron Star Observations*

Neutron stars are fairly unique among objects discussed thus far. Planets, stars, nebulae, and galaxies were all observed for millennia before the true natures of these objects were uncovered. In contrast, neutron stars (along with black holes) were discussed theoretically long before any observational evidence was found.

Unfortunately the observational measurements are frustratingly sparse. Even the fastest spin rates don't much push the physical limits. As far as maximum masses go, Fig. 44 shows that most measured NS masses are around $1.4M_\odot$. The few especially massive examples ($M_* \gtrsim 2M_\odot$) do help kill quite a few models, though. And for radii it's worse: while some masses are measured to $\lesssim 2\%$, there are no comparably precise NS radius measurements (despite many efforts). Anyway, only $\sim$10 neutron stars are close enough that we can study their thermal emission (in X-rays; $kT \gtrsim 50$ keV) — if they are more than $\gtrsim 500$ pc away then the ISM absorbs most of the radiation; and even when

detections are made, detailed atmospheric modeling (with many unknowns) is needed to accurately infer radii.

Most observational data of neutron stars come from **pulsars** – neither truly pulsating nor truly stars, but rapidly-rotating neutron stars that emit periodic radio (or other EM) emission. These were first discovered in 1967 by Jocelyn Bell, a 2nd year graduate student.

21.6 *Pulsars*

First discovered in 1967, thousands of pulsars are now known (see Fig. 48). Most are detected in radio, but a subset are also seen in X-rays and even gamma rays. The period of the EM emission ranges from as long as 10 s in a few cases to just 1–2 ms at the other extreme.

It was recognized almost immediately that these objects must be very small. E.g., the Crab nebular pulsar (the remnant of SN 1054) has a period of $P = 33$ msec, implying a maximum diameter of

$$L \lesssim cP = (3 \times 10^5 \text{ km s}^{-1})(0.033) \approx 10^5 \text{ km}. \quad (551)$$

The size is consistent with a white dwarf but the period isn't. From Eq. 547

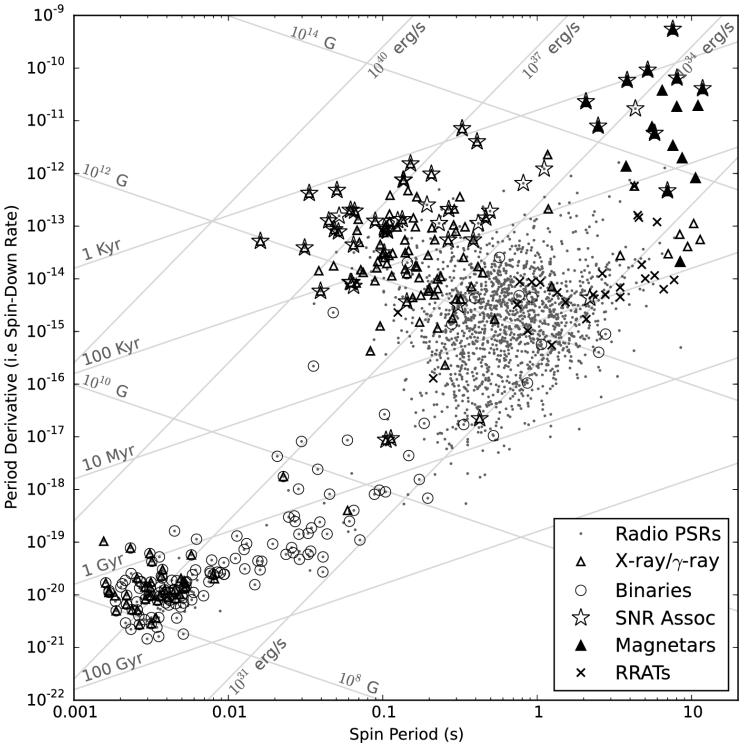

Figure 48: Pulsar observations in the traditional P-$\dot{P}$ plane. Straight lines indicate characteristic ages, spin-down luminosities, and maximum magnetic field strengths. (from `https://www.cv.nrao.edu/~sransom/web/Ch6.html`).

a white dwarf spinning that fast couldn't hold together, and the timescale for pulsations (whether freefall, Eq. 198, or sound-crossing, Eq. 201) shouldn't be lower than a few seconds. And a black hole shouldn't have any surface with which to anchor coherent, precisely-repeatable EM radiation. Thus by process of elimination, a neutron star is the most likely culprit.

The phenomenological view is that an intense beam of EM radiation is misaligned with the neutron star's rotation axis. This presumably arises from a magnetic dipole misaligned with the NS's spin axis; nonetheless many details remain unclear, and pulsar emission mechanisms remain an active area of research. But it must somehow involve a rotating magnetic field generating a large electric field from equator to pole. This in turn accelerates electrons and generates synchrotron radiation that is highly coherent and highly polarized.

Rotation and Magnetic Fields

To explain the observed emission requires rapid rotation and an extremely strong magnetic field; both can be understood from basic conservation principles. As noted previously, white dwarfs typically have $P_{WD} \sim 1000$ s and $B \sim 10^6$ G (the Earth and Sun both have magnetic fields of just $\sim$1 G). Assuming angular momentum is conserved during the collapse from white dwarf to neutron star, then we should expect

$$I_{WD}\Omega_{WD} = I_{NS}\Omega_{NS} \tag{552}$$

and so

$$\frac{P_{NS}}{P_{WD}} = \frac{M_{NS}R_{NS}^2}{M_{WD}R_{WD}^2} \sim \left(10^{-3}\right)^2. \tag{553}$$

Thus we should expect

$$P_{NS} \sim 10^{-6}P_{WD} \sim 10^{-3} \text{ sec} \tag{554}$$

which is roughly consistent with the shortest periods seen in Fig. 48.

As for the strong magnetic field, that can also be inferred from the known field strengths of white dwarfs. Magnetohydrodynamics tells us that magnetic flux Φ_B is conserved through any surface moving with a plasma. Thus the magnetic flux through a loop enclosing solid angle $\Delta\Omega$ around either the WD progenitor or NS progeny should be

$$\Phi_B = B_{WD}\Delta\Omega R_{WD}^2 \approx B_{NS}\Delta\Omega R_{NS}^2 \tag{555}$$

and so

$$\frac{B_{NS}}{B_{WD}} \approx \left(\frac{R_{WD}}{R_{NS}}\right)^2 \approx 10^6. \tag{556}$$

Thus, we expect neutron stars to have surface magnetic field strengths of order 10^{12} G.

These strong magnetic fields induce an electromagnetic "backreaction,"

slowing the rotation over time. Unlike most stellar objects, which are in quasi-steady state, this spindown is precisely measured in many pulsars. The traditional value is the time derivative of the period, or $\dot{P}$ (i.e., P-dot), a dimensionless quantity plotted as the vertical axis of Fig. 48. Because neutron stars spin down we almost always see $\dot{P} > 0$ (i.e., spin period increasing). Occasionally some neutron stars will show transitory "glitches" indicating sudden rearrangements of their moments of inertia (like a spinning ice skater rearranging their limbs). Glitches are usually seen in young, relatively hot neutron stars whose interiors are still stabilizing and reaching a more stable equilibrium.

When P and $\dot{P}$ are plotted against each other as in Fig. 48, we obtain the observational equivalent of the HR diagram – but for neutron stars. The periods span a range of $10^{-3} - 10$ s, with a peak near 0.5 s; meanwhile $\dot{P}$ has a much broader range, from $10^{-20} - 10^{-10}$ with a peak near 10^{-15}. For the lowest values of $\dot{P}$, the emission from these pulsars is more stable than the most precise atomic clocks (which have comparable stabilities of $\sim 10^{-16}$).

Pulsar luminosity

Fig. 48 also lets us estimate the energy loss rate of pulsars. Assuming that their energy reservoir is mainly rotational kinetic energy, then (in the classical approximation)

(557)
$$E_{\rm rot} = \frac{1}{2} I \omega^2$$

(558)
$$= 2\pi^2 \frac{I}{P^2}$$

(559)
$$\approx \frac{4\pi^2}{5} M \left(\frac{R}{P}\right)^2$$

and so

(560)
$$\frac{dE}{dt} = \frac{d}{dt}\left(\frac{1}{2} I \omega^2\right)$$

(561)
$$= I \omega \dot{\omega}$$

(562)
$$= \frac{8\pi^2}{5} M \frac{R^2}{P^3} \dot{P}.$$

For the Crab Nebula ($P = 33$ ms, $\dot{P} \sim 10^{-13}$, $M_* \approx 1.5 M_\odot$, $R_* \approx 10$ km) we find

(563) $$L = -\frac{dE}{dt} \approx 10^{38} \text{ erg s}^{-1}$$

which is comparable to the bolometric luminosity of the entire Crab Nebula; pulsars essentially convert their rotational energy into light. (Also, note that this power far outstrips the Solar luminosity of $L_\odot \approx 4 \times 10^{33}$ erg s^{-1}).

The mechanism of that radiation, as previously noted, is the strong, rapidly rotating magnetic field. For a given magnetic moment m, the magnetic equivalent of the Larmor formula gives the emitted power as

$$P = \frac{2|\ddot{m}|^2}{3c^3}. \tag{564}$$

Following Rybicki & Lightman (pp. 323–324), the surface magnetic field is

$$B_0 = \frac{2m}{R^3}. \tag{565}$$

The component of $\vec{m}$ along the rotation axis is constant; given an angle α between the rotation and magnetic dipole axes,

$$|\ddot{\vec{m}}| = \omega^2 |\vec{m}| \sin\alpha. \tag{566}$$

Thus the total radiated power is

$$L = \frac{\sin^2\alpha}{6c^3} B_0^2 \omega^4 R^6. \tag{567}$$

Setting Eqs. 562 and 567 equal to each other, we see that

$$B_0^2 \propto P\dot{P} \tag{568}$$

and so the P-$\dot{P}$ diagram of Fig. 48 should allow us to directly estimate the magnetic field strength of a pulsar. Typical values are $10^8 - 10^{15}$ G; objects with the strongest fields are termed **magnetars**. These sometimes exhibit huge outbursts, affecting terrestrial satellites and modifying the Earth's ionosphere from kpc away.

Pulsar ages and the braking index

Most importantly, the combination of P and $\dot{P}$ allows us to estimate the age of a pulsar. If we assume that the spindown rate depends on the current spin rate to the n^{th} power, then

$$\dot{\omega} = a\omega^n. \tag{569}$$

If we fold in information about the second derivative,

$$\ddot{\omega} = an\omega^{n-1}\dot{\omega}, \tag{570}$$

then

$$\ddot{\omega}\omega = an\omega^n\dot{\omega}^2 \tag{571}$$

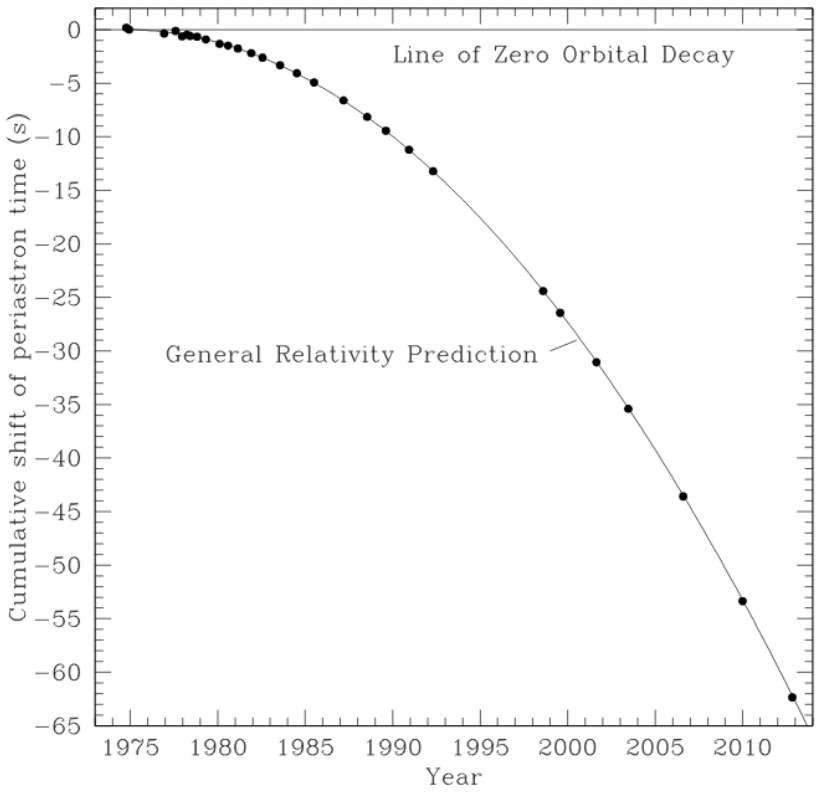

Figure 49: Period evolution of the famous Hulse-Taylor pulsar, with $P = 7.75$ hr.

and so

$$n = \frac{\omega\ddot{\omega}}{\dot{\omega}^2} \tag{572}$$

is defined as the **braking index** of the pulsar. For magnetic dipole radiation as described by Eqs. 562 and 567, we have

$$I\omega\dot{\omega} \propto \omega^4 \tag{573}$$

and so the braking index $n = 3$ for pure magnetic dipole radiation.

Traditionally, one then models the period evolution as

$$P(t) = ct^{1/(n-1)} \tag{574}$$

which yields

$$\dot{P} = \frac{c}{n-1} t^{1/(n-1)-1} = \frac{P}{t(n-1)} \tag{575}$$

and so the **characteristic age** of a pulsar is given by

$$\tau_{\rm pulsar} = \frac{1}{n-1}\frac{P}{\dot{P}} = \frac{P}{2\dot{P}} \quad \text{(for n = 3).} \tag{576}$$

Note from Eq. 574 that $\tau_{\rm pulsar}$ actually corresponds to the time for the period to increase by a factor of two. Nonetheless it's a pretty good age indicator: for the Crab pulsar ($P = 33$ ms, $\dot{P} = 4.2 \times 10^{-13}$) we find $\tau = 1200$ yr. Since this pulsar formed in SN 1054, our estimate is in pretty good agreement.

As seen for the Crab, characteristic ages are only approximate. Note from Fig. 48 that many millisecond pulsars have inferred ages > 10 Gyr, older than the universe! These are thought to have massively spun up by accreting high-angular-momentum material that inspiraled from a neighboring star (note that almost all ms pulsars are in binary systems). For other stars, the ages seem reasonable but the measured braking index (from P, $\dot{P}$, and $\ddot{P}$) is not 3.0 – for example, $n_{\rm crab} = 2.515 \pm 0.005$. This reflects the fact that the radiation is only approximately dipolar.

Other tidbits, bibs, and bobs about pulsars:

- **Binary neutron stars.** When one (or both) of the objects in a binary is a neutron star, we can use the variations in the pulse arrival times to precisely map the orbit. Fig. 49 shows 40 years of data on the Hulse-Taylor pulsar, indicating inexorable inspiral of the binary due to emission of gravitational radiation. These provide excellent tests of GR, and also provide some of the most precise NS masses known.

- **Pulsar planets.** A diminutive, multibody of binary pulsars. It is not commonly known that the first confirmed planets beyond the Solar system were discovered by pulsar timing measurements. These revealed a three-planet system with orbital periods of 25, 66, and 98 days and masses of 0.02 (!!), 3.9, and 4.3 $M_\oplus$, respectively. These have withstood the test of time, but they are not representative of the general population of extra-solar planets. Only ~ 6 such planets are known, in 3–4 systems.

22 Black Holes

22.1 *Useful references*

- Kippenhahn, Weiger, and Weiss, 2nd ed., Ch. 39

22.2 *Introduction*

We've almost completed our astrophysical survey of stars, their evolution, and the final end products. Just to recap:

Initial Mass	Fate	Final Mass
$\lesssim 13 M_{\rm Jup}$	Planet	same
$\sim 13 M_{\rm Jup} - \sim 0.08 M_\odot$	Brown dwarf	same
$\lesssim 0.08 M_\odot$	Brown dwarf	same
$0.08 M_\odot - 0.8 M_\odot$	Lives on MS for $> t_{\rm Hubble}$	same
$0.8 M_\odot - \boxed{7 M_\odot}$	White dwarf	$0.6 M_\odot - 1.4 M_\odot$
$\boxed{7 M_\odot} - \boxed{20 M_\odot}$	Neutron star	$1.4 M_\odot - \underline{3 M_\odot \text{ (?)}}$
$\boxed{\gtrsim 20 M_\odot}$	Black hole	$\underline{\gtrsim 3 M_\odot \text{ (?)}}$

In this table, initial masses in $\boxed{\text{boxes}}$ are uncertain due to poorly understood aspects of mass loss during stellar evolution. On the other hand, final masses that are underlined above are uncertain because the equation of state of neutron stars is only poorly known. But at final masses $\gtrsim 3 M_\odot$, no known physics provides a pressure that can hold up a star. The increase in pressure itself is ultimately self-defeating: it gravitates! Eventually the point is reached where support would require infinite pressure; nothing can hold it up. General relativity tells us that it must collapse, leaving a black hole behind.

22.3 *Observations of Black Holes*

Like neutron stars, the concept of black holes was invented before any observational evidence arose. Even 18th-century natural philosophers considered the impact of sufficient gravity on corpuscular light (i.e., photons). Relativity put the discussion on firmer and more accurate footing, but decades passed before the impact of event horizons, rotating black holes, etc. were recognized. In the last half-century observers have steadily built up a catalog of objects that are

- **Massive** — i.e., $> 3 M_\odot$ and so more massive than any plausible neutron star equation-of-state can support;
- **Compact**
- **Dark.**

This catalog includes many objects of masses $M \sim 5 - 25 M_\odot$ (stellar remnants; see Fig. 44), along with objects with $M \sim 10^6 - 10^9 M_\odot$ (**supermassive black holes**) at the centers of our and other galaxies. Evidence for **intermediate-mass black holes** remains inconclusive despite considerable searches.

Many of the first such stellar-mass black holes were discovered as bright X-ray sources. One of the earliest was Cygnus X-1 (i.e., the brightest X-ray source in the constellation Cygnus), over which Steven Hawking lost a bet with Kip Thorne. Another was V404 Cygni (a variable star in the same constellation), identified earlier but which underwent a massive outburst in 2015 – at peak brightness, the system was 50× brighter than the Crab Nebula (supernova remnant) in X-rays. In all these systems, the X-rays arise from hot gas (at millions of K) in an accretion disk spiraling down into the black hole. Most of these systems are binaries, and the accreting material is stripped from a "normal" star (pre-collapse, pre-supernova) by the black hole. Thus the component masses can be measured using the tools discussed in Sec. 4.

For V404 Cyg, the binary mass function (Eq. 7) is

$$f_m = \frac{(M_X \sin I)^3}{(M_X + M_c)^2} = 6.26 \pm 0.31 M_\odot. \tag{577}$$

The companion star is a K giant with $M \sim M_\odot$, implying that

$$M_x \sin^3 I \sim 6.3 M_\odot \tag{578}$$

and so

$$M_X \gtrsim 6.3 M_\odot. \tag{579}$$

However, from the binary period ($P = 6.4$ d) we find only that

$$a \gtrsim 0.12 \text{ AU} \tag{580}$$

which is far larger than the Schwarzschild radius for a black hole of this mass. Thus it was some time before evidence for V404 Cyg's black hole nature was widely accepted.

Observational evidence for supermassive black holes came initially from the velocity dispersion of stars near the centers of nearby galaxies. More recently, unambiguous evidence for these beasts came from orbital monitoring of stars around Sagittarius A* (in the Milky Way, $M \sim 4 \times 10^6 M_\odot$) and an image of the accretion disk and black hole shadow in the center of M87 ($M \sim 6 \times 10^9 M_\odot$); both are shown in Fig. 50.

22.4 *Non-Newtonian Orbits*

In general, sufficient evidence for a black hole requires demonstrating that too much mass is in too small of a volume, such that the mass much be enclosed within one Schwarzschild radius:

$$R_S = \frac{2GM}{c^2}. \tag{581}$$

But another key sign can be orbits with strongly non-Keplerian features that encode the nature of strong (relativistic) gravity.

Recall that the Keplerian two-body problem (Sec. 2) can be reduced to a

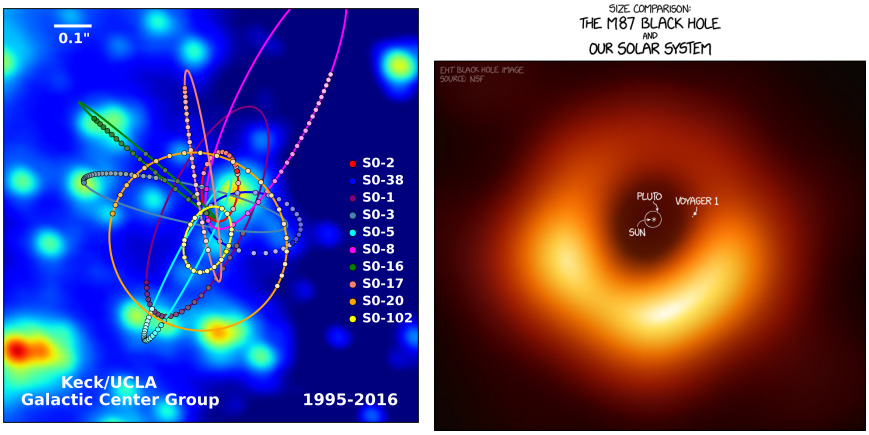

Figure 50: *Left:* Stellar orbits around Sgr A*, the supermassive black hole at the center of the Milky Way. Star S0-2 has a period of 16 yr, while other orbits are longer-period. (From `http://www.astro.ucla.edu/~ghezgroup/gc/`). *Right:* Accretion disk and shadow of the supermassive black hole at the center of nearby galaxy M87. The bright ring's diameter is 42μas, or $\sim 2000\times$ smaller than the scale bar at *left*.

one-dimensional effective potential:

$$E = \frac{1}{2}m\left(\frac{dr}{dt}\right)^2 + \frac{L^2}{2mr^2} - \frac{GMm}{r} \tag{582}$$

or

$$\epsilon = \frac{1}{2}\dot{r}^2 + \frac{l^2}{2r^2} - \frac{GM}{r} \tag{583}$$

$$= \frac{1}{2}\dot{r}^2 + V_{\text{eff}} \tag{584}$$

where ϵ and ℓ are the energy and angular momentum per mass, respectively. Fig. 51 recalls this scenario, with different values of ϵ corresponding to unbound, elliptical, or circular orbits.

The equivalent for orbits in general relativity looks more interesting. If we have a non-spinning black hole, then

$$\left(\frac{dr}{dt}\right)^2 = \frac{\epsilon^2}{c^2} - \left(1 - \frac{2GM}{rc^2}\right)\left(c^2 + \frac{\ell^2}{r^2}\right) \tag{585}$$

where ϵ and ℓ have the same meanings (but ϵ now includes the full relativistic energy, including rest mass energy). But one can again define a relativistic

effective potential,

$$V_{\text{eff,rel}} = \left(1 - \frac{2GM}{rc^2}\right)\left(c^2 + \frac{\ell^2}{r^2}\right). \tag{586}$$

For a particular value of ϵ^2, the orbital dynamics are determined by $V_{\text{eff,rel}}$ (analogously to the Newtonian case). Fig. 51 compares this case to the classical Keplerian case. A few interesting features that distinguish this new scenario:

- Circular orbits still exist if ϵ^2 is tangent to and just touches V_{eff} at a local minimum.
- Now there is an extra "hump" in the profile whose height depends on ℓ. This means that for certain values of ℓ^2, no local minimum exists – and thus in these cases there are no stable circular orbits.
- If ϵ is high enough for a given ℓ, the trajectory can reach $r = 0$ (this never happens in the classical case for nonzero angular momentum). This is a singularity: here tidal forces become infinitely strong, and anything approaching it will be shredded.

The local minimum disappears for

$$\ell = \sqrt{12}\frac{GM}{c} \tag{587}$$

which corresponds to a stable circular orbit at $r = 3R_s$. We therefore expect no orbits inside of this radius. So even inside an accretion disk, we should have

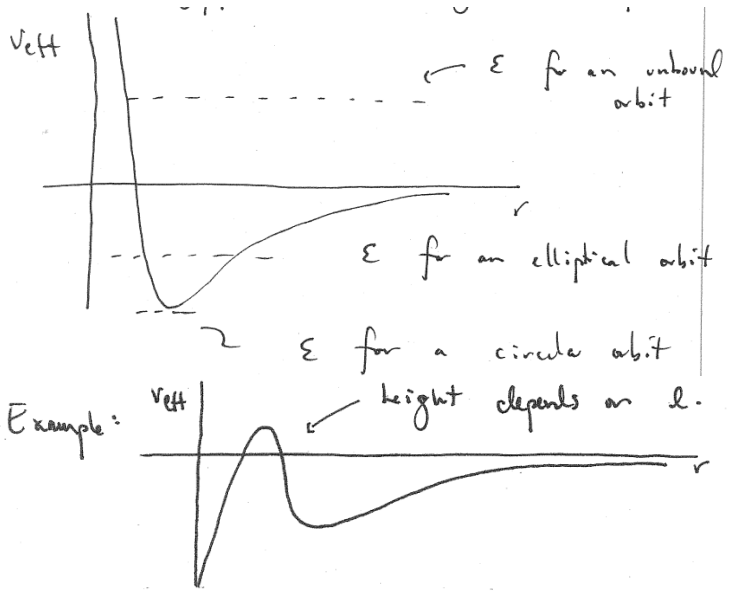

Figure 51: Effective potential vs. separation. *Top:* in a classical, Keplerian two-body system; *Bottom:* in the relativistic limit.

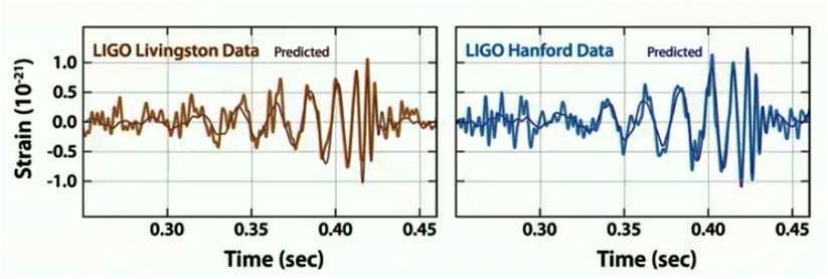

Figure 52: Gravitational wave event GW150914, indicating the inspiral and merger of two black holes.

a hole a few times larger than any black hole's event horizon.

Note that things get even more exciting once we bring rotation into the picture. The spin of a black hole has several interesting effects:

- The event horizon changes size and shape
- Orbits have a much more complicated (non-spherical) potential.
- Orbital frequencies become affected by "frame-dragging" as the spinning black hole twists spacetime around itself.

Thanks to the **no-hair theorem**, it turns out that everything about a black hole (including the orbits around it) can be described by just three parameters: mass, angular momentum (spin), and electric charge.

22.5 *Gravitational Waves and Black Holes*

Black holes must solve the Einstein equations in vacuum, $G_{\mu\nu} = 0$. This is true even if two black holes are close together. In this case, they emit gravitational waves – potentially with a much higher GW luminosity than the neutron star binaries whose inspiral also indicates GW emission (Sec. 21.6). It wasn't until the mid-2000s that computational relativity calculations first predicted what happens when two black holes orbit each other. The result, later spectacularly verified by gravitational wave measurements (see Fig. 52) includes three epochs:

1. **Inspiral:** Long before the merger, the binary is on a nearly-periodic orbit - but energy is being lost due to GW emission, so the semimajor axis (and period) steadily shrinks. Motion here is determined by the effective potential $V_{\text{eff,rel}}$, but with ϵ and ℓ slowly evolving.
2. **Plunge and Merger:** As the gravitational field grows in strength, eventually the orbits become unstable and the binary members rapidly come together, forming a single object.
3. **Ringdown:** A few, last oscillations are seen as the merged remnant settles down to the exact Kerr solution for a rotating black hole (enforcing the no-hair theorem).

This structure matches most of the gravitational wave events found so far (see e.g. Fig. 44). *Only* a black hole model, including all the necessary (very!) strong gravity physics, is able to explain these observations.

23 Accretion

23.1 *Useful references*

- Murray & Dermott, Ch. 3
- Choudhuri, Secs. 4.5.1, 5.6
- Hansen, Kawaler, and Trimble, Sec. 2.13

Much of our empirical knowledge of neutron stars and black holes comes from **accretion**: the flow of material from some object (usually a star) onto another. Accretion is a ubiquitous process in astrophysics, contributing to the formation and growth of planets ($< 10^{-3} M_\odot$), stars ($\sim M_\odot$), stellar remnants such as white dwarfs, neutron stars and black holes ($\lesssim 40 M_\odot$), and even the supermassive black holes that lie at the centers of galaxies ($10^6 - 10^9 M_\odot$).

23.2 *Lagrange Points and Equilibrium*

Our first goal is to identify the points of equilibrium in a two-body binary system with orbital period P. Imagine a test particle (e.g., an atom of potentially accretable gas) near the binary: what forces act on it? To answer this we examine the system in a frame co-rotating with the binary, as sketched in Fig. 53. We have two objects with masses $m_1 > m_2$,

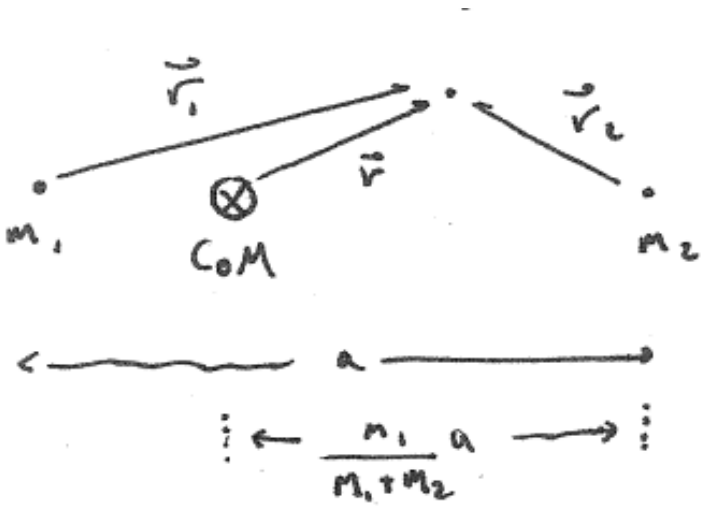

Figure 53: Schematic view of a coordinate frame co-rotating with a binary. "CoM" indicates the center of mass.

total mass M, mass ratio $q = m_1/m_2$, and a systemic angular velocity

(588)
$$\vec{\Omega} = \frac{2\pi}{P}\hat{z}$$

(589)
$$= \left(\frac{GM}{a^3}\right)^{1/2}\hat{z}$$

We expect to find a zone of influence near each body in the binary, such that our test particle will remain near that body. Any material inside this zone will stay on or near its dominating body; any material outside the zone will not be bound and could accrete onto the other object. For two stationary masses the effective potential would merely be the sum of their gravitational wells; the key difference here is that since we are considering the test particle within a rotating (non-inertial) reference frame, we must include a fictitious centrifugal force as well. In this **Roche potential**, we then have

(590) $$\psi_R(\vec{r}) = -G\frac{m_1}{r_1} - G\frac{m_2}{r_2} - \frac{1}{2}\Omega^2 r^2.$$

Note that the Roche potential, including only the centrifugal term, is just fine for considering equilibrium points (at which our test particle would be stationary). To consider dynamics and particle trajectories (i.e. nonzero velocities), we would also need to consider the (also fictitious)

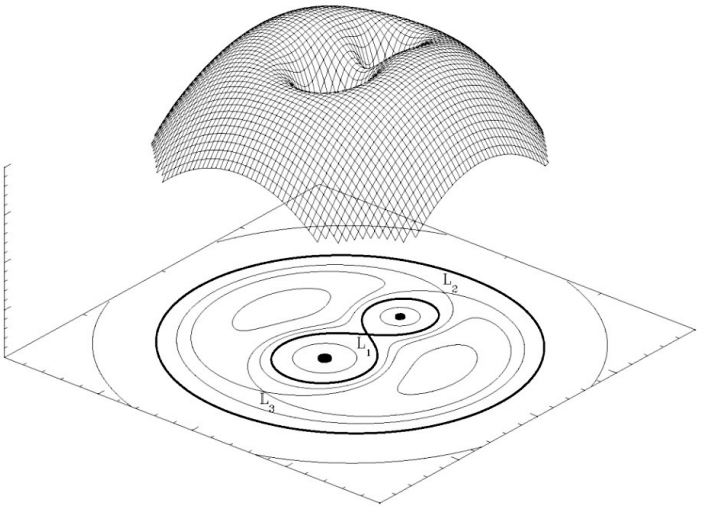

Figure 54: Roche potential (Eq. 590) as a surface plot (above) and as contour plot (below). Lagrange points 1–3 are noted; points 4 and 5 would be to either side of the "figure eight."

Coriolis term:

(591) $\vec{F}_{\text{Cor}} = 2m\vec{v} \times \vec{\Omega}$.

But so long as $v = 0$, we can neglect it.

Fig. 54 depicts the Roche potential as both a 3D mesh surface plot and a 2D contour plot. Note several key features:

- The gravitational well of each star shows up prominently for small $\vec{r}_1$ and $\vec{r}_2$. At large r, the centrifugal term dominates.
- If we take a cross-sectional cut along the line connecting the masses, ψ_R shows three local maxima. These are the first three **Lagrange Points** (actually found by Euler). L_1 is between the two objects (it is *not* the center of mass), L_2 is outside the low-mass object, and L_3 is outside the high-mass object.
- Expanding from the cross-section to the full 2D plane, there are two local maxima to each side: these are the final Lagrange points, L_4 and L_5. Furthermore, note that $L_1 - L_3$ are actually saddle points, and not truly local maxima.

All five of the Lagrange points can be identified as equilibrium points by setting

$$\vec{\nabla}\psi_R = 0.$$

As is apparent from Fig. 54, in the Roche description none of these five points appear to be truly stable equilibria. As noted above, this is because we have neglected Coriolis forces. When these are included $L_1 - L_3$ remain at least mildly unstable (or worse), but spacecraft can still maintain orbits around these points with only minimal use of thrusters.

Points L_4 and L_5 turn out to be true equilibria: given a small perturbation from those points, the Coriolis force will keep the test particle in funny-looking orbits around one or the other of these two points. If given a relatively small perturbation the test particle will exhibit so-called **tadpole orbits**, oscillating around L_4 or L_5 with a greater displacement toward L_3 than toward L_2. Thousands of asteroids are seen librating around Jupiter's L_4 and L_5 points; such objects are often terms **Trojans**. If given sufficient impetus, the test particle can be sent into a **horseshoe orbit**, wherein it oscillates around most of the system (as viewed from within the rotating frame). An object is a horseshoe orbit is less tightly bound and ranges over a much broader range of parameter space; nonetheless numerous such objects are also known.

23.3 *Roche Lobes and Equipotentials*

In this rotating reference frame, a star in equilibrium will still satisfy the equation of hydrostatic equilibrium. Now we no longer have spherical

symmetry, so our 3D equivalent of Eq. 192 is

$$\vec{\nabla} P = -\rho \vec{g}_{\text{eff}} = -\rho \vec{\nabla} \psi_R. \tag{592}$$

This means that the contours of ψ_R shown in Fig. 54 correspond to surfaces of constant pressure.

One often speaks of a Roche lobe radius – i.e., the radius of a sphere with the same volume as the Roche lobe. For star one, an approximation good to 1% is

$$\frac{R_1}{a} = \frac{0.49 q^{2/3}}{0.6 q^{2/3} + \ln(1 + q^{1/3})}. \tag{593}$$

If $q \ll 1$, then an even simpler approximation is

$$\frac{R_1}{a} \approx \frac{1}{2} q^{1/3}. \tag{594}$$

In particular, the outermost layer of the star will itself be shaped like one of these contours; in binary-speak, we say that the star only partially fills its **Roche lobe.** If neither star completely fills its Roche lobe, then we have a **detached binary**. As we consider a larger and larger star (of constant mass), the star will become increasingly almond-shaped. Eventually it will become so large that it completely fills its Roche lobe; if it becomes any larger, some of its material will fall through the narrow neck of the hourglass and enter the potential well of the other mass. An astronomer would say that the star is overflowing its Roche lobe; we then have a **semi-detached binary** (Algol is a classic example). If both stars fill their Roche lobes, then the "binary" is now a dumbbell-shaped **contact binary** rotating at the Keplerian period. In the most extreme case, a **common-envelope binary**, the cores of two stars can orbit together deep inside of a single, common envelope that now may rotate at a speed wholly unrelated to the Keplerian period. Regardless of the type of overflow, substantial mass transfer will occur and so the stellar evolution of the stars involved can be significantly affected.

23.4 *Roche Lobe Overflow*

When Roche lobe overflow occurs, material spills over at L_1 and falls down the companion's gravity well. Roche Lobe overflow can dramatically complicate stellar evolution in a binary system. Given a binary composed of two main-sequence stars, we might naively expect the smaller lobe to overflow first. But the more massive star (with the larger Roche lobe) will have a shorter life and will evolve first into a giant.

At this point, something interesting happens: as the star (say, m_1) expands and mass transfer begins, by Eq. 594 its Roche radius will shrink. The combined effect is to accelerate mass transfer; until in some cases m_2 may become more massive than m_1. Material may even slosh back

and forth between the two objects a time or two, but before too long one object or another will end its stellar life, as either a white dwarf, neutron star, or black hole.

23.5 *Accretion Disks*

Once our binary contains a compact stellar remnant, if the binary separation and mass ratio are right then one last phase of mass transfer can occur. When overflow occurs in a system with a compact object (WD, NS, or BH; call it m_2), the material has a long way to fall. It is pushed over the brink by the unbalanced pressure at L_1, and falls down toward m_2 with a velocity $v \approx c_s \sim 10s$ km s^{-1} — much smaller than the orbital speeds of ~ 100 km s^{-1}. When m_2 had a large radius this material would easily hit its target, but in this later phase of evolution the target is far smaller.

Now, the overflowing gas heads down, down toward m_2 — but all the while, the $\vec{v} \times \vec{\Omega}$ Coriolis force is steadily acting on the material, causing it to veer away from a direct path. The combined potential leads to the matter entering into an orbit around m_2, with the material's trajectory passing through its former position and smashing into the material that was coming along behind it.

Shock heating sets in where the infalling stream impacts the growing disk of matter, converting bulk kinetic energy into heat. Radiation can try to cool the hot, shocked material but it can't transport much angular momentum: so the accreted material ends up in a circular **accretion disk.**

Further evolution of the disk is set by its ability to transport mass inward through the disk while simultaneously moving angular momentum outward – these parameters are set in turn by the viscosity of the disk. Each concentric annulus of material in the disk wants to travel at a slightly different Keplerian speed. Very close to m_2 at the center of our accretion disk, orbits are determined solely by m_2 and so travel at the Keplerian angular velocity

$$\Omega_K(r) = \frac{v}{r} = \sqrt{\frac{GM}{r^3}}. \tag{595}$$

Meanwhile, the angular momentum per unit mass is

$$\ell(r) = rv = r^2\Omega_K = \sqrt{GMr}. \tag{596}$$

So as we go outward through successive annuli of the disk, Ω decreases but ℓ increases. These rings, rotating at different speeds, are coupled by viscosity – this effectively acts like friction. So each interior ring tries to speed up the rotation of its exterior neighbor, sending angular momentum outward and pushing out that exterior neighbor. At the same time, the ring interacts viscously with the next ring inward, trying to slow it down and so causing it to fall inward. The net effect is that the disk

will spread toward smaller and larger radii, transporting angular momentum outward. Energy is dissipated by the viscous interactions (plus emitted radiation), so material falls steadily inward.

23.6 *Alpha-Disk model*

Our modest goal here is to find a steady-state model for an accretion disk with fixed mass transfer rate $\dot{M}$. When disk material spills into the compact object's potential well it has near-zero velocity but a long way to fall. Thus the ultimate power source of an accretion disk comes from the conversion of gravitational potential energy. Dropping in some small amount of mass m will liberate

$$\Delta E = \frac{GMm}{R} \tag{597}$$

and so the overall luminosity of the accretion disk should scale as

$$L_{\rm acc} \approx \frac{GM\dot{M}}{R}. \tag{598}$$

The Stress Tensor

We will shortly introduce the so-called "α-disk" model that is often used to provide a phenomenological description of accretion disk physics. As background to this discussion, we first describe two useful foundational concepts. The first is the **viscous stress tensor** T_{ij}. (Some students have already encountered a variant of this tensor, the stress-energy tensor, in a general relativity class. For our discussion here, we only need the 3-D purely spatial stress tensor.) The quantity T_{ij} represents a flux of momentum:

$$T_{ij} = \text{Flux of momentum } p^i \text{ in the } j\text{-th direction .} \tag{599}$$

Imagine you have a box with sides parallel to the x, y, and z axes:

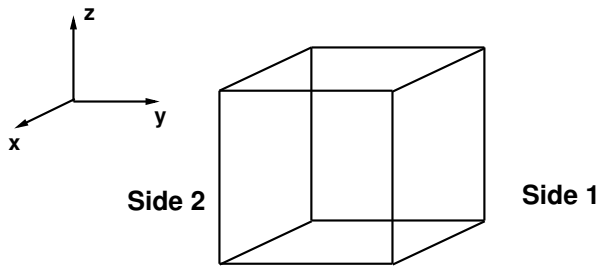

Figure 55: Fiducial box for computing fluxes.

The net rate of change of (for example) p^x associated with flow through the sides normal to the y axis is

$$\left.\frac{dp^x}{dt}\right|_{\hat{y}} = \int_{\text{side 1}} T_{xy}\, dx\, dz - \int_{\text{side 2}} T_{xy}\, dx\, dz \ . \tag{600}$$

Similar equations describe the rates of change of components associated with momentum flow through the sides normal to the other axes.

Viscosity

The second concept is the notion of **viscosity**. In a fluid, viscosity is the quantity which transports momentum component i in some direction that is not i — a *non-normal* stress. (Momentum component i transported in direction i is probably much more familiar: it is pressure.) It is related to the density of the fluid and the velocity *gradient*. In Cartesian coordinates, the coefficient of dynamic viscosity ν is defined as

$$T_{ij} = \rho\nu \frac{\partial v^i}{\partial x^j} \ . \tag{601}$$

When we convert to cylindrical coordinates (which we'll want to use to model an accretion disk), one particularly important component is

$$T_{\phi r} = \rho\nu r \frac{d\Omega}{dr} \ . \tag{602}$$

This tells us how axial motions in a disk are coupled to one another in the radial direction.

In fluids we typically encounter in our daily lives, the value of ν is of order the mean free path of the molecules in the fluid, λ, times their typical speed, $\bar{u}$. This intuition fails for accretion disks, which means that their viscosity (or their effective viscosity) must arise from some different physical mechanism. Determining this mechanism and thereby understanding the viscosity of astrophysical accretion disks is an important problem in modern astrophysics research.

Overview

Turn now to accretion disks. In steady state, accretion disks are a stable assembly of fluid in which various energy sources and various forces are in balance. This is very similar to the root underlying physics of stars; as such, it is not too surprising that the equations which govern the structure of accretion disks bear a more than passing resemblance to the equations of stellar structure. They are slightly more complicated, however, because of the different symmetry of the two systems: Stars are spherically symmetric, whereas accretion disks are cylindrically symmetric. A

stellar model tells us how key quantities (temperature, pressure, density) vary with spherical radius r. An accretion disk model tells us how key quantities (temperature, pressure, density) vary with cylindrical radius r and with height z above or below the disk's midplane, $z = 0$. (If there is any ambiguity, we will sometimes write the radius r_c to emphasize the cylindrical symmetry.)

Beyond the difference in symmetry, the basic physics describing stars and accretion disks are more-or-less identical. In particular we have

1. **Force balance.** In stars, we balance gravity with hydrodynamic pressure. Thanks to spherical symmetry, we only need to do this in the radial direction. In an accretion disk, we balance gravity, pressure, centrifugal forces, and viscous coupling of adjacent fluid elements. The single force balance equation we found for stars splits into 3 separate equations (one for each component) in an accretion disk.
2. **Mass conservation.** The donor star pumps mass into the disk; it is transported inward and eventually falls onto the object that is accreting. In steady state, the mass in a fluid element does not change; mass flows in and out, and the sum is constant.
3. **Power generation.** In a star, we generate power by nuclear fusion. In an accretion disk, we generate power by fluid elements rubbing against one another.
4. **Radiation transport.** That power is generated throughout the disk, and has to flow out to the surface before it is radiated away. To understand this process, we need to know about the opacity of the material in the disk, and how the radiation gets out.
5. **Equation of state.** Just as in stars, we need to relate pressure to density.

We now go through these, though not quite in this order. Our final disk model will display a well-ordered hierarchy of velocities:

(603) $v_z \ll v_r \ll c_s \lesssim v_\phi$.

I.e., the accreting material rapidly swirls around the disk, at Keplerian velocities typically faster than the sound speed. Much slower than those speeds will be a steady inward radial drift; even slower will be vertical settling toward the disk midplane.

The Alpha-Disk Model

1. **Radial force balance.**

   We assume here that the orbital speed is much larger than the sound speed of the gas. If this is the case, then we can neglect gas forces in favor of the centrifugal force: Considering a fluid element

of mass Δm, and a central body of mass M onto which the accretion flows, we have

$$\frac{GM\Delta m}{r^2} = \Delta m \Omega^2 r \longrightarrow \boxed{\Omega(r) = \Omega_K = \sqrt{\frac{GM}{r^3}}} \tag{604}$$

This has a built-in consistency check: After we build our model, we compare dP/dr with $GM\rho/r^2$. If the pressure gradient is not small in this comparison, then we should not have neglected it, and we need to revisit this.

2. **Vertical force balance.**

   We cannot neglect pressure gradients for this force component — they are the whole effect. We look at the z component of the usual equation of hydrostatic balance:

$$\frac{\partial P}{\partial z} = -g_z \rho \tag{605}$$

$$= -\frac{GM}{r^2}\left(\frac{z}{r}\right)\rho\ . \tag{606}$$

   Integrate this up using the fact that pressure is zero outside the disk, $z \geq H/2$ (defining H as the disk's height, and $z = 0$ as the disk's midplane):

$$\int_0^{H/2} \frac{\partial P}{\partial z} dz = P_{H/2} - P_m = -P_m\ . \tag{607}$$

   Here P_m is pressure on the midplane. We pull various factors out of the integral on the right-hand side, and find

$$P_m \simeq \frac{GM}{r^3} \int_0^{H/2} z\,\rho\, dz \approx \frac{GM\rho H^2}{r^3}\ . \tag{608}$$

   In the final approximate result, we neglected factors of order unity. Errors due to this neglect should be comparable to any errors made in neglecting how ρ varies with z.

   In some applications, we need somewhat better approximations than this. Note that the r which appears here is strictly speaking the *spherical* radius, not the cylindrical one. One way to improve the calculation would be to replace r with $\sqrt{r_c^2 + z^2}$ in the equation for dP/dz. For the applications we will pursue in 8.901, we use $r \simeq r_c$. This is known as the "thin disk" approximation. It is used quite widely, but it is worth being aware of its limitations.

   Another approximation we have made is that the disk has a well-

defined upper edge at $H/2$, when in reality the vertical pressure will tend to have an exponential decrease – in this case, H becomes the disk's vertical scale height.

3. **Mass conservation.**

   Mass flows from large radius to small radius. Consider a cross section of one annulus of the disk, as shown in Fig. 56. Think about mass flowing into and out of the volume associated with this cross section in a time Δt:

$$\begin{aligned}\Delta M &= \text{Mass entering outer radius in } \Delta t - \text{Mass leaving inner radius in } \Delta t \\ &= \{[\text{Cross section at } r_o]\,[\text{Mass flux at } r_o] - [\text{Cross section at } r_i]\,[\text{Mass flux at } r_i]\}\,\Delta t \\ &= \{[2\pi r_o H(r_0)]\,[\rho(r_o)v_r(r_o)] - [2\pi r_i H(r_i)]\,[\rho(r_i)v_r(r_i)]\}\,\Delta t\end{aligned}$$

   Now divide everything by the volume of this annulus, $2\pi r H(r)\Delta r$, and take the limit as $\Delta r \to 0$, $\Delta t \to 0$:

$$\frac{\partial \rho}{\partial t} = \frac{1}{2\pi r H(r)} \frac{d}{dr}\left(2\pi r H \rho v_r\right) \ . \tag{609}$$

   Strictly speaking Eq. 609 should be a partial derivative rather than a total derivative on the right-hand side. In the thin disk model, we neglect the dependence of quantities on z. As such, taking $\partial/\partial r \to d/dr$ is a fine approximation as long as the thin-disk conditions are met. We'll similarly use $\partial \to d$ in the calculations that follow.

   In steady state, $\partial\rho/\partial t = 0$. Imagining that everything depends only on r, we then have

$$2\pi r H \rho v_r = \text{constant} \ . \tag{610}$$

   We can tell by inspection that this constant is just the rate at which mass enters one side of the volume and then leaves the other, so we have

$$\boxed{2\pi r H \rho v_r = \dot{M}} \tag{611}$$

   Note that the above calculation is equivalent to starting from the

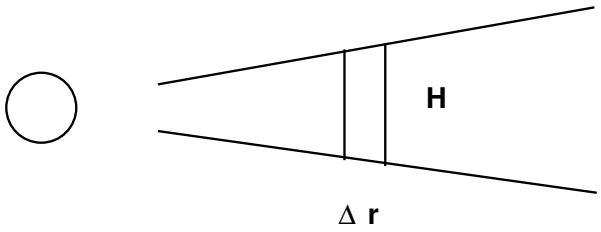

Figure 56: Cross section of one annulus of thickness Δr, height H.

mass continuity equation,

$$\frac{\partial}{\partial r}(\rho v_r r) = 0. \tag{612}$$

This implies that $\rho v_r r$ is constant, which one then integrates:

$$\int \rho v_r r \, d\phi \, dz = 2\pi r H \rho v_r = \dot{M}. \tag{613}$$

4. **Angular momentum.**

How to handle the transport of angular momentum in the disk is a little bit delicate. We begin by essentially repeating the mass transport analysis, but looking at how angular momentum flows radially through the disk:

$$\begin{aligned}
\Delta L &= L \text{ entering outer radius} - L \text{ leaving inner radius} \\
&= \{[\text{Cross section at } r_o]\,[L \text{ flux at } r_o] - [\text{Cross section at } r_i]\,[L \text{ flux at } r_i]\}\,\Delta t \\
&= \left\{[2\pi r_o H(r_0)]\left[\rho(r_o) v_r(r_o)\Omega(r_o) r_o^2\right] - [2\pi r_i H(r_i)]\left[\rho(r_i) v_r(r_i)\Omega(r_i) r_i^2\right]\right\}\Delta t
\end{aligned}$$

I've used the fact that the angular momentum of a mass element is $\Delta m r^2 \Omega$, so the radial flux associated with this angular momentum is $(\rho v_r) r^2 \Omega$. Divide by Δt, by the volume $2\pi r H \Delta r$, and take the limits. The result is

$$\tau = \frac{1}{2\pi r H}\frac{d}{dr}\left(2\pi r H \rho v_r \Omega r^2\right) \ . \tag{614}$$

We have defined $\tau \equiv dL/dV dt$, the torque on the annulus per unit volume. We massage this one step further, using the result from our analysis of mass conservation to simplify:

$$\boxed{\tau = \frac{1}{2\pi r H}\frac{d}{dr}\left(\dot{M}\Omega r^2\right)} \tag{615}$$

Now comes the tricky bit: What do we use for τ? Fundamentally, we know that τ arises from viscosity coupling adjacent annuli of the disk to one another: viscosity "wants" the disk to rotate as a solid body, so it tries to slows down annuli on the inside and speed up annuli on the outside. Our goal is to compute the torque associated with the ϕ component of momentum that flows in the r direction, as shown in Fig. 57.

We compute the angular momentum ΔL delivered to this annulus:

$$\begin{aligned}
\Delta L &= [r_o(\text{axial force at } r_o) + r_i(\text{axial force at } r_i)]\,\Delta t \\
&= \left[r_o \left(\int_{\text{outer face}} T_{\phi r}\, dA \right) - r_i \left(\int_{\text{inner face}} T_{\phi r}\, dA \right) \right] \Delta t \\
&= \left\{ T_{\phi r}(r_o) \left[2\pi r_o^2 H(r_o) \right] - T_{\phi r}(r_i) \left[2\pi r_i^2 H(r_i) \right] \right\} \Delta t \qquad (616)
\end{aligned}$$

Note on the first line that we *add* the two torques together: the torque associated with momentum flux at both the outer and the inner boundaries of the annulus contributes to the angular momentum in this volume. The math which follows determines the signs of these contributions; we find a relative minus sign because the normal associated with the inner face of the annulus points in, and that associated with the outer face points out.

Dividing and taking limits appropriately, we find

$$\tau = \frac{1}{rH} \frac{d}{dr} \left(T_{\phi r} r^2 H \right) \ . \qquad (617)$$

So far, our analysis has effectively just moved our ignorance from one place to another. This isn't a bad thing, since we've now moved our unknown into one quantity, the stress-tensor component $T_{\phi r}$.

To proceed, we need to figure out what to use for this quantity. If we could estimate the viscosity ν, we would use Eq. (602) to estimate $T_{\phi r}$. Estimating ν is rather tricky; however, we know that the resulting stress $T_{\phi r}$ must have the same dimensions as pressure. A very quick-and-dirty approximation is to imagine that P and $T_{\phi r}$ are proportional to one another:

$$T_{\phi r} = \alpha P \ . \qquad (618)$$

This approximation yields what is known as the **Shakura-Sunyaev α-disk model**. The key idea here is that, since the pressure P is *a* stress, it gives us a reasonable guess for typical values of *all* stresses in the disk. The parameter α parameterizes our ignorance, and is

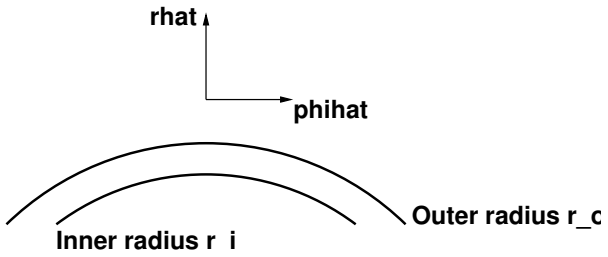

Figure 57: Top view of disk, looking down on our fiducial annulus.

typically taken to be between 0 and 1.

A slightly less handwavy approach demands that $\nu \approx \alpha H c_s$ (where c_s is sound speed) — these are the only dimensional quantities we can combine to make a quantity that looks like a viscosity. Since c_s is related to the pressure, this way of building a disk model yields an α that is nearly identical to what we find using Eq. (618), differing by a factor of order unity. This is in fact what Shakura and Sunyaev's original paper actually does.

Taking α to be a constant, our torque equation becomes

$$\boxed{\tau = \frac{\alpha}{rH}\frac{d}{dr}\left(Pr^2H\right)} \tag{619}$$

Using this in Eq. (615), we have

$$\frac{\alpha}{rH}\frac{d}{dr}\left(Pr^2H\right) = \frac{1}{2\pi rH}\frac{d}{dr}\left(\dot{M}\Omega r^2\right) \ . \tag{620}$$

Clearing out common factors of rH, both sides are perfect d/dr derivatives and can be integrated up to relate quantities at some inner radius $r_{\rm inner}$ to quantities at an outer radius r.

Looking ahead a bit, the solutions that we construct in this way have a pressure profile that decreases as we move to smaller radius. Let us assume that there is a radius $r_{\rm inner}$ at which disk pressure vanishes, i.e. that $P(r_{\rm inner}) = 0$. We find

$$\dot{M}\left[\Omega r^2 - \Omega_{\rm inner} r_{\rm inner}^2\right] = 2\pi\alpha P(r) H(r) r^2 \ . \tag{621}$$

Using $\Omega = \sqrt{GM/r^3}$, this further simplifies to

$$\boxed{2\pi\alpha PH = \dot{M}\Omega f^4} \tag{622}$$

where we define

$$f^4 \equiv 1 - \sqrt{r_{\rm inner}/r}. \tag{623}$$

(The reason for the power of 4 included in the definition of f will be explained shortly.)

5. **Power generation.**

   All these annuli rubbing against one another not only transfer angular momentum, they also make the disk hot. The power that is generated on an annulus takes the schematic form

   (624)

   Power $= 2 \times$ (torque) $\times$ (relative angular velocity of neighboring annuli)

   This equation is just the angular equivalent of the Fv power you get

for a force F acting at a speed v. The leading 2 is because we get contributions from both the inner and outer face of the annulus. To understand why we use the relative angular velocity, imagine that we sit in the center of our fiducial annulus. The angular velocities that matter to compute this power are the angular velocity of the neighboring annuli with respect to us — the outer one a distance $\Delta r/2$ farther out, the inner one a distance $\Delta r/2$ further in. This relative angular velocity is given by

$$\Delta\Omega = \left|\frac{d\Omega}{dr}\right| \frac{\Delta r}{2} \,. \tag{625}$$

The absolute value is included here because this heat is generated by a dissipative process. It doesn't matter if the relative speeds of neighboring annuli are positive or negative; as long as they are nonzero, they will generate heat.

We next need to compute the torque that appears in the power formula. There's a somewhat confusing point to be made here: the torque we want looks a bit different from the torque that we computed previously, in our analysis of angular momentum transport.

The key point is that in that previous step, our goal was to compute the angular momentum that *accumulates in the annulus* due to the momentum flux. Here, we just want to know what the torque is *at some particular radius*. It is enough to just to compute things on one face of the annulus to get this torque:

$$\begin{aligned} \text{torque} &= r \times \int_{\text{annulus at } r} T_{\phi r}\, dA \\ &= r \times (\alpha P \times 2\pi r H) \\ &= 2\pi\alpha r^2 P H \,. \end{aligned} \tag{626}$$

This means that the power generated in this annulus is

$$\boxed{\text{Power} = 2\pi\alpha r^2 P H \Delta r \left|\frac{d\Omega}{dr}\right|} \tag{627}$$

The quantity of direct observational relevance is the flux, or power per unit area, from the disk. We denote this $\dot{Q}$:

$$\dot{Q} \equiv \frac{\text{Power}}{\text{Area}} = \frac{2\pi\alpha r^2 P H \Delta r \left|\frac{d\Omega}{dr}\right|}{2 \cdot 2\pi r \Delta r} \,. \tag{628}$$

The disk has two sides, hence the extra factor of two in the denominator. This gives us

$$\dot{Q} = \frac{1}{2}\alpha P H r \left|\frac{d\Omega}{dr}\right| = \frac{3}{4}\alpha P H \Omega \,, \tag{629}$$

using the fact that $r|d\Omega/dr| = (3/2)\Omega$.

Let us combine this result with the expression for αPH we found previously, Eq. (622):

$$\boxed{\dot{Q} = \frac{3}{8\pi}\Omega^2 \dot{M} f^4} \tag{630}$$

The power per unit area depends only on the input $\dot{M}$, with Ω and f providing a bit of radial variation. The "fudge factor" α we introduced drops out, which is satisfying.

Since $\dot{Q}$ is itself a flux, so we can use it to define an effective temperature:

$$\dot{Q} = \sigma_{\rm SB} T_{\rm eff}^4 \longrightarrow \boxed{T_{\rm eff} = \left(\frac{3\Omega^2 \dot{M}}{8\pi\sigma_{\rm SB}}\right)^{1/4} f} \tag{631}$$

This is why the definition of f includes that 4th power.

6. **Energy transport.**

The energy generated in this way is buried in the disk and has to come out. We treat the disk like a stellar atmosphere, and return to our analysis of transport analysis. The most relevant equation here is the moment of the radiation transport equation that relates the gradient of radiation pressure to opacity and flux. See Sec. 2.5 of Choudhuri for a reminder [especially Eq. (2.74)]:

$$\frac{dP_{\rm rad}}{dz} = -\frac{\bar{\rho}\bar{\kappa}}{c} F \ . \tag{632}$$

Here, $P_{\rm rad}$ is radiation pressure, $\bar{\kappa}$ is a Rosseland mean opacity, $\bar{\rho}$ is a similar mean for the density, and F is the flux.

For our purposes, it suffices to approximate the derivative as

$$\frac{dP_{\rm rad}}{dz} \approx \frac{P_{\rm rad,\ surf} - P_{{\rm rad},z=0}}{H} = -\frac{P_{{\rm rad},z=0}}{H} \ , \tag{633}$$

using the fact that the surface of the disk by definition has zero pressure of any kind. The flux is $F = \sigma T_{\rm eff}^4$; radiation pressure is $P_{\rm rad} = (4\sigma/3c)T^4$. Notice that this is actual thermodynamic temperature, not effective temperature. This equation thus gives us a relation between the effective temperature we determine from observations and the thermodynamic state of the disk:

$$\boxed{T^4 = \frac{3}{4} H\bar{\rho}\bar{\kappa} T_{\rm eff}^4} \tag{634}$$

Finally, we need to an opacity. Two commonly used examples are

$$\begin{aligned} \bar{\kappa} &= \kappa_{\rm es} \qquad \text{(electron scattering)} \\ &= \kappa_0 \rho T^{-7/2} \qquad \text{(Kramer's law)} \ . \end{aligned} \tag{635}$$

7. **Equation of state.**
   Two choices are typically used:

$$\begin{aligned} P &= \frac{\rho}{\mu} k_B T \qquad \text{or} \\ &= \frac{4\sigma}{3c} T^4 \ , \end{aligned} \tag{636}$$

   depending on whether you think gas pressure or radiation pressure is more important. Which do you use? That's a question of phenomenology: you try both, and see which describes your data better.

To summarize, the α-disk model uses the following set of coupled equations:

$$T_{\rm eff} = \left(\frac{3G}{8\pi}\right)^{1/4} M^{1/4} \dot{M}^{1/4} f \tag{637}$$

$$PH = \alpha^{-1} \frac{\sqrt{GM}}{2\pi} \dot{M} r^{-3/2} f^4 \tag{638}$$

$$T^4 = \frac{3}{4} \bar{\kappa} \bar{\rho} H T_{\rm eff}^4 \tag{639}$$

$$P = \frac{GM}{r^3} \rho H^2 \tag{640}$$

$$= \rho k_B T / \mu \qquad \text{or} \qquad \frac{4\sigma}{3c} T^4 \tag{641}$$

with a choice for the $\bar{\kappa}$ we use. Once the opacity and the equation of state are specified, we can build remarkably (well, relatively) simple solutions for the whole thing.

23.7 *Observations of Accretion*

The single simplest signature of accretion onto a compact object is the luminosity. If a disk is optically thin, a single proton falling through it and onto the central object releases

$$\Delta E = \frac{GMm_p}{R} \approx 0.2 m_p c^2 \tag{642}$$

(for a neutron star). If all this went into thermal energy, we'd then expect from

$$\Delta E \sim k_b T \tag{643}$$

to find

$$T \sim \frac{GMm_p}{k_b R} \sim 100 \text{ MeV} \quad (644)$$

(again, for a neutron star).

Based on this simple estimate, we should expect accreting neutron stars to be gamma-ray sources. But in fact, disks are typically quite optically thick. Emitted photons are scattered and reprocessed many times, so that the luminosity comes out at lower energies. Things saturate at the Eddington luminosity (Eq. 455); when this is set equal to the Stefan-Boltzmann law

$$\frac{4\pi cGMm_p}{\sigma_T} = 4\pi R^2 \sigma_{SB} T_{\text{eff}}^4 \quad (645)$$

the result is that

$$k_b T_{\text{eff}} \approx \text{ keV} \quad (646)$$

for neutron stars – i.e., at X-ray energies.

To map the disk itself in more detail, we can use spectroscopy. A rotating disk exhibits a gradient of radial velocities along its surface, determined by both the disk's Keplerian velocity profile and by the viewing angle. This turns the emission from your favorite, single emission line in the disk into a double-peaked shape, with each velocity component corresponding to a particular velocity. Especially when combined with the orbital motion of the disk in the binary system, and sometimes also with eclipses of the disk by the secondary star, one can infer quite a detailed picture of the disk in question.

Different types of stars exhibit different types of behavior when undergoing accretion:

- **Normal stars** (i.e., not compact remnants). These add mass from one member of the binary to the other. As discussed in Sec. 23.4, these can have the odd situation that the more evolved member of the binary is less massive. This is because it swelled up, overflowed its Roche lobe, and dumped mass onto its companion. One such example is the eclipsing binary Algol.
- **White dwarfs.** These are particularly interesting, since they exhibit variable behavior – these are the so-called **cataclysmic variables.** There are a few types:
  1. *Dwarf nova:* an instability in $\dot{M}$ leads to sudden, occasional brightenings of the source.
  2. *Classical nova:* sufficient H accumulates on the WD's surface until it gets hot and dense enough to initiate fusion. In a degenerate medium, this initiates flash burning: the whole layer fuses very rapidly.

3. *Supernova Ia:* It is possible for a white dwarf to accrete enough mass to go over the Chandrasekhar mass limit and collapse. As described in Sec. 19.6, this is one (though probably not the dominant) pathway to forming SNe Ia.

– **Neutron stars.** These are seen in X-rays and have two categories.

1. *High-mass X-ray binaries* (HMXBs): In this case the companion to the neutron star is a young, massive O or B star. The NS has a strong magnetic field, and X-ray flux is seen to pulsate. Most of these will evolve into NS-NS binaries.

2. *Low-mass X-ray binaries* (LMXBs): The companion to the NS is $\lesssim 1 M_\odot$, and so the system is considerably older. As we saw in Fig. 48 and Sec. 21.5, the NS's magnetic field is thus somewhat weaker. As with the HMXBs, the X-ray flux is seen to pulsate in some cases. Most of these LMXBs will likely evolve into millisecond pulsars.
   Before they become ms pulsars, LMXBs also exhibit two types of behavior. "Type I" show a sharp rise in luminosity, followed by a slow decline; this indicates the thermonuclear detonation of accreted material on the NS, similar to cataclysmic variables. "Type II" show more frequent, lower-amplitude variations indicative of instabilities in the accretion flow – i.e., sudden changes in $\dot{M}$.

In either case, the magnetic field is crucial for understanding the pulsations. A strong $\vec{B}$ field channels the accreting material to the NS's magnetic poles, and one gets lots of emission from these "hot spots," with the emission modulated by the NS spin.

We can make a rough estimate of the $\vec{B}$ strength needed to channel the incoming accretion flow by examining the radius $r_{\rm mag}$ at which the magnetic field's energy density equals the kinetic energy density of the accretion flow. If we assume that the neutron star's magnetic field is approximately a dipole, then $B \propto r^{-3}$. If the magnetic field at the pole is B_p, then

$$u_B = \frac{B^2}{8\pi} = \frac{B_p^2}{8\pi}\left(\frac{R}{r}\right)^6. \tag{647}$$

We then define

$$\eta = \frac{v_{\rm rad}}{v_{\rm Kepler}} \ll 1 \tag{648}$$

And then consider energy density balance:

(649)
$$\frac{B_p^2}{8\pi}\left(\frac{R}{r}\right)^6 = u_{\text{kinetic}} \quad \text{(K.E. per mass of infalling gas)}$$

(650)
$$= \frac{1}{2}\rho\left(v_{\text{Kepler}}^2 + v_{\text{rad}}^2\right)$$

(651)
$$\approx \frac{1}{2}\rho v_{\text{Kepler}}^2$$

(652)
$$\approx \frac{GM\rho}{2r_{\text{mag}}}$$

The mass inflow rate of the disk (which subtends a solid angle Ω_{disk}) is

(653) $\dot{M} = \rho v_r A_{\text{disk}} = \rho\eta v_K r_{\text{mag}}^2 \Omega_{\text{disk}}$.

Solving for ρ, we find

(654) $\rho = \dfrac{\dot{M}}{\eta v_K r_{\text{mag}}^2 \Omega}$,

We substitute this expression for ρ along with $v_K = \sqrt{\frac{GM}{r}}$ into our expression for u_K at the disk's inner edge.

(655) $u_K = \dfrac{\dot{M} v_K}{8\pi\eta r_{\text{mag}}^2 \Omega} = \dfrac{\dot{M}\,(GM)^{1/2}}{2\eta r_{\text{mag}}^{5/2}\Omega}$.

Equating u_K and u_B, and solving for r_{mag} we find,

(656) $r_{\text{mag}} \propto \left(\dfrac{B_p^2 R_*^6}{\dot{M}\sqrt{M}}\right)^{2/7}$

(where R_* is the size of the compact object). It turns out that if $r_{\text{mag}} > R_*$, then the accretion flow is significantly affected by $\vec{B}$ and becomes magnetically channeled.

– **Black Holes:** These have no surface, and so no pinned $\vec{B}$ fields, no pulsations, and no bursts. These characteristics are found in all sources with $M \gtrsim 3M_\odot$. What we see instead is messy hydrodynamics in strong (relativistic) gravity. The disk itself is still magnetized; the field gets "wrapped up" by the black hole spin, producing jets.

24 Fluid Mechanics

24.1 *Useful References*

- F. Shu, Vol. II, "Gas Dynamics."
- Boyd & Sanderson, "Plasma Dynamics," Chs. 2, 3, and 6.

24.2 *Vlasov Equation and its Moments*

The **Vlasov Equation** describes the time evolution of particles in a system dominated by long-range interactions, and is of general utility for many issues relating to fluids (especially those at high temperatures). The Vlasov equation is derived from Liouville's theorem; it describes the phase space density $f(\vec{r}, \vec{p})$ and takes the form

$$\frac{df}{dt} = \frac{\partial f}{\partial t} + \vec{v} \cdot \nabla f - \nabla \Phi \cdot \frac{\partial f}{\partial \vec{v}} \tag{657}$$

where $\vec{v}$ is velocity and Φ is the potential, such that for force F and mass m

$$\nabla \Phi = -\frac{\vec{F}}{m}. \tag{658}$$

The Vlasov equation can be used to derive several fundamental equations in the study of fluids. This is done by calculating the moments of the equation: multiplying Eq. 657 by $(\vec{v})^n$ for n=0, 1, and 2, integrating over all of velocity space, and considering the result.

Conservation of Mass

Taking the zeroth moment, we first find

$$\int \frac{\partial f}{\partial t} d^3v + \int \frac{\partial}{\partial x_i}(v_i f) d^3v + \int \frac{F_i}{m} \frac{\partial f}{\partial v_i} d^3v = 0 \tag{659}$$

We can recognize and simplify a few terms in this thicket. For example,

$$\int \frac{\partial f}{\partial t} d^3v = \frac{\partial}{\partial t} \int f d^3v \tag{660}$$

$$= \frac{\partial \rho}{\partial t} \tag{661}$$

is the time rate of change of the density. If forces are dominated by the Lorentz force

$$\vec{F} = q(\vec{E} + \vec{v} \times \vec{B}) \tag{662}$$

then it turns out that

$$\int \frac{F_i}{m} \frac{\partial f}{\partial v_i} d^3v = 0. \tag{663}$$

It is furthermore customary to define the first moment of the distribution function f as

$$\vec{u} = \frac{1}{\rho} \int \vec{v} f d^3v. \tag{664}$$

The result for each component is then

$$\frac{\partial \rho}{\partial t} + \frac{\partial}{\partial x_i}(\rho \vec{u}_i) = 0. \tag{665}$$

In its full vector form, this is the **Continuity Equation** of fluid dynamics,

$$\boxed{\frac{\partial \rho}{\partial t} + \vec{\nabla} \cdot (\rho \vec{u}) = 0} \tag{666}$$

which indicates that particle number (or equivalently, fluid mass) is conserved during fluid motions. The first term indicates the time rate of change in a particular volume, which is equal in magnitude to the net amount of fluid leaving that volume.

Conservation of Momentum

By taking the first moment of the Vlasov equation (i.e., multiplying by $\vec{v}$ and integrating as above) one ultimately obtains

$$\boxed{\frac{\partial}{\partial t}(\rho \vec{u}) + \vec{\nabla} \cdot (\rho \vec{u} \cdot \vec{u}) = -\vec{\nabla} \cdot (\rho \vec{\vec{\sigma}}^2) + \rho \frac{\vec{F}}{m}} \tag{667}$$

which is the equation of **Momentum Conservation** in fluid dynamics. Here $\vec{\vec{\sigma}}$ is the generalized velocity dispersion tensor,

$$\rho \sigma_{ij}^2 = \int v_i v_j f d^3v \tag{668}$$

$$= P\delta_{ij} - \Pi_{ij} \tag{669}$$

where the last expression is the difference between the pressure tensor and the viscous diffusion tensor,

$$\Pi_{ij} = \mu \left(\frac{\partial u_i}{\partial x_j} + \frac{\partial u_j}{\partial x_i} \right) + \eta \frac{\partial u_i}{\partial x_j} \delta_{ij}. \tag{670}$$

Here η is

$$\eta = \beta - \frac{2}{3}\mu \tag{671}$$

which relates β, the bulk velocity coefficient, with μ, the shear velocity coefficient.

Conservation of Energy

The $n = 2$ moment expresses conservation of energy in the fluid, and equivalently determines the pressure P as well. Its derivation is truly marvelous but these notes are too narrow to contain it (well, almost). Nonetheless for completeness the final result is:

$$\frac{\partial}{\partial t}\left(\frac{\rho u^2}{2} + e\right) + \vec{\nabla}\cdot\left(\rho\vec{u}u^2/2 + \vec{u}\mu\right) = \frac{\rho\vec{u}\cdot\vec{F}}{m} + \vec{\nabla}\cdot\left(\vec{u}\cdot\vec{\vec{\Pi}}\right) - \vec{\nabla}\cdot\vec{q} \tag{672}$$

where $\vec{\vec{\Pi}}$ is still the viscous diffusion tensor, e is the internal energy

$$e = \frac{P}{\gamma - 1}, \tag{673}$$

q is the heat flow

$$q_i = \Sigma_i \int v_i v_j^2 f d^3v, \tag{674}$$

and μ (a different μ than immediately above) is the enthalpy (total heat content)

$$\mu = e + P = \frac{\gamma P}{\gamma - 1}. \tag{675}$$

24.3 *Shocks: Rankine-Hugoniot Equations*

Shocks are a frequent topic of study in astrophysical (and other) fluid studies. A **shock** occurs whenever a propagating wave is sufficiently intense that nonlinear wave theory no longer applies. In this case, the increased pressure at the traveling wave front builds up and ultimately leads to a sharp discontinuity in fluid velocity, ρ, and P.

In a coordinate system moving with a shock, under the right conditions the three moment equations are simplified greatly. The resulting, simplified statements of conservation of number (mass), momentum, and energy are the **Rankine-Hugoniot jump conditions**:

$$\rho\vec{u} = \text{const.}, \tag{676}$$

$$P + \rho u^2 = \text{const.}, \tag{677}$$

and

$$\frac{P}{\rho}\frac{\gamma}{\gamma-1}+\frac{1}{2}\rho u^2 = \text{const.}. \tag{678}$$

Using these three conservation equations, if we know the pre-shock conditions (in region 1) then we can calculate the post-shock (region 2) conditions. Fig. 58 shows the relevant quantities and situation as seen in the moving frame of the shock front.

Velocity and Density

A shock wave zooms through; in the shock's frame of reference, the unshocked material is moving at speed u_1. What will be the speed of the shocked medium: i.e., what is u_2?

From the energy equation,

$$\frac{1}{2}\left(u_1^2-u_2^2\right) = \frac{\gamma}{\gamma-1}\left(\frac{P_2}{\rho_2}\frac{P_1}{\rho_1}\right). \tag{679}$$

Invoking the continuity equation and rearranging gives

$$\frac{\rho_1 u_1}{2}\left(u_1^2-u_2^2\right) = \frac{\gamma}{\gamma-1}(P_2u_2-P_1u_1). \tag{680}$$

Applying the momentum equation and dividing out a factor of $(u_1 - u_2)$

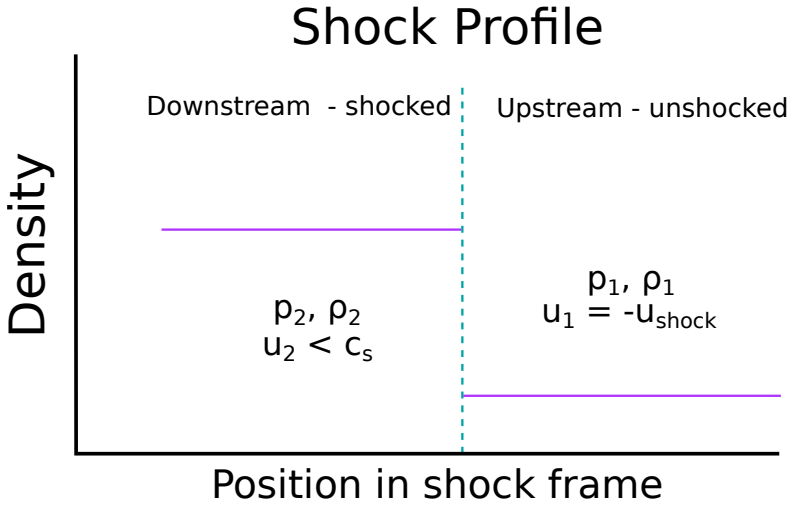

Figure 58: Shock schematic: relevant quantities as seen in the reference frame of the moving shock front. (figure courtesy of T. Johnson)

yields

$$\frac{\rho_1 u_1}{2}(u_1 + u_2) = \frac{\gamma}{\gamma - 1}(-P_1 + \rho_1 u_1 u_2). \tag{681}$$

We now bring in the **Mach number**, defined as the velocity relative to the local soundspeed:

$$M = \frac{u}{c_s} = u\sqrt{\frac{\rho}{\gamma P}}. \tag{682}$$

This, plus another round of algebra, gives

$$\frac{u_1 + u_2}{2} = \frac{\gamma}{\gamma - 1}\left(u_2 - \frac{u_1}{\gamma M_1^2}\right). \tag{683}$$

Finally one can factor out the terms containing u_1 and u_2, divide, and find that

$$\frac{u_2}{u_1} = \frac{\gamma - 1}{\gamma + 1} + \frac{2}{\gamma + 1}\frac{1}{M_1^2}. \tag{684}$$

Since $\gamma \approx 1.5$ and shocks are supersonic $M > 1$, this means $u_2 < u_1$. The velocity after the shock has passed will always be less than the speed of the shock front. In the limit of a very fast-moving shock,

$$\lim_{M \to \infty} \frac{u_2}{u_1} = \frac{\gamma - 1}{\gamma + 1}. \tag{685}$$

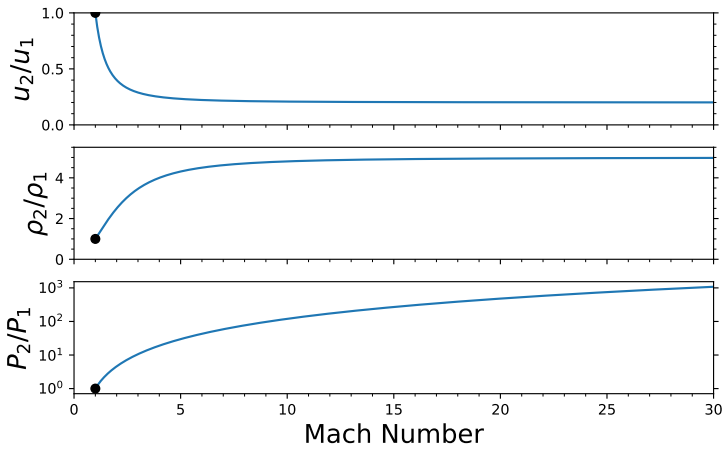

Figure 59: Post-shock conditions vs. shock speed: velocity (top; Eq. 684), density (middle; Eq. 686), and pressure (bottom; Eqs. 691 and 692). The black dot indicates $M = 1$; below this speed, there is no shock.

From Eq. 684 and the continuity equation, the density relation is then also quickly derived:

$$\rho_2 = \rho_1 \frac{u_1}{u_2} \tag{686}$$

So as the shock speed increases the density will asymptotically approach

$$\lim_{M\to\infty} \frac{\rho_2}{\rho_1} = \frac{\gamma+1}{\gamma-1}. \tag{687}$$

Thus the density is always greater after the shock has passed through, but never more than a ∼few times greater.

Pressure

To determine the new pressure, we start with the combined continuity and momentum equations

$$P_2 = P_1 + \rho_1 u_1 (u_1 - u_2) \tag{688}$$

$$= P_1 + \rho_1 u_1^2 \left(1 - \frac{u_2}{u_1}\right). \tag{689}$$

Using Eq. 682 to substitute for P_1 and Eq. 684 for u_2/u_1, after some algebraic gymnastics we have

$$P_2 = \rho_1 u_1^2 \left(\frac{1}{\gamma M_1^2} + \frac{2(M_1^2-1)}{M_1^2(\gamma+1)}\right) \tag{690}$$

$$= \rho_1 u_1^2 \left(\frac{1}{\gamma M_1^2} + \frac{2}{\gamma+1} - \frac{2}{M_1^2(\gamma+1)}\right). \tag{691}$$

The ratio of pressures requires a bit more work; defining $r = \rho_2/\rho_1$, it is

$$\frac{P_2}{P_1} = \frac{(\gamma+1)r - (\gamma-1)}{(\gamma+1) - (\gamma-1)r} \tag{692}$$

The pressure will also be greater after the shock has passed through; unlike for density, a shock can increase the pressure to arbitrarily large values.

24.4 *Supernova Blast Waves*

A common shock is the sudden, cataclysmic injection of energy into the interstellar medium by a supernova. The outer layers of the dying star are ejected from the remnant core at extremely high velocities, where they interact with

an ISM that is essentially at rest. The evolution of the SN blast wave can be considered in two distinct phases: the initial (energy-conserving) **Sedov-Taylor** expansion phase, and the later (momentum-conserving) **snowplow phase**.

Sedov-Taylor Expansion Phase

Soon after the supernova goes off, the ejecta's energy content (thermal plus kinetic) is much greater than what is being radiated away. Thus we can approximate the expansion as adiabatic. (Note that the Sedov phase really only begins when the mass swept up in the blast wave shell becomes comparable to the initial ejecta mass; this takes roughly 70–100 yr.)

A common approach is to assume (reasonably) that the shock wave's expansion will depend on the shock front radius r at time t, the ISM's initial density ρ_1, and the energy injected E. One defines a characteristic, dimensionless quantity

$$\xi \equiv r t^l E^m \rho_1^n. \tag{693}$$

For ξ to be dimensionless and not retain units of length (L), mass (M), or time (T) it must be true that

$$[\xi] = 1 = L T^l \left(\frac{ML^2}{T^2}\right)^m \left(\frac{M}{L^3}\right)^n \tag{694}$$

which implies

$$\begin{aligned} l &= -2/5 \\ m &= -1/5 \\ n &= +1/5. \end{aligned}$$

This dimensional argument immediately implies that the shock front radius scales as

$$r_{\rm sh} = \xi_0 \left(\frac{E t^2}{\rho_1}\right)^{1/5}. \tag{695}$$

For reasonable assumptions, ξ_0 is of order unity (typically within $\lesssim 20\%$). This also gives an expression for the speed of the expanding shock front,

$$u_{\rm sh} = \frac{2}{5}\xi_0 \left(\frac{E}{\rho_1 t^3}\right)^{1/5} \tag{696}$$

$$= \frac{2}{5} r_{\rm sh}/t. \tag{697}$$

We can compare these predictions to observations, e.g. of the relatively young Crab Nebula. For $E = 10^{51}$ erg, $\rho_1 = 10^{-24}$ g cm^{-3}, and $t = 1000$ yr

our predictions come moderately close to reality:

(698)
$$r_{\rm pred} \approx 5 \text{ pc} \sim r_{\rm obs} \approx 3 \text{ pc}$$

(699)
$$u_{\rm pred} \approx 2000 \text{ km s}^{-1} \sim u_{\rm obs} \approx 900 \text{ km s}^{-1}.$$

With the size and speed of the shock wave in hand, we can use the Rankine-Hugoniot conditions to determine the density, bulk velocity, and pressure inside the shock front (just after the blast wave has passed through). Using the nomenclature of Fig. 60, for a very strong (highly supersonic) blast wave, *immediately* inside the blast front Eqs. 684, 686, and 691 will give

$$u_{2,Lab} = -u_{2,Shock} + u_{\rm sh} = -\left(\frac{\gamma-1}{\gamma+1}\right) u_{\rm sh} + u_{\rm sh} = \frac{2}{\gamma+1} u_{\rm sh}$$
$$\rho_2 = \frac{\gamma+1}{\gamma-1}\rho_1$$
$$P_2 = \frac{2}{\gamma+1}\rho_1 u_{\rm sh}^2.$$

By combining these with the fluid equations (Eqs. 666, 667, and 672) and setting $u = (2/5) r_{\rm sh}/t$ (Eq. 697), one obtains a set of analytically-tractable relations for the pressure, density, and velocity as a function of radius. These relations are plotted in the right-hand panel of Fig. 60.

Snowplow Phase

Long after the supernova goes off, the ejecta has lost enough energy and is expanding slowly enough that energy losses via radiation become significant. This happens with the total radiated energy is comparable to the initial input energy E, which typically takes $\sim 10^5$ yr. At this point the energy of the shock wave is no longer conserved, but its momentum should still be conserved. In this case, the shock front acts like a snowplow coasting into a snow bank; the series of collisions is inelastic and the wave continues to slow down at a new, different rate.

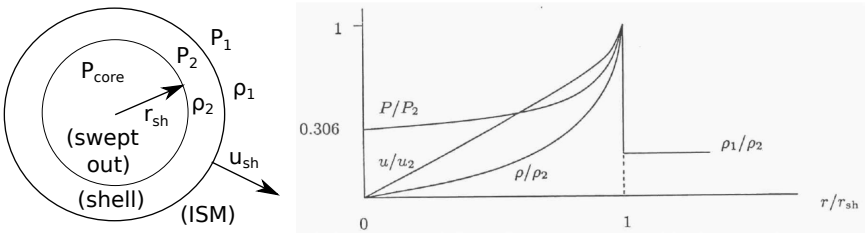

Figure 60: *Left:* Schematic diagram of a supernova shock wave with finite shell width. *Right:* Sedov solution for $\gamma = 5/3$ (Fig. 17.3 of Shu, Vol. II).

At this late stage, the supernova blast wave with radius r has swept up a spherical region of mass, which is carried along with the shock: this is just

(700) $$M_{\text{shell}} = \frac{4}{3}\pi r^3 \rho_1.$$

In the momentum-conserving phase, we should have

(701) $$p_{\text{shell}} = M_{\text{shell}}(t) u_{\text{sh}}(t) = \text{ const.}$$

This means

(702) $$r^3 \dot{r} = \text{ const,}$$

which implies

(703)
$$r_{\text{sh}} \propto t^{1/4} \quad \text{and}$$

(704)
$$u_{\text{sh}} \propto t^{-3/4}.$$

24.5 *Rayleigh-Taylor Instability*

Another common use of fluid dynamics is to determine when a given system becomes unstable. The approach used here is perturbation theory: assume some initial conditions in (perhaps unstable) equilibrium, assume a small perturbation to those conditions, and observe the results: if the perturbation grows with time then an instability is indicated.

One such scenario is the **Rayleigh-Taylor Instability**: given two media

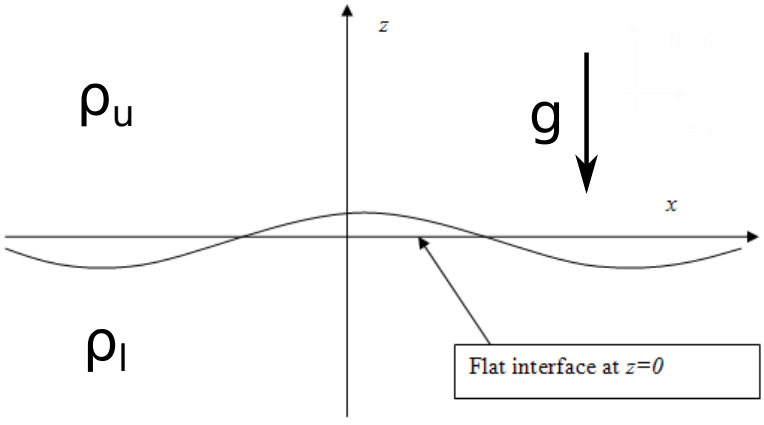

Figure 61: Initial conditions for considering the Rayleigh-Taylor instability, just after an initial perturbation has been applied.

with densities ρ_u and ρ_ℓ and a local acceleration (i.e. gravity) field $\vec{g}$ perpendicular to the interface between the media, the media will be unstable if the denser material is "on top."

We assume initial conditions $u = 0$, $\rho = \rho_0(z)$, and $P = P_0$. We then examine the situation if a small density perturbation ρ_1 is applied. This perturbation may also change the velocity and pressure, so the new conditions are

$$\begin{aligned}\rho &= \rho_0 + \rho_1 \\ \vec{u} &= u_1 \\ P &= P_0 + P_1.\end{aligned}$$

The standard approach is to model ρ_1 as the complex function

$$\rho_1 = \rho_1(z)e^{i(kx-\omega t)}. \tag{705}$$

The utility of this approach is that ω will determine when our situation is stable or not. Specifically, if $\omega^2 > 1$ then ω is real and the perturbation (i.e., its real part) will merely oscillate with time; but if $\omega^2 < 1$ then our perturbation will grow exponentially with time, indicating an unstable system.

We then proceed to apply each of the fluid equations of Sec. 24.2, beginning with the continuity equation (Eq. 666):

$$\frac{\partial \rho}{\partial t} + \vec{\nabla} \cdot (\rho \vec{u}) = 0.$$

Applying Eq. 705, we then obtain

$$-i\omega\rho_1 + \vec{\nabla} \cdot (\rho_0 \vec{u_1}) + \vec{\nabla} \cdot (\rho_1 \vec{u_1}) = 0. \tag{706}$$

Since ρ_1 and $\vec{u_1}$ are both small their product is negligible, and the last term can be dropped. Furthermore, if the fluids are incompressible then

$$\vec{\nabla} \cdot \vec{u} = 0. \tag{707}$$

We then have

$$\begin{aligned}-i\omega\rho_1 + \vec{u_1} \cdot \vec{\nabla}\rho_0 &= 0 \\ -i\omega\rho_1 + \frac{\partial \rho_0}{\partial z} u_1^z &= 0\end{aligned}$$

and so the amplitude of the density perturbations is

$$\rho_1 = \frac{(\partial \rho_0 / \partial z) u_1^z}{i\omega}. \tag{708}$$

The next step is to determine the pressure perturbation, P_1, that results from the applied density perturbation. For this we begin with the next moment equation, of momentum conservation. A simplified statement of mo-

mentum conservation (Eq. 667) is

$$\frac{\partial}{\partial t}(\rho\vec{u}) = -\vec{\nabla}P + \rho\vec{g}.$$

Expanding this using our perturbed quantities gives

$$\frac{\partial}{\partial t}(\rho_0\vec{u_1}) = -\vec{\nabla}P_1 - \rho_1 g\hat{z}.$$

The gradient of the pressure perturbation (which has a form analogous to Eq. 705), is

$$\vec{\nabla}P_1 = ikP_1\hat{x} + \frac{\partial P_1}{\partial z}\hat{z}. \tag{709}$$

We thus have two equations for each of the two component directions:

$$-i\omega\rho_0 u_1^x = -ikP_1 \qquad (\hat{x} \text{ direction}) \tag{710}$$

and

$$-i\omega\rho_0 u_1^z = -\rho_1 g - \frac{\partial P_1}{\partial z} \quad (\hat{z} \text{ direction}). \tag{711}$$

From the first of these (Eq. 710), we have

$$P_1 = \frac{\omega}{k}\rho_0 u_1^x \tag{712}$$

which is usually recast using the definition of incompressibility,

$$\vec{\nabla}\cdot u = iku_1^x + \frac{\partial u_1^z}{\partial z} = 0 \tag{713}$$

to give

$$P_1 = \frac{i\omega}{k^2}\rho_0\frac{\partial u_z^z}{\partial z}. \tag{714}$$

For the final piece of the puzzle, to determine ω^2 and so determine whether our stratified fluid is stable or not, we begin with Eq. 711:

$$-i\omega\rho_0 u_1^z = -\rho g - \frac{\partial P_1}{\partial z} \tag{715}$$

$$= -\rho_1 g - \frac{\partial}{\partial z}\left(\frac{i\omega}{k^2}\rho_0\frac{\partial u_1^z}{\partial z}\right) \tag{716}$$

$$= -\rho_1 g - \frac{i\omega}{k^2}\left(\frac{\partial}{\partial z}\left(\rho_0\frac{\partial u_1^z}{\partial z}\right)\right). \tag{717}$$

The density gradient is zero in all directions but $\hat{z}$, and even then it is zero everywhere except at the boundary $z = 0$. Thus we have

$$\vec{\nabla}\rho_0 = \frac{\partial \rho_0}{\partial z}\hat{z} = (\rho_u - \rho_\ell)\,\delta(z)\hat{z}. \tag{718}$$

With this and Eq. 708, we then have

$$\frac{\partial}{\partial z}\left(\rho_0 \frac{\partial u_1^z}{\partial z}\right) - k^2\rho_0 u_1^z = \frac{gk^2}{\omega^2} u_1^z\,(\rho_u - \rho_\ell)\,\delta(z). \tag{719}$$

Because of the delta function, two different expressions will result depending on whether or not $z = 0$. If not, then $\delta(z) = 0$ and so Eq. 719 becomes

$$\frac{\partial^2}{u_1^z}\partial z^2 = k^2 u_1^z \tag{720}$$

whose solution has the usual form:

$$u_1^z = u_{10}^z e^{-k|z|}. \tag{721}$$

On the other hand, if $z = 0$ then we take Eq. 719 and integrate up across the boundary layer; schematically, we are calculating $\int_{0^-}^{0^+} dz$. Since $\rho_0 u_1^z$ is continuous at $z = 0$ (by Eq. 721),

$$\int_{0^-}^{0^+} k^2 \rho u_1^z dz = 0. \tag{722}$$

Again making use of Eq. 721, integrating the second term in Eq. 719 will give

$$\int_{0^-}^{0^+} \frac{\partial}{\partial z}\left(\rho_0 \frac{\partial u_1^z}{\partial z}\right) dz = -k u_{10}^z\,(\rho_u + \rho_\ell)\,. \tag{723}$$

Finally, integrating over the delta function in the right-hand side of Eq. 719 yields

$$\int_{0^-}^{0^+} \frac{gk^2}{\omega^2} u_1^z\,(\rho_u - \rho_\ell)\,\delta(z) = \frac{gk^2}{\omega^2} u_{10}^z\,(\rho_u - \rho_\ell)\,. \tag{724}$$

The key result of all this that we have now shown that

$$\boxed{\omega^2 = -gk\frac{\rho_u - \rho_\ell}{\rho_u + \rho_\ell}.} \tag{725}$$

The implication is that if the denser material is "on top," $\rho_u > \rho_\ell$, $\omega^2 < 0$, and the situation is unstable. If the denser material starts out underneath, then the

situation is stable. This is why oil always floats on water (even if you try to pour a layer of water onto a pre-existing layer of oil). It is also responsible for the fascinating surface shape of the interface between supernova remnants and the ISM, as seen (e.g.) in the Crab Nebula, and it is of fundamental importance for inertially-confined fusion experiments.

In the case of instability, the density perturbation grows exponentially with time so long as the perturbations are small. One sometimes defines the Atwood Number

$$A \equiv \frac{\rho_u - \rho_\ell}{\rho_u + \rho_\ell} \tag{726}$$

in which case the characteristic growth timescale is

$$\tau_{\rm RT} = (Agk)^{-1/2} . \tag{727}$$

Since the wavenumber $k = 2\pi/\lambda$, this means

$$\tau_{\rm RT} = \left(\frac{\lambda}{2\pi A g} \right)^{1/2} \tag{728}$$

So the shortest-wavelength perturbations grow most rapidly.

Once the perturbation amplitude is comparable to its wavelength, this linear regime begins to break down. We will then have alternating rising and sinking plumes, moving at different relative velocities. In the presence of a velocity shear and different densities, we have the **Kelvin-Helmholtz-Rayleigh-Taylor instability.** It turns out that in the presence of velocity shear ω is always complex, and so the fluid will always be unstable. The Kelvin-Helmholtz instability is responsible for some cloud patterns on Earth, and it sculpts the shapes of outflow jets from compact, accreting sources. The combined KHRT instability is responsible for the characteristic "mushroom clouds" that form above large (or even nuclear) explosions.

25 The Interstellar Medium

25.1 *Useful References*

- Choudhuri, Secs. 6.5–6.6
- Rybicki & Lightman, Sec. 10.5

25.2 *Introduction*

The **interstellar medium**, or ISM, is the nearly-empty space inside our Galaxy in which all the objects we've studied thus far are embedded (note that there is also an intergalactic medium in the spaces between galaxies). The Milky Way is full of gas, dust, cosmic rays, and radiation, all at comparable energy densities. This forms a very complex medium, that often affects many processes involving stars and compact objects, as well as our observations of these objects.

Our focus here is on the gas and the plasma. On average, the ISM is composed of $\sim 75\%$ H and $\sim 25\%$ He, by mass. Typical densities are $n \sim 1$ cm^{-3} – about $100\times$ emptier than the so-called "ultra-high" vacuums found in terrestrial laboratories. The ISM is strongly inhomogeneous the material sits in various reservoirs, which are characterized using different observing techniques:

Reservoir	n [cm^{-3}]	T [K]	observed by:
H I gas (neutral)	0.3–30	30–3000	radio (typ. 21 cm)
Molecular clouds (H_2)	$\gtrsim 10^3$	30	radio
H II regions (ionized)	0.3–10^4	10^4	radio $\rightarrow$ optical
Coronal gas (ionized)	~ 0.004	$\gtrsim 10^6$	radio, X-ray

The neutral species, atomic (H I) and molecular (H_2), contain most of the gas mass. Molecular clouds are where stars form, as discussed briefly in Sec. 18.1. These tend to be highly obscured, but disks and jets around young stars are often visible. H II regions require a hot, ionizing source: e.g. a white dwarf or a massive, young star. Coronal gas is blown out by supernovae.

25.3 *H_2: Collapse and Fragmentation*

Earlier we introduced the concept of the Jeans Mass (Eq. 435), the mass required for gravitational collapse to occur,

$$M_{\rm Jeans} = 2.3\, M_\odot \left(\frac{T}{10\ {\rm K}}\right)^{3/2} \left(\frac{n}{10^5\ {\rm cm}^{-3}}\right)^{-1/2}.$$

Given the density and temperature of various stages of the ISM, we can calculate the Jeans mass in each phase:

Reservoir	$M_{\rm Jeans}/M_\odot$
H I	$10^4 - 10^8$
H_2	~ 300
H II	$10^7 - 10^9$
Coronal gas	$\sim 10^{12}$

So we can see why stars form in the molecular (H_2) regions.

Once the Jeans mass has been reached and gravitational collapse sets in (see Sec .18.1), both n and T will increase in the cloud. These have competing effects: increasing n will tend to decrease the Jeans mass, while increasing T will increase the Jeans mass. If "density wins" and the net effect is a decrease in M_{Jeans}, the large collapsing cloud will then be able to collapse on much smaller scales: the cloud fragments, and the result is multiple collapsing objects. If the collapsing object can no longer easily cool, then it has likely become a protostar.

25.4 *H II Regions*

H II regions are zones of ionized atomic hydrogen. They are often associated with nebulae, and require gas that contains a continuous source of ionizing radiation ($h\nu > 13.6$ eV). This could be a massive star or a white dwarf, but either way it must be very hot (and so fairly young). Without that central source, the protons and electrons in the ISM will quickly recombine – even with the ionizing source, it can only ionize a region of some given volume before recombinations will be happening as quickly as ionizations. The result will be a bubble of ionized gas, termed a **Strömgren Sphere**. Such H II regions are easily observable via the strong emission lines resulting from recombination. Thus to add further to the nomenclature, they are also sometimes known as emission-line nebulae.

Our goal in the following section is to understand the size of the ionized bubble and its detailed ionization structure. In this effort, we will define the ionization fraction

$$f \equiv \frac{n_{\text{H}^+}(r)}{n_{\text{H}}(r)}. \tag{729}$$

For a fully neutral, atomic ISM $f = 0$, while full ionization implies $f = 1$. As hinted at in the preceding argument, to maintain a constant f we will want to make use of ionization equilibrium, where

(number of ionizing photons/sec from source)	=	(number of recombinations/sec in bubble)
Q_*	=	$R_{\text{recom}}\left(\frac{4}{3}\pi R^3\right)$

(under the assumption of spherical symmetry). Here

$$Q_* \equiv \int_{\nu_m}^{\infty} \frac{L_\nu}{h\nu} d\nu \tag{730}$$

is the number of ionizing photons emitted per second, with $h\nu_m = 13.6$ eV. On the right-hand side, R_{recom} is the volumetric recombination rate (recombina-

tions per sec per cm^3):

(731)
$$R_{\rm recom} \equiv n_p n_e \langle \sigma_{\rm recom} v \rangle$$

(732)
$$= n_p n_e \alpha(T).$$

Here $\sigma_{\rm recom}$ is the free-bound cross-section for recombination. The function $\alpha(T)$ can be computed from the theory of radiative transitions; it is approximately

(733)
$$\alpha(T) \approx (2.6 \times 10^{-13} {\rm cm}^3 \ {\rm s}^{-1}) \left(\frac{T_{\rm gas}}{10^4 {\rm K}} \right)^{-1/2}$$

Regardless of the exact form of $\alpha(T)$, if we assume that our bubble is fully ionized (presumably with some recombinative transition zone at the edges), we will have

(734)
$$n_p n_e = n^2$$

and so then

(735)
$$Q_* = n^2 \alpha(T) \left(\frac{4}{3} \pi R^3 \right).$$

This gives the classic **Strömgren Radius** of a Strömgren sphere,

(736)
$$R = \left(\frac{3 Q_*}{4 \pi \alpha n^2} \right)^{1/3}.$$

Note that this has the expected scalings: the bubble is larger for a stronger ionizing source (larger Q_*), for a lower ambient density n, and for higher temperature $T_{\rm gas}$. One can expand on this simple model a bit in a few ways. One is to consider multiple transitions in the H atoms, which gives rise to much more complicated forms for $\langle v\sigma \rangle$. Another is to require equilibrium in each of a series of nested spherical shells. In each shell, one then sets the local ionization rate (which depends on the flux reaching that radius) equal to the local recombination rate (depending on the local temperature and neutral fraction).

25.5 *Plasma Waves*

As noted above, much of the ISM is ionized: thus we should really treat it as a plasma, rather than a gas. This ionized mixture affects the propagation of EM radiation (especially radio waves) in several observable ways.

In what follows we focus on these propagation effects. We need to consider a dilute proton-electron plasma, possible with a background magnetic field. We will first revisit the wave equation, in order to compare it to non-vacuum wave propagation.

The wave-plasma interactions will be dominated by the electrons, because they are very light and so can respond much more quickly to changing fields. To understand how they respond, we revisit the momentum equation (Eq. 667). We have

$$\rho_e \left[\frac{\partial \vec{v}}{\partial t} + \left(\vec{v} \cdot \vec{\nabla} \vec{v} \right) \right] = -\vec{\nabla} P - n_e e \left(\vec{E} + \frac{\vec{v}}{c} \times \vec{B} \right) \tag{737}$$

where $\vec{v}$ is the velocity induced by the radiation; we'll assume this is a small value. We'll also neglect $\vec{\nabla} P$, since it is often unimportant in the ISM. Under these assumptions, and with $\rho_e = m_e n_e$, we then obtain

$$m_e \frac{\partial \vec{v}}{\partial t} = -e \left(\vec{E} + \frac{\vec{v}}{c} \times \vec{B} \right). \tag{738}$$

This is just the old Lorentz force law – which makes sense, since we're just considering changes in the electrons' momenta. Here $\vec{E}$ comes from the EM radiation involved, whereas $\vec{B}$ comes from whatever background $\vec{B}$ is in the ISM. The contribution to $\vec{B}$ from the EM radiation will be smaller by $\sim v/c$, so we ignore it.

Let's recall Maxwell's equations, specifically Faraday's Law

$$\vec{\nabla} \times \vec{E} = -\frac{1}{c} \frac{\partial \vec{B}}{\partial t} \tag{739}$$

and the Maxwell-Ampere Law

$$\vec{\nabla} \times \vec{B} = \frac{4\pi}{c} \vec{J} + \frac{1}{c} \frac{\partial \vec{E}}{\partial t}. \tag{740}$$

In our plasma,

$$\vec{J} = n_e (-e) \vec{v}. \tag{741}$$

We take the time derivative of Eq. 740, which is

$$\vec{\nabla} \times \frac{\partial \vec{B}}{\partial t} = \frac{4\pi}{c} \frac{\partial \vec{J}}{\partial t} + \frac{1}{c} \frac{\partial^2 \vec{E}}{\partial t^2}. \tag{742}$$

Taking these terms one by one, we first see that

$$\frac{\partial \vec{J}}{\partial t} = -n_e e \frac{\partial \vec{v}}{\partial t} \tag{743}$$

$$= \frac{n_e e^2}{m_e} \vec{E}. \tag{744}$$

I.e., the rate of change of the current depends on the electric field. And we can

rewrite Faraday's Law as

$$\frac{\partial \vec{B}}{\partial t} = -c\vec{\nabla} \times \vec{E}. \tag{745}$$

Thus from Maxwell's equations in a plasma we obtain

$$\vec{\nabla} \times \vec{\nabla} \times \vec{E} = \frac{4\pi n_e e^2}{m_e c^2}\vec{E} + \frac{1}{c^2}\frac{\partial^2 \vec{E}}{\partial t^2}. \tag{746}$$

To see how electromagnetic waves propagate through the plasma (and their effects on the plasma), we assume that the waves can be decomposed into a series of Fourier modes — plane waves:

$$\vec{E} \equiv \vec{E_0} e^{i(\vec{k}\cdot\vec{r} - \omega t)}. \tag{747}$$

Applying this expression to Eq. 746, we then obtain the dispersion relation

$$\vec{k} \times \vec{k} \times \vec{E_0} = \left(\frac{\omega_p^2}{c^2} - \frac{\omega^2}{c^2}\right)\vec{E_0}. \tag{748}$$

Here we have defined the **plasma frequency,**

$$\omega_p = \left(\frac{4\pi n_e e^2}{m_e}\right)^{1/2} \left(\approx 2\pi \times 10^4 \text{ Hz}\right) \left(\frac{n_e}{1 \text{ cm}^{-3}}\right)^{1/2}. \tag{749}$$

This dispersion relation has the character of an eigenvalue problem: an operator acting on $\vec{E_0}$ equals $\vec{E_0}$ times a constant. We can determine the velocities of each eigenmode solution via $d\omega/dk$ for each component.

We can gain further insight into this situation if we define a coordinate direction for our propagating wave:

$$\vec{k} = k\hat{z}. \tag{750}$$

This means that our wave equation (Eq. 748) now becomes

$$k^2\left(E_y\hat{y} + E_x\hat{x}\right) = \frac{\omega_p^2 - \omega^2}{c^2}\left(E_x\hat{x} + E_y\hat{y} + E_z\hat{z}\right) \tag{751}$$

which is really three equations, one for each vector component.

$$\begin{bmatrix} \omega_p^2 + c^2k^2 & 0 & 0 \\ 0 & \omega_p^2 c^2 k^2 & 0 \\ 0 & 0 & \omega_p^2 \end{bmatrix} \begin{bmatrix} E_x \\ E_y \\ E_z \end{bmatrix} = \omega^2 \begin{bmatrix} E_x \\ E_y \\ E_z \end{bmatrix} \tag{752}$$

This has three solution. The one along $\hat{z}$ has the form $\omega^2 = \omega_p^2$, i.e. ω is a

constant. This is a longitudinal mode and does not propagate, since

$$v_{\text{group}} = \frac{d\omega}{dk} = 0. \tag{753}$$

The remaining two solutions lie along $\hat{x}$ and $\hat{y}$. These degenerate solutions represent transverse waves and have the form

$$\omega^2 = c^2k^2 + \omega_p^2 \tag{754}$$

and so have nonzero velocities

$$v_{\text{group}} = \frac{d\omega}{dk} = \frac{c^2k}{\omega} \tag{755}$$

$$= c\left(1 + \frac{\omega_p^2}{c^2k^2}\right)^{-1/2} \tag{756}$$

$$= c\left(1 - \frac{\omega_p^2}{\omega^2}\right)^{+1/2} \tag{757}$$

The longitudinal modes are **plasma modes**: non-propagating disturbances in the plasma, indicating local bunching and rarefactions (i.e., density fluctuations). The electric field then sets up a restoring force, as sketched schematically in Fig. 62. If charge carriers in a neutral block of gas with volume $A\Delta x$ are separated, a plane-parallel electric field will be set up with

$$E = 4\pi\sigma = \frac{4\pi n_e e A\Delta x}{A}. \tag{758}$$

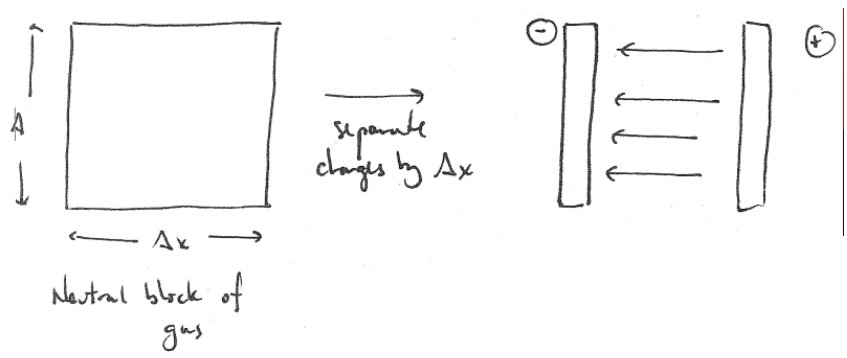

Figure 62: Intuitive picture: charges are separated in a neutral block of gas (*left*), setting up an electric field (*right*) which itself sets up a restoring force.

The restoring force on the charge carriers will then be

$$F = m_e \frac{d^2 \Delta x}{dt^2} = -eE \tag{759}$$

and so

$$\frac{d^2 \Delta x}{dt^2} + \frac{4\pi n_e e^2}{m_e} \Delta x = 0 \tag{760}$$

$$\frac{d^2 \Delta x}{dt^2} + \omega_p^2 \Delta x = 0. \tag{761}$$

So in plasma modes, when charges are initially perturbed they will subsequently oscillate with frequency ω_p (Eq. 749).

Fig. 63 shows the dispersion relation $\omega(k)$. The frequency ω has its minimum value at $\omega(k = 0) = \omega_p$ and increases with $|k|$. Thus, modes with $\omega < \omega_p$ cannot propagate through the ISM.

Plasma modes play an important role in both the ISM as well as closer to home, in the Earth's ionosphere.

Medium	n_e [cm^{-3}]	f_p [Hz]	λ_p
ISM	~ 0.03	1700	180 km
ionosphere	$\sim 10^5$	3×10^6	100 m

The ionospheric cutoff means that radio waves with $\lambda \gtrsim 100$ m cannot propagate through the Earth's atmosphere: ground-based radio astronomy is impossible at these frequencies! On the other hand, the same argument holds for terrestrial radio emissions: they are blocked from reaching space, but can instead be reflected beyond direct line-of-sight and far around the globe.

As a final note, solid metals look very much like a free electron gas to incident photons. In this case, the characteristic $\lambda_p \sim 10$s of nm ($f_p \sim 3 \times 10^{16}$ Hz) and longer-wavelength radiation cannot propagate through the metal. Thus solid metals reflect visible light, but are (largely) transparent to high-energy

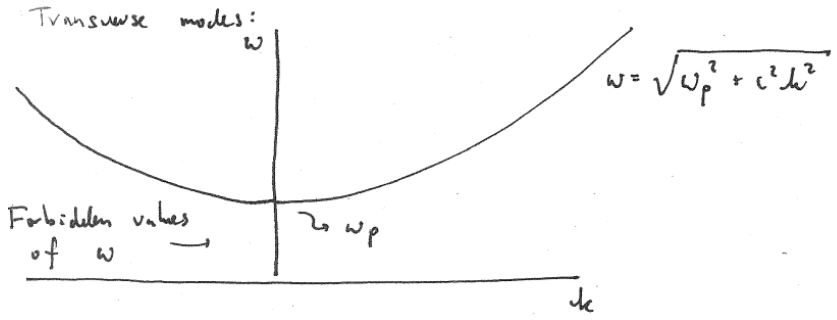

Figure 63: Dispersion relation for transverse plasma modes. Modes with $\omega < \omega_p$ cannot propagate.

UV and X-ray radiation.

25.6 *ISM as Observatory: Dispersion and Rotation Measures*

Some of the most-observed radio sources embedded in the ISM are pulsars (though there are many others). Each emitted pulse travels through the ISM, and its wave speed will be affected by its propagation through the plasma. If it is a distance d away, the travel time of the pulse is

(762)
$$t_{\text{pulse}} = \int_0^d \frac{d\ell}{v_{\text{group}}}$$

(763)
$$= \frac{1}{c}\int_0^d \left(1 - \frac{\omega_p^2}{\omega^2}\right)^{-1/2} d\ell.$$

If we are observing at fairly high frequencies compared to the ISM's cutoff frequency (just ~ 2 kHz) then we can simplify this somewhat as

(764)
$$t_{\text{pulse}} \approx \frac{d}{c} + \frac{1}{c}\int_0^d \frac{\omega_p^2}{2\omega^2} d\ell$$

(765)
$$= \frac{d}{c} + \frac{2\pi e^2}{m_e c\omega^2}\int_0^d n_e d\ell$$

We don't know when the pulse was actually emitted, so a measurement at a single frequency won't help us much. But we can look at the offset in the time of arrival as a function of frequency (or wavelength):

(766)
$$\frac{dt_p}{d\omega} = -\frac{4\pi e^2}{m_e c\omega^3}\int_0^d n_e d\ell$$

(767)
$$= -\frac{4\pi e^2}{m_e c\omega^3}\langle n_e\rangle d.$$

The initial fraction is just a set of physical or observed constants; the remaining quantities are defined as the **Dispersion Measure**

(768) $\text{DM} = \langle n_e\rangle d.$

Using sources with known distances, we have established that $\langle n_e\rangle \approx 0.03\,\text{cm}^{-3}$

in most areas of the Milky Way. We can then measure $dt_p/d\omega$ to directly estimate the distances to pulsars! Fig. 64 shows the dispersion measure for an assortment of Galactic pulsars and magnetars.

We can also examine the propagation of waves through the ISM in the presence of a time-changing $\vec{B}$ (which we have ignored up to now). The calculation is not trivial! But the key, final result is that right-hand and left-hand circular polarization states will travel at different speeds:

$$k_{L/R} = \frac{\omega}{c}\left(1 - \frac{\omega_p^2}{\omega(\omega \pm \omega_c)}\right)^{1/2} \tag{769}$$

where

$$\omega_c \equiv \frac{eB_{||}}{m_e c} \tag{770}$$

and

$$B_{||} = \vec{B} \cdot \vec{k}/k. \tag{771}$$

Since any linearly-polarized wave can be regarded as the combination of two circular polarizations, any linearly-polarized plane wave will see its direction of polarization rotate as the two circular waves move at different speeds.

$$\Delta\theta_p = \int_0^d \frac{k_L - k_R}{2} dz \equiv \mathrm{RM}\lambda^2 \tag{772}$$

where RM is the observed **Rotation Measure**. Observationally we again look at how this changes with frequency:

$$\frac{d\theta}{d\omega} = -\frac{1}{\omega^3}\frac{4\pi e^3}{m_e^2 c^2}\int_0^d n_e B_{||} dz. \tag{773}$$

This gives us a way to infer magnetic field strengths throughout the ISM, just using radio wave observations (and a bit of astrophysics). Fig. 64 shows the rotation measure vs. dispersion measure for various radio sources.

26 Exoplanet Atmospheres

26.1 *Temperatures*

Like stars or brown dwarfs, planets are born hot. But they cool off quickly, and so the energy budgets of all but the youngest exoplanets are dominated by stellar irradiation reprocessed by the planet's atmosphere (or surface). When internal heat sources are small, a planet in energy balance should satisfy

$$E_{\text{out}} = E_{\text{abs}} = (1 - A_B)E_{\text{inc}} \tag{774}$$

where the E's above are the outgoing (emitted), absorbed, and incident energies, respectively. The term A_B is the **Bond Albedo** of a planet, and indicates the bolometric fraction of incident energy absorbed by the planet. (Thus the reflected energy is $A_B E_{\text{inc}}$ — shinier planets reflect, i.e. scatter, more light.)

Given a planet with radius R_p, orbital separation a, and stellar radius R_*,

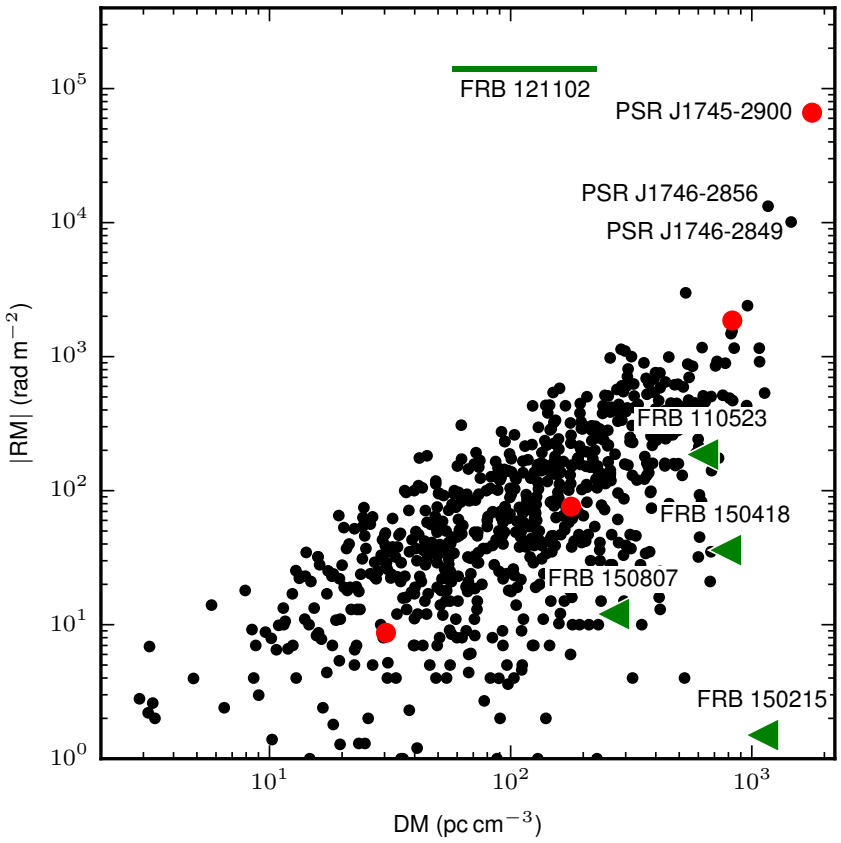

Figure 64: Dispersion and rotation measures for Galactic pulsars (black dots) and magnetars (red dots) and for Fast Radio Bursts (green triangles and green line at top). Reproduced from Micchili et al. (2018), Fig. 3.

energy balance then implies that over the entire planet

$$4\pi R_p^2 F_p = (1 - A_B) \left(\frac{R_*}{a}\right)^2 \pi R_p^2. \tag{775}$$

Invoking the Stefan-Boltzmann law for the star in terms of its effective temperature $T_{\rm eff}$, we can then calculate the **equilibrium temperature** of the planet's irradiated day side,

$$T_{\rm eq} = T_{\rm eff} \left(\frac{R_*}{a}\right)^{1/2} [f\,(1 - A_B)]^{1/4} \tag{776}$$

Here f accounts for the fact that on a planet with an atmosphere (or ocean), bulk motion can transport heat from the hot day side to the colder night side: in this case the planet effectively radiates with a greater effective surface area, and so $T_{\rm eq}$ is lower. Valid values of f range from $1/4$ (lower $T_{\rm eq}$, indicating full heat circulation around the planet) to $2/3$ (no circulation). Note that the equilibrium temperature is really just a parameterized incident irradiation that lets us sweep our uncertainty about f and A_B under the rug. There is also an **irradiation temperature**,

$$T_{\rm irr} = T_{\rm eff} \left(\frac{R_*}{a}\right)^{1/2} = \frac{S_0^{1/4}}{\sigma_{SB}} \tag{777}$$

which describes the incident radiation coming in at the substellar point (noon on the equator). Here S_0 is (for Earth) the **Solar constant** of about 1400 W m^{-2} incident at the top of the atmosphere.

Typical values for A_B are 0.12 for Mercury, 0.75 for Venus, and $\sim$0.3 for the other Solar system planets. Thus Venus actually has a lower $T_{\rm eq}$ than the Earth despite being closer to the Sun (i.e., having greater $T_{\rm irr}$). Nonetheless the Venerean surface is hot enough to melt lead. This hints at a key issue with the use of equilibrium temperature: it is only a rough proxy and can sometimes lead to expectations at variance with observations.

We know comparatively little about the albedos of most exoplanets. Most measurements to date are of hot Jupiters (highly irradiated gas giants, $T_{\rm eq} >$ 1000 K and $R_p \sim R_{\rm Jup}$) and indicate quite low albedos, $A_B \lesssim 0.2$. But a few exceptions have quite high albedos; these are thought to be covered in especially reflective clouds.

26.2 *Surface-Atmosphere Energy Balance*

It may surprise you to consider that some planets have atmospheres, which can absorb and emit radiation on their own. If the planet also has a solid surface, then we can equate the radiation absorbed and re-emitted by both the atmosphere and the surface to gain insight into the planet's energy balance.

The overall picture is shown in Fig. 65. The scenario is similar in some ways to the two-layer stellar model introduced in Sec. 7.2, but now we have a surface. We split the radiation into two wholly separate components: in-

coming radiation from the star, and outgoing radiation from the surface and atmosphere. For the Earth around the Sun, $T_P \approx 290$ K and $T_* \approx 5800$ K, so from Wien's Law (Eq. 82) $\lambda_{P,\max} \approx 10\mu$m while $\lambda_{*,\max} \approx 500$ nm. These very different wavelengths are not typically affected by the same opacity sources, and so we are justified in treating these two radiation streams separately. For hotter planets and/or cooler stars, this assumption can break down: e.g. the hottest of the hot Jupiters have $T_{\rm eq} \gtrsim 2000$ K, not so much cooler than the coolest stars.

We assume that the atmosphere has a thermal emissivity ϵ, where

$$\epsilon = 1 - e^{-\tau}. \tag{778}$$

For a fairly thin atmosphere (like the Earth's), $\tau < 1$ and so $\epsilon \approx \tau$. We will define F_S and F_A as the flux emitted by a blackbody at the temperatures of the surface and atmosphere, respectively.

If we require energy balance at the planet's surface, we have

$$\frac{S_0}{4} + \epsilon F_A = \frac{A_B S_0}{4} + F_S. \tag{779}$$

The atmosphere is transparent to the incoming radiation but absorbs some of the thermal radiation from the surface, so atmospheric energy balance gives

$$\epsilon F_S = 2\epsilon F_A. \tag{780}$$

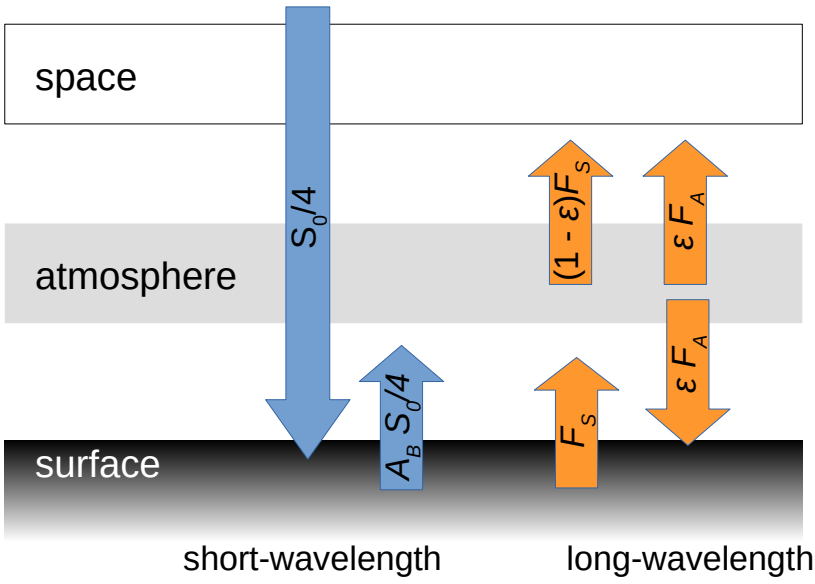

Figure 65: Energy balance on a planet with an atmosphere. Short-wavelength (visible) radiation is shown in blue, and long-wavelength (thermal) radiation in orange.

Combining these two relations gives

$$\sigma T_S^4 = S_0 \frac{1 - A_B}{4} \frac{1}{1 - \epsilon/2} \tag{781}$$

which relates the surface temperature T_S to the planetary albedo and atmospheric emissivity. If A_B is low the planet's surface will cool off – but as the atmosphere becomes more opaque to thermal radiation (i.e., as ϵ rises from $\sim$0 toward unity) the surface temperature will increase. This second point is one simple version of the **greenhouse effect**. It is part of the reason that Venus' surface is much hotter than its upper atmosphere (i.e., because $\epsilon_{\text{Venus}} \approx 1$), and is one reason that Earth's surface temperature is slowly but steadily increasing (i.e., because $\epsilon_\oplus$ is being increased).

If one sets T_S to 273 K and 373 K, with reasonable values of ϵ one can calculate the inner and outer orbital semimajor axes a for which liquid water can persist on the planet's surface. This is the first step toward calculating the **habitable zone**; planets in this zone orbiting a star are often particularly intriguing prospects for atmospheric characterization.

26.3 *Transmission Spectroscopy*

Long ago in Sec. 4.3 we briefly alluded to transiting planets. The transit method is the most productive method to date for finding new planets; it also provides a way to study the chemical composition of their atmospheres. This is useful because planets are so much fainter than stars that measuring their composition via spectroscopy of their thermal emission (as we do with stars) is impossible in all but a few of the most favorable cases. Instead, we use **transmission spectroscopy**.

In an atmosphere in hydrostatic equilibrium (Eq. 192), the pressure is

$$P = nkT = P_0 e^{-z/H} \tag{782}$$

where H is the **atmospheric scale height**, the characteristic e-folding scale of the atmosphere:

$$H \equiv \frac{k_B T}{\mu g_P}. \tag{783}$$

If we assume that the atmosphere is isothermal, then similarly

$$n(z) = n_0 e^{-z/H}. \tag{784}$$

When observing a transit at a particular wavelength, we will only observe down to an altitude z such that the tangent optical depth is roughly unity. The ray will travel from one side of the atmosphere through to the other, with a

minimum altitude z. The full optical depth along that tangent line is

$$\begin{aligned}\tau_\nu &= 2\int_z^R n\sigma_\nu ds \\ &= 2\sigma_\nu n_0 \int_z^R e^{-r/H} ds.\end{aligned}$$

Due to the dependence of z and s this integral isn't totally trivial. What's important is that n drops off rapidly (exponentially!) with altitude, so that the optical depth is dominated by the minimum altitude z hit by the ray. This means that

$$\tau_\nu \propto e^{-z/H} = 1. \tag{785}$$

Because z depends on the opacity — which is wavelength-dependent — a different altitude is reached for the rays at each wavelength. If we observe transits at two different wavelengths, then the two altitudes probed will be

$$\frac{z_1 - z_2}{H} = \frac{\delta z}{H} = \ln\frac{\sigma_1}{\sigma_2}. \tag{786}$$

The result is that each transit observation probes effectively one scale height of the atmosphere, modulated by the atmospheric opacity at that wavelength. The characteristic transit signal of one scale height is just the ratio of the projected area of the planet's annulus to the area of the host star:

$$\delta = \frac{\delta A}{A} = \frac{2\pi R_P H}{\pi R_*^2}. \tag{787}$$

By observing the transit at multiple wavelengths, one builds up a **transmission spectrum** – the wavelength-dependent transit depth. The difference between the transit depths at two wavelengths is then just

$$\left(\frac{\delta F}{F}\right)_1 - \left(\frac{\delta F}{F}\right)_2 \approx \delta \ln\frac{\sigma_1}{\sigma_2}. \tag{788}$$

In the strongest lines, the core-to-wing opacity ratio might be as high as 10^4, but the logarithmic dependence means that only roughly $10H$ will be probed. Most lines are weaker than this, so in practice transmission spectroscopy probes a moderately narrow range of the atmosphere — frustrating because we can't measure pressures outside of this range, but nice because some of our assumptions (such as that the atmosphere is isothermal) are moderately valid.

One simple, analytic example is Rayleigh scattering, in which $\sigma \propto \lambda^{-4}$ due to small particles (molecules or tiny particulates) high in a planet's atmo-

sphere. In transit, the transit depth will then scale as

$$\delta \ln \frac{\sigma_1}{\sigma_2} \propto (-4 \ln \lambda) \frac{H R_p}{R_*^2}. \quad (789)$$

Equivalently, this means that the apparent planetary radius should increase to shorter wavelengths as

$$R_P(\lambda) \propto -H \ln \lambda \propto \frac{T}{\mu g} \ln \lambda. \quad (790)$$

If transits and radial velocities have measured a planet's R_P, M_p, and so also g, then by measuring the transit spectrum one obtains (in principle) a degenerate measurement of the mean molecular weight μ and the atmospheric temperature T.

In practice, only a few atmospheres obviously show a clear signature of Rayleigh scattering; most have a multitude of opacity sources (often including mid-level-sized clouds or hazes) which complicates the picture. But the general result that transit-inferred planet size is proportional to $\ln \sigma$ remains valid.

26.4 *Basic scaling relations for atmospheric characterization*

There are several fundamental ways that the atmospheres of exoplanets are characterized:

- **Transits.** These measure the planet-to-star radius ratio $\delta = R_P^2/R_*^2$. By inferring the star's properties, we measure the planet size. If we also know its mass, then we know its density and so might know whether it is a puffy gas giant or dense rock. However, the bulk compositions of planets with sizes of 2–6$R_\oplus$ are degenerate – they cannot be uniquely determined by mass and radius measurements alone.
- **Transmission.** As described above, the signal amplitude is roughly HR_P/R_*^2. This is $\propto TR_P/(\mu g_P R_*^2) \propto T/(\mu \rho_P R_*^2)$. So a hot, low-density planet with a H_2-dominated atmosphere will have a large signal – as one moves to cooler and denser planets with heavier atmospheric constituents (i.e., towards more Earth-like planets) characterization becomes progressively more difficult.
- **Thermal Emission: eclipses.** When a transiting planet passes behind its host star, its thermal emission is blocked. To first order, if the planet and star both emit as blackbodies then the measured signal is $\delta(B_\nu(T_P)/B_\nu(T_*))$. If the planets are hot and we observe in the infrared near the Rayleigh-Jeans tail, then (very roughly) we will instead have $\delta T_P/T_*$ – infrared eclipses give us the temperature of the planet. More specifically, this is the brightness temperature of the planet's day side (the only hemisphere seen right around the time of eclipse).
- **Thermal Emission: phase curves.** Most exoplanets are hotter (and brighter) on their daysides and colder (and dimmer) on their nightsides. By ob-

serving throughout a planet's orbit, we can sometimes measure the roughly sinusoidal change in system brightness during a full planet orbit. The full (peak-to-valley) amplitude of this flux variation (assuming blackbody emission) will be $\delta(B_\nu(T_{\mathrm{p,hot}}) - B_\nu(T_{\mathrm{p,cold}}))/B_\nu(T_*))$. In the Rayleigh-Jeans limit, this becomes $\delta(T_{\mathrm{p,hot}} - T_{\mathrm{p,cold}})/T_*$. With the eclipse observed "for free" during the phase curve, we thus measure the day-to-night temperature contrast. We can actually get a low-resolution 1D (longitudinally-averaged) temperature map of the entire planet.

- **Thermal Emission: direct imaging.** Most known exoplanets are in very short periods and cannot be spatially resolved by telescopes. These observations are dominated by stellar flux and Poisson (photon) noise limits the achievable precision. A few planets are on very wide orbits, such that the stellar light is well-separated from the planet. In these cases one can "simply" point a spectrograph at the planet and measure its emission spectrum, just like one does for a planet. The relative signal amplitude will be the same as for the eclipse case described above, but the relative noise levels will be lower (all else being equal). Like eclipses and phase curves, direct imaging can also in principle be done at visible wavelengths; here the observed planet flux will often be dominated by scattering (and so by the planet's albedo) and not so much by T_P.

The following table gives approximate estimates for the signal amplitude for several different types of planetary systems. It should be apparent why so many more hot Jupiters than habitable, Earthlike planets have been studied: the atmospheric signals for those hot gas giants are orders of magnitude larger.

Method	Scaling	Earth, G2 Dwarf	Hot Jupiter, G2 Dwarf	Earth, M dwarf	Hot Jupiter, M dwarf
T_{eq}	$T_{\mathrm{eff}}\left(\frac{R_*}{2a}\right)^{1/2}$	280 K	1600 K	280 K	1000 K
Transit	$\left(\frac{R_P}{R_*}\right)^2$	10^{-4}	10^{-2}	6×10^{-4}	6×10^{-2}
Transmission	$\frac{HR_P}{R_*^2}$	10^{-7}	10^{-4}	6×10^{-7}	3×10^{-4}
Emission (5μm)	$\left(\frac{R_P}{R_*}\right)^2\frac{B_\nu(T_P)}{B_\nu(T_*)}$	2×10^{-9}	10^{-3}	2×10^{-8}	6×10^{-3}

26.5 *Thermal Transport: Atmospheric Circulation*

Thermal phase curves in particular offer the intriguing possibility of studying global conditions all around the planet — in contrast to eclipses (which probe only the day-side) and transits (which probe only the day-night terminator). Fully modeling a planet's global atmospheric circulation requires so-called

general circulation models (GCMs) that solve some version of the Navier-Stokes fluid equations (and perhaps also accounting for other physics such as ionization, magnetic fields, etc.). Nonetheless we can build a simple thermal transport model to describe what we might expect to see when observing phase curves.

We will consider a day in the life of an individual gas parcel on a tidally-locked, short-period exoplanet. The planet is on a circular orbit and receives incident bolometric flux from its star

$$F_{\rm inc} = \sigma T_{\rm eff}^4 \left(\frac{R_*}{a}\right)^2. \quad (791)$$

However, the gas parcel only absorbs a fraction of this incident flux. This fraction accounts both for the albedo (discussed previously) but also for planetary geometry: planets are spheres, and a gas parcel near the planet's limb or equator will absorb less stellar energy than at noon on the equator (the substellar point). Another way of thinking about this is that solar cells tend to be a lousy investment in Antarctica. Assume the parcel is at latitude θ and longitude ϕ. We define $\theta = 0$ at the North pole and π at the South pole, while $\phi = 0$ at the substellar longitude, $-\pi/2$ at dawn, and $\pi/2$ at sunset.

The net flux of the parcel will be

$$\Delta F = (1 - A_B) F_{\rm inc} \sin\theta \max(\cos\phi, 0) - \sigma T^4. \quad (792)$$

(The "max" function takes the maximum of the two arguments, and accounts for the fact that when our atmospheric parcel is on the night side, it absorbs zero (not negative) flux.) If the parcel has density ρ, specific heat capacity c_P, and thickness H then we obtain a differential equation for the parcel's temperature:

$$\frac{dT}{dt} = \frac{1}{c_h}\left((1 - A_B) F \sin\theta \max(\cos\phi, 0) - \sigma T^4\right) \quad (793)$$

where

$$c_h = \rho c_P H. \quad (794)$$

If we set $dT/dt = 0$ in Eq. 793, then we obtain an expression for the *local* equilibrium temperature of the gas parcel.

Since one parcel is as good as another, if we can solve Eq. 793 for one gas parcel and relate time to the parcel's longitude then we will know how the surface temperature of the entire planet varies with longitude – i.e., we will have constructed a planetary temperature map.

To make things a bit more tractable, we define a fiducial temperature

$$T_0 \equiv T_{\rm eff}(1 - A_B)^{1/4} \sin^{1/4}\theta \left(\frac{R_*}{a}\right)^{1/2} \quad (795)$$

and also define the **radiative timescale**

$$\tau_{\rm rad} \equiv \frac{c_h}{\sigma T_0^3}. \quad (796)$$

If we then define a dimensionless temperature $T' \equiv T/T_0$ and time $t' \equiv t/\tau_{\rm rad}$, then Eq. 793 is simplified to

$$\frac{dT'}{dt'} = \max(\cos\phi, 0) - T'^4. \quad (797)$$

This is a function of time, but we could also write things in terms of longitude if we could describe the motion of our gas parcel around the planet. We assume that our gas parcel is advected around the planet (e.g., by the globally circulating winds predicted on hot gas giants) with a characteristic windspeed $v_{\rm adv}$, giving rise to a characteristic **advective timescale**

$$\tau_{\rm adv} \equiv \frac{2\pi R_P}{v_{\rm adv}}. \quad (798)$$

An important quantity is the ratio of these two timescales, which we denote

$$\epsilon \equiv \frac{\tau_{\rm rad}}{\tau_{\rm adv}}. \quad (799)$$

When $\epsilon \ll 1$, radiation is "faster" (i.e., more efficient) than advection and energy is almost immediately radiated away before it can be transported around the planet. When $\epsilon \gg 1$, the reverse is true and energy is swept away by winds much more rapidly than it can be re-radiated. Eq. 797 then becomes

$$\frac{dT'}{d\phi} = \frac{2\pi}{\epsilon}\left(\max(\cos\phi, 0) - T'^4\right). \quad (800)$$

Eq. 800 has two solutions, depending on whether the parcel is on the day side (absorbing energy while re-radiating) or on the night side (emitting only). The analytic solution for the night-side temperature can be found by integrating from dusk (when the parcel stops absorbing energy, $\phi = \pi/2$) until some later phase ϕ (up until dawn). The solution is

$$T'_{\rm night}(\phi) = \left(\frac{6\pi}{\epsilon}\left[\phi - \frac{\pi}{2}\right] + (T'_{\rm dusk})^{-3}\right)^{-1/3}. \quad (801)$$

If advection is extremely efficient, then the first term in parentheses is zero and $T_{\rm night} = T_{\rm dusk}$ — the planet's night side has a uniform temperature. But as radiative transport begins to dominate advective heat transport, the night side temperature will drop steadily from dusk (consisting of parcels that only just stopped seeing their star) to dawn (after they have been radiating away thermal energy for the entire night). Note that this process happens even though the planet itself is tidally locked; global winds still circulate.

On the day side, there is no general analytic solution to Eq. 800 (though it

can be solved numerically). Nonetheless (as with the night side) the solution will depend sensitively on the ratio of advective and radiative timescales. If $\epsilon \gg 1$ then advection is very efficient, and

$$\frac{dT'_{\rm day}}{d\phi} = 0 \;\rightarrow\; T_{\rm day} = \text{const.} \tag{802}$$

If energy transport is very efficient, the temperature is the same, day and night. On the other hand, if $\epsilon \ll 1$ then radiation is extremely efficient and winds have negligible effect on heat transport. In that case,

$$T'_{\rm day} = \cos^{1/4}\phi. \tag{803}$$

As the next-order approximation, one can assume that T' is a quadratic function of ϕ and similarly expand $\cos\phi$ to second order. This is a pretty crude model, but it provides one or two final insights. Under this assumption,

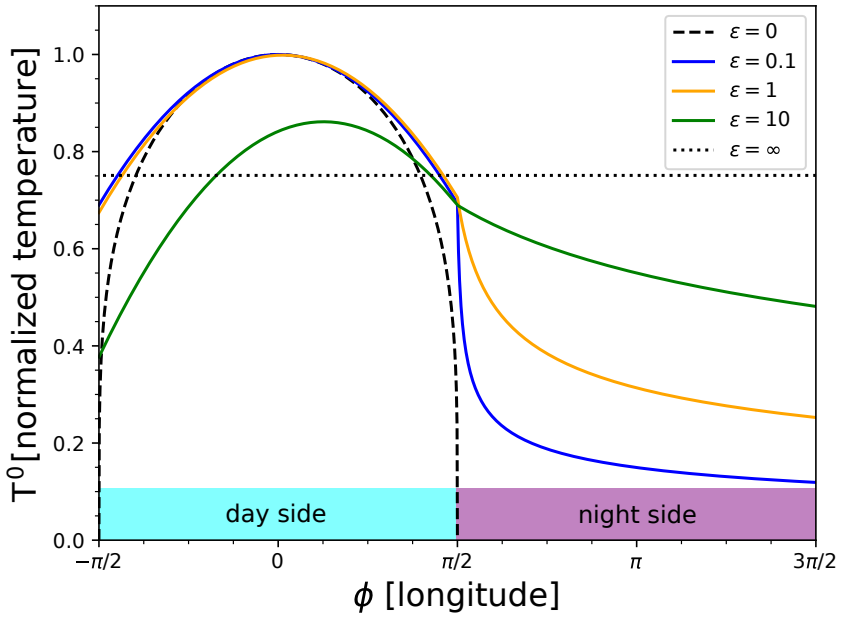

Figure 66: Planetary temperature vs. longitude for a simple energy transport model, for different values of $\epsilon = \tau_{\rm rad}/\tau_{\rm adv}$. The substellar longitude is at $\phi = 0$. The solid curves on the day side are the second-order approximate solutions of Eq. 804, while on the night side are plotted the exact solutions of Eq. 801. The broken black curves are the exact solutions for the limiting cases indicated, i.e. atmospheres dominated by radiation (dashed) and advection (dotted).

setting $\epsilon \equiv \tau_{\rm rad}/\tau_{\rm adv}$ yields

$$T_{\rm day} \approx \left(1 - \frac{\epsilon^2}{64\pi^2}\right) + \frac{\epsilon}{32\pi}\phi - \frac{1}{8}\phi^2. \quad (804)$$

These approximate solutions are plotted in Fig. 66 for several values of ϵ. Note that the low-ϵ curves are a decent match to the exact analytic solution for $\epsilon = 0$ (i.e., Eq. 803), but the quadratic models overpredict the temperature at dawn and dusk. They also leave a discontinuity in T' at dawn; this can be fixed by computing the full numerical solution to Eq. 800.

The temperature of our circulating gas parcel reaches a maximum when $dT'/d\phi = 0$, which implies a longitude of maximum temperature

$$\phi_{\rm max} \approx \frac{1}{8\pi}\frac{\tau_{\rm rad}}{\tau_{\rm adv}}. \quad (805)$$

Thus the hottest part of the planet is located to the East of the substellar point; this shift in peak temperature is the **phase offset**, and gives an estimate of the relative timescales operating in a planet's atmosphere. (This is *not* the reason that on Earth it's warmer in the early afternoon than at dead noon; that's because of the Earth's thermal inertia and its rapid rotation, $P_{\rm rot}/P_{\rm orb} \ll 1$.)

By setting $\phi = \phi_{\rm max}$ in Eq. 804, we obtain the maximum dayside temperature:

$$T'_{\rm day,max} = T'_{\rm day}(\phi_{\rm max}) \approx 1 - \frac{7\epsilon^2}{512\pi^2}. \quad (806)$$

Thus radiative-dominated atmospheres have the maximum possible day side temperatures. As advection plays an increasingly important role, more energy is distributed around the planet and the maximum day side temperature decreases. In the exact solution, the maximum temperature also correlates with the phase offset, as

$$T'_{\rm max} = \cos^{1/4}\phi_{\rm max} \quad (807)$$

down to a minimum of $\pi^{-1/4}$ (as plotted in Fig. 66).

Many typical hot Jupiters have phase offsets of $\sim 20^o$ — indicating typical values of $\epsilon \approx 10$, day side temperatures 10–15% cooler than in local equilibrium, and moderate day-to-night temperature contrasts. As one observes hotter and hotter planets (e.g., $T_{\rm eq} \gtrsim 2000$ K), radiation increasingly dominates over heat transport, $\epsilon \to 0$, day sides become hotter, and day-night temperature contrast increases. In practice, processes other than radiation and advection become important when considering atmospheric circulation; in particular, various drag forces and their associated timescales can become at least as relevant as the advective processes that they inhibit.

27 The Big Bang, Our Starting Point

27.1 *A Human History of the Universe*

As humans, we have for centuries tried to understand the nature of the universe we live in. It is a slow process, often impeded by old beliefs that are not easily replaced by new theories, even when they better support the available evidence. The earliest Greek and Roman astronomers believed that the earth was the center of the universe, with all of the objects in the heavens surrounding our world in fixed, crystalline spheres. Aided by Christian doctrine, the belief that earth was at the center of the universe persisted until the 17th century, even though observations of the motions of the planets in the second century began to require adjustments to this model that verged on the absurd in their complexity (see the epicycles of Ptolemy for an example of this). Even when Copernicus developed a simpler theory of a heliocentric universe that perfectly fit the data available, it took Galileo observing the phases of Venus and a set of moons orbiting Jupiter with his telescope to definitively prove that not everything in the heavens orbits the earth. Even then, this new idea was not easily adopted: for his contributions to astronomy, Galileo was convicted of heresy and imprisoned in his home until his death. While the heliocentric theory of Copernicus led us to our modern view of the solar system and set the stage for understanding we were not located in a special place in the universe, it would be many more years before we understood that the universe consisted of more than just the known planets (up to Saturn) and the 'fixed stars'.

One of the most important figures in our next big leap in understanding the extent of the universe we inhabit was Henrietta Swan Leavitt. In the early 20th century, nearly 300 years after the controversy of Copernicus and Galileo, Leavitt discovered that there was a simple relationship between the intrinsic, peak brightness of a type of variable star and the period of time over which its brightness varied. By measuring the period of these Cepheid variables, one could then determine exactly how bright this star should be (like a light bulb) and thus infer its distance. Critically, these stars were bright enough to be seen at enormous distances, and so using one of the biggest telescopes of that time, Edwin Hubble observed Cepheid stars in the so-called 'Andromeda Nebula' and showed that this source was in fact not part of the Milky Way Galaxy. Andromeda and all of the other 'spiral nebulae' like it were actually so far away that they must be considered 'island universes' of their own: other galaxies full of other stars, just like the Milky Way we inhabit. This discovery was a breakthrough, as astronomers began at last to understand the universe for what it was: not merely a solar system surrounded by fixed stars, but a collection of thousands of galaxies, each containing billions of stars, and our own solar system surrounding just one of these stars. Modern studies have added additional detail to this picture: we know now that the visible universe contains as many as two trillion galaxies, and that most of the stars in these galaxies are statistically likely to have solar systems like our own, but Hubble, aided by Leavitt's discovery, was the first to really define our modern view of the universe.

Hubble made another critical contribution to our understanding of the universe during his career: having determined the distances to galaxies outside of the Milky Way, he also measured the speed at which these galaxies were moving, using the degree to which spectral features in these galaxies were Doppler shifted. To everyone's surprise, he found that the distant galaxies he observed were all moving away from the Milky Way, faster and faster the further away they were. There was one simple explanation for this: the universe was expanding. Assuming (thanks to the Copernican principle that we are not in a special place in the universe), that any observer at another place and time would observe the same phenomenon, it must be that the space itself between the galaxies was growing every larger. Hubble reasoned that if one took the constant speed of expansion that he measured, and if one then reversed this expansion, one would reach a time at which all of the galaxies in the universe would be at the same place. This would then be the origin of the universe: the Big Bang. Using this model, he calculated for the first time a finite age for the universe we live in. Modern scientists have improved upon his measurement of the speed at which the galaxies are moving away from is, and we now believe from this and other independent evidence that the age of the universe is 13.8 billion years old

27.2 *A Timeline of the Universe*

As the universe has expanded since the Big Bang, its conditions have changed drastically from an inferno of pure energy in the first few fractions of a second to the dark, expansive void we inhabit presently. With its continuing expansion, its average temperature has decreased, as has the average matter density, and so the universe has passed through different eras of being dominated by radiation, matter, and its current state today: dominated by dark energy. However, while the average matter density has decreased, gravity has been at work locally to counter this expansion by taking initial quantum fluctuations in the mass/energy field and amplifying them to form dense condensations separated by enormous voids of expanding space. These gravitationally-bound structures are dominated by dark matter, and in the present day they form the backbone of what are now enormous filaments and nodes; clusters and superclusters containing millions and billions of galaxies. However, it was not until a few hundred million years after the Big Bang that the gas in the early universe cooled and condensed sufficiently to form the first generation of stars, and perhaps at the same time, the first galaxies. Over the billions of years since that time, the space between individual galaxies and galaxy clusters has increased, to the point that many of the most distant galaxies that we see, we could never send a signal to, as relative to us they appear to be moving away faster than the speed of light. Due to the acceleration of the expansion of the universe (caused by the dominance of dark energy), the universe will continue to expand in this way, faster and faster, until eventually the only light we see comes from our own galaxy: all other galaxies having apparently moved away from us so fast that their light can no longer reach us.

27.3 *Big Bang Nucleosynthesis*

For this class, one of the most important events in the early universe was a short (a few minutes) period beginning 100 seconds after the Big Bang. By this time, the universe had cooled enough that particles were able to condense out of the energy soup, and the temperature of the expanding universe began to approach that of the interior of stars today: around a billion K. The conditions were then ideal for taking the single protons that existed in the universe, and fusing them to create deuterium, helium and a few other molecules. Because the universe was still rapidly expanding, the temperatures needed for hydrogen fusion did not last long, but it was sufficient to turn approximately 25% of the mass of hydrogen in the universe into helium. In addition to helium, a very small fraction of the gas was able to undergo multiple fusion reactions and create tritium (which is unstable and quickly decayed), and a detectable amount of lithium. This is shown in Figure 67: all non-manmade elements heavier than this must have been in stars and their associated processes.

Figure 67: A periodic table showing the different processes by which the elements observed in the universe today were formed

27.4 *The Cosmic Microwave Background*

Approximately 300,000 years after the Big Bang, the universe cooled enough to undergo another important change. All of the hydrogen, helium, and lithium created in Big Bang Nucleosynthesis were, up to this point, technically in an ionized state. That is, they consisted only of protons and neutrons, and had no attached electrons. Electrons were present in the universe, but as a free gas. As such, they frequently underwent collisions with the photons, causing those photons to scatter in random and unpredictable paths, and making the universe opaque to radiation. However, once the universe reached a temperature of around 3000 K, the electrons began to combine with the atomic nuclei, as their thermal energy was no longer greater than the electrostatic binding energy between themselves and the protons. As soon as the majority of the electrons were bound to nuclei, photons became free to travel unimpeded throughout the universe. As observers then, we can only see back to this time when the universe first became transparent to radiation, and the barrier between us and earlier times is known as 'the surface of last scattering'. The imprint of the radiation from this period is still detected today as the 'Cosmic Microwave Background' or CMB, at a present-day temperature of 2.7 K, peaking at a wavelength near 1 mm. The information encoded in the structure of this all-sky pattern of emission is one of the most important pieces of data used by precision cosmology studies, and has been used as evidence for inflation in the early universe, and to infer the fraction of non-baryonic (dark) matter in the universe.

27.5 *The first stars and galaxies*

We have seen that we are fundamentally limited in looking back in time by the CMB (though, physicists can in a way 'look back' to in time to the conditions that dominated at higher energies that occurred before this time using particle colliders). What are the oldest objects that we have seen? At present, the record holder is a galaxy that is 13.4 billion light years away, having formed by only 400 million years after the Big Bang. Galaxies like this are detected primarily through their extremely red (red-shifted) colors: though they are full of young, hot and blue stars, the extreme speed at which they appear to be moving away from us shifts this radiation to infrared wavelengths. We believe that the first stars and galaxies could have formed as early as a hundred million years after the Big Bang, and new observatories like the James Webb Space Telescope continue to be built in order to search for evidence of their formation at these early times. When the first stars formed, and what they were like, is important to understanding just how our universe went from nearly pure hydrogen and helium to the current day, in which we live on a planet largely made out of silicon, carbon, and metals.

28 Thermal and Thermodynamic Equilibrium

28.1 *Molecular Excitation*

How do molecules exchange energy with their environment? In the vacuum of interstellar space, there are really only two ways to get energy from the environment: by absorbing a photon, as we have seen, and by colliding with another body (typically either an electron, an atom, or another molecule).

However, molecules are typically far apart in space. How likely is it that two molecules will collide? The probability of collision can be determined by considering several parameters, namely the effective size of the molecule, how fast it is moving, and the number density of collision partners. This is illustrated in Figure 31. The effective size of a molecule is determined not just by the physical size of the molecule, but by any relevant long-range attractive forces (in this case, electromagnetic attraction between the molecule and its collision partners) which will effectively increase the collision cross-section. The larger the cross-section, the higher the probability of collision. Likewise, the faster a molecule is moving, the more distance it covers and the more likely it is to undergo a collision faster. Finally, the higher the number density of collision partners, the more likely it is that a collision will occur.

The typical time t_{col} over which a molecule is expected to have at least one collision (the collisional timescale) is given by

$$t_{col} = \frac{v}{nA} \tag{808}$$

Here, A is the collisional cross section, and n is the number density of collisional partners in the medium through which the molecule is traveling at a speed v. Related to this, the typical distance that a molecule will be able to travel before undergoing a collision (the mean free path, first mentioned in Section 8.3) is given by:

$$l = \frac{1}{nA}. \tag{809}$$

How can molecules store the energy they get from their surroundings? There are four places. The first of course is in their macroscopic, translational movement, in the speed at which they move through space. However, molecules can also store significant energy internally: in rotational, vibrational, and electronic forms. These internal energies are quantized into different excitation states. As a molecule undergoes a collision or absorbs a photon of the appropriate energy, it can move up into a higher excitation state. A molecule can also emit a photon or undergo a collision to move down into a lower excitation state.

The population of these different excitation states of a molecule (that is, the number of molecules with a given internal energy configuration) can be described in terms of the typical rates of each of these processes. The simplest model to consider is that of a two-level system, in which the molecule

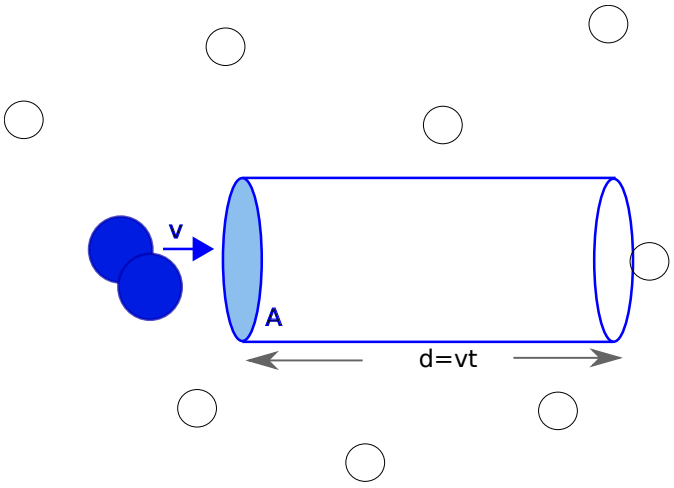

Figure 68: A diagram illustrating the probability of collision for a molecule moving at a speed v through a medium of other particles (assumed to have a number density n). The collisional cross section of the molecule is A. In this diagram, the molecule is presumed to undergo a single collision in a time t after traveling a distance d.

can be either in a low-energy state l or a higher-energy state u. The population of both levels is given by consideration of the rates going into and out of each, shown in Figure 69. The first rates to consider are C_{lu} and C_{ul}, or the collisional rate coefficients (Here, C is essentially equal to the collisional cross section$A$ multiplied by the speed v, and has units of s^1 cm^3. If you multiply this by the number density, you will get a simple rate of the number of collisions resulting in excitation per second). The next set of rates are the so-called 'Einstein B' coefficients. These are the rates for the absorption of photons (B_{lu}) and the *stimulated* emission of photons (B_{ul}). The latter is really only relevant in cases of laser (or at the typical wavelengths corresponding to molecular excitation, maser) emission. The final rate is the 'Einstein A' coefficient A_{ul} that represents the de-excitation through the spontaneous emission of a photon. This spontaneous emission is typically how spectral lines from molecules are observed.

Figure 69: An illustration of the different processes that lead to excitation and de-excitation in a hypothetical two-level system like the energy levels in an atom or a molecule. Upward arrows represent the excitation processes– collisional (in blue) and radiative (in red) – that can cause a transition from a lower l to an upper u energy state. Downward arrows represent the corresponding de-excitation processes.

Of course, in real life a molecule has dozens to hundreds or more different rotational, vibrational, and electronic energy states. Determining how each of these states is populated then requires quite complex computer codes to find

the equilibrium based on all of the rates into and out of each level.

In the cold interstellar medium, rotational excitation will be the most typical form of molecular excitation, as the energies involved in vibrational excitation (to bend or stretch the bonds of a molecule) are typically measured in excitation temperatures of hundreds to thousands of K.

Exactly how much energy is stored in these different levels, and how are these energy levels spaced in real molecules? Although this is a quantum problem, we can consider a classical analog for a rotating, diatomic molecule: two weights fixed to each end of a rigid rod. We will only deal with rotational energy levels, however vibrational energy levels can also be understood through the classical analog of weights on a spring. In real life, these analogs begin to break down at high energies, when fast-spinning molecules start stretching and increasing the previously fixed molecular spacing, or begin to spin AND vibrate, all of which is much too complicated to think about here without becoming the stuff of our nightmares.

Figure 70: A rigid rotor model for the rotation of a diatomic molecule like CO. The molecule is assumed to rotate around a central axis, with the two atoms of a molecule having a fixed separation r.

For a classical rigid rotor, we would define the angular momentum of this system as $L = I\omega$ where L is the total angular momentum, I is the moment of inertia, and ω is the angular speed. For such a system, the moment of inertia is

$$I = mr^2 \tag{810}$$

where r is the separation between the two atoms, and m is the reduced mass:

$$m = \frac{m_1 * m_2}{m_1 + m_2} \tag{811}$$

However, in our case, the angular momentum is quantized:

$$L^2 = J(J+1)\hbar \tag{812}$$

We can plug this in to the classical formula for the energy of a rigid rotor to get an expression for the energy of the J^{th} rotational level:

$$E = \frac{J(J+1)\hbar}{2I} \tag{813}$$

With knowledge of the moment of inertia of a molecule, one can then use Equation 813 to determine the energy of each of its rotational transitions, to

determine the energy separation between levels, and to determine the frequency of a photon ($E = h\nu$) that will be emitted as a result of a transition between two levels.

28.2 *Typical Temperatures and Densities*

The cold molecular interstellar medium, while not the bulk of gas in our Galaxy, is the gas that is the most relevant for forming stars, and so knowledge of its physical conditions are important both for understanding and observing that process. The dominant constituent of gas in this phase is molecular hydrogen (H_2). Typical temperatures in this gas range from 5 K up to 100 K, and typical number densities n range from $10^4 - 10^6$ particles per cubic centimeter, though they can be as high as $n \sim 10^7 - 10^8$ cm^{-3} in condensations that will form massive stars. Most gas in this phase is found in giant molecular clouds, objects with sizes of many tens to hundreds of parsecs, and masses of a few tens of thousand to a million times that of our sun. Inside of these clouds, the structure is quite fractal, and consists of smaller 'clumps' capable of forming a small cluster of stars, and 'cores' that will form a single stellar system. Molecular clouds contain dust as well as gas, and while typically by mass, there is 100 times more gas than dust, the dust is responsible for significant extinction: blocking short wavelength light from penetrating to the center of the cloud, and making the cloud appear as a dark silhouette against the background stars at optical wavelengths.

The temperatures of molecular clouds are measured by using many of the tools we have described so far. Astronomers observe emission lines from molecules, and (with the rough analogy that each molecule acts like a lightbulb, so counting up the total flux coming from a spectral line gives you an idea of the number of molecules present and emitting light) count the number of molecules in several rotational energy states. They then use the Boltzmann equation (Equation 96) to determine an excitation temperature for the gas. If the cloud is in local thermodynamic equilibrium, this is equivalent to the kinetic temperature; otherwise it can be a (significant) underestimate.

To first order, the gas density can be determined based on the critical (number) density of the molecular transitions that are observed to emit in a given region of a cloud. Referring back to Figure 69, the critical density can be written as

$$n = \frac{A_{ul}}{C_{lu}} \tag{814}$$

and is the number density n at which collisional excitation at a rate of C_{lu} will populate the upper J level for a particular molecular transition (say, the $J = 1$ level for the observed $J = 1 - 0$ rotational transitions of CO) at a rate equal to that at which spontaneous emission of a photon acting at a rate A_{ul} will depopulate that level. This is the turning point between the case in which you do not expect to see significant emission from a spectral line (when molecules de-excite due to spontaneous emission faster than collisions

can excite a significant number of them) and the case in which there should be strong emission: molecules are excited into a state faster than they decay, and so at any given time there is a significant population of excited molecules to emit a photon as they spontaneously de-excite).

In general however, to get an accurate density (and temperature), particularly in cases when the gas is not in local thermodynamic equilibrium, one must rely on complex computer codes that determine both how collisions (the rates of which are dependent on the temperature and density of the gas) populate all of the different energy levels through collisions, and then also predict how photons emitted by transitions between these levels make it out of the gas cloud (using the equations of radiative transfer).

28.3 *Astrochemistry*

How do chemical reactions proceed in the unique environment of space? In space we already know that we will not find the sort of liquid chemistry we see on earth. One of the main alternatives is then gas-phase chemistry, and here we find that the environment of a typical cloud of gas in space is extremely different from anything found on earth. As we noted in the previous section, temperatures are cold (typically around 10 K, vs near 300 K for the earth) and the densities are much lower than the air we breathe: typical gas densities in space range from a hundred to a million particles per cubic centimeter, rather than 10^{19} particles in a cubic centimeter of our atmosphere (or even 10 billion particles per cubic centimeter in the best vacuum we can create in the lab!).

Initially, astronomers weren't sure that in these kinds of environments chemical reactions would happen at all! In fact these days however, we know that chemical reactions in the interstellar medium can make molecules with more than ten (or even 60 or 70) atoms! So how does gas-phase chemistry work? In Section 28.1, we discussed the likelihood of molecules in space colliding with each other (Equations 808 and 809) and described how these collisions can lead to the excitation of the molecules involved, making them rotate or vibrate slower or faster. Depending on the molecules involved however, these collisions also have the possibility of bringing the molecules close enough together that you will have a reaction that creates entirely new molecules. In general, at the densities relevant for the interstellar medium, these will all be two-body interactions from the ballistic collision of particles. At higher densities, three-body interactions are possible, but we will ignore these for this discussion.

There are a number of types of different reactions that are possible. We will highlight a few of the more common and/or important, and for each of these, we will give an associated rate k that indicates how frequently this reaction will proceed. Like C_{lu} and C_{ul} this coefficient has units of $\mathrm{cm}^3\ \mathrm{s}^1$ and is determined by the typical speed of a molecule v (or technically the relative speed between the two reacting molecules) and the reaction cross section σ: $k = \langle v\sigma \rangle$. This cross section is not strictly geometric (e.g., due to the size of the reacting molecule): it also depends on any long-range forces like electromagnetic attractions between the molecules. Essentially, k gives you the number of reactions per second, if you multiply by the number density of the gas.

1. **Dissociative Recombination**

   $AB^+ + e^- \rightarrow A + B.$

   This reaction is one of several (**photodissociation**, **collisional dissociation**) that destroys molecular bonds. Thus, as its name implies, this reaction is not generally one that creates more complex molecules in the ISM, and instead leads to breaking apart rather than building up molecules. Dissociative recombination has a relatively high reaction rate, due to the large σ from the Coulomb force ($\propto \frac{1}{r}$) between the two molecules involved. Typical rates are $k \sim 10^{-6}$ cm^3 s^{-1}.

2. **Radiative Association**

   $A^+ + B^- \rightarrow AB + \gamma$

   As opposed to dissociative recombination, this is one of a class of reactions in which bonds are formed rather than destroyed. (Other reactions of this type include **associative detachment**, in which an anion and a neutral combine and release an electron, and **grain surface** chemistry, which we will discuss in more detail shortly). In a radiative association reaction, two species (typically in the ISM these are a neutral species and a charged species, though one can also consider neutral-neutral or charged-charged reactions) combine to create a new molecule. Depending on the reactants, the cross section σ can be affected by electromagnetic attraction. In the case illustrated above, there is an attraction due to the dipole moment induced in the neutral species by the charged species ($\propto \frac{1}{r^4}$). The success of this reaction is however hindered by an additional condition for success: the emission of a photon (γ). This photon is necessary in order to stabilize the molecule and conserve energy: the energy of the two colliding molecules must go somewhere, and so initially it goes into internal excitation (rotational, vibrational, or electronic) states of the molecule, leaving it in a highly-excited state AB^*. If a photon is not promptly emitted to release this energy, the molecule will just break apart again. So, in fact, the reaction can be more correctly written to reflect this additional step:

   $A + B \rightleftharpoons AB^* \rightarrow AB + \gamma$

   Note that this problem is particularly unique to astrochemistry: in terrestrial chemistry, higher densities typically allow for three-body interactions, and this additional reactant can then carry away the excess energy of formation. Depending on the interaction cross section of the reactants and how quickly an excited molecule is able to give off this photon (you will recall that this timescale is exactly set by the size of the Einstein A coefficient (A_{ul} with units of s^{-1}) we discussed in Section 28.1) these reactions can have rates of $k \sim 10^{-9} - 10^{-17}$ cm^3 s^{-1}, if they are able to proceed at all.

3. **Neutral - Neutral**

   $A + BC \rightarrow AB + C$

This reaction is one of several (including **charge-transfer** reactions and **ion-molecule** reactions which we will discuss below) in which the bonds between molecules are rearranged. These interactions have the smallest cross sections of the types considered here. Here, the only 'long-range' force is due to the Van der Waals force in the molecules, which is extremely weak ($\propto \frac{1}{r^6}$). As a result, the typical rates of these reactions are $k \sim 10^{-11}$ cm^3 s^{-1}.

4. **Ion-Molecule**

   $A^+ + BC \rightarrow AB^+ + C$

   This is one of the most important reactions in gas phase chemistry of the interstellar medium. It has higher rates than neutral-neutral reactions because of the electromagnetic attraction between the reactants from the dipole moment induced by the charged species. Because of the nature of this electromagnetic interaction, these reactions are largely independent of temperature (i.e., the relative speed of the reactants). Typical rates for ion-molecule reactions are $k \sim 10^{-9}$ cm^3 s^{-1}

5. **Grain Surface**

   $A + B{:}g \rightarrow AB + g$

   In these reactions (like **radiative association**, they are a type of bond-formation reaction), the presence of a dust grain acts as a third body to stabilize the formation of a single molecule out of two reactants. This is a particularly nifty solution to the problem we have with radiative dissociation (forming one molecule out of two leaves a bunch of excess energy that must somehow be carried away) and the inability to apply the typical terrestrial solution (as it is difficult to have a three-body interaction in the low densities of the interstellar medium). Instead of waiting for a third body to come to them, here the reactants just go to a dust grain, becoming trapped on its surface. While larger atoms and molecules will typically find themselves stuck in a potential well on the surface of the grain, smaller atoms like hydrogen can hop around the surface from well to well, until they find a species that they can combine with. As a result, grain surface chemistry tends to be responsible for making many saturated, hydrogen-rich molecules found in space (for example, CH_3OH). When two species combine to form a third, the energy does not need to be transferred to a photon, but can be transferred to the dust grain, and is often enough to detach the new molecule from the grain, and kick it back out into space.

One of the most famous problems in astrochemistry relies on grain surface chemistry for its solution: the formation of molecular hydrogen, or H_2. Despite being the most basic molecule one could form out of the most abundant species (H) in the interstellar medium, the sheer abundance of this molecule was initially puzzling to explain. This is because there are numerous barriers to its formation in the gas phase. The first barrier is due to the symmetry of

this molecule, which has no permanent dipole moment. As a result, it radiative efficiency, or ability to emit a photon once excited (measured by A_{ul}), is extremely low. This means that the simplest reaction for forming H_2:

$$H + H \rightarrow H_2 + \gamma$$

does not proceed.

Other gas-phase mechanisms for forming H_2 require two reactions, and so are limited both by the slowest of these reactions, and the availability of the other necessary reactants. The first of these routes requires a radiative association reactions ($k \sim 10^{-17}$ cm^3 s^{-1}) followed by a faster associative detachment reactions ($k \sim 10^{-9}$ cm^3 s^{-1}):

$$H + e^- \rightarrow H^- + \gamma$$
$$H^- + H \rightarrow H_2 + e^-$$

Problems with this route include the fact that it is both hard to create H^-, and once it is created, it can also be easily destroyed by other interactions (photodetachment of its electron, or mutual neutralization with H^+).

Another route involves a similar set of reactions, in this case radiative association ($k \sim 10^{-20}$ cm^3 s^{-1}) followed by charge transfer ($k \sim 10^{-9}$ cm^3 s^{-1}):

$$H + H^+ \rightarrow H_2^+ + \gamma$$
$$H_2^+ + H \rightarrow H_2 + H^+$$

Here we have the same problem with creating H^+ as we did with H^- (but worse): an extremely slow radiative association rate. After creating H^+ it is at least slightly harder to destroy, as lacking an electron it cannot undergo photodetachment.

In summary, none of these rates are anywhere near what is required for H_2 to be the most abundant molecule in the ISM. The solution for a rapid formation of H_2 is then the existence of dust grains, such that:

$$H + H{:}g \rightarrow H_2 + g$$

While this solves our problem in the present day, it still suggests that the formation of H_2 may have been a problem in the early universe, when dust grains were absent (as in the formation of the first stars) or hard to come by.

29 Energy Transport

Questions you should be able to answer after these lectures:

- Which processes are important for blocking the free movement of photons in stars, leading to opacity?
- How does temperature vary with radius in a star, and what variables does this temperature gradient depend on?
- Under what conditions will convective instability occur in a star?

29.1 *Opacity*

In the interiors of stars, we have previously considered that energy can be locally created through nuclear processes, and used this to define one of our equations for stellar structure: the energy equation, or Equation 240. However, we now also need to return to our description of radiative transfer within stars and consider that energy can also be locally lost to absorption processes. The first step is to define the processes that contribute to absorption or opacity within stars.

For the physical conditions that dominate in stars, we will consider four types of interactions between photons and electrons that result in the scattering or absorption of incident photons, and thus increase the opacity of the gas.

Figure 71: An illustration of four sources of opacity that are relevant for the conditions in the interior and/or atmospheres of stars. **Thomson Scattering**: An elastic collision of a low-energy photon with an electron, which does not increase the kinetic energy of the electron, and does not alter the wavelength of the photon. **Free-Free Absorption**: A photon is absorbed by an electron in the vicinity of another charged particle. **Bound-Free Absorption**: An electron in an atom absorbs a photon, ionizing the atom. **Bound-Bound Absorption**: An electron in an atom absorbs a photon, exciting it to a higher energy state.

The first of these is **Electron scattering**, or for the typical (low-energy and non-relativistic) conditions inside of stars: Thomson scattering. In this case, illustrated in the top left panel of Figure 71, a photon elastically collides with an electron, and is redirected or scattered away. For Thomson scattering, the low energy of the photon means that the momentum it imparts into the electron is negligible. As a result, the electron does not recoil, and the photon does not change its energy (or wavelength). In contrast, in the higher-energy regime of Compton scattering (which is unlikely to occur in normal stars), the inelastic collision of a much higher-energy photon with an electron imparts a momentum that is significant in comparison to the mass of the electron. The electron then recoils, leaving the photon with with a reduced energy (and thus wavelength).

The second process that can occur is **Free-free absorption**, the absorption of a photon by a free electron. In order to simultaneously conserve energy and

momentum in this interaction however, the free electron must actually still be near a third body (another charged particle) with which it can exchange energy through a long-distance interaction. This is illustrated in the middle panel of Figure 71. Basically, the electron is accelerated through the absorption of a photon. The inverse of this process is known as 'Bremsstrahlung' or electron braking: basically, an electron that passes close to a positively charged particle will alter its course due to the electromagnetic interaction, decelerating and emitting a photon in the process. This is actually an important source of astrophysical emission from ionized gas, particularly at radio wavelengths. However, as we are concerned here with processes that contribute to stellar opacity, an emission process of this sort is not important to our discussion.

A third process, which results in the absorption of a photon, is **Bound-free absorption**. Unlike the two previous processes, this process requires an electron that is not free, but is bound to a nucleus. An incident photon of sufficient energy can be absorbed by this electron, freeing it from the nucleus and ionizing the atom. This process, also known as photoionization, is shown in the bottom-left panel of Figure 71. An example of this type of opacity is the H^- opacity in the sun.

The final opacity-generating process we will consider is **Bound-bound absorption**. As with bound-free absorption, a photon is absorbed by an electron that is bound to the nucleus of an atom. However, instead of escaping the atom, the electron is instead excited into a higher electronic state of the atom (as shown in the left panel of Figure 71). As the electron remains bound, this process is more selective than bound-free absorption, requiring an incident photon of the correct energy to excite the electron to the next allowed quantum state.

The first two processes require large amounts of free electrons, and so are more likely to occur in the highest-temperature regions of stars, where the gas can be assumed to be fully ionized. These processes can be assumed dominate in these regions, as there will correspondingly be few to no of the bound electrons required for the last two processes to occur. In the outer layers of stars including stellar atmospheres, the reverse will be true. (Note that the extremely cool outer atmospheres of red giants, an additional source of opacity can come from the absorption of photons by molecules, exciting any combination of their electronic, vibrational, or even rotational states, like those discussed in Section 28.1. However, gas in most stellar atmospheres is so hot that the thermal energy of atoms is greater than than the molecular binding forces, and so is almost exclusively atomic rather than molecular.)

We will not go in detail into the expressions for each of these types of opacity, and how they depend on the local physical conditions. However, we will briefly describe the opacity for the two processes that are most important in stellar interiors. The first, opacity from electron scattering, is independent of temperature and gas density. It scales only by the number density of free electrons present (and hence, with the metallicity of the gas, which is assumed to be fully ionized). This type of scattering is called Thomson scattering, and

can be described with the relation:

$$\kappa_{th} = \frac{1}{2}\kappa_{th,0}(1+X) \tag{815}$$

Here, $\kappa_{th,0}$ = 0.04 m^2 kg^{-1}

In contrast, free-free absorption is dependent on both temperature and density. It can be described by Kramer's opacity law:

$$\kappa_{ff} = \frac{1}{2}\kappa_{ff,0}(1+X)\langle\frac{\mathcal{Z}^2}{\mathcal{A}}\rangle\rho T^{-7/2} \tag{816}$$

Here, $\kappa_{ff,0}$ is a scaling coefficient with a value of 7.5×10^{18} m^5 kg^{-2} $K^{7/2}$. As described at the end of Section 11.2, X is the composition or metallicity of the gas, $\mathcal{A}$ is the baryon number or the number of total protons and neutrons in a typical atom, and $\mathcal{Z}$ is the typical charge of that atom. We will return to this relationship when we describe massive stars, and discuss the limits that physics puts on their mass and luminosity.

29.2 *The Temperature Gradient*

Having identified what drives opacity in a star on the microscopic scales of interactions between individual particles, we now zoom back out to ask what effect this opacity has on the macroscopic scales of entire stars.

To do this, we will formally define the opacity coefficient κ. This has units of the fraction of flux that is absorbed (unitless) *times* area per mass, which at first seems a little strange. However, what this actually corresponds to is the amount of absorption per a given mass surface density of absorbing material. This mass surface density is the typical mass of junk that will be encountered in a unit of area through which the energy flux of a star passes, so it makes sense that absorption coefficient would be proportional to the inverse of this quantity.

Figure 72: An illustration of a small slab of area dA and thickness dr taken from a shell within the star at a radius r from the center. The local density of the shell is ρ and the local opacity coefficient is κ. As in Figure 22, the slab experiences an upward pressure on its lower surface of $P + dP$ and feels a downward pressure of P on its upper surface. However, now we also consider that an upward flux of energy $F_r + dF_r$ enters through its lower surface, while only a flux of F_r leaves its upper surface.

We can visualize this using Figure 72. Here, we have a slab with thickness dr, density ρ and absorption coefficient κ taken from a shell inside the star at a radius of r. An energy flux of $F_r + dF_r$ is incident on the bottom surface of the slab, however, the energy flux leaving the slab is only F_r. To satisfy conservation of energy, the amount of energy lost must be equal to the amount that is absorbed in this slab. To get the total amount of flux absorbed, we have

to multiply the fraction of flux that is absorbed per mass surface density κ by the incident flux F_r, by the thickness of the slab dr (so that we now have the amount of flux absorbed for a given volume density) and finally to multiply this by the volume density ρ, yielding the total amount of flux absorbed in a slab of area dA. We can write this as:

$$dF_r = -\kappa F_r \rho dr. \tag{817}$$

For completeness, we can also relate the opacity coefficient κ to the previously-defined optical depth τ:

$$d\tau = -\kappa \rho dr. \tag{818}$$

Another useful relation is to use κ to define the mean free path (Equation 809) that a photon will travel in the presence of this opacity. Remembering that the mean free path is $\frac{1}{\tau}$, the mean free path as a function of κ is

$$l = \frac{1}{\kappa \rho} \tag{819}$$

(Note, in case you are comparing this to the Prialnik textbook, the author is some kind of sadist who using H to define the energy **flux** at a radius r inside of a star, and F to define the **luminosity** at a radius r.)

One consequence of the absorption of photons by this slab is that the photons are imparting a net momentum onto the slab. We can define a momentum flux (momentum per area per time) imparted onto this slab as $\left(\frac{dp}{dA\,dt}\right)$. From previous physics courses, we know that the momentum of a photon can be written as

$$p = \frac{E}{c} \tag{820}$$

We can use this to rewrite the momentum flux as $\frac{dF_r}{c}$. Now, we know from Newton's second law that a change in momentum with time is equivalent to a force:

$$F = \frac{dp}{dt}. \tag{821}$$

We also know that the definition of pressure is a force per unit area, so we can rewrite the left side of this equation:

$$dA\,dP_{rad} = \frac{dp}{dt}. \tag{822}$$

Note that as we are dealing with the momentum imparted by photons, this is specifically the radiation pressure P_{rad}. Substituting $\frac{dp}{dt}$ with our expression for the momentum flux, we can now rewrite the right side of this equation:

$$dA\, dP_{rad} = \frac{dF_r}{c} dA. \tag{823}$$

We can use Equation 817 to replace dF_r:

$$dA\, dP_{rad} = -F_r \frac{\kappa\rho}{c} dr dA. \tag{824}$$

Rearranging this and canceling out dA on each side, we get the following relation:

$$\frac{dP_{rad}}{dr} = -\frac{F_r\, \kappa\rho}{c} \tag{825}$$

As we are dealing with the radiation pressure, we know that we have an expression for this pressure purely as a function of temperature. We then choose to define the left hand side of this equation as a temperature gradient rather than a pressure gradient. To do this, we use the chain rule:

$$\frac{dP}{dr} = \frac{dP}{dT}\frac{dT}{dr} \tag{826}$$

This requires us to take the derivative of the radiation pressure (Equation 258) with respect to temperature:

$$\frac{dP}{dT} = \frac{d}{dr}\left(\frac{1}{3} a T^4\right) = \frac{4}{3} a T^3 \tag{827}$$

We can then rewrite Equation 825 as

$$\frac{dT}{dr} = -F_r \frac{3}{4ac}\frac{\kappa\rho}{T^3} \tag{828}$$

Finally, we can use Equation 39 to replace F_r with L_r and we have an expression for the temperature gradient in a star that regulates the radiative transport of energy in a star:

$$\frac{dT}{dr} = -\frac{L_r}{4\pi r^2}\frac{3}{4ac}\frac{\kappa\rho}{T^3} \tag{829}$$

Having defined the temperature gradient in a star, we now have all four of the fundamental equations of stellar structure. Putting all of them in an

identical time-independent form, we see that we have defined the variation of radius, pressure, temperature, and luminosity all as a function of mass:

$$\frac{dr}{dm} = \frac{1}{4\pi r^2 \rho} \tag{830}$$

$$\frac{dP}{dm} = -\frac{Gm(r)}{4\pi r^4} \tag{831}$$

$$\frac{dT}{dm} = -\frac{L_r}{(4\pi r^2)^2}\frac{3}{4ac}\frac{\kappa}{T^3} \tag{832}$$

$$\frac{dL_r}{dm} = \epsilon_m \tag{833}$$

Adding an equation of state, and expressions for κ and ϵ_m as a function of composition, we now (theoretically) have everything that we need to fully describe the structure of a star at a given point in time.

30 References

1. 'Astrophysics for Physicists' Textbook by Arnab Rai Choudhury
2. Notes on Radiative Transfer from Kees Dullemond at the University of Heidelberg
3. Notes on Molecular Spectra from Essential Radio Astronomy by James Conden at NRAO
4. Notes on the Virial Theorem from Astronomy 1100 at the University of Oslo
5. A nicer proof of the Virial Theorem from Anatoly Klypin at NMSU
6. Notes on the Jeans Mass by Chris Mihos at Case Western
7. Notes on the luminosity of a collapsing cloud by Bob Mutel at the University of Iowa
8. 'The Origin of Stars' Textbook by Michael D. Smith
9. 'Online ISM Textbook by Alyssa Goodman and grad students at Harvard
10. Notes on Astrochemistry from Claire Vallance at Oxford
11. Star Formation lectures by Andrea Stolte, formerly at Bonn University
12. Star Formation talk by Christoph Mordasini, MPIA

31 Acknowledgements

W.C. Ng, K. Shin, E. Lee, A.S. Biscoveanu, and other students for identifying frequent errors in earlier versions of these lecture notes. T. Johnson for allowing me to use his shock profile figure (Fig. 58). N. Mehrle for pointing out the informative analysis described in Sec. 26.2.